LOSS OF TIP30 ACCELERATES PANCREATIC CANCER PROGRESSION AND METASTASIS

Imade E. Imasuen Williams

Submitted to the faculty of the University Graduate School
in partial fulfillment of the requirements
for the degree
Doctor of Philosophy
in the Department of Biochemistry and Molecular Biology,
Indiana University

July 2019

Accepted by the Graduate Faculty of Indiana University, in partial fulfillment of the requirements for the degree of Doctor of Philosophy.

Doctoral Committee

_____
Thomas Hurley, Ph.D., Chair

_____
Maureen Harrington, Ph.D.

October 22, 2018

_____
Brittney-Shea Herbert, Ph.D.

_____
Harikrishna Nakshatri, BVSc., Ph.D.

DEDICATION

I dedicate this dissertation to my late grandparents, Tamara and Mikhail Antonyuk, and my husband, Dwight Williams, as without them none of this would have been possible.

ACKNOWLEDGEMENTS

I would like to express my sincerest gratitude to my doctoral committee: Dr. Maureen Harrington, Dr. Brittney-Shea Herbert, Dr. Hari Nakshatri, and Dr. Thomas Hurley. Thank you for your scientific advisement, support, and guidance. Without your service I would not have made it this far. I would like to especially thank Dr. Thomas Hurley and Dr. Hari Nakshatri for co-advising me through the completion of my doctoral training and dissertation. I am also especially grateful for and am humbled by the entire committee's dedication and feedback over the years, especially in regards to this dissertation and my grant writing. Your support and encouragement gave me an extraordinary amount of strength and courage. In addition to my committee, I would like to thank Dr. Francis Enane, Brandy Boyer-Wood (Indiana Biomedical Gateway (IBMG) Program for PhD Studies), Debra Barker (Indiana University Purdue-University of Indianapolis (IUPUI) Graduate Office), and Dr. Kimberly S. Collins for their feedback and assistance in regards to the formatting of this dissertation.

I would like to express my sincerest gratitude to Dr. Murray Korc, and present and past members of the Korc Laboratory, especially Dr. Francis Enane, Samantha Deitz McElyea, Dr. Jesse Gore, Dr. Sudha Savant, Dr. Kelly Craven, Alison Bates, and Abass Conteh for their support and guidance during my doctoral training. I would like to thank my funding source, the National Institutes of Health (NIH) and National Cancer Institute (NCI). This work and my PhD training was supported by a Diversity Supplement to RO1-CA075059, and more recently by a Ruth L. Kirschstein National Research Service Award (NRSA) Individual

Predoctoral Fellowship to Promote Diversity in Health-Related Research (Parent F31) awarded by the NCI/NIH under Award Number F31-CA236332. I would like especially thank the Center to Reduce Cancer Health Disparities, especially Dr. Nicole McNeil Ford, for their professional development and grant writing workshops, and their support. I would also like to thank the Lustgarten Foundation for the travel award that allowed me to attend the 2017 Cold Spring Harbor Workshop on Pancreatic Cancer, as well as all the facilitators of the workshop. The experience truly enriched my research training in the field of pancreatic cancer.

The interpretation of the mouse studies in this dissertation would not have been possible without Dr. George E. Sandusky, whom I would like to especially acknowledge and thank for the pathological evaluation of the tissues sections associated with these studies, and for allowing me to shadow and learn under his guidance. I would like to thank Rachael Topolski for assistance with tissue sectioning and thank Khalid Mohammad's Laboratory for assistance with tissue processing. I thank Samantha Deitz McElyea for creating the AsPC-1-miR-10b-OX-GFP and AsPC-1-miR-10b-GFP-C human pancreatic cancer cell lines. I would like to thank Dr. Francis Enane for his expertise and assistance with whole genome sequencing and The Cancer Genome Atlas (TCGA) analyses.

I would also like to thank the following individuals and research cores for supporting my work: Mary Brown and IU School of Medicine Indiana Center for Biological Microscopy for confocal microscopy training and guidance; Susan Perkins and the Department of Biostatistics walk-in clinic for guidance with statistical analyses; the Medical and Molecular Genetics Departments and Erica

Clickenbeard for assistance with imaging; the Indiana University Simon Cancer Center (IUSCC) Flow Cytometry Core for the sorting of green fluorescent protein (GFP)-labeled cell lines; and Robert Brankamp from The Jackson Laboratory for his consultation on mouse strain genetics and resources for mice obtained from The Jackson Laboratory.

The IU Simon Cancer Center Summer Research Program (IUCCSRP) first exposed me to the field of cancer research; and I would like to thank the IUCCSRP and my mentor Dr. Marc Mendonca, Helen Chin-Sinex, Dr. Joseph Dynlacht, and Dr. Gwendolyn Johnson, the program director at the time. I would also like to thank Dr. Robert J. Coffey and Dr. Michelle Demory Beckler, Dr. Patrick Ma, Dr. Periasamy Selvaraj, and Dr. Erica Bozeman for their mentorship during my baccalaureate and post-baccalaureate training. I am grateful for the Southern Regional Education Board especially Dr. Ansley Abraham and the Yale Ciencia Academy for providing me with networking and professional development resources for a career in science and education as well as moral support.

I am grateful for the supportive faculty and staff at IU School of Medicine, especially, Dr. Millie Georgiadis, Dr. John Turchi, Dr. Travis Jerde, Dr. Hari Nakshatri, Dr. Teresa Zimmers, and Dr. Andrea Bonetto for support of my scientific development and training and enthusiastic support of opportunities for students to present their research through entities such as departmental seminars and the Cancer Research Club. I would like to thank the leadership of the IBMG Program for PhD Studies, especially Tara Hobson, Dr. Joseph Bidwell, and Brandy Boyer-Wood, the Biochemistry and Molecular Biology Department at IU School of

Medicine, especially Graduate Advisor Dr. Mark Goebl, Grants Specialist Sheila Reynolds, Computer Support Specialist Jack Arthur, Melissa Tarrh, and Darlene Lambert; the IUPUI Graduate Office, especially Dr. Tabitha Hardy and Dr. Janice Blum, Kim Burrows, Vicki Bonds, Dr. Jason Kwon, and my cohort for their advice, mentorship, and feedback during my PhD training. The commitment of the IUPUI faculty and staff to pedagogy has been inspiring beyond measure. The IBMG program provided me with abundant access to opportunities and resources that enabled me to grow intellectually and professionally. It has been an absolute honor learning from and conversing with such a large pool of brilliant scientists with the highest caliber of intellect and creative thinking. Thank you all for seeing my potential, believing in me, and supporting me. And thank you for collectively preparing me for a very exciting future of endless possibilities.

I owe many thanks to my center and foundation, God, and my husband, Dwight Williams. This would not have been possible without the unwavering love and support of my family and friends that saw me through this incredible journey and completion of this dissertation, especially, Ayshai Jones, and Frank and Sissy Wade, who were present every step of the way. Thank you. To my beloved mother-in-law, Meme, who passed away of metastatic breast cancer on October 23, 2013, the semester I began the PhD program, I would like to say thank you for your countless support. Your presence in my life made an everlasting impact and helped carry me through. Lastly, I would be remised to not acknowledge all those affected by cancer, poverty, or oppression, the reason behind my motivation and passion.

Imade E. Imasuen Williams

LOSS OF TIP30 ACCELERATES PANCREATIC CANCER PROGRESSION AND METASTASIS

Pancreatic ductal adenocarcinoma (PDAC) is currently the fourth leading cause of cancer-related death in the United States, and is characterized by key driver mutations (e.g. *KRAS*, *TP53*, *CDKN2A*, and *SMAD4*), elevated expression of growth factors such as TGF-βs and the EGF receptor (EGFR), a markedly desmoplastic stroma, and a propensity to develop multi-organ metastases and chemoresistance. Consistent with its aggressive nature, the 5-year survival rate for PDAC is 8-9%, which demonstrates an urgent need to develop novel therapies. High expression levels of microRNA-10b (miR-10b) in PDAC tissues are associated with decreased patient survival and earlier appearance of metastatic disease following neoadjuvant chemoradiotherapy. miR-10b downregulates the expression of transcription coactivator Tat-Interacting Protein 30 (TIP30) by targeting its 3'UTR. TIP30 has multiple reported functions. TIP30 suppresses tumor formation and metastasis, forms a complex that regulates EGFR trafficking and degradation, and transcriptionally upregulates pro-apoptotic genes. Alterations in *TIP30* have been reported in multiple human cancers, including pancreatic cancer. We hypothesized that *Tip30*-deficiency accelerates PDAC progression and metastasis in a murine model of PDAC. To test this hypothesis, we crossed mice with oncogenic *Kras* (KC) localized to the pancreas epithelium, with *Tip30*-deficient mice (K30C). We compared PDAC histopathology between *Tip30*-heterozygous ($K30^{+/-}C$) and *Tip30*-null ($K30^{-/-}C$) mice. *Tip30*-heterozygosity

accelerated PDAC-lesion-associated pancreatic cancer cell (PCC) pulmonary seeding. By contrast, total loss of *Tip30* enhanced PCC micrometastatic seeding to the liver and hepatic metastasis. $K30^{+/-}C$ mice also presented with an early, increased penetrance of lung lesions and lung adenocarcinoma; and PCCs isolated from $K30^{+/-}C$ pancreata exhibited increased EGFR protein levels. These findings suggest that TIP30 deficiency can have a dose-dependent effect on organotropic metastasis and EGFR levels in PCCs. Future studies will delineate the molecular consequences of TIP30 loss in PDAC and contribute to a broader understanding of pancreatic cancer metastasis.

Thomas Hurley, Ph.D., Chair

TABLE OF CONTENTS

LIST OF TABLES

LIST OF FIGURES

ABBREVIATIONS

+/+	Wild-type
+/-	Heterozygote (one wild-type and one mutant copy)
-/-	Null (two mutant copies)
°	Degrees
°C	Degrees Celsius
µL	Microliters
µm	Micrometers
2D	Two-dimensional
3D	Three-dimensional
3'UTR	Three prime untranslated region
5-FU	5-fluorouracil
aa	Amino acids
AA	African American
ab	Abcam
ACSL4	Acyl-CoA Synthetase Long Chain Family Member 4
ADM	Acinar to ductal metaplasia
AKT	Serine/threonine-protein kinase (or protein kinase B, PKB)
AMP	High level amplification (GISTIC score "2")
APS	Ammonium persulfate
BAX	Bcl-2-associated X protein
Bcl-2	B-cell lymphoma 2
bp	Base pairs

BSA	Bovine serum albumin
C	Common primer
CA	Celiac axis or artery
CA 19-9	Cancer-associated antigen 19-9
CAF	Cancer-associated fibroblast
CC3	(TIP30)
CD	Cluster of differentiation
CDKN2A	Cyclin dependent kinase inhibitor 2A
cDNA	Complementary DNA
CIA	Estrogen receptor alpha-interacting coactivator
CK-19	Cytokeratin 19
Cm	Centimeters
CAN	Copy number alterations
CO_2	Carbon dioxide
CRC	Colorectal cancer
CRE	Causes recombination
CST	Cell Signaling Technology, Inc.
CT	Computed tomography scan
CXCR4	C-X-C chemokine receptor type 4
ddH2O	Ultrapure, double deionized Milli-Q water (EMD Millipore)
DFS	Disease-free survival
DIABLO	Direct inhibitor of apoptosis-binding protein
DNA	Deoxyribonucleic acid

dNTPs	Deoxyribonucleotide triphosphate
DPC4	Deleted in pancreatic cancer, locus 4 or SMAD4
ECM	Extracellular matrix
EDTA	Ethylenediaminetetraacetic acid
EGF	Epidermal growth factor
EGFP	Enhanced green fluorescent protein
EGFR	Epidermal growth factor receptor
EMH	Extramedullary hematopoiesis
EMT	Epithelial-mesenchymal transition
EpCAM	Epithelial cellular adhesion molecule
ERBB2	Erb-b2 receptor tyrosine kinase 2
ERK1/2	Extracellular signal-regulated protein kinases 1 and 2
ESA	Epithelial-specific antigen
ESCC	Esophageal squamous cell carcinoma
EUS-FNA	Endoscopic ultrasound-guided fine-needle aspiration
F	Female
F	Forward primer
FACS	Fluorescence-activated cell sorting
FBS	Fetal bovine serum
FOLFIRINOX	Folinic acid (leucovorin), 5-FU, irinotecan, and oxaliplatin
g	Gram
G12D	Point mutation (Glycine, G, to Aspartic acid, D)
G28V	Amino acid substitution (28^{th} Glycine to Valine)

G31A	Amino acid substitution (31st Glycine to Alanine)
GAIN	Amplification (GISTIC score “1”)
GEMM	Genetically engineered mouse model
GISTIC	Genome Identification of Significant Targets in Cancer score
Gross	Frank, or clearly visible by eye (see Burnet et al., 2004)
GTP	Guanosine triphosphate
HA	Hepatic Artery
HBSS	Hank’s Balanced Salt Solution
HCC	Hepatocellular carcinoma
HeLa	Immortalized cervical cancer cell line from Henrietta Lacks
HETLOSS	Heterozygous loss
HER2	Human epidermal growth factor receptor type 2
HER3	Human epidermal growth factor receptor type 3
HOMDEL	Homozygous loss
HPAP	Human placental alkaline phosphatase
hPDAC	Human PDAC
HTATIP2	HIV-1 tat-interacting protein 2 (TIP30)
ID	Identifier
IL-6	Interleukin 6
K30$^{+/+}$C	KC + *Tip30*-wild-type
K30$^{+/-}$C	KC + *Tip30*-heterozygous
K30$^{-/-}$C	KC + *Tip30*-null
K30Ctd	KC + *Tip30*$^{+/+;\ +/-;\ -/-}$ + tdTom$^{+/-;\ -/-}$

KC	*LoxP-STOP-LoxP-Kras$^{G12D/+}$; Pdx1-Cre*
kD	Kilodaltons
KLF4	Kruppel like factor 4
KO	Knockout mouse or cell line
Kras	Kirsten rat sarcoma viral oncogene
L	Liter
LB	Lower buffer (for SDS-PAGE)
***Lox*P**	***L**ocus **o**f crossing over (**x**)*-bacteriophage **P1**
LoxP-Kras^{G12D}	Recombined *LSL-Kras^{G12D}, Kras$^{G12D/+}$* (1 *Lox*P site)
LSL	*LoxP-STOP-LoxP* cassette
LSL-Kras^{G12D}	Transgene, *Kras^{G12D}* expression is prevented by the *STOP*
M	Male
M	Molar
MAPK	Mitogen-activated protein kinase
MDS	Myelodysplastic syndrome
MDSC	Myeloid-derived suppressor cell
MEF	Mouse embryonic fibroblast
MEK1/2	Mitogen-activated protein kinase kinase 1 and 2
Met	Metastatic
MET	Mesenchymal-epithelial transition
$MgCl_2$	Magnesium chloride
MHV	Mouse hepatitis virus
mL	Milliliters

min	Minutes
miR	MicroRNA
mm	Millimeters
mM	Milimolar
MMTV	Mouse mammary tumor virus
MNV	Mouse norovirus
mp53	Mutant p53
mPDAC	Murine PDAC
MPV	Metapneumovirus
mRNA	Messenger ribonucleic acid
MS	Median Survival
MT	Mutant
mTOR	Mammalian target of rapamycin
MTT	Mehtylthiazolyldiphenyl-tetrazolium bromide
Mut	Mutant
MVM	Minute virus of mice
NaOH	Sodium hydroxide
NCI	National Cancer Institute
Neu	ErbB2
neoR	Neomycin resistance cassette
NF1	Neurofibromatosis 1
ng	Nanograms
NHB	Non-Hispanic black

NHW	Non-Hispanic white
No.	Number
nm	Nanometer
Null	*Tip30*$^{-/-}$
OCT	Optimal cutting temperature compound
OS	Overall survival
p	Probability value or significance is
p16	Protein encoded by CDKN2A
PanIN	Pancreatic intraepithelial neoplasia
PAAD	Pancreatic adenocarcinoma project ID
PAGE	Polyacrylamide gel electrophoresis
pAKT	phosphorylated AKT
PBS	Phosphate-buffered saline
pCA	Chicken beta actin core promoter with a CMV enhancer
PCC	Pancreatic Cancer Cell
PCR	Polymerase Chain Reaction
PDAC	Pancreatic ductal adenocarcinoma
PDK	Pyruvate dehydrogenase kinase 1
PD-L1	Programmed death-ligand 1
Pdx1	Pancreatic duodenal homeobox 1
Pdx1-Cre	Transgene
pEGFR	Phosphorylated EGFR
pERK1/2	Phosphorylated ERK1/2

PI3K	Phosphoinositide 3-kinase
P/S	Penicillin-Streptomycin
PV	Portal vein
PVM	Pneumonia virus of mice
qRT-PCR	Quantitative reverse transcription-polymerase chain reaction
R	Reverse primer
Rac	Ras-related C3 botulinum toxin substrate
RAF	Rapidly accelerated fibrosarcoma kinase
RB	Retinoblastoma
Re	Repeated sampling
Rho	Ras homologous protein
RNAseq	RNA sequencing
RPKM	Reads per kilobase per million (RPKM) mapped reads
Rps6	Murine ribosomal protein S6
RTK	Receptor tyrosine kinase
SBRT	Stereotactic body radiation therapy
SC	Santa Cruz Biotechnology, Inc.
SCA1	Stem cell antigen 1
SCC	Single cell clone cell line
SDC1	Syndecan 1
SDS	Sodium dodecyl sulfate
Shh	Sonic hedgehog
SEM	Standard error of the mean

SEX	“Male” versus “female” biology
SMA	Superior mesenteric artery
Smac	Second mitochondria-derived activator of caspases
SMAD4	Mothers against decapentaplegic homolog 4
SMAD7	Mothers against decapentaplegic homolog 7
SMV	Superior mesenteric vein
SNP	Single nucleotide polymorphism
STR	Short tandem repeat
T3cDM	Type 3c diabetes
TAM	Tumor-associated macrophage
TAE	Tris base, acetic acid and EDTA buffer
TBS	Tris-buffered saline
TBST	Tris-buffered saline-Tween-20
TC3	Alternatively spliced product of CC3
TCGA	The Cancer Genome Atlas
td$^{+/-}$	See tdTom, one copy
td$^{-/-}$	See tdTom, two copies
tdTom	*LoxP-tdTomato-LoxP-EGFP* transgene
TGF-β	Transforming growth factor – β
TGFβR2	TGF-beta type II receptor
T_H17	T helper 17 cell
TIP30	Tat-interacting protein (30 kD)
TP	K30C and K30Ctd mouse ear tag identifier

TP30	Mouse colony (K30C and K30Ctd mouse models)
TP53	Tumor protein 53 gene, codes for p53
T_{reg}	Regulatory T-cell
Tris	Tris(hydroxymethyl)aminomethane
Trp53	Transformation related protein 53 (house mouse) or p53
UB	Upper buffer (for SDS-PAGE)
UCSC	University of California Santa Cruz
UTSW	UT Southwestern Medical Center, Dallas, Texas
UV	Ultraviolet
v-SCLC	Variant-Small cell lung cancer
WT	Wild-type or diploid

CHAPTER 1. INTRODUCTION

Cancer is the second leading cause of death in the United States (US), and the leading cause of death among Hispanics and Asian Americans (Heron et al., 2016). As described by Hanahan and Weinberg in their seminal review, *Hallmarks of Cancer*, cancer, is the permanent alteration in a normal cell's physiology (Hanahan and Weinberg, 2011). These alterations can allow uncontrolled cell proliferation and malignant growth of various tissues in the body. According to Hanahan and Weinberg, the six original hallmarks include:

- evasion of apoptosis (programmed cell death)
- the ability to produce growth signals
- resisting anti-growth signals
- an ability to promote the growth of new blood vessels
- a capacity for tissue invasion and metastasis
- unlimited capacity for replication (Hanahan and Weinberg, 2000).

In 2011, four additional hallmarks were added, including 1) hijacking cellular metabolism, 2) harboring genetic mutations and genomic instability, 3) evading the immune response, and 4) inflammation (Hanahan and Weinberg, 2011).

Cancer death rates have declined by 26% since 1991, and as of 2016, more than 15.5 million cancer survivors were living in the United States (*American Cancer Society*, 2018). Research and technological strides have contributed to an improvement in cancer detection methods. These strides have impacted early diagnosis and the development of therapies for some cancers, such as testicular, prostate, thyroid, skin, and breast cancers. These five cancers currently have a

survival rate of greater than 90% (*American Cancer Society*, 2018). This statement is based on cases diagnosed between 2007-2013 and followed through 2014.

Despite these advances for the general population, not all populations have seen the broad benefits. Survival rates are lower in Black Americans compared to White Americans for many cancers ("Cancer Disparities", 2018). Since the late 1980s, testicular cancer has had near-cure survival rates, at greater than 95%. In addition, the five-year survival rate for breast cancer is currently 91%, for all races. However, the survival percentages drop drastically for patients diagnosed at later stages (American Cancer Society, 2018). It should also be noted that epidemiological statistics above are based on data collected by the Surveillance Research Program in the National Cancer Institute's Division of Cancer Control and Population Sciences ("Surveillance, Epidemiology", 2010). However, data availability and underreporting limit the broad utility of the data, as these studies represent only one-third of the population of the United States (Yu et al., 2009). Continued research and collaborations between clinicians and translational and basic scientists in fields of surgery, radiation oncology, immunology, genetics, biochemistry, chemistry, and molecular and cellular biology, will one day allow for similar advances for other cancers, including one the most deadly: pancreatic cancer, where the survival rate has only increased by a few percentage points, since the 1970s (*American Cancer Society*, 2018).

1.1 Pancreatic Ductal Adenocarcinoma (PDAC)

Pancreatic cancer is currently the fourth leading cause of cancer-related death in the United States and is projected to become the second by 2020 (Rahib,

2014). In 2018, there were roughly 55,000 new pancreatic cancer cases, and roughly 44,000 estimated deaths (Siegel et al., 2018). Although the risk of developing pancreatic cancer is rare, it is almost always fatal. The median survival for PDAC is six months, with an overall five-year survival rate of 8-9% (Siegel, 2014; Siegel et al., 2018; American Cancer Society, 2018). This poor prognosis is due in large part to its high metastatic prevalence. The most common sites of metastasis are the liver, followed by the lung (Hezel et al., 2006). More than 80% of patients have non-localized disease at diagnosis and are not eligible for surgery (Li et al., 2004; Hezel et al., 2006; *American Cancer Society*, 2018).

Pancreatic ductal adenocarcinoma, PDAC, makes up approximately 94% of all pancreatic cancers (Warshaw et al., 1992, *American Cancer Society*, 2018). PDAC is characterized by heightened desmoplasia (Pandol et al., 2009), a hypoxic tumor environment (Koong et al., 2000), pancreatic cancer cell (PCC) chemoresistance, a high frequency of key driver mutations [*KRAS* (95%) (Raphael et al., 2017; Almoguera et al., 1988), *SMAD4 (*55%), *TP53* (70%), and *CDKN2A* (90%) (Rozenblum et al., 1997; Kern, 2000; Hruban et al., 2000)], and upregulation of growth factors including transforming growth factor-betas (TGF-βs) (Friess et al., 1993) and epidermal growth factor (EGF) receptor (Navas et al, 2012; Barton et al., 1991; Korc et al., 1992; Friess et al., 1996; reviewed by Bardeesy and DePhino, 2002). The complexity of the tumor microenvironment, the heterogeneity of the disease, the lack of useful biomarkers for early detection, and inadequate therapeutic response makes PDAC a challenging cancer to treat (Siegel et al., 2018).

There are seven distinct stages of PDAC progression (0-IV), with stage IV being the most advanced. Stages I and II have two sub-stage classifications: A and B (Alteri et al., 2017). Disease stage is determined by tumor size, lymph node involvement, and metastasis to distant organs. The American Joint Committee on Cancer determined this tumor-node-metastasis classification system (Edge et al., 2010). In Stage 0, or carcinoma *in situ*, cancer is confined to the pancreatic duct cells and the pancreas (Alteri et al., 2017). In Stage IA, the tumor is 2 cm or less, while in Stage IB, the tumor is between 2 and 4 cm. In Stage IIA, the tumor is bigger than 4 cm across. In Stage IIB, the tumor size can be anywhere between that as described in Stage I-IIA but also involves spread to a few lymph nodes (Hidalgo, 2010; Saka et al., 2016). In Stage I or II, the tumor is classified as resectable (Varadhachary et al., 2006). Stage III cancer may or may not be confined to the pancreas and varies in size, and lymph node involvement, but spread to distant sites is not detected; this stage is classified as locally advanced and unresectable (Varadhachary et al., 2006; Hidalgo, 2010). In Stage IV, or metastatic disease, PDAC has spread to either the liver, peritoneum (lining of the abdominal cavity), lungs and/or bones (Peixoto et al., 2015). It is important to note that in humans diagnosed with Stage IV cancer, both the cancer size and lymph node spread can vary (Alteri et al., 2017; Hidalgo, 2010). This variability highlights the heterogeneity of the disease and challenges the prevailing paradigm that tumor invasion precedes metastasis.

1.1.1 Pancreas Anatomy and Physiology

Pancreas is derived from Greek, meaning “all flesh”. The human pancreas is a glandular organ that lies in the abdomen just behind the stomach (reviewed in Williams, J, 2012). The pancreas is in direct proximity to the portal vein (PV), aorta, celiac axis (CA), and the superior mesenteric vein (SMV) and artery (SMA) (Longnecker, 2014; **Figure 1**). The head of the pancreas sits in a crevice of the duodenum, and the tail of the pancreas connects to the spleen. The majority of the pancreas tissue is exocrine, and aids in the digestion of proteins and carbohydrates. The exocrine pancreas is comprised of acinar and ductal compartments that are responsible for pro-enzyme secretion and release of pancreatic juices into the duodenum of the small intestine (Kern, 1993). The major pancreatic duct, which connects with the common bile duct, allows pancreatic secretions to reach the duodenum. Key enzymes produced by the pancreas are trypsin, which aids in protein digestion, and amylase and lipase, which aid in the breakdown of carbohydrates and fats, respectively. Additional enzymes stored in the pancreas are DNase and RNase (Pandol, 2011).

The remaining pancreatic tissue is endocrine in function and is responsible for releasing hormones into the bloodstream. The islet compartment of the pancreas (**Figure 1**), or the islets of Langerhans house the endocrine function of the pancreas. Somatostatin, growth inhibitory hormone, is one such hormone released by the pancreas (Longnecker, 2014), in addition to the hormones insulin and glucagon that are released from alpha and beta cells, respectively. Insulin and glucagon regulate the responses to the fed and fasting states relative to circulating

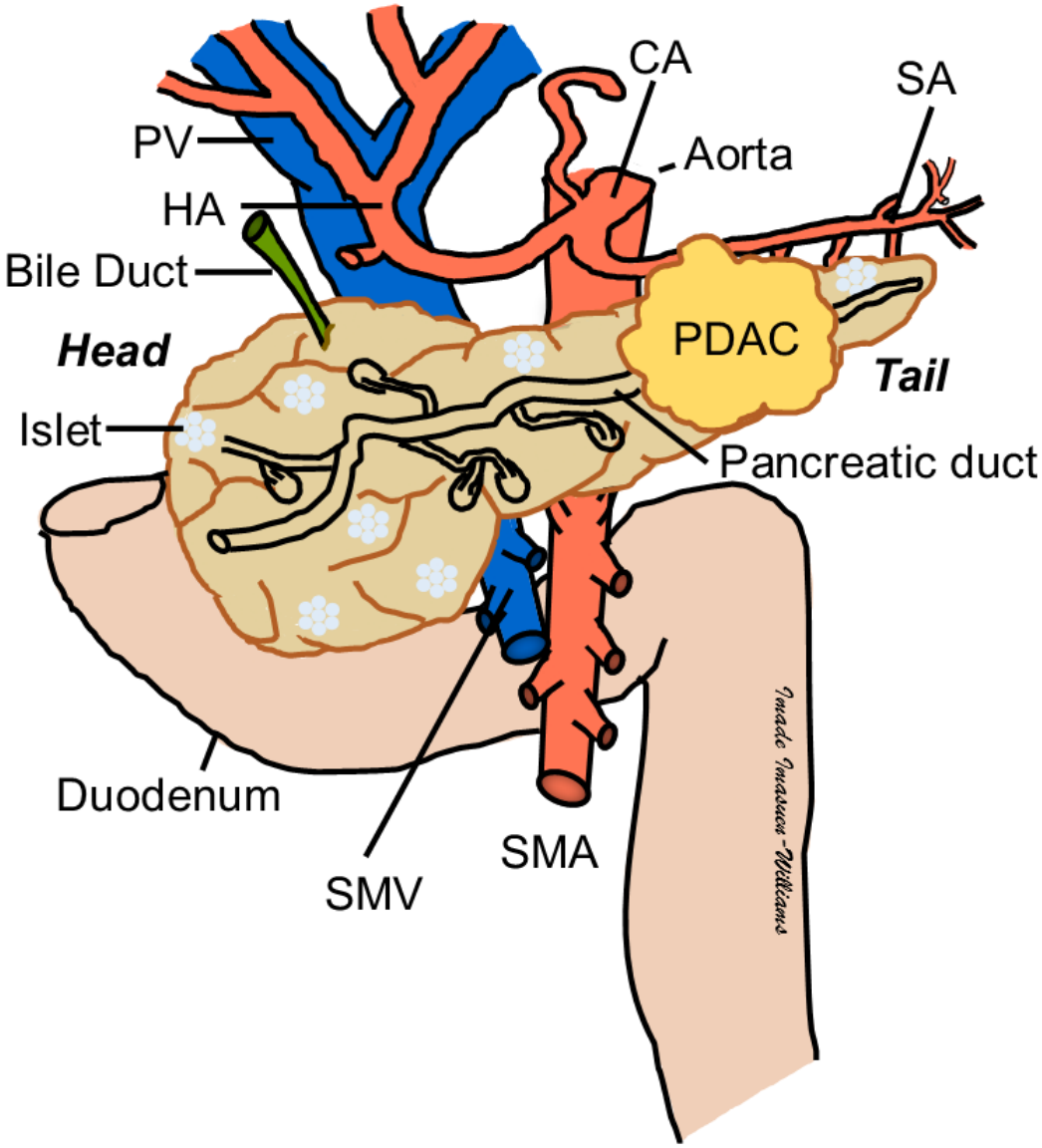

Figure 1. The pancreas with neighboring arteries and blood vessels

A depiction of the human pancreas with a tumor (PDAC), sitting in the groove of the duodenum. CA-Celic Axis, HA-Hepatic Artery, PV-Portal Vein, SA-Splenic Artery. SMA-Superior Mesenteric Artery. SMV-Superior Mesenteric Vein. The head and tail of the pancreas are marked.

blood glucose levels. Glucagon stimulates the breakdown of the energy reserve glycogen in the liver in order to maintain blood glucose levels. Decreased insulin production or resistance to insulin is linked to type 1 or 2 Diabetes Mellitus (reviewed by Kharroubi and Darwish, 2015).

1.1.2 PDAC Presentation and Risk Factors

Patients diagnosed with pancreatic cancer often present late in the disease stage. The clinical presentation for PDAC includes unexplained weight loss, jaundice, acute onset of diabetes, and can include acute pancreatitis, floating stools, pain, nausea, and vomiting (Tempero et al., 2017). However, these symptoms often appear only during advanced disease stages (*American Cancer Society*, 2018). Early stage disease symptoms can be vague and non-specific, further contributing to late diagnoses. By the time most patients reach the clinic, their cancer has already metastasized to distant organs.

Jaundice is associated with patients with tumors in the head of the pancreas, while patients with tumors in the tail or body of the pancreas are more likely to present with symptoms only late in the development of the disease (reviewed in Tempero et al., 2017). As a consequence, only 15% of PDAC patients present with resectable disease (Hidalgo et al., 2015). Furthermore,

- 75% of patients experience recurrence in approximately 2.5 years (Groot et al., 2018)
- ~35% of PDAC patients present with locally advanced disease (Stage III) (Hidalgo et al., 2015)
- 50-60% of PDAC patients present with metastatic disease (Stage IV) (*American Cancer Society*, 2017; Varadhachary, 2006; Hidalgo et al., 2015).

In locally advanced disease, a pancreatic tumor can fall under the category of borderline resectable where the tumor partially wraps around vital blood vessels (**Figure 2A**) or locally advanced surgically unresectable disease. A borderline resectable tumor either encases the hepatic artery without extending to the celiac axis (and without SMA encasement) or some distortion or narrowing of the SMV is present, but safe resection and reconstruction are feasible (Al-Hawary et al., 2013). If a tumor makes venous or arterial vessel contact that exceeds 180° in circumference, it is classified as “vessel encasement” (**Figure 2B**). In the case of unresectable disease, the relationship and proximity between the tumor and vein or artery decrease the safety for surgical removal of the tumor. Unresectable PDAC involves tumor encasement of the celiac axis, more than 180° around the superior mesenteric artery (SMA), or occlusion of the superior mesenteric vein (SMV), the portal vein (PV), or the superior mesenteric-portal vein (SMPV) (Varadhachary, 2006; Al-Hawary et al., 2014, **Figure 2C**). This would result in an unreconstructable SMV or PV, and the patient’s disease is therefore considered inoperable.

PDAC is associated with a variety of different risk factors. The demographic factors associated in developing pancreatic cancer include age (> 50 years), male gender, and ethnicity (black populations have the highest mortality) (reviewed in Li et al., 2004). Outside of these demographic factors, lifestyle risk factors include tobacco, obesity and heavy alcohol use. The latter of which is defined as more than 20 drinks per week (Alsamarrai et al., 2014) or >60 mL ethanol/day (Hassan et al., 2007). In a different report and meta-analysis of 117 pooled datasets,

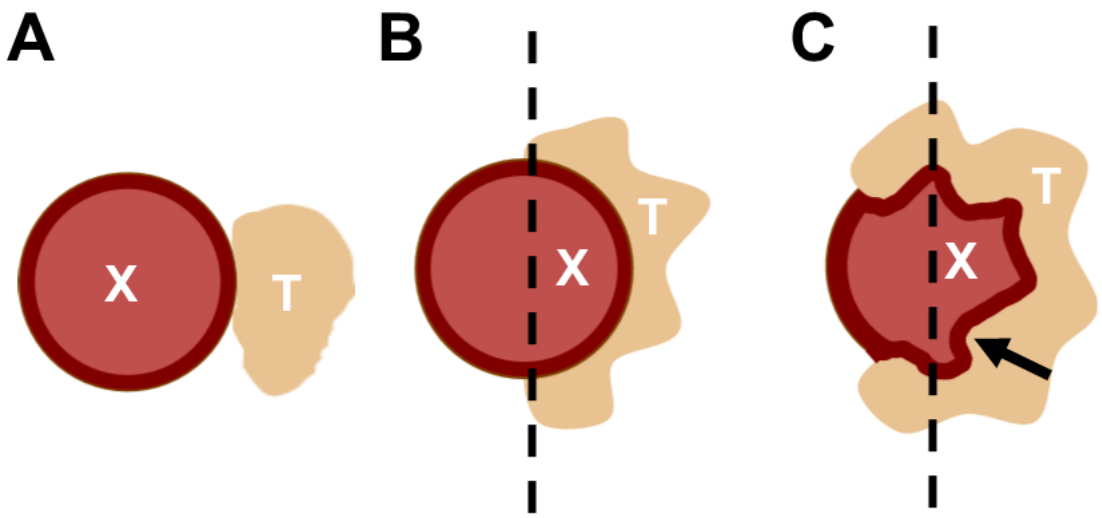

Figure 2. PDAC tumor contact with arterial or venous wall influences surgical resection

(A) Tumor contact is less than 180°. No arterial or vein encasement or distortion. **(B)** Tumor contact is 180°. Tumor is encasing the artery or vein. **(C)** Tumor contact of greater than 180° with arterial or venous occlusion and distortion. Black arrow notes an example of distortion. X, Artery or Vein, T, Tumor. Dashed line, 180° lumenal circumference. Image reproduced with permission from reference Al-Hawary et al., 2014.

tobacco smoking was one of the highest associated risk factors (Maisonneuve and Lowenfels, 2014). The risk of developing pancreatic cancer is two-fold higher in smokers as compared to non-smokers (Lin et al., 2002; Iodice et al., 2008). Lastly, genetic predisposition, Diabetes Mellitus, a history of pancreatitis (Hassan et al., 2007; *American Cancer Society*, 2017), *Helicobacter pylori* infection (moderate risk, Maisonneuve and Lowenfels, 2014), smokeless tobacco use, Lynch syndrome, presence of mutations in BRCA1 and/or BRCA2, more than four cups of coffee per day (*American Cancer Society*, 2017, Lin, Y, 2002), low fruit and vegetable intake, and the consumption of charred food from grilling (Li, D., 2004) are additional reported risk factors. Epidemiology studies demonstrate that 1 in 62 individuals can expect to be diagnosed with pancreatic cancer at least once in their lifetime (Noone, 2018).

Most PDAC cases result from somatic mutations. However, roughly 10% of cases result from germline or familial mutations. To be considered at risk for familial PDAC, the patient must have at least two immediate relatives (parent, sibling, or child) diagnosed with the disease (Petersen, 2016). Genetic risk factors and medical conditions that contribute to pancreatic cancer predisposition are hereditary pancreatitis, hereditary non-polyposis colorectal cancer, ataxia-telangiectasia, Peutz-Jeghers syndrome, familial breast cancer, familial atypical multiple mole melanoma, chronic pancreatitis, diabetic mellitus, gastrectomy and deficiencies in carcinogen metabolism and DNA repair (reviewed in Li et al., 2004). Common genes involved in hereditary pancreatic cancer are BRCA2, CDKN2A, PALB2, and ATM (Roberts et al., 2016). The time between a diagnosis of chronic

pancreatitis and onset of PDAC is 10-20 years (Bang et al., 2014). Chronic pancreatitis, although a risk factor, is considered to confer very low risk for PDAC, with only 4-6% of chronic pancreatitis patients presenting with PDAC over 20 years (Bang et al., 2014). To reduce the risk of pancreatic cancer, a tobacco- and a smoke-free lifestyle, lower body mass index (BMI), and a diet consisting of fruit and whole grains is recommended (Pericleous et al., 2014).

When compared to age-matched controls, PDAC patients had at least a 40% higher prevalence of diabetes compared to breast, colon, lung or prostate cancer patients (Andersen et al., 2017). Although PDAC arises in the exocrine pancreas, alterations in the endocrine compartment may predispose people to disease development and vice versa. Type 3c diabetes (T3cDM) is used to describe diabetic patients that developed diabetes after first being diagnosed with exocrine pancreatic disease (reviewed in Andersen et al., 2017). It is also referred to as PDAC-associated diabetes or new-onset diabetes associated with PDAC (reviewed in Andersen et al., 2017). Although pancreatic disease and PDAC are believed to cause diabetes in a subset of patients, the mechanism for this is not yet known. The causation-association between the two are based on findings that in PDAC patients with diabetes, the diagnoses for the latter occurred less than 24 months before the diagnosis of PDAC (Pannala et al., 2008; Andersen et al., 2017). Researchers have even encouraged clinicians to use new-onset diabetes as a biomarker for PDAC diagnosis.

1.1.2.1 Pancreatic Cancer Disparities

Non-Hispanic Blacks (NHBs) and African Americans have the highest cancer incidence and mortality rates compared to other races (Siegel et al., 2018). In the most recent report, African Americans (AA) had both the highest incidence and mortality rates for cancers of the kidney and renal pelvis, the liver and intrahepatic bile duct, the lung and bronchus (male), the prostate, the stomach, and the uterine cervix (Siegel et al., 2018). Although the incidence for patients with breast cancer were similar in both non-Hispanic Black (NHB) and non-Hispanic White (NHW) women, NHB breast cancer patients had a higher mortality rate. Overall cancer deaths in NHBs were 14% higher than NHWs and were independent of gender (Siegel et al., 2014; Siegel et al., 2018); the racial disparity was more substantial for individuals 65 years old or younger. These and other disparities were attributed to lower access to quality healthcare (Siegel et al., 2018). Emerging studies point to the impact of genetic ancestry on the biology and disease course in breast cancer, a field where disparities in breast cancer have been well established. For instance, the observation that US Hispanic women have the second lowest breast cancer incidence compared to NHW, AA, Asian American, and Indigenous American women is attributed to their mixed European and Indigenous American ancestry (reviewed in Fejerman et al., 2008). Fejerman et al., (2008) found that after adjusting for place of birth and known risk factors, the association between higher European ancestry and breast cancer risk was statistically significant. In contrast, there is disproportionate presentation of an aggressive subtype of breast cancer in women of African descent. Young women

of African descent have a higher incidence of triple-negative breast cancer (reviewed in Jenkins et al., 2019). According to Jenkins et al. (2019), these women are reported to have tumors with a distinct genetic signature. An example is the *DARC/ACKR1* mutation, which is known as the duffy variant and is restricted to populations with West African Ancestry (Jenkins et al., 2019). This recent study shows that the West African-specific duffy variant strongly associates with an increase in proinflammatory chemokines involved in cancer progression.

The incidence of pancreatic cancer is 25% higher in NHBs compared to NHWs (*American Cancer Society*, 2018). A multi-institutional study based out of Houston, Texas, reported that African American (AA) PDAC patients had a lower survival status compared with Caucasian PDAC patients (after adjusting for age, sex, and stage at diagnosis). They further suggested that the factors that attributed to these differences included financial pressures, cultural differences, and underlying comorbidities that prevented therapy (Wray et al., 2012). These factors also decreased the probability of receiving treatment, Wray et al. (2012) reported. In a review by Khawja et al. (2015), AA patients were younger at the time of diagnosis, and had more difficult-to-treat tumors, specifically tumors found in the tail or body of the pancreas. Although the percentage of patients with mutations at codon 12 in *KRAS* were not significantly different in AA PDAC patients, the presence of the $KRAS^{G12V}$ mutation was more than double that of Caucasian patients (Pernick et al., 2003). Additional studies into the impact of genetic ancestry on PDAC incidence and patient survival are needed in the pancreatic cancer research field.

Health disparity studies are limited based on self-reporting of race without mapping of genetic ancestry (Mersha and Abebe, 2015). As reviewed by Mersha and Abebe in *Human Genomics*, race refers to a person's physical appearance, i.e., skin color. Ethnicity can refer to a person's cultural heritage. However, these groupings do not account for the variability in genetic ancestry and the specific percent of African or European ancestry in an individual, uncovered by genetic analysis (Mersha and Abebe, 2015). Research studies should account for commonalities in single nucleotide polymorphism (SNP) variants to more accurately identify and group populations of individuals (Mersha and Abebe, 2015). This approach could improve treatment options for people of color diagnosed with PDAC. Bridging gaps identified in health disparities research may also include more representation of minorities in clinical trials and stages of drug development, and in the use of human samples for research. Addressing these concerns, especially for PDAC, could help advance the field and translate to the broader population within the United States.

1.1.3 Current Therapy

PDAC is currently detected by endoscopic ultrasound-guided fine-needle aspiration (EUS-FNA) (Hewitt et al., 2012). This method, however, cannot be used to exclude the presence of cancer and EUS-FNA cannot distinguish between PDAC and chronic pancreatitis (Hartwig et al., 2009, Fritscher-Ravens et al., 2002). The current standard of care for PDAC is gemcitabine plus nanoparticle albumin-bound (nab)-paclitaxel (a microtubule inhibitor) or the combination of leucovorin, 5-fluorouracil (5-FU), irinotecan and oxaliplatin (FOLFIRINOX)

(reviewed in Hidalgo et al., 2015). Surgery and radiation therapy, with a combination of any of the three chemotherapies, are also current treatment options for patients diagnosed with pancreatic cancer. For patients with borderline resectable pancreatic cancer, the standard of care is a chemotherapeutic as a neoadjuvant, followed by chemoradiation therapy after surgery (Varadhachary et al., 2006).

1.1.3.1 Surgery

Surgery and removal of the tumor is currently the only way to cure pancreatic cancer (reviewed in Bardeesy and DePinho, 2002; Ducreux et al., 2015). Unfortunately, due to the typically late presentation, only about 20% of patients are candidates for surgery. During the surgical process, resection of the tumor is difficult and must be accompanied by clear disease-free margins. Positive margins after surgery can result in disease re-occurrence and translate to poor survival outcome (reviewed in Varadhachary, 2006). In addition, the reported five-year survival rate for surgery-eligible candidates is still only 20% (Ahrendt and Pitt, 2002). A computed tomography (CT) scan, using submillimeter (0.5-1 mm) axial (horizontal plane) sections, is used to stage the tumor and determine resectable or non-resectable tumor classification (stage I or II) (Lu et al., 1997). CT is the preferred method for pancreas imaging and staging; however, pathological diagnosis is not required before surgery (Tempero et al., 2017).

The relationship between the pancreatic tumor and any nearby vessel or arterial wall, introduced in section 1.1.2, is especially critical in determining what type of surgery, if any, can be performed (Tempero et al., 2017). Degree of contact

with either the vessel or arterial wall as well as vessel or arterial deformity or narrowing are two criteria that surgeons must take into account to determine if a pancreatic tumor can be resected (Tempero et al., 2017, **Figure 2**). A pancreatic tumor is resectable when fat planes are present around the celiac axis and superior mesenteric (SMA) and hepatic arteries without superior mesenteric (SMV) or portal vein distortion (Al-Hawary et al., 2013). Venous or arterial vessel contact that exceeds 180° in circumference precludes surgical removal of the tumor **(Figure 2C**, Al-Hawary et al., 2013). Aortic encasement or invasion (**Figure 1**) would also hinder the surgical resection of a tumor (Al-Hawary, 2014). Negative resection margins (the outer edge of tissue devoid of cancer cells) are imperative for improved prognosis after surgery (Sohn et al., 2000). If the pancreatic tumor is ever in an inaccessible location that may potentially prevent vasculature reconstruction or leave negative margins, then surgeons will not operate.

Tumors in the pancreas tail and body are typically not eligible for surgical resection due to advanced disease at the time of diagnosis. However, if eligible then a pancreatectomy is performed (surgical excision of the tail and body of the pancreas and spleen). A total pancreatectomy is performed if the cancer is not confined to just one region of the pancreas. These surgeries also typically include removal of a portion of the small intestine, a portion of the stomach, the common bile duct, the gallbladder, the spleen, and nearby lymph nodes. Patients that present with tumors in the head of the pancreas receive a minimally invasive pancreaticoduodenectomy termed a “Whipple” which is a complex technique required to be performed only by highly skilled and trained surgeons. The Whipple

is a form of laparoscopic surgery that was performed first by Walter Kausch and then Allen Whipple in the early 1900s (reviewed in Gagner and Palermo 2009). This procedure results in the removal of the head of the pancreas, the duodenum, the gallbladder, and the bile duct resulting in resection and reconstruction in one step (Tempero et al., 2017; reviewed in Masiak-Segit et al., 2018).

1.1.3.2 Chemotherapy

Current therapeutic modalities for PDAC are gemcitabine plus nab-paclitaxel or FOLFIRINOX. Before administration of neoadjuvant therapy, a fine-needle aspiration (FNA) biopsy guided by endoscopic ultrasound (EUS) or CT is required. The biopsy is used to confirm malignancy and for pathological staging. Neoadjuvant therapy is administered first to shrink the tumor before surgery. Gemcitabine is recommended for patients with either metastatic or locally advanced disease, as well as good performance status (Tempero et al., 2017). In a large phase 3 clinical trial of gemcitabine-treated patients, the median disease-free survival (DFS) was 13.4 months for the gemcitabine-treated group compared to only 6.7 months in the control group (Oettle et al., 2013).

Although, gemcitabine and gemcitabine combinations are recommended as first-line treatment for PDAC, fixed-dose-rate gemcitabine or other gemcitabine combinations are also acceptable forms of treatment for patients with advanced or metastatic disease. Some combinations include gemcitabine plus cisplatin, gemcitabine plus erlotinib (an epidermal growth factor receptor (EGFR) inhibitor), and gemcitabine plus capecitabine. However, these latter combination therapies did not result in a median DFS that was better than gemcitabine alone. An

exception is the case of gemcitabine plus cisplatin, which did provide benefit to a certain subgroup of patients. All combinations also were associated with extreme toxicities, such as in the case of gemcitabine plus capecitabine (Tempero et al., 2017). The most recent chemotherapy regimen for patients with metastatic pancreatic cancer includes cocktail leucovorin (**fol**inic acid), 5-FU (**f**luorouracil), **irin**otecan, and **ox**aliplatin (FOLFIRINOX). In a randomized phase 3 clinical trial patients treated with FOLFIRINOX exhibited a significant three-four month progression-free survival (PFS) and median overall survival (OS) advantage compared to patients treated with gemcitabine alone (Conroy et al., 2011). FOLFIRINOX is also used as a second-line treatment for patients that have been previously treated with gemcitabine.

1.1.3.3 Radiation Therapy

Patients with pancreatic cancer are given radiation therapy in combination with chemotherapy. Chemotherapy is used to sensitize cancer cells to radiation (Tempero et al., 2017); this maximizes the impact of the radiation. To date, the addition of radiation therapy only results in a modest survival advantage at best when compared to treatment with chemotherapeutic regimens alone (reviewed in Tempero et al., 2017). Advances in radiation therapy will be beneficial for those patients with localized PDAC and poor performance status: patients who cannot tolerate surgery and are inoperable due to age. Stereotactic body radiation therapy (SBRT) is one such approach that delivers precise radiation therapy via cyberknife and linear-accelerator-based methods (Ryan et al., 2018).

1.1.4 PDAC Pathobiology and Tumor Microenvironment

In addition to heterogeneous, PDAC tumors are often described as desmoplastic, which means they are dense and abundant in fibrous or connective tissue (reviewed in Hezel et al., 2006). PDAC tumor tissue, also referred to as stroma, makes up 80% of the pancreatic tumor mass and plays an important role in carcinogenesis (Erkan et al., 2010). PDAC stroma is rich in type I collagen and fibronectin (Mollenhauer et al., 1987). In addition to collagen and fibronectin, the PDAC tumor microenvironment is also abundant in hyaluronic acid (Provenzano et al., 2012; Olive et al., 2009; Jacobetz et al., 2013; Chen et al., 2015). Cancer heterogeneity describes the cell population diversity commonly found within a tumor and the distinct molecular signatures of those cell populations (Dagogo-Jack and Shaw, 2017). The extracellular matrix (ECM) of a PDAC tumor is the molecular network that connects the various cell types within the tumor (Feig et al., 2012). These cells include cancer epithelial cells, stromal cells (stellate cells), fibroblasts, a variety of cancer-associated fibroblasts (CAFS), endothelial cells, and all immune cells (Öhlund et al., 2017).

In addition to being widely fibrotic as a result of desmoplastic reaction (Pandol et al., 2009), the PDAC tumor microenvironment is hypovascular, which leads to a low oxygen or a hypoxic - environment (Koong et al., 2000). Hypoxia is reported to increase pancreatic stellate cell activity (Couvelard et al., 2005). Indeed, vessels in PDAC tumors appear collapsed (Longo et al., 2016) which is a phenomenon attributed to the interstitial fluid pressure in solid tumors. The decreased vasculature adversely impacts drug delivery and is a factor in chemo-

resistance (Jacobetz et al., 2013). Reports on the role of the vasculature in PDAC tumors are conflicting. Although blood vessels are compressed, in a recent report, 35% of human PDACs (hPDACs) exhibit an up-regulation of an angiogenic gene signature (Craven et al., 2016). Targeting lymphangiogenesis using a combinatorial therapy approach has also led to tumor growth and metastasis suppression in an orthotopic model of PDAC (Gore et al., 2016). These and other reports of high vascular endothelial growth factor (VEGF) expression in PDAC tumors challenge the current dogma that angiogenesis does not actively play a role in PDAC (Itakura et al., 1997; Seo et al., 2000).

Another characteristic of the PDAC tumor microenvironment is its highly immunosuppressive nature. Immunosuppression is one way that tumor cells evade immune surveillance, which typically serves to destroy pathogens (reviewed in Vinay et al., 2015). Understanding the relationship between the immune system and PDAC tumor biology will be necessary for developing effective immunotherapies. Immune infiltrates of PDAC tumors include high numbers of M2-type tumor-associated macrophages (TAMs), a subset of neutrophils, regulatory T-cells (T_{reg}), and T helper 17 (T_H17) cells (reviewed in Protti and De Monte, 2013; Clark et al., 2007; Zou and Restifo, 2011), and myeloid-derived suppressor cells (MDSCs) (Zhang et al., 2014). Although the number of CD68+ macrophage infiltrates in human PDAC tumors vary, one study demonstrated that an increase in CD163+ and CD204+ M2-type TAMs were associated with invasion and lymph node metastasis (reviewed in Protti and De Monte, 2013). In an inducible genetically engineered mouse model (GEMM) of PDAC, macrophages and a

second subset of myeloid cells, MDSCs, were found to inhibit CD8+ T-cell anti-tumor activity by activating PD-L1 expression through an EGFR/MAPK signaling axis (Zhang et al., 2016). Targeting CD11b myeloid cells in this model restored anti-tumor immunity. The emerging field of tumor immunology, as it applies to PDAC is an area that warrants further investigation, and may allow for a better understanding of PDAC pathobiology and the complex tumor microenvironment.

1.1.5 PDAC Initiation, Progression, and Maintenance

The head of the pancreas is the most common site of PDAC formation (Hezel et al., 2006). However, tumors are also found in the organ's tail or body. If tumors of the body or tail of the pancreas go undetected, it results in more aggressive tumor formation and poorer patient outcome (Dreyer et al., 2018). In addition to a desmoplastic stromal reaction, other histological features of PDAC include abnormal gland formation and well-to-poorly-differentiated tumors (Hansel et al., 2003). Of the three identified PDAC precursor lesions: pancreatic intraepithelial neoplasia (PanIN), mucinous cystic neoplasm (MCN), and intraductal papillary mucinous neoplasm (IPMN), PanIN is the most common and widely studied (reviewed in Hezel et al., 2006). PanIN lesions are microscopic and progress stepwise, from PanIN-1A/B to PanIN-2 to PanIN-3, accumulating genetic alterations as they progress to PDAC (reviewed in Hruban, 2000; Bardeesy and DePinho, 2002; Brosens et al., 2015). As PanIN lesions progress in histological stage they exhibit increasing architectural and nuclear atypia (Kern et al., 2001). High-grade PanIN, such as PanIN-3, are found less frequently in human pancreas

tissues from individuals who have not been diagnosed with PDAC and are associated with invasive PDAC (Konstantinidis et al., 2013; Hruban et al., 2004).

There are four key genetic driver mutations of PDAC. These are genetic mutations that predominate and are found at high frequency in PDAC patients. These drivers are *KRAS*, $p16^{INK4A}$, *SMAD4/DPC4*, and *TP53* alterations (Kern, 2000; Yachida and Iacobuzio-Donahue, 2009), and all can contribute to PDAC initiation and progression (Bardeesy and DePinho, 2002). PDAC formation is believed to follow a genetic progression model, and telomere shortening contributes to this genomic instability (Bardeesy and DePinho, 2002; Hruban et al., 2000). Additionally, telomere shortening is an event that is detected beginning in early grade PanIN (van Heek et al., 2002), and contributes to PDAC when coupled with inflammatory conditions (Brosens et al., 2015).

Low-frequency driver mutations of PDAC include alterations in the retinoblastoma gene (*RB1)* (Kern, 2000) and hyperphosphorylation and inactivation of its protein product, RB (Gore et al., 2013) and the overexpression of growth factors such as transforming growth factor-βs (TGF-βs) (Friess et al., 1993) and the epidermal growth factor (EGF) family of receptors (R) and their ligands (Barton et al., 1991; Korc et al., 1992; Friess et al., 1996). Alterations in TGFβR2 are also seen at lower frequency (Goggins et al., 1998). Dysregulation in pathways such as these promotes uncontrolled proliferation in human and murine pancreatic cancer cell lines (Gore et al., 2013; Jaganathan et al., 2010).

The specific cell of origin in PDAC is still unclear. PDAC was initially thought to originate from ductal cells due to the duct-like histology of PanIN precursor

lesions. However, attempts to transform normal ductal cells into PanIN precursor lesions or PDAC were unsuccessful (Brembeck et al., 2003). A vast body of literature supports the acinar cell as the PDAC cell of origin (Wagner, 2001; Carrière et al., 2007; reviewed in Guerra and Barbacid, 2013). Acinar to ductal metaplasia (ADM) is reported to precede PanIN formation and PDAC (Crawford et al., 2002), and PanIN precursor lesions are thought to originate through the transdifferentiation of acinar cells (reviewed by Stanger and Dor, 2006; Guerra and Barbacid, 2013). However, pancreata, resected for reasons other than PDAC have a 50% incidence of PanIN-1 (Konstantinidis et al., 2013), challenging a definitive association between early lesions and stepwise progression to PDAC. The concept of pancreas insult or injury either through inflammation, a genetic event, or an environmental oxidative stress event is widely accepted as an associated event for PDAC initiation (reviewed by Kolodecik et al., 2013). Although a combination of one or more of these events is a likely initiator of the disease, it is generally perceived that “inflammatory-driven pancreatic carcinogenesis” is a significant contributor (reviewed in Neesse et al., 2015). In this model, a damaged acinar cell releases inflammatory cytokines such as interleukin-6 (IL-6) or tumor necrosis factor (TNF) in response to pancreatic injury. The immune system then attempts to clear the cells, albeit unsuccessfully. Additional pro-inflammatory cytokines are released into the parenchyma and inadvertently result in an increase in the population of pre-malignant and malignant pancreatic cells (reviewed in Neesse et al., 2015).

Cancer cell and cancer cell-associated fibroblast (CAF) cross-talk contributes to the formation of a pancreatic tumor and disease progression. Pancreatic stellate cells are a small population of initially quiescent cells in the periacinar pancreas parenchyma (Erkan et al., 2010). They have a myofibroblast-like morphology and are responsible for depositing extracellular matrix (ECM) protein into the periacinar space upon activation (Erkin et al., 2009). The sole purpose of activated stellate cells, in the context of PDAC, is to facilitate cancer progression by interacting with pancreatic cancer cells (PCCs).

Pancreatic cancer cells interact with stellate cells and stimulate stellate cell activation (Bachem et al., 2005). Although PCCs express a few of the ECM components such as type I, III, and IV collagen, fibronectin, laminin, vitronectin, or undulin (Löhr et al., 1994), activated stellate cells secrete excessive amounts of ECM proteins to produce the stromal reaction or fibrosis (Xu et al., 2010). Stellate cells are therefore critical in establishing a web that allows for inflammatory, acinar, and cancer cell association and cross-talk that could then initiate tumor formation.

1.1.5.1 KRAS, EGFR and other Drivers of PDAC

Mutations in *KRAS* are one of the four key drivers of hPDAC (Guerra et al., 2003; Hingorani et al., 2003; Collins et al., 2012; Ying et al., 2012); and genetic *KRAS* aberrations have been detected as early as pancreatic intraepithelial lesion (PanIN)-1 (Kanda et al., 2012). *KRAS* is a proto-oncogene and belongs to a family of small GTPases involved in the regulation of cell growth and proliferation. An oncogenic *KRAS* mutation is not only necessary for the initiation of PDAC, but continuous KRAS signaling has been proven to be essential for PDAC progression

and maintenance in inducible mouse model studies (Collins et al., 2012). Activating point mutations in codon 12 of *KRAS* make up 98% of all *KRAS* mutations in PDAC (Eser et al., 2014). EGFR induction appears close to the same time as a mutation in *KRAS* in the genetic progression model of human PDAC (Bardeesy and DePhino, 2002). EGFR or other receptor tyrosine kinases can influence KRAS activity via autocrine and paracrine stimuli (Eser et al., 2014). This process is initiated when ligand binds to the EGFR's extracellular domain and promotes receptor dimerization and transactivation of the receptor's tyrosine kinase domains. Kinase activation then promotes downstream activation of Ras through GDP/GTP exchange. An activated Ras binds to its effector protein Raf to elicit downstream signaling responses through the canonical mitogen-activated protein kinase signaling pathway, RAF-MEK1/2-ERK1/2, or through PI3K-AKT pathways (reviewed in Downward, 2002, **Figure 3**). Studies by Navas et al. (2012) show that *Kras*-driven PDAC is dependent on EGFR signaling, except in the case of complete p53 loss (*p53*^{lox} mouse) which led to EGFR-independent, *Kras*-driven PDAC formation (Navas et al., 2012). In addition, ablation of EGFR decreases ERK and PI3K activity in an oncogenic *Kras* model of murine PDAC (reviewed in Crawford et al., 2019; Ardito et al., 2012).

The remaining three driver mutations of PDAC (*TP53*, *CDKN2A* (p16^{INK4A}), and *SMAD4 or DPC4*) have tumor-suppressive properties (Rozenblum et al., 1997). Tumor-suppressor loss, through genetic mutation and epigenetic silencing, as in the case of *CDKN2A* (p16^{INK4A}) (Fukushima et al., 2002), results in aberrant signaling. p16^{INK4A}, encoded by *CDKN2A,* is a cell-cycle inhibitor of G1-S transition

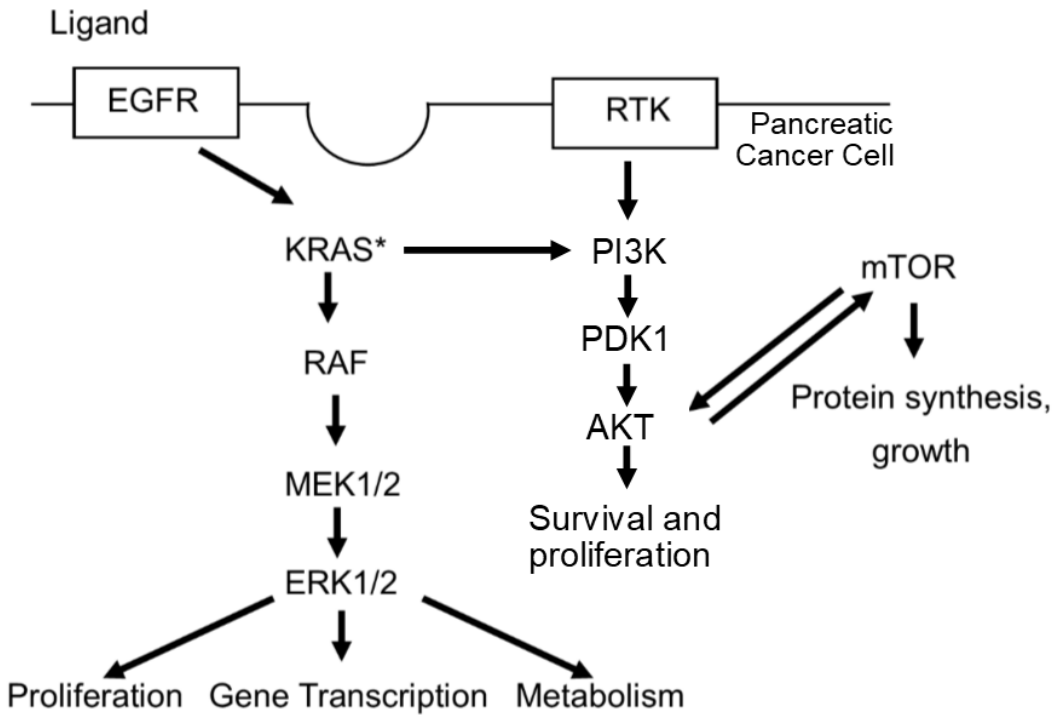

Figure 3. EGFR-KRAS signaling in PDAC

Alterations in the microenvironment that are pro-tumor contribute to PDAC initiation, progression and maintenance. Oncogenic KRAS (KRAS*) activity can be enhanced by other upstream receptor tyrosine kinases (RTKs), the epidermal growth factor receptor (EGFR) and its family members, and downstream effectors such as PI3K and AKT. Image adapted from (Eser et al., 2014).

and is dysregulated in cancer (Romagosa et al., 2011). *TP53* is one of the most widely studied tumor suppressor genes (Muller and Vousden, 2014), and point mutations in *TP53* provide a growth advantage to cancer cells (Muller and Vousden, 2014). One such example is the *R175H* point mutation (Morton et al., 2010), $Trp53^{R172H}$ in mouse models (Hingorani et al., 2005). Inactivating point mutations in either *p53 or p16(Ink4a)* accelerated pancreatic lesion formation in a murine PDAC model of oncogenic *Kras* (Bardeesy et al., 2006a). Hingorani et al. (2005) were the first to show that *Trp53*-mutant mice succumbed to disease at five months and had high metastatic burden in a $Kras^{G12D}$ mouse PDAC model (Hingorani et al., 2003). In contrast, mice with both oncogenic *Kras* and an *Ink4a* tumor suppressor deletion formed PanIN lesions early and died due to metastatic disease by 11 weeks of age (Aguirre et al., 2003).

Mothers against decapentaplegic homolog 4 (SMAD4), also known as deleted in pancreatic cancer, locus 4 or *DPC4*, is the gene that encodes a transcription factor involved in canonical TGF-β signaling and message transport to the cell nucleus (Shi and Massagué, 2003). *SMAD4* inactivating mutations make up around 50% of PDAC cases (Kern, 2000). While *Smad4*-deficient mice do not develop pancreatic tumors, *Smad4* loss combined with oncogenic *Kras* also accelerated PDAC development (Bardeesy et al., 2006b). This mouse model utilizes a pancreas-specific promoter to drive germline expression of an activating $Kras^{G12D}$ point mutation and deletion of *Smad4* exons 8 and 9 (Bardeesy et al., 2006b).

Numerous studies in mice demonstrate the relevance of oncogenic *Kras* in the initiation, progression and maintenance of PDAC (Hingorani et al., 2003, Hingorani et al., 2005; Bardeesy et al., 2006a, Bardeesy et al., 2006b; Aguirre et al., 2003; Collins et al., 2012). The progression model for human PDAC is limited by the uncertainty of the temporal sequence of each genetic event subsequent to the initiating *KRAS* mutation (Bardeesy and DePhino, 2002; Pasca di Magliano and Logsdon, 2013). Over the last 16 years, and with the use of genetically engineered mouse models (GEMMs) of PDAC that recapitulate human pancreatic neoplasia, substantial advances have been made in the field. Continued rigorous experimentation of the biochemical and cellular components of these genetic alterations and their contributions to disease progression are still intensely underway in the field.

1.1.6 PDAC Metastasis

Metastasis allows a tumor to spread and kill its host organism (reviewed in Gupta and Massagué, 2006). Almost 90% of all cancer deaths are the result of metastasis, or the malignant spread of a tumor to a secondary site, or sites (Chaffer and Weinberg, 2011). Metastasis requires cancer cell detachment from the primary tumor site, followed by cancer cell motility and intravasation into the circulatory system. Next, bypass of immune surveillance, extravasation at capillary beds, followed by invasion at the secondary site precedes colonization of a distant organ (reviewed in Gupta and Massagué, 2006). Epithelial to mesenchymal transition (EMT) was initially believed to be a requirement for cancer invasion and metastasis (Kang and Massagué, 2004). However, the concept that a cancer cell needs to

undergo EMT in order to metastasize and become invasive was challenged in the pancreas field when the Raghu Kalluri laboratory reported that the deletion of two common EMT inducers, Snail and Twist, did not alter PDAC invasion, dissemination or metastasis (Zheng et al., 2015). A study in the breast cancer field found that EMT was not essential for tumor initiation (Xie et al., 2014). Although EMT in PDAC differs from that in breast cancer, others reported that EMT and pancreatic cancer cell dissemination preceded pancreatic tumor formation (Rhim et al., 2012). These discrepancies in the field could be due to variations among model systems (Hruban et al., 2006) and/or differences in genomic-aberration-associated EMT dependencies. PDAC is a disease laden with genetic alterations. Consequently, certain subtypes of PDAC may influence genetic aberrations that are more prone to an EMT-dependent metastatic progression. Delineating the EMT program in the context of specific genomic aberrations may help to resolve the role of EMT in PDAC progression and metastasis.

More than 50% of PDAC patients (Hidalgo et al., 2015) present with metastatic disease. In a separate report, 20% of PDAC patients were classified as having resectable disease presentation with hepatic or peritoneal metastasis at the time of laparoscopy or laparotomy (Varadhacary et al., 2006). This reflects the limitations of PDAC detection by CT. The liver is the most frequent site of PDAC metastasis, although distant metastases have been found at almost all anatomical sites (Yachida and Iacobuzio-Donahue, 2009). A review of autopsy data from four different reports that combined 413 autopsies in which PDAC was the primary tumor found that the liver is involved in 80% of metastatic PDAC cases (Yachida

and Iacobuzio-Donahue, 2009). For the one-third of PDAC patients reported not to have liver metastases at autopsy, those patients instead have lung and abdominal lymph node metastasis (Yachida and Iacobuzio-Donahue, 2009). The lung is the third most commonly involved site of metastasis with a frequency of 45% total involvement at autopsy (reviewed in Yachida and Iacobuzio-Donahue, 2009; Embuscado et al., 2005). The reported percentages take into account autopsies in which multiple sites of metastasis were identified in some patients with a primary neoplasm in the pancreas (diSibio and French, 2008).

Distant metastases occur late in the clonal evolution of PDAC (with the first subclone with metastatic potential appearing roughly seven years after the appearance of the founder cell of the parental clone) (Haeno et al., 2012). Based on sequencing and evolutionary mapping of primary and metastatic clonal populations from seven rapid autopsy patients, a computational analysis suggested that primary pancreatic cancers and their matched metastases shared only a weak relationship (Haeno et al., 2012). The presence of large tumors without metastases at autopsy and small tumors with metastases at autopsy support that an increase in tumor size does not necessarily have to influence metastatic burden. Metastatic cells can also exist in a dormant state and bypass detection (Obenauf and Massagué, 2015; Giancotti, 2015). Requirements for colonization of metastatic cells are site-specific (Obenauf and Massagué, 2015).

The TGF-β signaling pathway relies on the SMAD4 transcription factor and additional SMAD cofactors; this pathway can be anti-mitogenic or cause pancreatic cancer cells to have a cell growth advantage and EMT (Massagué, 1998). For

these reasons, TGF- β actions are considered to be context dependent (see Friess et al., 1993), and can be cancer-metastasis promoting (Padua and Massagué, 2008). SMAD4 inactivation disrupts canonical TGF-β signaling (Massagué, 1998). In addition, *TGβR2*-deficient mice develop oncogenic *Kras*-driven PDAC and liver metastases as early as seven to ten weeks (Ijichi et al., 2006). In a compound *Smad4*-deficient/*Ink4a*$^{+/-}$/*Kras*-mutant mouse model of PDAC, 37.5% of mice developed liver invasion or metastases (Bardeesy et al., 2006b). The Sonic Hedgehog signaling pathway, initially discovered for its role in embryogenesis, is an additional signaling pathway associated with PDAC metastasis. Misregulation of the Hedgehog signaling pathway is common in PDACs (Berman et al., 2003; Thayer et al., 2003). Together with Notch (another embryonic signal transduction pathway) signaling, Hedgehog can promote pancreatic cancer initiation and maintenance if left unchecked (Mullendore et al., 2009). Primary and metastatic cell lines established from a murine PDAC model have sustained activation of Hedgehog signaling (Thayer et al., 2003). Lastly, hypoxia-inducible factors 1 and 2, when elevated, are associated with increased metastasis in multiple cancers including pancreatic cancer (Rankin and Giaccia, 2016). Therefore both the hypovascular and hypoxic PDAC tumor environment may promote metastatic disease (reviewed in Tuveson and Neoptolemos, 2011). Since these factors and aforementioned signaling pathways contribute to metastatic disease, additional studies delineating the biochemical processes and therapies targeting this signaling may be extremely valuable in improving patient outcome.

Due to their self-renewal properties, cancer stem cells (CSCs) have been linked to the origin of cancer metastasis. CSCs contribute to intratumoral heterogeneity and are also a mechanism of tumor resistance to therapy (Shibue and Weinberg, 2017). Pancreatic CSCs play a significant role in the promotion and dissemination of PDAC (Lee et al., 2008; Zhu and Yuan, 2015; Valle et al., 2018). In 2007, studies in Diane Simeone's laboratory led to the identification of CD44/CD24/epithelial specific antigen (ESA)-positive pancreatic cancer cells with self-renewal properties and the capacity to produce progeny that can fully differentiate (Li et al., 2007). Additional CSC studies found that migratory CD133- and CXCR4-positive human pancreatic cancer stem cells are essential for PDAC metastasis (Hermann et al., 2007). Depletion of this pool prevented PDAC metastasis but not tumor initiation. More recently, highly metastatic pancreatic cancer cells have tested positive for EpCAM, CD24, CD44, CD133, and SCA1 markers (Ischenko et al., 2014).

1.1.7 Advances and Progress

According to a study reliant on data from the Survival, Epidemiology and End Results (SEER) Database of human metastatic PDAC cases from 1993 to 2013, the percent of patients that died within two months of PDAC diagnosis decreased from 63.5% to 50.6% (Golan et al., 2017). In addition, patient survival (12 months after diagnosis) increased from 4.9% to 12.7% (Golan et al., 2017). These improvements have been linked to advances in chemotherapy. Gemcitabine increased the 12-month survival rate for PDAC from 2% to 18%, when compared to the first chemotherapeutic used for the treatment of PDAC (5-

FU) (Burris et al., 1997). Single therapeutic targeting of the most frequently mutated genes in PDAC has not proven successful. However, combinatorial targeting of signaling molecules such as phosphoinositide 3-kinase (PI3K), with MEK, and AKT inhibitors is being investigated in clinical trials (reviewed in Hidalgo et al., 2014). The combinatorial approach has been used in the development of more efficacious chemotherapeutics for the treatment of pancreatic cancer, for example, FOLFIRINOX and gemcitabine/nab-paclitaxel. FOLFIRINOX significantly improved patient outcome, by increasing the median OS of PDAC after treatment to 11.1 months (Conroy et al., 2011). The median overall survival of gemcitabine, when compared to FOLFIRINOX in this study, was 6.4 months (Conroy et al., 2011).

The majority of PDAC patients are deemed inoperable at the time of diagnosis due to late presentation and advanced stage by the time they reach the clinic. A recent study that focused on identifying circulating tumor cells (CTCs) in the blood of PDAC patients had promising results. The investigators detected CTCs in 62.5% of patients with a 94.4% specificity rate (Ankeny et al., 2014). In a follow-up study, three or more CTCs per 4 mL of blood was a prognostic marker and an accurate identifier of patients with metastatic disease (Court et al., 2018).

To detect pancreatic cancer efficiently and effectively, one needs to have a pancreatic cancer-associated (CA) antigen, also referred to as a biomarker that is specific to the disease. In order for a cancer-associated antigen to be reliable, it needs to be specific for PDAC patients. The utility of serum carbohydrate and carcinoembryonic antigens have proven to be useful when distinguishing PDAC

from healthy tissues; however, these antigens prove useful only in Stage III PDAC or greater (Chen et al., 2015). In a comprehensive meta-analysis that included 2,316 participants, carbohydrate antigen 19-9 (CA 19-9), a candidate biomarker for the diagnosis of pancreatic cancer, was found to have a sensitivity of 0.8 and a specificity of 0.8. These findings translate to an 80% detection rate for pancreatic cancer patients using this marker, with 80% accuracy (Huang and Liu, 2014).

Since the vast majority of PDAC tumor consists of stroma (Erkan et al., 2010), efforts to target the stroma have been made. The reasoning behind stromal targeting was to allow for better delivery of chemotherapeutic agents into the tumor. Surprisingly, investigators found that targeting stromal elements of PDAC resulted in a more aggressive and undifferentiated cancer (Rhim et al., 2014). These studies utilized a genetically engineered mouse model (GEMM) of PDAC with a deletion in sonic hedgehog (Shh) (Rhim et al., 2014). Shh was targeted due to its notable involvement in PDAC tumor stroma development according to Rhim et al. (2014). Their findings were consistent with human trial data in which stromal targeting was not successful (Ozdemir et al., 2014). The HALO 202 phase II clinical trial explored targeting elevated hyaluronan levels, in a subset of PDAC patients, and demonstrated a modest increase in survival when combined with nab-paclitaxel/gemcitabine therapy (Hingorani et al., 2018). Consequently, additional studies need to be conducted in the area of combined stromal and epithelial targeting to establish whether this is a therapeutic option.

Quantitative analysis using a mathematical model predicted a window of roughly 20 years between the initiation of PDAC tumorigenesis and the metastatic

lesion presentation in the clinic (Yachida et al., 2010). The last three years of the timeline were attributed to the birth of a metastatic subclone. This subclone would, therefore, hold the capacity to give rise to a liver or lung metastatic lesion (Yachida et al., 2010). These findings highlight a 17-year window of opportunity where further biomarker and targeted therapy could help save the lives of a vast majority of PDAC patients.

Although endoscopic and radiographic imaging technologies still have limitations for diagnosis of PDAC and pancreatitis, especially for early-stage disease, significant improvements have been made. Endoscopic ultrasound (EUS) and endoscopic retrograde pancreatography (ERP) methods have the potential to aid in early diagnosis and delivery of therapeutic agents to the tumor site. ERP was first used to image the pancreatic duct, but advances have since improved the outcomes for this device (Coté et al., 2013). Some advances include pancreatoscopy which allows for more straightforward and direct visualization of both the bile duct and the pancreas duct. Albeit, biopsy during this process is not feasible due to a time limitation. There have also been advances in resolution and high-definition video imaging. High-resolution microendoscopy allows for the visualization of PanIN precursor lesions of PDAC, and tissue at a cellular level (reviewed by Coté et al., 2013).

1.1.8 Cre-*loxP* Technology: Site-Specific Recombination for Genetically Engineered Mouse Models (GEMMs) of PDAC

Cre is a 38-kDa tyrosine recombinase enzyme that is derived from the P1 bacteriophage (Sauer and Henderson, 1988). Sternberg and Hamilton (1981)

coined the term Cre, which means *c*auses *re*combination. Sernberg and Hamilton (1981) proved that the P1 bacteriophage contained a hot spot for recombination and natural ability to resolve its genome using Cre recombinase proteins and target ***l****ocus* ***o****f crossing over (****x****)*-bacteriophage **P1** (*lox*P*)* sites (Sternberg and Hamilton, 1981; Hoess and Abremski, 1984). *Lox*P and the *cre* gene were confirmed to be separate yet adjacent segments of *Eco*R1-7 DNA (Sternberg and Hamilton, 1981). Cre-*lox*P-mediated site-specific homologous recombination (specific transgene deletion) was developed by Brian Sauer and is used in transgenic mouse model systems to control the expression of transgenes of interest (Sauer and Henderson, 1988). Since Cre is a site-specific DNA recombinase, it only relies on the location and orientation of its direct target: *lox*P sites, which are short strands of DNA with Cre-specific binding sites. *Lox*P sites are 34-bp in length and consist of two 13-bp palindromic DNA sequences separated by an 8-bp spacer region. The spacer region is where the cleavage event occurs (Lakso et al., 1992). When *Lox*P sites are oriented in the same direction (in cis) around or flanking a specific gene, it allows for deletion of that gene; *lox*P sites in opposite orientation result in inverted floxed genetic sequences (Kuzminov et al., 2011).

Cre uses a topoisomerase mechanism to introduce site-specific cuts and ligations in DNA sequences. Cre's conserved tyrosine residue participates in nucleophilic attack and linkage formation with a phosphate group on the targeted DNA strand (Van Duyne, 2001). This results in a DNA-protein complex and 3'-phosphotyrosine linkage (Van Duyne, 2001). This homologous recombination event allows for controlled expression of genetic mutations in tissues or cells of

interest. Through an adenoviral vector, *Cre* can be introduced close to the targeted organ (Jackson et al., 2001) or can be introduced by cell- or tissue-specific promoters introduced and passed down in the germline. Since the two *lox*P DNA regions are positioned on the same chromosome, the homologous recombination event occurs through the formation of a circle (Kuzminov et al., 2011). This leaves one resolved linear strand of DNA with a *lox*P site, and one deleted circular DNA strand holding the genetic region targeted for deletion and the other *lox*P. Investigators have found that recombination efficiency between two *loxP* sites on the same chromosome decreases with increasing genetic distance (Zheng et al., 2000).

Genetic engineering of tissue and cell-specific mutations in animal model systems allows scientists to understand the development and progression of human disease. Genetically engineered mouse models (GEMMS) have been precious and critical for expanding the knowledge base for pancreatic ductal adenocarcinoma (PDAC) development and progression, mostly due to the similarity in disease progression shared between *Homo sapiens* and *Mus musculus* (house mouse). Studies in mice are performed only when necessary and can lead to the development of novel patient therapies. The advantage of using autochthonous mouse models of PDAC is that they allow for spontaneous tumor formation in the mouse's own pancreas (Tao et al., 2018). Using Cre-*lox*P technology and systems, conditional (restrictive) mutations in the pancreas of genetically engineered mice can be spatially controlled through the introduction of pancreas-specific promoters (reviewed in Walrath et al., 2010). In addition to

spatial control, temporal control of a specific mutation can be employed using a Cre fused to the hormone-binding domain of the estrogen receptor (Cre-ER) (Feil et al., 2009). Cre-ER technology in mice exposed to the ligand tamoxifen through feed or drink allows activation of the ER and drives Cre to the nucleus where it can recombine DNA (Feil et al., 2009; Walrath et al., 2010). These GEMMs are referred to as inducible models.

Pancreatic duodenal homeobox 1 (Pdx1) is a transcription factor involved in the development of the pancreas. It is expressed early during embryogenesis at embryonic day 8.5 (E8.5) (Offield et al., 1996). In transgenic mouse models of pancreatic cancer, the *Pdx1* promoter is commonly used to drive preferential expression of a mutation of interest to the pancreas epithelium. *Pdx1-Cre*-transgenic mice (Gu et al., 2002) will express the Cre recombinase protein, which will facilitate a site-specific DNA recombination event in all cells that express the Pdx1 transcription factor. P48 is a second transcription factor expressed around E9.5 essential for pancreas fate (Hingorani et al., 2003). Together, Pdx1 and P48 double-positive expressing cells give rise to all of the cells of the mature pancreas (Hingorani et al., 2003).

The KC mouse model (*LoxP-STOP-LoxP (LSL)-**K**ras^{G12D};Pdx1-**C**re* or *LSL-**K**ras^{G12D};P48-**C**re)* of pancreatic cancer utilizes the Cre-*lox*P technology via a *Pdx1* or *P48 promoter*. The recombination event that occurs results in the excision of a synthetic transcriptional/translational ‘stop’ cassette (STOP) (Lakso et al., 1992; reviewed in Dragatsis and Zeitlin, 2001) that sits just upstream of the mutant *Kras* sequence. Thus, one copy of oncogenic *Kras* (*G12D*) (*Kras$^{G12D/+}$* or *Kras^{G12D}*) is

driven to the pancreas epithelium during embryogenesis (Hingorani et al., 2003). In addition to the pancreas epithelium, *Pdx1*-Cre has been detected in the antral stomach and duodenum in neonates and the adult islet (Hingorani et al., 2003). While *Pdx1*-Cre results in a reported stochastic pattern of expression in pancreas tissues, *P48*-Cre results in a more uniform distribution of Cre in the pancreas when assessed in the background of a ROSA26 (R26) Cre reporter. This is thought to be potentially due to the knock-in-strategy used to develop the transgenic mouse model (Hingorani et al., 2003; Kawaguchi et al., 2002). The ROSA26 gene locus is ubiquitously and constitutively expressed in all tissues, and during embryonic development in mice. The ROSA26 reporter line is used to monitor Cre expression by detection of beta-galactosidase expression (Soriano, 1999-Seidler, et al., 2008; Friedrich and Soriano, 1991). KC mice develop a full range of pre-malignant lesions in the pancreas, similar to the human PDAC with long latency to PDAC (Hingorani et al., 2003). The *Pdx1-Cre;LSL-Kras*^{G12D} mouse can develop metastatic disease as early as 6.25 months to both the liver and the lung (Hingorani et al. 2003; reviewed in Guerra and Barbacid, 2013).

Another group of investigators developed a temporal oncogenic *Kras* mouse model of PDAC using a R26-tetracycline transactivator transgene to control Kras^{G12D} expression in the pancreas epithelium (Collins et al., 2012). Using this model, they were able to show that oncogenic *Kras* is required for PDAC initiation and tumor maintenance (Collins et al., 2012). The investigators reported “rare areas of ADM and low-grade PanIN in 1 of 3 mice” at three weeks of age (Collins et al., 2012, p.641). At five weeks of age, 2 of 3 mice had areas of ADM and low-

grade PanIN formation. A more even distribution of PanIN precursor lesions of PDAC and areas of fibrosis was detected in mice 18 weeks of age, and at six months 1 of 2 mice developed PDAC (Collins et al., 2012).

1.2 MicroRNAs and miR-10b in PDAC

MicroRNAs (miRs) are small non-coding ribonucleic acids (RNAs), that are between 18-25 nucleotides long, and are commonly overexpressed in PDAC (Garzon et al., 2010; Szafranska et al., 2007; Bloomston et al., 2007). miR-10b is one of the most frequently upregulated miRs in PDAC (Bloomston et al., 2007; Preis et al., 2011). High miR-10b levels in human hPDAC are associated with decreased therapeutic response to neoadjuvant therapy, shorter time to metastasis, and decreased patient survival (Preis et al., 2011). miR-10b was significantly overexpressed in cytokeratin (CK)-19 positive pancreatic cancer cells (PCCs) in human PDAC tissues (Preis et al., 2011). CK-19 is a marker used to identify pancreatic cancer cells in precursor lesions and PDAC in tissues. In addition, an analysis of plasma samples from a patient cohort undergoing evaluation for PDAC indicated that high plasma miR-10b levels distinguish PDAC from chronic pancreatitis (CP) and patients without pancreatic pathology (Ouyang et al., 2017). miR-10b enhances pancreatic cancer cell (PCC) invasion *in vitro* by suppressing Tat-interacting protein 30 (TIP30) gene expression, which leads to sustained epidermal growth factor (EGF) signaling (Ouyang et al., 2017). microRNA-dependent mechanisms are an example of epigenetic alterations, or alterations in gene expression that do not result from modification of the DNA sequence itself (reviewed by McCleary-Wheeler et al., 2014).

1.3 TIP30, Direct Target of miR-10b

In a recent PDAC study, miR-10b-overexpressing PCCs had a significant decrease in TIP30 gene expression levels (**Table 1**, Ouyang et al., 2013). In both PDAC and esophageal squamous cell carcinoma (ESCC), miR-10b is reported to directly target the 3' untranslated region (UTR) of TIP30 mRNA and lead to decreased TIP30 expression (Ouyang, 2013; Dong et al., 2014). miR-10b and TIP30 expression were also inversely correlated in 15 human ESCC cases (Dong et al., 2014). As noted in **Table 1**, TIP30 is not the only target of miR-10b (Ouyang et al., 2013, Supplemental). A microarray analysis by Ouyang et al. (2013, Supplemental) revealed that 55 genes were down-regulated in a human pancreatic cancer cell line engineered to overexpress miR-10b (pMir-10b). A miR can have more than a hundred different targets (Brennecke et al., 2005). In addition to *HTATIP2* or *TIP30*, and genes listed in **Table 1**, miR-10b is reported to target kruppel like factor 4 (KLF4) (Tian et al., 2010) and RAS-signaling modulator NF1 (Chai et al., 2010) among others (Ouyang et al., 2013). In addition to a reported tumor-suppressive function, Klf4 overexpression induced PanIN formation in the presence of oncogenic *Kras* (Wei et al., 2016).

1.3.1 TIP30

Tat-interacting-protein (TIP) 30 or (30 kilodaltons (kD)) [also known as **H**uman Immunodeficiency Virus-1 (HIV-1) **TAT-I**nteractive **P**rotein **2** (HTATIP2) or CC3 in the literature] is a small transcriptional coactivator, metastasis suppressor and antiangiogenic factor that predisposes cells to apoptosis (Shtivelman, 1997; Xiao et al., 1998; Baker et al., 2000; NicAmhlaoibh and Shtivelman, 2001).

Table 1. Genes down-regulated by miR-10b

Gene symbol	pMir-10b/ctrl FC	p-value
FBXO45	**0.58**	**0.002801**
RAB15	**0.51**	**0.014403**
AGR2	**0.50**	**0.039114**
SDC1	**0.45**	**0.001458**
CDK6	**0.38**	**0.024854**
SKA1	**0.38**	**0.024388**
HTATIP2 (TIP30)	**0.38**	**0.034162**
EPHB2	**0.35**	**0.022975**

Adapted from Ouyang et al. (2013, Supplemental). FC, fold change

The name HTATIP2 came from a 1998 study, in which investigators reported a transcription cofactor that accelerated tat-mediated transcription by binding the C-terminal domain of RNA polymerase II and enhancing Tat-activated transcription of HIV-1 (Xiao et al., 1998). Around the same time, and in a separate study, loss of a gene by the name of CC3, was reported in an RNA differential display analysis of highly metastatic variant small cell lung cancer (v-SCLC) cell lines compared to non-metastatic cell lines (Shtivelman, 1997). Shtivelman found that CC3-low or -absent v-SCLC cells were resistant to apoptosis (Shtivelman, 1997). CC3 and HTATIP2 were found to be the same gene and gene product, and the role of TIP30 as a metastasis suppressor through proapoptotic properties were further examined. A role for TIP30 kinase activity was even postulated (Xiao et al., 2000). However, the kinase activity of TIP30 is highly unlikely due to the lack of an ATP-binding site (Omari et al., 2005).

TIP30, located on chromosome 11 in humans, and chromosome 7 in mice is ubiquitously expressed in normal tissues, including the pancreas (**Figure 4**, Shtivelman, 1997). The TIP30 protein has been found in both the nucleus (Xiao et al., 1998; Ito et al., 2003; Jiang et al., 2004; Zhao et al., 2008; Li et al., 2013) and cytoplasm (Ito et al. 2003; King and Shtivelman, 2004; Zhao et al., 2007; Zhao et al., 2008; Tong et al., 2009; Li et al., 2013; Guo et al., 2014) as well as localized to the nuclear envelope (King and Shtivelman, 2004; Guo et al., 2014). Ito et al. (2003) reported that 90% of TIP30 is found in the cytoplasm, and 10% in the nucleus. Three isoforms of TIP30 have been reported in human cell lines: isoforms

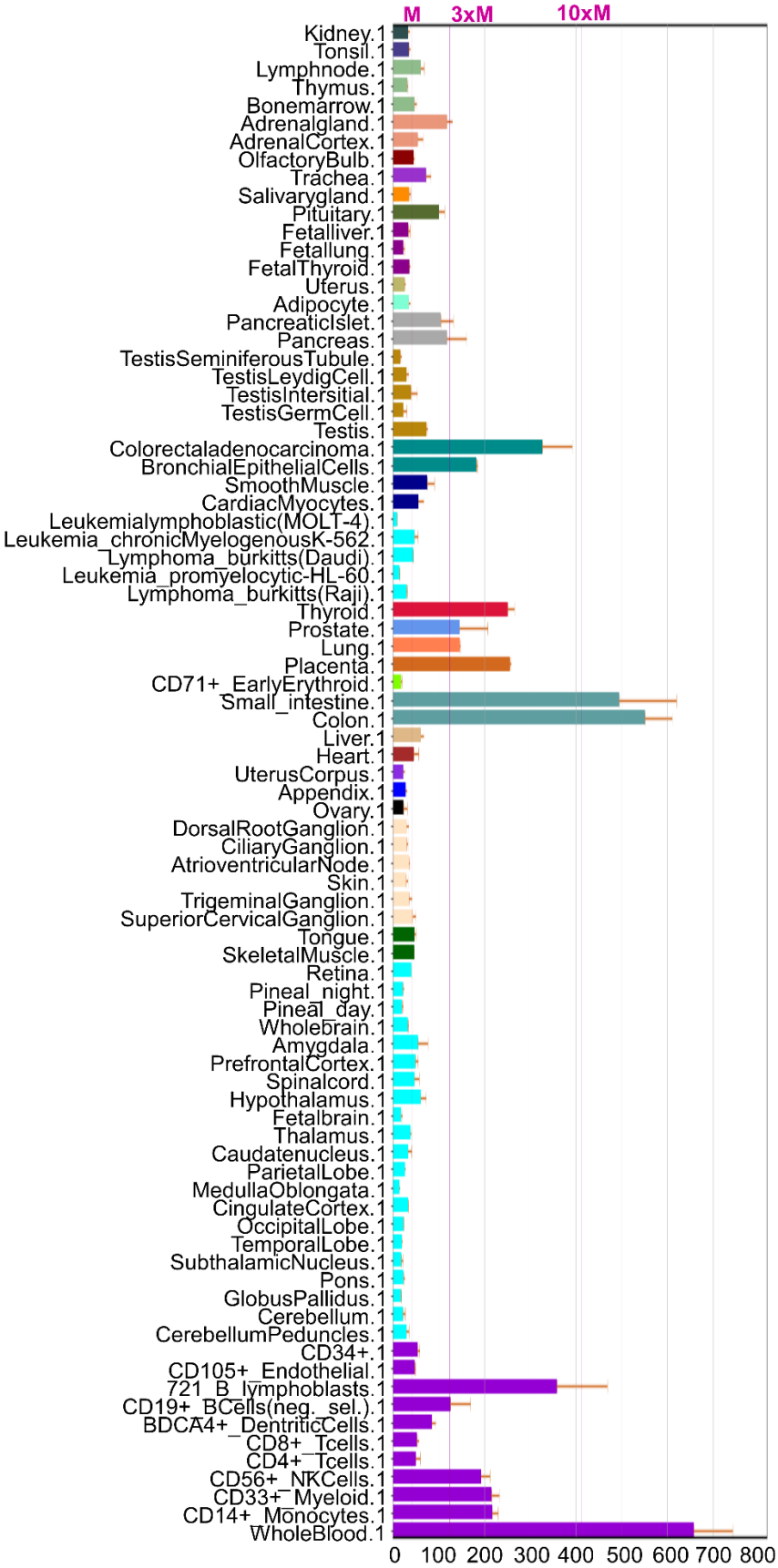
M
3xM
10xM
Kidney.1
Tonsil.1
Lymphnode.1
Thymus.1
Bonemarrow.1
Adrenalgland.1
AdrenalCortex.1
OlfactoryBulb.1
Trachea.1
Salivarygland.1
Pituitary.1
Fetalliver.1
Fetallung.1
FetalThyroid.1
Uterus.1
Adipocyte.1
PancreaticIslet.1
Pancreas.1
TestisSeminiferousTubule.1
TestisLeydigCell.1
TestisInterstitial.1
TestisGermCell.1
Testis.1
Colorectaladenocarcinoma.1
BronchialEpithelialCells.1
SmoothMuscle.1
CardiacMyocytes.1
Leukemialymphoblastic(MOLT-4).1
Leukemia_chronicMyelogenousK-562.1
Lymphoma_burkitts(Daudi).1
Leukemia_promyelocytic-HL-60.1
Lymphoma_burkitts(Raji).1
Thyroid.1
Prostate.1
Lung.1
Placenta.1
CD71+_EarlyErythroid.1
Small_intestine.1
Colon.1
Liver.1
Heart.1
UterusCorpus.1
Appendix.1
Ovary.1
DorsalRootGanglion.1
CiliaryGanglion.1
AtrioventricularNode.1
Skin.1
TrigeminalGanglion.1
SuperiorCervicalGanglion.1
Tongue.1
SkeletalMuscle.1
Retina.1
Pineal_night.1
Pineal_day.1
Wholebrain.1
Amygdala.1
PrefrontalCortex.1
Spinalcord.1
Hypothalamus.1
Fetalbrain.1
Thalamus.1
Caudatenucleus.1
ParietalLobe.1
MedullaOblongata.1
CingulateCortex.1
OccipitalLobe.1
TemporalLobe.1
SubthalamicNucleus.1
Pons.1
GlobusPallidus.1
Cerebellum.1
CerebellumPeduncles.1
CD34+.1
CD105+_Endothelial.1
721_B_lymphoblasts.1
CD19+_BCells(neg._sel.).1
BDCA4+_DentriticCells.1
CD8+_Tcells.1
CD4+_Tcells.1
CD56+_NKCells.1
CD33+_Myeloid.1
CD14+_Monocytes.1
WholeBlood.1
0
100
200
300
400
500
600
700
800

Figure 4. Ubiquitous expression of TIP30

TIP30 (HTATIP2) tissue-specific gene expression from BioGPS database (Wu et al., 2016). Probe-based microarray data (GeneAtlas U133A). Expression values are units of fluorescence intensity. M = mean fluorescent intensity of 41.3 (baseline). Image retrieved from http://biogps.org/#goto=genereport&id=1055 on November 14, 2018.

1 and 3 weigh 27 kD and 30 kD, respectively. Isoform 1 is considered to be the canonical form and is associated with TIP30's proapoptotic and antiangiogenic properties (Shtivelman, 1997). Isoform 3 was isolated as a binding cofactor of Tat in pull-down assays (Xiao et al., 1998). Isoform 2, 14.9 kD, referred to as TC3 or alternatively spliced product of CC3 (Whitman et al., 2000), is missing amino acids 134-242 [according to the National Center for Biotechnology Information database (NCBI)] (Greer et al., 2009, Shtivelman, 1997). Although this study did not focus on isoform 2, TC3 is reported to have an antiapoptotic effect and protect cells from apoptosis. This isoform is also reported to be highly unstable and susceptible to degradation (Whitman et al., 2000). TIP30 is mutated or lost in a vast majority of human cancers including hepatocellular (Ito et al., 2003), breast (Zhao et al., 2007), colorectal (Chen et al., 2010), lung (Tong et al., 2009), and brain (Hu et al., 2016). Loss of TIP30 has also been associated with EMT and enhanced invasiveness of both hepatocellular carcinoma (HCC) and pancreatic cancer cells (Zhu et al., 2015; Ouyang et al., 2013). Furthermore, TIP30 loss was associated with lymph node metastasis and poor survival outcome in PDAC patients (Guo et al., 2014). TIP30 loss was also correlated with lymph node metastasis in a lung cancer study (Tong et al., 2009).

1.3.2 TIP30 Functions

TIP30 is most closely related to the enzymatic family of short-chain dehydrogenases/reductases or SDRs (Baker, 1999). Oxioreductases catalyze oxidation-reduction reactions and are commonly dependent on nicotinamide adenine dinucleotide phosphate (NAD(H) or NADP(H)) coenzymes (Kallberg et al.,

2002). Indeed, NADPH is the preferred cofactor for TIP30. However, X-ray crystallography studies have failed to identify substrate-binding or associated enzyme activity (Omari et al., 2005). TIP30 shares the greatest sequence identity with the *E. Coli* SDR UDP galactose-4 epimerase and has the common Tyr143-Lys147Ser132 motif found in SDR catalytic domains (Baker, 1999). However, unlike SDRs, the dimer interface does not involve typical packing of two pairs of helices. Consequently, the catalytic tyrosine is not positioned appropriately for catalysis (Omari et al., 2005). SDRs are typically active only as dimers or heterodimers (Jornvall et al., 1995) and have identified substrates. However, TIP30 is reported to interact with other proteins, including importin-β2 to inhibit nuclear import and ACSL4 to mediate endosomal trafficking. TIP30 also interacts with the estrogen receptor alpha-interacting coactivator CIA to repress c-Myc transcription (Jiang et al., 2004).

In the STRING consortium and database for protein interactomes (Szklarczyk et al., 2015), TIP30 interactors are mostly NAD(P)H dehydrogenases, synthetases, including ATP synthase, and involve mitochondrial proteins (**Figure 5**). The TIP30 interactors that are labeled as “known” in **Figure 5** were identified in curated databases or were experimentally determined (Szklarczyk et al., 2015).Zhang et al. (2011), report that TIP30 forms a complex with ACSL4, endophilin B1, and Rab5a that is essential for receptor-mediated endocytosis and helps to regulate EGFR signaling and degradation. Endophilin B1 maintains mitochondrial membrane compartmentalization and architecture (Karbowski et al., 2004). The mitochondria are not only the powerhouse of the cell, but upon

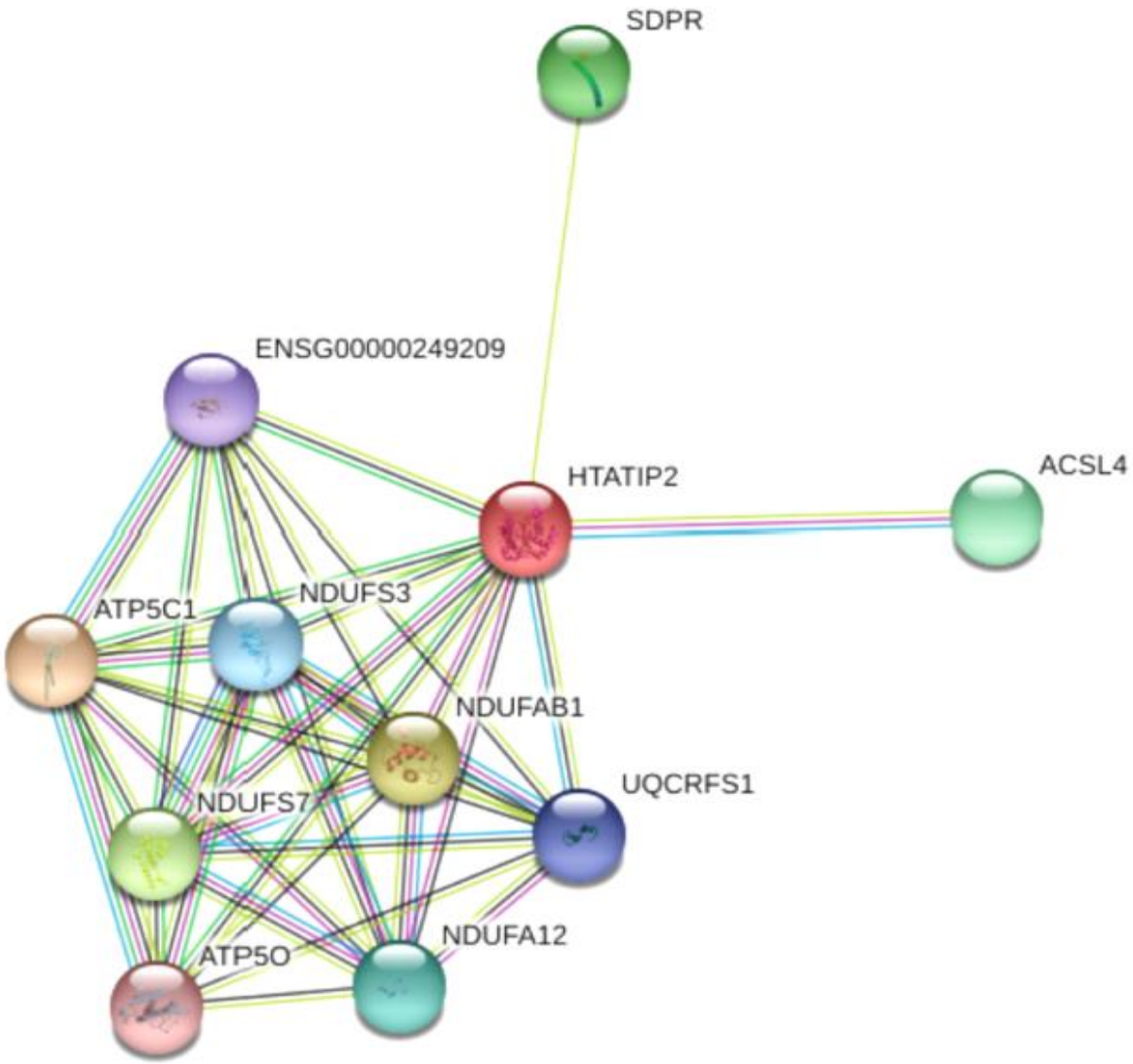
SDPR
ENSG00000249209
HTATIP2
ACSL4
ATP5C1
NDUFS3
NDUFAB1
UQCRFS1
NDUFS7
NDUFA12
ATP5O

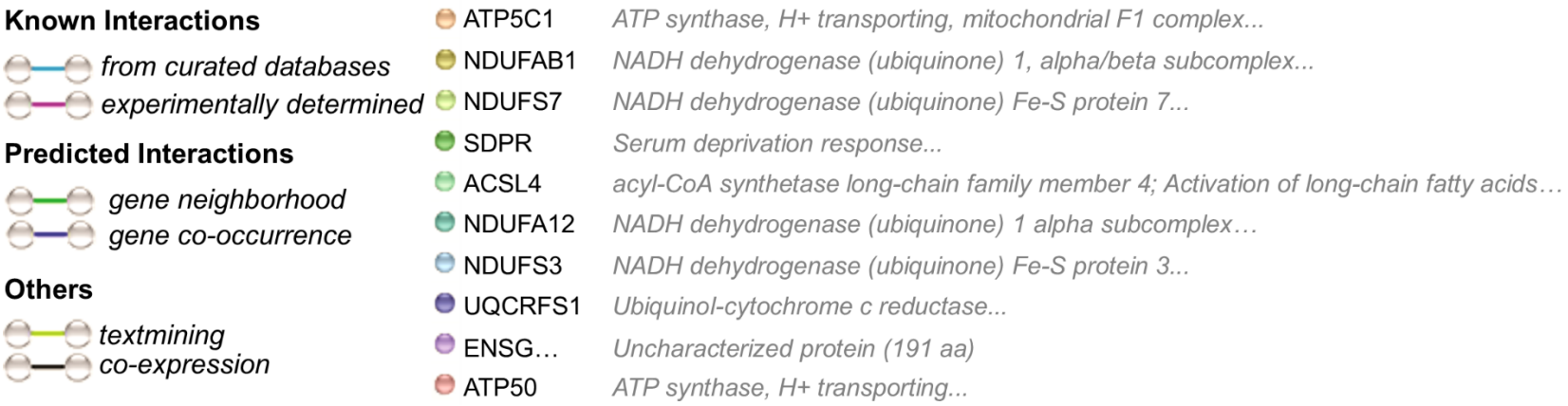

Figure 5. Gene and protein interaction network for TIP30

HTATIP2 is the query node for TIP30 in the Search Tool for the Retrieval of Interacting Genes/Proteins (STRING) database (Szklarczyk et al., 2015). Nodes surrounding HTATIP2 are the first shell of interactors. Empty nodes are those proteins with unknown 3D structures. Image retrieved from STRING v11, https://string-db.org/ on July 7, 2018.

membrane permeabilization, this organelle is responsible for reported TIP30-mediated release of proapoptotic factors such as cytochrome c and second mitochondria-derived activator of caspases/direct inhibitor of apoptosis-binding protein (Smac/DIABLO) (Shi et al., 2008). Mitochondrial-associated proteins Bax and Bcl-2 are also involved in cell death response and were found to work in concert with TIP30 to induce apoptosis (Shi et al., 2008). Given these multiple roles for TIP30 in literature, the overarching theme of its activity is that of a redox sensor. As such, TIP30 would be involved in processes that affect gene transcription in addition to some of the other properties identified in the literature such as coactivation, apoptosis and nuclear import as described below.

1.3.2.1 Coactivation

Coactivators play an important role in regulating biological processes by regulating gene expression (Puigserver and Spiegelman, 2003; Spiegelman and Heinrich, 2004). In a protein affinity chromatography assay, TIP30 was one of the two proteins identified to bind the activation domain of tat, a nuclear regulatory protein encoded by HIV-1 that enhances HIV-1 transcription (Xiao et al., 1998; reviewed in Jones and Peterlin, 1994). The role of tat in HIV-1 transcription is to increase the efficiency of RNA polymerase II transcription elongation (Jones and Peterlin, 1994). As mentioned previously, neither oxioreductase nor kinase activity has been confirmed for TIP30. There have been reports of serine and threonine kinase activity, autophosphorylation, as well as direct phosphorylation of the serine and threonine residues on the C-terminal domain of RNA polymerase II (Xiao et al., 2000); however, an ATP-binding site was not found in TIP30 (Omari et al.,

2005). One speculation for the discrepancy has been potential kinase contamination from the baculovirus expression system preparations used in the original studies (Omari et al., 2005). Xiao et al. (2000) also reported that TIP30 did not behave as a global transcription factor. TIP30 depletion did not affect basal transcription or Gal-VP16-activated transcription (Xiao et al., 1998). Gal-VP16 is a class of transcriptional activators involved in activating yeast, plant, insect and mammalian cell transcription (reviewed in Sadowski et al., 1988). With the lack of confirmed catalytic activity, classification of this protein as a coactivator may be more appropriate. Although TIP30 cannot act as a transcriptional regulator, it may still be involved in regulating transcription by interacting with other coactivators and/or acting as a sensor.

1.3.2.2 Apoptosis

TIP30's metastasis suppressor and proapoptotic functions were first identified by the lack of expression of TIP30 in a differential display of highly metastatic variant-small cell lung cancer (v-SCLC) compared to classic small-cell lung cancer cell lines. Reintroduction of TIP30 in v-SCLC cells sensitized cells to apoptosis both *in vitro* and *in vivo* and upregulated an apoptotic pathway that may have involved down-regulation of anti-apoptotic factor Bcl-2 (Shtivelman, 1997). In a separate study, TIP30 overexpression led to an increase in NIH 3T3 and v-SCLC cell death as detected in a trypan blue exclusion assay and the upregulation of an apoptotic gene signature (Xiao et al., 2000). Overexpression of TIP30 in v-SCLC cells led to increased levels of the apoptotic genes Bad and Siva (Xiao et al., 2000). Shi et al. (2008), found that TIP30 triggers the release of cytochrome c from the

mitochondrial intermembrane space into the cytosol and the release of second mitochondria-derived activator of caspases/direct inhibitor of apoptosis-binding protein (Smac/DIABLO). Cytochrome c and Smac/DIABLO are two well-known precursors and initiators of a mitochondrial apoptotic pathway, leading to cell death (Shi et al., 2008; Arnoult et al., 2002; Martinez-Ruiz et al., 2008). TIP30 regulated the translocation of Bax through a TIP30-P53-Bax signaling cascade ending with activation of Caspase-9 and -3 (Shi et al., 2008).

1.3.2.3 Nuclear Import

Another explanation for TIP30-mediated apoptosis is demonstrated through studies of its role in nuclear import. Inhibition of nuclear import by TIP30 induces cell death according to King and Shtivelman (2004). TIP30 is reported to bind importin betas and inhibit the nuclear import *in vitro* and *in vivo* of classic nuclear localization signal- (NLS) or M9-tagged proteins (King and Shtivelman, 2004). The addition of purified TIP30 cytosol [transport buffer] to permeabilized HeLa cervical cancer cells decreased nuclear import rates in *in vitro* nuclear import assays; while the addition of recombinant protein from TIP30 (G28V) and (G31A) mutants decreased cell-binding interactions with transportin (importin β2) and the nuclear pore complex (King and Shtivelman, 2004). These TIP30-mutant conditions further led to a decrease in nuclear import inhibition (King and Shtivelman, 2004). The physiological implications of these findings still need to be elucidated.

1.3.3 TIP30 in Cancer, Metastasis, and PDAC

The seminal work on TIP30 in cells derived from small cell lung cancer (SCLC) as well as in other tumor cells *in vitro* support its anti-metastatic properties

(Shtivelman, 1997, Xiao et al., 2000). In 1997, and under the name CC3, *TIP30* gene expression was absent in highly metastatic variant-SCLC (v-SCLC) cell lines; the reintroduction of CC3 suppressed metastasis *in vivo* in a tail vein assay (Shtivelman, 1997). Similar results were obtained with highly metastatic hepatocellular carcinoma (HCC) cell line LM3 after intratumoral injection of TIP30-overexpressing adenovirus (Zhao et al., 2008). The majority of the literature supports TIP30 as a metastasis suppressor and tumor suppressor. However, most of these studies are cell-line based (Ito et al., 2003; Zhao et al., 2007; Chen et al., 2010; Tong et al., 2009). There is also literature that reports TIP30 overexpression in Her-2/neu-positive breast cancer tissues and in metastatic prostate cancer (Zhang et al., 2005; Zhang et al., 2008). The impact of both TIP30 loss and overexpression in cancer is not understood and will need further elucidation.

GEMMs with full-body *Tip30* loss develop hepatocellular carcinoma (Ito, et al., 2003) or lung adenocarcinoma (Li, et al., 2013) with long latency. TIP30 loss has also been shown to enhance cytoplasmic and nuclear epidermal growth factor receptor (EGFR) signaling and to promote human lung cancer tumorigenesis (Li et al., 2013). In HeLa cervical cancer cells, TIP30 silencing enhanced mitochondrial respiration and glycolysis (Chen and Shtivelman, 2010). TIP30 loss is relevant across multiple cancer subtypes and may also play a role in the metabolic regulation of various cancer cells. Given the contrasting results obtained with cell line based studies, a meta-analysis was performed by Xu et al. (2016) to determine the prognostic value of TIP30. Analysis of 1705 cancer patients with high versus low TIP30 expression determined that patients with high TIP30 levels

showed favorable overall/recurrence-free survival whereas lack of TIP30 expression was associated with lymph node and tumor metastasis (Xu et al., 2016).

The relationship between TIP30 expression and cancer is a subject of intense investigation. Ouyang et al. (2013), reported that TIP30 is a direct target of microRNA (miR)-10b, one of the most frequently upregulated microRNAs (miRs) in PDAC (Bloomston et al., 2007; Preis et al., 2011). In these studies, pancreatic cancer cells that overexpressed miR-10b had decreased TIP30 mRNA levels. These levels were reversed when the 3'UTR of TIP30 was mutated and unable to be recognized by miR-10b (Ouyang et al., 2013). Pancreatic cancer cells with decreased TIP30 levels by miR-10b overexpression or by direct silencing of TIP30 mRNA showed an increase in EGF- and TGF-β-mediated invasion as well as an increase in epithelial-mesenchymal transition (EMT)-associated gene expression levels (Ouyang et al., 2013). TIP30 is also involved in EGFR endocytic trafficking and degradation by associating with Rab5a when complexed with endophilin B1 and ACSL4 to modulate EGFR endocytosis and signaling (Zhang et al., 2011; Li et al., 2013). While Rab5 is a GTPase involved in the fusion of the vesicles with the early endosome (Gorvel et al., 1991), endophilin B1 maintains mitochondrial morphology and organization in addition to its involvement in receptor trafficking (Karbowski et al., 2004). One study points to the association between decreased TIP30 protein expression and increased lymph node metastasis and poor prognosis in pancreatic cancer patients (Guo et al., 2014). It is therefore not fully understood if and how TIP30 loss exerts an essential role in PDAC pathobiology.

To summarize, TIP30 is a putative metastasis suppressor, whose current function is not yet fully understood. Although classified as an oxioreductase, it does not act as an oxioreductase or as a kinase, but has been reported to bind proteins that enhance transcription. What is clear, is that TIP30 alterations are prominent in multiple different cancers including PDAC, and loss of TIP30 has been reported to associate with poor survival outcome. Further research is needed in this regard, and for the role of TIP30 loss in PDAC specifically, due to the connection made between miR-10b overexpression in PDAC and miR-10b-TIP30 targeting in human pancreatic cancer cells (Ouyang et al., 2013). To this end, we generated a novel genetically engineered mouse model to study the role of *Tip30* loss in the autochthonous model of oncogenic *Kras*-driven PDAC. We hypothesized that *Tip30* loss accelerates pancreatic cancer progression and metastasis.

CHAPTER 2. MATERIALS AND METHODS

2.1 Mice

B6.FVB-Tg(Ipf1-Cre)1Tuv (*Pdx1-Cre*) mice were obtained from the National Cancer Institute (NCI) Repository, Stock No. 01XL5 (mouse ID's TP427 or greater). Mouse ID's preceding TP427 received the *Pdx1-Cre* transgene from The Jackson Laboratory (B6.FVB-Tg(Pdx1-cre)6Tuv/J, Stock No. 014647. B6.129S4/SvJae-Kras^{Tm4Tyj}/J (*LSL-Kras$^{G12D/+}$*) and C.129P2(B6)-Htatip2^{tm1Hx}/J (*Tip30$^{-/-}$*) were purchased from The Jackson Laboratory, Stock No. 008179 and 018767, respectively, and have been previously described (Jackson et al., 2001; Hingorani et al, 2003; Ito et al., 2003). A mouse ID "TP" ear tag and mouse identification system (National Band & Tag, Newport, KY, and Style No. 1005-1P) was used to identify each mouse subject. To expand the *Tip30* mouse colony ("TP"), founders were crossed with *Pdx1-Cre* from an existing colony in our laboratory from the background Stock Rb1<tm2Brn>/J. Mice used for these experiments were therefore of mixed background, with more than four identified strains, and *LSL-Kras$^{G12D/+}$;Tip30$^{+/+}$;Pdx1-Cre* (K30$^{+/+}$C), and *Tip30*-deficient (K30$^{+/-}$C or K30$^{-/-}$C) and wild-type controls were generated internally and rigorous genotyping was performed. Introduction of only one *Pdx1-Cre* and one *LSL-Kras^{G12D}* allele was controlled by breeding with parents that were positive for only one mutant allele between the two parents. Brother-sister mating was employed. Mice were born with near-expected Mendelian genetic ratios, but ratios varied between litters. For example, in one litter the *Tip30* transgene was distributed as follows: 0 *Tip30$^{-/-}$*; 6 *Tip30$^{+/-}$*; and 3 *Tip30$^{+/+}$* (for a litter whose parents were K30$^{+/-}$

and $30^{+/-}$C); and in another litter from a different pair of breeders, but with the same genotype: 2 *Tip30*$^{-/-}$; 5 *Tip30*$^{+/-}$; and 1 *Tip30*$^{+/+}$. *LSL-Kras*^{G12D} was passed on at a rate of roughly 50%, as was the *Pdx1-Cre* transgene in both of these litters. Three mice from both litters received both a *LSL-Kras*^{G12D} and *Pdx1-Cre* transgene. In a breeding cross of $30^{+/-}$ and $30^{-/-}$ the *Tip30* transgene was distributed as follows: 4 *Tip30*$^{-/-}$; 5 *Tip30*$^{+/-}$; and 0 *Tip30*$^{+/+}$. As reported previously, the *Tip30* gene was not essential for mouse development (Ito et al., 2003). Animal experiments were approved by the Institutional Animal Care and Use Committee (IACUC) at Indiana University School of Medicine, Indianapolis, IN, and were cared for by Laboratory Animal Resource Center (LARC) per the IACUC protocol No. 10785 and 11344.

2.2 Tail DNA Extraction

Tail snips were taken when pups were two weeks of age, in accordance with IACUC and LARC standards. Tails snips, measuring approximately three to four millimeters in length, were digested in 150 microliters of tail lysis buffer (50 mM NaOH + 2 µM EDTA) for 45 minutes at 95°C using a Perkin Elmer Thermal Cycler. The reaction was stopped using a 10 microliter neutralization solution of 1 mM tris(hydroxymethyl)aminomethane (Tris) in ultrapure laboratory grade double deionized water (ddH2O), pH 8.2. One microliter of tail DNA was used in genotyping reactions. These steps amounted to roughly 200-300 ng of DNA. Tail DNA was stored at -20°C.

2.3 Tissue and Cell Line DNA Extraction

Proteinase K and Phenol DNA extraction method was used to extract DNA from tissues and cell lines. Phenol/chloroform/isoamyl alcohol, pH 6.7 (Fisher

BP17521) and 0.3 mL digestion buffer for cell lines per well (6-well plate, in duplicate) or 0.5 mL tissue dust was used. Digestion Buffer was composed of 100 mM NaCl, 10 mM Tris [pH 8.0], 25 mM EDTA [pH 8.0], 0.5% SDS, and 0.1 mg/mL proteinase K (Roche #03115836001). Digests were incubated at 50°C for 12-18 hours, rotating to activate Proteinase K. DNA was precipitated with 1/10 volume of 3 M sodium acetate (pH 5.2) ammonium acetate and 2 volumes of 100% ethanol, then washed with 70% ethanol. DNA pellets were dissolved in ultrapure, deionized, nuclease-free H2O (Fisher Scientific BP2819-1). For DNA sequencing, a DNA and RNA purification kit was used to purify DNA (Qiagen 80204). For whole genome sequencing, DNA was extracted using the DNA purification kit (Qiagen 80204) from cell lines and outsourced to Novogene (Sacramento, CA) for library preparation, sequencing, and alignment to the mm10 mouse reference genome. Sequencing results were viewed in the Integrative Genomics Viewer (retrieved from https://software.broadinstitute.org/software/igv/ and accessed June 13, 2018. Dr. Francis Enane, a member of our laboratory with expertise in genomic analysis, assisted with the interpretation of the whole genome sequencing data.

2.4 Genotyping

For genotyping, genomic DNA isolated from mouse tails, pancreas, lung, or liver tissues or from murine cell lines isolated from primary tissue was subjected to polymerase chain reaction (PCR) using recommended sequence-specific oligonucleotide primers and agarose gel electrophoresis. HotStarTaq polymerase (Qiagen 203607), PCR (dNTPs) Nucleotide Mix (Roche 04638956001), Coral Red 10X PCR buffer, 15 mM $MgCl_2$ (Qiagen N1032568), 25 mM $MgCl_2$ (Qiagen

1018999), and ultrapure laboratory grade deionized water (ddH2O) from a Milli-Q IQ 7000 water purification system (EMD Millipore) was used as listed in Section 2.27. Oligomers used and thermocycler conditions were performed as instructed by The Jackson Laboratory, and are listed in Section 2.28. Oligomers were reconstituted to 100 µM stock solutions and used at a final concentration of 0.5µM, unless otherwise indicated. PCR products were separated over 1.5%-3% agarose (Lonza 50004)/1X TAE gel. A 1% ethidium bromide (Fisher BP1302-10) solution was added to the gel at a ratio of 1:15,000 during gel preparation for the purposes of DNA fragment detection. DNA fragments (visualized as bands) were imaged using a Bio-Rad ChemiDoc MP Imaging System. Genotyping was also outsourced to TransnetYX (Cordova, TN, USA) for genomic DNA from tail and pancreas to confirm in-house genotyping. Methods sections 2.26-2.28 describe PCR primers, reactions, and cycling conditions for the *Kras*^{G12D} transgene (Kras), “Cre” of the *Pdx1-Cre* transgene (PDX), the *Tip30* transgene: *Tip30* wild-type (WT) versus *Tip30* mutant (MT), and the EGFP of the tdTomato-EGFP transgene. *Pdx1-Cre* genotyping was confirmed using primers that spanned both *Pdx1* and *Cre* regions in one reaction (see Methods 2.26, “Pdx1-Cre (NCI)”. Genotyping of additional transgenes commonly used in GEMM research of PDAC (Westphalen and Olive, 2012) and previously used by the Korc Laboratory (*Trp53*^{R172H} or mp53 (Hingorani et al, 2005), Rb (Carrière et al., 2011), miR-155 (The Jackson Laboratory 007745), Bmal (The Jackson Laboratory 007668), miR-21 (Hatley et al., 2010), Smad7 (Snider et al., 2010), Ink4a (Aguirre et al., 2003), Agr2 (Norris et al., 2013; Park et al., 2009), human HER3, Smad4L/L (Bardeesy et al., 2006b), p16 (Bardeesy et

al., 2006a), and Syndecan 4 mouse models as well as genotyping for other transgenes related to research studies by the developers of the *Tip30*-deficient mouse model [MMTV-Neu (Zhang et al., 2010), NCOA5 (S. Gao et al., 2013), and IL-6 (S. Gao et al., 2013) mouse models] was also completed to exclude contamination and the presence of other genes than what is reported in the "TP30" mouse colony generated for these studies (**Appendix A**).

2.4.1 The Kras G12D Conditional PCR Method

The PCR reaction for Kras G12D Conditional PCR can be used to confirm successful recombination of the *LSL-Kras*^{G12D} transgene with Cre recombinase (Jacks, 2017). This protocol, published by the The Jacks Lab (Jacks, 2017) and utilized in Hingorani et al. (2003), results in the detection of three bands: an unrecombined LSL cassette (a 500-bp PCR product also referred to as "Unrecombined 2lox"), the wild-type *Kras* sequence (a 622-bp PCR product), and a third 650 base pair product confirming the presence of a remaining *lox*P site and the *Kras*^{G12D} mutation ("Recombined 1loxP" PCR product). For this assay, one primer recognizes the upstream region of the *Kras* sequence (LSL-FP1), a second primer anneals downstream of primer one and recognizes the first coding exon of *Kras* (LSL-RP2), and a third primer anneals to a portion of the LSL cassette (LSL-FP3). The positioning of primers LSL-FP1 and LSL-RP2 will result in a PCR product whose size reflects the presence or absence of the recombination event, through the insertion of a *lox*P site (roughly 34 bp) on the *Kras*^{G12D} sequence. A mouse with just a *LSL-Kras*^{G12D} transgene and no *Pdx1-Cre* will test positive for the unrecombined 2-*lox*P PCR product and the 622 bp wild-type *Kras* product, and

has both one copy of a wild-type allele in addition to one copy of a the *LSL-Kras*^{G12D} transgene. A *LSL-**K**ras*^{G12D}*;Pdx1-**C**re* (KC, Hingorani et al., 2003) mouse that has undergone successful recombination in the pancreas tissue will also be positive for the third PCR product, 1-*lox*P-*Kras*^{G12D} at around 650 bp (Hingorani et al., 2003). This recombination event will not be 100% efficient in pancreatic tissues, however, due to the stochastic expression of *Pdx1* (Hingorani et al., 2003). If recombination was 100%, then one would also observe the complete loss of the 500 bp unrecombined 2-*Lox*P PCR product.

2.5 Tissue Preparation

Necropsies were performed and tissues were harvested in accordance to our IACUC protocol. First, a small piece of pancreas tissue was quickly excised and snap frozen in liquid nitrogen after quick gross examination to prevent autolysis. Following removal, pancreas tissue is reported to undergo rapid autolysis (Hruban et al., 2006). *In situ* and *ex vivo* images of tissues were taken with a Sony DSLR-A390 camera. In addition to pancreas tissue, a sample of the liver, lung and muscle were snap frozen into separate cryovials, stored at -80°C, and used for protein, mRNA, and DNA analysis. A sample from pancreas, lung, and liver tissues were also excised and establish cell lines as indicated (see Methods 2.13, 2.14). The remaining tissue from these organs, as well as whole kidney, spleen, and muscle were placed in 10% neutral buffered formalin (VWR International BDH0502) for paraffin embedding and histological analysis (see Methods 2.11). A second sampling of the tail was taken at sacrifice to confirm

genotyping. Fluorescent tissues from the K30Ctd mouse model were frozen in optimal cutting temperature (OCT) compound without fixation.

2.6 Tissue Pulverization for Protein, mRNA, or DNA

Snap frozen pancreata or tissues were pulverized using liquid nitrogen-cooled tissue guns in RNAase-free conditions (Ambion AM9780) to a fine dust substance. Tissue dust was immediately transferred into original cryovials on dry ice and stored at -80°C.

2.7 Extraction of mRNA from Tissues

Pancreas RNA was extracted using an adapted guanidine isothiocyanate method (Chang, et al., 1990; Han et al, 1987). In brief, pulverized tissue dust was added to pre-cooled RNA Extraction Buffer with guanidine thiocyanate (Sigma #50981), prepared on the day of extraction. Sodium acetate pH 4.0, saturated phenol, pH 4.5 (Amresco #0981), and chloroform was added sequentially for phase separation, and RNA was precipitated overnight in isopropanol at a 1:1 volume ratio at -20°C. RNA pellets were dissolved in nuclease-free H2O (Fisher Scientific BP2819-1).

2.8 Extraction of mRNA from Cell Lines

mRNA was extracted from cell lines using 0.5 mL TRIzol (Invitrogen 15596018) per six-well, in duplicate after washing cells two times in ice-cold RNAse free 1X phosphate-buffered saline (PBS). Chloroform extraction was used, followed by an overnight precipitation in 100% isopropanol at 4°C, then 75% ethanol before centrifugation and resuspension in nuclease-free H2O (Fisher Scientific BP2819-1). An Ultraviolet-visible (UV-Vis) spectrophotometer

(NanoDrop 2000, Thermo Fisher Scientific) was used to measure sample absorbances and determine final mRNA concentrations.

2.9 Conversion of mRNA to cDNA

For the synthesis of complementary DNA (cDNA), 1000 ng of mRNA was converted to cDNA using a High-Capacity cDNA Reverse Transcription Kit (Applied Biosystems 4387406) and its protocol. For microRNA (miR) analysis, 10 ng of mRNA was converted to cDNA using the Applied Biosystems TaqMan MicroRNA Reverse Transcription Kit (Thermo Fisher Scientific 4366596) and its protocol.

2.10 Quantitative Reverse Transcription-Polymerase Chain Reaction

Complementary DNA (cDNA) was prepared for real-time quantitative reverse transcription-polymerase chain reaction (qRT-PCR) using 1X TaqMan Fast Advanced Master Mix (Applied Biosystems 4444557) and TaqMan Probes or a multiplex SYBR Green quantitative PCA assay with Power SYBR PCR Master Mix (Applied Biosystems 4367659). Applied Biosystems (AB) TaqMan probes (Thermo Fisher Scientific TaqMan Assays, Catalog No. 4331182) were common to: exon 2-3 of Htatip2, murine Tip30 (AB No. Mm00457476_m1); murine Rps6 (AB No. Mm02342456); murine Egfr (AB No. Mm00433023_m1); or murine β-actin (AB No. MM0607939_s1). Human miR-10b was assessed using the hsa-miR-10b primer/probe set (Thermo Fisher Scientific Assay ID 002218) and the internal control RNU6B (Thermo Fisher Scientific Assay ID 001093). SYBR Green qPCR and SYBR Green Master Mix (Applied Biosystems 4444557) was used to confirm *Tip30* mRNA expression levels using Tip30 exon 6. Forward (“Tip30 Exon 6-a”):

5’GTCCTACTGTGTGACAGGCAAG, Reverse (“Tip30 Exon 6-b”): 5’ACTCAGCTACATGCAGCCCA. Rps6 was used as the internal gene expression control. SYBR Green qPCR was also used to detect c-Myc mRNA levels (Forward: GCCCAGTGAGGATATCTGGA, Reverse: ATCGCAGATGAAGCTCTGGT). c-Myc levels were normalized to beta-actin (Forward: ATCATGTTTGAGACCTCCAACACC, Reverse: GGATCTTCATGAGGTAGTCTGCA). Real-time qRT-PCR was run on the Applied Biosystems ViiA7, and cycle threshold (CT) values were obtained after 40 cycles. All qRT-PCR experiments were run in duplicate per run, and pancreas tissues or cells lines from at least three different mice per group were analyzed. The relative quantity of gene expression values was calculated using the 2(-ΔΔ(C)T) method (Livak and Schmittgen, 2001). Fold increases were calculated relative to control or wild-type after normalization to an internal control. Statistical analysis was performed by using a Student’s two-tailed t-test when two groups were compared (in excel), or one-way analysis of variance (ANOVA) if comparing more than two groups, with a Tukey post-hoc test (SigmaPlot 12.5). For experiments using cell lines, at least two cell lines were from K30C mice, and at least one cell line was derived from K30Ctd mice, for *Tip30*-wild-type, and both *Tip30*-deficient groups (*Tip30*$^{+/-}$, *Tip30*$^{-/-}$).

2.11 Histological Analysis and Immunohistochemistry-Immunofluorescence

Mice were sacrificed at the times indicated or were monitored until moribund. Tissues were fixed in 10% neutral buffered formalin (VWR International

BDH0502) overnight, before transfer to 70% ethanol. Tissues were embedded in paraffin on the KD BM II Tissue Embedding Station after processing using a Microm STP420 Tissue Processor (Thermo Fisher Scientific). Hydrated tissue blocks were faced, then tissues were sectioned at 4-5 µm thick using a Thermo Fisher Scientific HM 3555 microtome. Roughly 4-5 consecutive sections were obtained per mouse tissue to use for analysis. Slides with tissue sections were baked for 30 mins at 65°C, in a Robbins Scientific 310 Hybridization Incubator, before tissue deparaffinization and rehydration. Hematoxylin (Sigma GH5232) and eosin (Acros organics #20193000) were used to perform hematoxylin and eosin (H&E) staining. Antigen retrieval and unmasking were performed using a citrate-based, pH 6 solution (Vector Laboratories H-3300) for immunohistochemistry (IHC), IHC immunofluorescence (IHC-IF), and Alcian Blue (Newcomer Supply 1003A) staining. Tissues were passed through a series of dehydration steps, mounting (Fisher SP15-500), and cover-slipping (Fisherbrand 12-544G). Tissues were probed with CK-19 (Troma III, Developmental Studies Hybridoma Bank, 1:10) overnight at 4°C, in a humidified slide chamber after 3% hydrogen peroxidase (Fisher H325) exposure and wash. Slides were then incubated in Biotinylated Rabbit anti-Rat IgG (Vector Laboratories BA-4001) 1:400 in 5% normal goat serum in PBS (Vector Laboratories S1000). For IHC, the avidin-biotin complex (ABC) technique was performed using the Vectastain ABC HRP kit from Vector Laboratories. 3,3'-Diaminobenzidine (DAB) exposure was performed for the same duration of time for all samples. For IHC-IF detection of amylase, insulin, and glucagon, antigen-unmasked tissue sections were incubated in anti-Pancreatic

rabbit amylase antibody 1:400 (Abcam ab21156), rabbit anti-Insulin antibody (ab63820) 1:600, and mouse anti-Glucagon antibody (ab10988) 1:400 overnight at 4°C, in a humidified slide chamber. Normal goat serum was used as the diluent, except for in mouse on mouse detection in which case, the M.O.M. kit was used (Vector Laboratories BMK-2202). The M.O.M kit included protein concentrate, Mouse Ig Blocking Reagent, and Biotinylated anti-Mouse IgG. Alpha-SMA (mouse origin, Sigma A2547, 1:500) was detected by IHC with the M.O.M. kit. Goat anti-Rabbit Alexa Fluor 488 (Thermo Fisher Scientific A11034) or Goat anti-Mouse Alexa Fluor 555 (Invitrogen A21429) were the secondary antibodies used in IHC-IF primary detection. Slides were mounted (Invitrogen P36931 Prolong Gold mounting medium with DAPI), coverslipped, (Fisherbrand 12-544G), and allowed to dry overnight before imaging.

Tissues were imaged using an Olympus BX60 Microscope with Lumen 200 Fluorescence Illumination System (Prior Scientific) and Image Pro Plus 7.0 software) at low (4X objective lens) and high (20X objective lens) power. For IHC-amylase, glucagon, and insulin imaging of pancreas tissues, images were captured using “Mono”, and for CK-19 and α-SMA images were captured using “RGB” Olympus BX60 Microscope/Image Pro Plus 7.0 settings. For the scale bars provided in images of this report and taken using the Olympus BX60 microscope, a ruler in micrometers (μm) was imaged at low and higher power (“scale bar” image specific to each magnification). These images were opened alongside the images of tissues for each corresponding magnification. Both images were formatted to “lock aspect ratio” in Microsoft Publisher software (which was used to create

figures), then scaled down (using the same conditions for both images). A line was drawn on the imaged ruler in the “scale bar” image spanning 100 μm in Microsoft Publisher. For “scale bar” images and imaged tissue that were the same size only (both in power and in Microsoft Publisher) the 100 μm scale bar was transferred to the right, bottommost corner of the tissue image. This was done for both low and high power images provided in this report. This method was also used to create scale bars for images of visceral tissues and both *in situ* or *ex vivo*, but only if the image was taken with a ruler at the time of imaging.

A Leica DM5000B microscope with Leica DFC 7000T camera and LASX software was used to image H&E sections of pulmonary tissues and liver in this report at low (2.5X objective lens) and high (20X objective lens) power. An image with an attached scale bar was taken for at least one field at each power. The scale bars provided by the LASX software for a 2.5X objective lens image was 750 μm in length, and for the 20X objective lens image was 100 μm in length; therefore for presentation of tissue at both low and high power, a scale bar that spanned 100 μm was drawn and saved with the image for both images for consistency. Scale bars presented in this report are an accurate representation of the scale bars provided by the software. This microscope and camera was also used for the representative fields in **Figure 15A-D** and **Figure 16**.

2.12 Lesion Scoring

Pancreas and organ pathology was determined by the board certified pathologist, Dr. George Sandusky. We first assessed an H&E stained section of the entire tissue for the pancreata of 21 $K30^{+/+}C$, 20 $K30^{+/-}C$, 24 $K30^{-/-}C$ mice. In

addition, if additional sections were available, including CK-19 sections, all images available at higher power were compiled to determine the extent of PDAC (whether it was in the beginning stages or full blown) and for an overall scoring of PDAC precursor lesions. PDAC was assessed with the visualization of a glandular pattern in pancreas tissue, ductal architecture, and cellular and nuclear atypia (Hezel et al., 2006). The Hruban et al. (2006) consensus report for evaluating genetically engineered mouse models for PDAC was referenced, and statistically significant). An increase in pERK1/2 was also observed in miR-10b-overexpressing AsPC-1 cells after 10-30 minutes of EGF treatment (**Figure 41**).of this report. An H&E section for seven to twelve lung, kidney, and spleen tissues was also examined by histopathological analysis.

2.13 Isolation of Primary and Metastatic Pancreatic Cancer Cells from Tissues

Fresh tissue biopsies were carefully minced (Exelint International, Size 10; 29550), washed in five passes of 1% antibiotic-antimycotic (Life Technologies 15240-62) and digested with 2 mg/mL Type IV Collagenase (Worthington LS004188) in plain HBSS, warmed to 37°C for 30-45 minutes. Cell suspensions were passed through a 70-micron mesh cell strainer (Corning 352350) and washed free of collagenase before plating. Pancreatic tumor, lung, and liver tissue biopsies were collected and processed in separate dishes; mincing scalpels were changed between tissues.

2.14 Cell Lines and Tissue Culture

Single cell clones from three $K30^{+/+}C$, three $K30^{+/-}C$, and two $K30^{-/-}C$ murine pancreatic cancer cell lines (mPCCs) isolated for these studies (see Methods 2.13) were authenticated by IDEXX BioResearch (Columbia, MO, USA) and underwent MHV, MNV, MPV, MVM, *Mycoplasma pulmonis*, *Mycoplasma sp*., PVM and Sendai testing, genetic evaluation for an Interspecies Contamination Test and mouse nine-marker STR profiling. All testing came back negative, confirming that original cell lines established in the lab were mycoplasma and pathogen free, and were indeed mouse (**Appendix B**). AsPC-1 human pancreatic cancer cells (hPCCs) were obtained from the ATCC the American Type Culture Collection (Manassas, VA, USA). Samantha Deitz McElyea, a member of our lab, with expertise in establishing GFP-positive-microRNA (miR)-10b overexpressing-stably transfected human pancreatic cancer cell lines generated at least three stable AsPC-1-miR-10b-overexpressing (AsPC-1-miR-10b-OX-GFP) and three AsPC-1-vector-control (AsPC-1-GFP-C) cell lines for the purposes of these studies. The materials and methods for miR-10b-overexpressing human PCCs has been reported (Ouyang et al., 2013). Briefly, 293T-based retroviral packaging Phoenix cells (Life Technologies) were transfected with either a MDH1-PGK-GFP microRNA-10b retroviral construct or an empty MDH1-PGK-GFP construct. Viruses were then harvested and AsPC-1 hPCCs were transduced. After 48 hours, GFP positive cells were isolated by flow cytometry.

mPCCs and AsPC-1 cells were grown in complete RPMI (Hyclone SH30027.01) culture medium supplemented with 5% heat-inactivated and filtered

fetal bovine serum (FBS) (Tissue Culture Biologicals 101H1) and 1% Penicillin-Streptomycin (P/S, Hyclone SV30010) in a HEPA filtered Thermo Scientific Forma Series II 3110 Water-Jacketed CO_2 Incubator at 37°C and 5% CO_2. Cell passage and plating for experiments were conducted in a biological safety cabinet with aseptic technique. Trypsin 0.05% (Hyclone SH30236) was used to dissociate cells in culture for passage. HBSS (Lonza 10-S43F) was used to wash cells before trypsinization and for experiments in culture. Trypan Blue Solution, 0.4% (Thermo Fisher Scientific 15250061) was used during cell counting to assess cell viability. Cell populations plated for experiment had greater than 80% viability. The majority of the experiments were performed using cell lines that were passaged less than 20 passages. All tissue culture was performed under aseptic conditions. Cells were routinely checked for mycoplasma (Lonza LT07). Cells in these experiments were free from mycoplasma contamination. Cells were frozen in 10% DMSO (Fisher Scientific NC0945470)/FBS and stored in -80°C and/or liquid nitrogen. Cell lines were imaged using brightfield settings with DMI 3000B Microscope and Leica DFC310 FX camera with Las V4.5 software. GFP images were captured using a GFP D5, YFP filter and the same settings in figures depicted. For experiments using murine cell lines, at least two cell lines were from K30C mice, and at least one cell line was derived from K30Ctd mice, for each *Tip30* wild-type, heterozygous, and homozygous-loss group.

2.15 GFP/RFP Visualization and Fluorescent Imaging of K30Ctd GEMM

Excitation of EGFP and Tomato were captured in a light box illuminated by fiber optic lighting (Illumatool BLS; Lightools Research, Encinitas, CA, USA). This

system allowed us to detect and visualize live recombined and nonrecombined cells and whole tissues expressing EGFP and Tomato. Whole-body images with the visceral abdominal cavity exposed (epidermal and dermal levels removed) were taken immediately after sacrifice, and allowed *in situ* GFP visualization of pancreas tissues as well as micrometastatic seeding of pancreatic cancer cells to distant organs. Pancreas, spleen, liver in part or full, and lungs were isolated and imaged *ex vivo* in a petri dish after being washed in 1X sterile PBS, to confirm detection of micrometastatic seeding visualized by whole body imaging. GFP and Tomato were illuminated with two Illumatool excitation lamps. GFP fluorescence was captured with a 470 nm +/- 40 nm emission filter. Tomato was illuminated with the same lamps and captured with a 572 nm +/- 35nm filter. Peak excitation for tdTomato is 554 nm (Muzumdar et al., 2007). High-resolution images were captured directly using an Olympus DP70 camera (DSP Technologies, Inc., Santa Barbara, CA, USA) secured to the top of the light box. Image-Pro Plus 7.0 software was used to preview and capture the images at camera's normal resolution which is 0.003 inches/pixel. Adobe Photoshop was used to auto contrast the images. Adjustments to brightness and contrast are as indicated.

2.16 Overexpression of microRNA-10b in a Human AsPC-1 Pancreatic Cancer Cell Line

Materials and methods for creating microRNA (miR)-10b-overexpressing AsPC-1 cells were described previously in Methods 2.14 and reported in Ouyang et al. (2013). qRT-PCR was used to analyze both human miR-10b (Thermo Fisher Scientific Assay ID 002218) and the internal control RNU6B (Thermo Fisher

Scientific Assay ID 001093), in duplicate from three biological replicates of AsPC-1-miR-10b-OX-GFP and AsPC-1-GFP-C stably transfected cell lines. CT values were obtained and normalized to RNU6B per experiment. AsPC-1-miR-10b-OX-GFP miR-10b levels are represented as a fold change normalized to control (AsPC-1-GFP-C) or relative quantity (RQ). The mean ± SEM of three independent experiments is depicted in **Figure 40**. Student's two-tailed t-test of RQ values was used to assess statistical significance. $p<0.05$ was considered statistically significant. 200,000 AsPC-1-miR-10b-OX-GFP or AsPC-1-GFP-C cells were serum starved (low-serum media: RPMI supplemented with 0.5% FBS, 0.1% Bovine Serum Albumin (BSA-Sigma A7906), 5 µg/mL apotransferrin, 5 ng/mL sodium selenite, and 1% P/S) for 24 hours (hrs) and then treated with 1 nM EGF (Millipore, Billerica, MA, USA) for 0, 10, 30 mins, or 24 hrs in low-serum media, as indicated. Densitometry was performed on at least three separate experiments using Image J. Protein levels from each experiment were normalized to a respective β-Actin or α-Tubulin loading control, and then to the 0 min time point for AsPC-1-GFP-C (Ctrl) cells (0 min-Ctrl), except for pAKT levels, which were only normalized to the loading control. This was because two pAKT experiments had "0 min-Ctrl" densitometry values of 0. For pEGFR Y1148 and EGFR, n=3; pAKT and AKT n=4. Data reported are the means ± SEM.

2.17 Flow Cytometry and Fluorescence-Activated Cell Sorting (FACS)

GFP-positive cell lines were established by sorting cells isolated from K30Ctd$^{+/-}$ mice after culture. GFP-positive cells were sorted using the BD FACS Aria II Cell Sorter or BD SORP Aria (IU Simon Cancer Center Flow Cytometry

Core). Cells were trypsinized and resuspended in 10 million cells/mL and passed through a 40-micron mesh cell strainer (Corning 352340). Similar settings (including gating to a GFP-negative cell line TP573) were applied for all cell sorting. GFP-positive and negative cells were collected and replated after sorting.

2.18 Protein Extraction from Tissues and Cell Lines and Immunoblotting

Pulverized pancreatic tissue dust was homogenized in cell lysis buffer (Cell Signaling Technology 9803) with 1X Protease Inhibitor Cocktail (cOmplete, Roche 11697498001), 1 mM beta-glycerophosphate (Sigma G5422), 1 mM sodium orthovanadate (Sigma S6508), and 1 mM PMSF (Sigma 78830). Tissue dust lysates and lysates from cells were sonicated twice using Fisher Scientific Model 120 Sonic Dismembrator and ultrasonic processor, with five second pulse-five second break intervals for one minute per sonication. Pierce BCA Assay (Thermo Scientific 23225) with a 562 nM wavelength was used to determine protein concentrations. 15 µg of protein was separated over 15% SDS-PAGE with 30% Acrylamide/Bis (Biorad 161-0158) and gel electrophoresis (Bio-Rad Criterion Cell 135BR0033528) and transferred to PVDF membrane (0.45 µm, Millipore IPVH00010). Membranes were blocked with 5% BD Difco skim milk (232100)/TBST, and incubated in primary antibody overnight at 4°C per company recommendations. Secondary antibody HRP-conjugated antibodies (1:5,000) in 5% milk/TBST were used to detect the primary antibody. Washes before and after secondary were in TBST at room temperature. Protein bands were visualized after adding Supersignal West Pico and Femto substrates (Thermo Scientific 34578, 34095) to membranes, and exposure to autoradiography film (Ultra Cruz SC-

201697) and a Konica Medical Film Processor (SRX-101A). More than three separate experiments were performed to confirm TIP30 protein levels in three-month-old pancreas tissues from $K30^{+/+}C$, $K30^{+/-}C$, $K30^{-/-}C$ mice.

For immunoblot analysis of cell lines mPCCs or hPCCs were washed twice with ice-cold 1X PBS, scraped in cell lysis buffer and 12 µg or 20 µg of protein, respectively, was separated over 10% SDS-PAGE and assessed as described above. The following antibodies were used: EGFR (CST 4267, 1:1000, 5% milk), N-cadherin (BD 610920, 1:2000, 5% milk), E-cadherin (BD 610181), CK-19 (Troma III, Developmental Studies Hybridoma Bank, 1:500 5% milk), α-Tubulin (Sigma T9026, 1:2000, 5% milk), ɣ-Tubulin (Sigma T5326, 1:1000, 1% milk), β-Actin (Sigma A1978, 1:100,000, 5% milk), HER2 (SC 284, 1:200, 5% milk, HER3 (CST 4754, 1:1000, 5% BSA), TIP30 (Abcam ab177961, Lot GR163258-1, 1:5000, 5% BSA). pEGFR Y1148 (CST 4404, 1:1000, 5% BSA), pAKT, AKT S473 (CST 4060, 1:2000, 5% BSA), pERK1/2 (CST 4370, 1:2000, 5% BSA), and total ERK1/2 (CST9102, 1:1000, 5% milk). A 250 kD protein ladder (BioRad 161-0375) was used for all immunoblotting experiments. The following secondary antibodies were used: Goat anti-Mouse (Biorad 170-6516), Goat anti-Rabbit (Biorad 170-6515), and Goat anti-Rat (EMD Millipore 401416). For tissues and cell lines at least three biological samples (from three different mice) were assessed. In addition, at least two (tissues) and three technical replicates (per cell line), in which protein was collected from a cell line on three different dates was assessed. Densitometric analysis of immunoblot data was performed using Image J software, to quantitate protein levels. Briefly, a rectangle with fixed dimensions per immunoblot (per

protein) was used to calculate background mean white pixel signal and mean white pixel signal per sample condition. The background mean white pixel was subtracted from the mean white pixel signal of each sample for the number of black pixels. The loading control was also quantitated in this manner. Normalization of data occurred in two steps 1) to the loading control and 2) to the $K30^{+/+}C$, wild-type *Tip30* control. For step 1, the black pixels of the samples were divided by the black pixels for the respective loading control for each sample. Then, for step 2, $K30^{+/+}C$ levels for three cell lines were averaged (n=3) and average values for $K30^{+/-}C$ or $K30^{-/-}C$ PCCs were divided by the average $K30^{+/+}C$ and depicted in bar graphs. For statistical analysis, values from step 1 were assessed.

2.19 Two-Dimensional Clonogenic Growth Assay

500 single cells were plated in duplicate in a six-well plate in complete media. After seven to eight days in culture, unless otherwise indicated, colonies were washed twice with ice-cold 1X PBS and fixed with 0.05% crystal violet (Sigma C6158) in 95% methanol solution for five minutes at room temperature. Crystal violet solution was removed and stained colonies were washed twice with 1X cold PBS and once with ddH2O to remove background dye. Dry plates were scanned and colony areas were assessed using the Image J Colony Area plugin software designed for six-well plates (Guzman et al., 2014). One representative experiment per cell line was used to determine mean two-dimensional growth.

2.20 Three-Dimensional Colony Growth Forming Assay

The three-dimensional (3D) culture system was described previously (Sempere et al., 2011). Briefly, for each experiment 5,000 mPCCs were plated in

duplicate (two wells) in a 48-well tissue culture plate. Cells were first resuspended in 200 µl of an ice-cold 3%-growth-factor-reduced matrigel (Corning 356231)/complete media, before plating on top of 200 µl of solidified 1% soft agar/complete media. Autoclaved aliquots of 3% agar noble (BD Diagnostic Systems 214220) were stored at 4°C. Cells were fed every 4-5 days with 100 µl ice cold 3% matrigel/complete media. After 14-20 days in culture, colonies were imaged at 4X and 20X magnification using a DMI 3000B Microscope and Leica CFC310 FX camera and Las V4.5 software. Captured formats were 1392x1040 units. Each well was then stained with a final concentration of 0.4 mg/mL MTT (Sigma M2128), for 3 hours at 37°C, before whole-plate imaging. Surface areas of 3D colonies were scanned using an HP Scanjet G4050. Colony areas from scanned images were quantitated using Image J Colony Area plugin for custom plates (Guzman et al., 2014). Mean threshold intensities were used per plate to account for background, and percent areas occupied were divided by total well area percentages per well. Three biological replicates or three separate cell lines per group: *Tip30*$^{+/+}$, *Tip30*$^{+/-}$, and *Tip30*$^{-/-}$ in the KC background (K30$^{+/+}$C-TP151-GFP, TP711, TP715; K30$^{+/-}$C-TP852-GFP, TP573, TP647; and K30$^{-/-}$C-TP735-GFP, TP592-1, TP889) were analyzed in this assay. Our cell line nomenclature uses the mouse ID number from which the cell line was derived. For each of the nine cell lines assessed, three separate experiments were first performed in duplicate on three different dates for each cell line, except for the cell line TP852-GFP, for which only one experiment was performed in duplicate; and data was collected. For statistical analysis, one representative experiment of 3D growth for

each cell line after 17-18 days in culture was utilized, and $K30^{+/+}C$, $K30^{+/-}C$, and $K30^{-/-}C$ groups, with n=3, were compared by one-way analysis of variance (ANOVA) (SigmaPlot 12.5). Results did not reach statistical significance.

2.21 Immunofluorescence Confocal Microscopy

10,000 cells were plated in 8-well glass chamber slide in normal tissue culture media, 5% FBS, 1% P/S, grown to 60% confluence before being serum starved overnight after washing 2X with HBSS. Serum starving media consisted of 0.5% FBS, 0.1% BSA, 5 µg/mL apotransferrin, 5 ng/mL sodium selenite, RPMI. Cells, 1% P/S were fixed with 4% paraformaldehyde at baseline (no EGF or 0 min time point) or following treatments with 1 nM EGF for 30 min or 120 min. Cell membranes were permeabilized during blocking with 1% BSA/0.15% TritonX/ 5% normal goat serum (Vector Laboratories S1000). PCCs were probed with anti-EGFR (CST 4267 1:50) and 1:400 Goat anti-Rabbit Alexa Fluor 488 (Life Technologies A11034, Lot 1851447) antibodies to detect EGFR. Slides were mounted with Prolong Gold mounting medium with DAPI (Invitrogen P36931) and coverslipped (Fisherbrand 12-544G) and imaged using the Leica SP8 Confocal microscope with a 40X/1.3 oil immersion, Zoom of 2.3 and LASX software. 15-30 cells were captured per field and two fields were imaged at a minimum after scanning the entire slide and processed using Fiji and Imaris 64 software for maximum intensity projection from a 3D volume. Background from a no primary antibody negative control image was removed from images shown during processing. Fiji software was used for image processing and to subtract background. The background was determined from a control image (obtained by

imaging a control field in the experiment that was incubated with the secondary antibody, but no primary antibody “no primary control”) and subtracted from all subsequent images. Antibodies detecting CK19 (rat origin, Troma III, Developmental Studies Hybridoma Bank) at a 1:200 dilution, and α-SMA (mouse origin, Sigma A2547) at a 1:100 dilution were used for representative staining in a cell line from each group. The following fluorophore-conjugated secondary antibodies were used for immunofluorescence detection: Goat anti-Mouse Alexa Fluor 555 (Invitrogen A21429) was used to detect α-SMA; Goat anti-Rat Alexa Fluor 647 (Invitrogen A21472) was used to detect CK19; Goat anti-Rabbit Alexa Fluor 488 (Thermo Fisher Scientific A11034) was used to detect EGFR.

2.22 MIR10B and TIP30 Expression in hPDAC

MIMAT0000254 (MIR10B) hPDAC RNAseq data was downloaded from UCSC Xena browser’s The Cancer Genome Atlas (TCGA) Pancreatic Cancer (PAAD) cohort (Goldman et al., 2019) and HTATIP2 (TIP30) from the TCGA provisional dataset (J. Gao et al., 2013; Cerami et al., 2012). Data was accessed on July 7, 2018. Patient-matched TIP30 and MIR10B expression values were used to create a scatterplot using SigmaPlot 13.0. An exponential decay curve was fit to the data, and the relationship between both values were assessed using the Spearman coefficient in SigmaPlot.

2.23 K30C Survival Analysis

$K30^{+/+}C$, $K30^{+/-}C$, and $K30^{-/-}C$ mice that were non-breeders were also monitored for survival in accordance with IACUC and LARC standards. Mice were monitored until moribund, which was determined by symptoms such as any and

first indication of difficulty breathing, short rapid breaths, irregular coat and grooming presentation (scruffiness), lack of eating and severe weight loss (as determined by LARC), and any other reasons determined by LARC to comply with humane treatment conditions. Mice monitored for survival were obtained from progeny with mouse ID numbers TP427 and higher (see Methods 2.1 for an explanation regarding the mouse identification system and Pdx1-Cre mouse strain background). This was to minimize any interference in differences in strain source on survival (see Methods 2.1). Mouse subjects used in the survival curve ranged from subject ID numbers TP431 to TP1217. Observations began with the first death occurrence on August 7, 2015. The survival study was terminated in July of 2018. Mice that were taken at specific and pre-determined time points were not included in the survival analysis.

Survival data were analyzed using the Kaplan-Meier estimator through GraphPad Prism 7.0 on July 20, 2018. Death was considered to be an event or occurrence (“1”). Mice were monitored for 12 months, however not all mice were able to be monitored for a total of 12 months due to rolling assignment to the study. If mice were alive at the conclusion of the study they were assigned a “0” or considered censored. Censored data and “0=censored” is reviewed by Rich et al. (2010) and Goel et al. (2010). For the purposes of these studies, these were mice that were alive before reaching the 12-month endpoint in the study ($K30^{+/+}C$, n=4; $K30^{+/-}C$, n=2; and $K30^{-/-}C$, n=5). Since the study was concluded before 12 months for these particular mice we had no way to know nor predict their survival (in months). Therefore all “1” (experienced death or occurrence) and “0” (censored)

events were included in the statistical analysis so as not to skew the data in favor any one particular cohort. A logrank (Mantel-cox) test was performed on all survival data (both “1” and “0” events). The total number of mice per group including the censored subjects were as follows: $K30^{+/+}C$, n=10; $K30^{+/-}C$, n=14; and $K30^{-/-}C$, n=13.

2.24 Statistics

A Student’s two-tailed t-test (Microsoft Excel) was performed, when two groups were compared. For more than two group comparisons, a one-way-analysis of variance (ANOVA) with Tukey post-hoc was performed in Sigma Plot 11.0. A power analysis was performed at the Biostatistics Walk-In Clinic to determine the number of animals needed for significance in tumor formation between groups, with a power of 0.80 and an alpha of 0.05. For statistical testing, $p<0.05$ was considered significant. Categorical data sets were analyzed with a Chi-square test (SigmaPlot 13.0) or Chi-Square test for trend (GraphPad Prism 4.0) for three groups ($K30^{+/+}C$, $K30^{+/-}C$, and $K30^{-/-}C$) using a 2x3 contingency table, followed by 2x2 contingency table and Fisher exact or Chi-square analyses between two groups with a Bonferroni Correction of 0.0167, to check for significance (SigmaPlot 13.0). Survival data were analyzed using a Kaplan Meir survival curve and Log-rank (GraphPad Prism 7.0), (see Methods 2.23). Continuous data (MIR10B and TIP30 expression in hPDAC, TCGA) was analyzed using a nonlinear fit (exponential decay) to the data derived from TCGA obtained from UCSC Xena browser using Sigmaplot 13.0, followed by statistical analysis using the Spearman’s rank correlation coefficient (Sigmaplot 13.0). Two separate

analyses were done, both with and without the outlier. For categorical and continuous data set statistical analyses we consulted with Dr. Susan Perkins, a Professor of Biostatistcs and member of both the Pancreatic Cancer Signature Center and the Biostatistics and Data Management Core of the Indiana Melvin and Bren Simon Cancer. Dr. Perkins is currently the Director of Design and Biostatistics Program of the Indiana Clinical and Translational Sciences Institute (CTSI).

2.25 Composition of Buffers

Laboratory grade double deionized water (ddH2O), from an EMD Millipore Milli-Q water purification system, was used in the composition of all buffers.

Immunoblotting Gel Electrophoresis:

Upper buffer (UB)-0.5 M Tris; 0.4% SDS; pH 6.8

Lower buffer (LB)-1.5 M Tris; 0.4% SDS; pH 8.8

SDS-PAGE Gels (per gel):

10% separating gel-3.33 mL 30% acrylamide; 2.5 mL LB, 4.17 mL ddH2O

12% separating gel-4.0 mL 30% acrylamide; 2.5 mL LB, 3.5 mL ddH2O

15% separating gel-5.0 mL 30% acrylamide; 2.5 mL LB, 2.5 mL ddH2O

Add 50 µL 10% APS, 10 µL TEMED per gel.

Stacking gel: 0.67 mL 30% acrylamide; 1.25 mL UB, 3 mL ddH2O

Add 25 µL 10% APS, 5 µL TEMED per gel.

6X Loading Dye: 1 g SDS; 7 mL UB; 3 mL Glycerol; 600 µL β-Mercaptoethanol (BME); 0.6% bromophenol blue

5X Running Buffer (Diluted to 1X):

0.96 M Glycine

125 mM Tris

For 4 L: 60.4 g Tris; 288 g Glycine; 20 g SDS

Transfer Buffer:

25 mM Tris; 192 nM Glycine; 20% Methanol

For 8 L: 115.2 g Glycine; 24 g Tris; 1.6 L Methanol; 6.4 L ddH2O

10X Tris-buffered saline (TBS)

For 8 L: 192 g Tris; 704 g NaCl, pH 7.6 (55 mL 12 M HCl)

Tris-buffered saline-Tween-20(TBST)

1X TBS, add 8 mL Tween-20 (0.1%)

50X Tris base, acetic acid and EDTA (TAE)

121 g Tris

28.55 mL Glacial Acetic Acid

18.6 g EDTA

Fill to 500 mL ddH2O, pH 8.5

2.26 Primers

Primers are listed in 5’ to 3’, left to right.

Kras

K005 (mut Kras): AGCTAGCCACCATGGCTTGAGTAAGTCTGCA

K006 (wt & mut Kras): CCTTTACAAGCGCACGCAGACTGTAGA

PDX (Cre-Cre)

Cre 1: TGATGAGGTTCGCAAGAACC

Cre 2: CCATGAGTGAACGAACCTGG

Pdx1-Cre (NCI)

Pdx-F: CTGGACTACATCTTGAGTTGC

Pdx-R: GGTGTACGGTCAGTAAATTTG

Tip30

MT (Reverse): GGC CTC TTC GCT ATT ACG C

Common (Forward): TGA GTC TCT GCC CAA CA

WTR (Reverse): TAA TGG ACA CCT TCC CCT CA

tdTomato

Wild-type Forward - CTC TGC TGC CTC CTG GCT TCT

Wild-type Reverse - CGA GGC GGA TCA CAA GCA ATA

Mutant Reverse - TCA ATG GGC GGG GGT CGT T

Kras G12D Conditional PCR

LSL-1 GTCTTTCCCCAGCACAGTGC

LSL-2 CTCTTGCCTACGCCACCAGCTC

LSL-3 AGCTAGCCACCATGGCTTGAGTAAGTCTGCA

2.27 PCR Reactions

19 microliters of master mix was combined with one microliter of tail DNA for each PCR reaction as described below. In genotyping DNA isolated from pancreas tissues, other organs, or cell lines, 17 microliters of mastermix was combined with three microliters of ddH2O + 200 ng of DNA sample. Two separate PCR reactions were performed for TIP30 genotyping: one to detect the wild-type allele and another to detect the mutant (LacZ) allele.

Kras/PDX	
Genotyping per reaction (µL)	
2	10x buffer
1.2	$MgCl_2$
0.5	dNTPs
0.1	Forward primer
0.1	Reverse primer
0.1	Taq
15	H2O

Tip30	
Genotyping per reaction (µL)	
2	10x buffer
1	$MgCl_2$
0.5	dNTPs
0.1	Common (Forward) primer
0.1	Reverse primer (MT or WTR)

0.1	Taq
15.2	H2O

tdTom	
Genotyping per reaction (µL)	
1.8	10x buffer
1	$MgCl_2$
0.5	dNTPs
0.15	Forward primer (WTF)
0.1	Reverse primer (WTR)
0.2	Mutant primer (MT)
0.1	Taq
15	H2O

Kras G12D Conditional PCR	
Genotyping per reaction (µL)	
1.8	10x buffer
1	$MgCl_2$
0.5	dNTPs
0.1	Forward primer (LSL-1)
0.1	Reverse primer (LSL-2)
0.1	Mutant primer (LSL-3)
0.1	Taq
13.3	H2O

Pdx1-Cre (NCI)	
Genotyping per reaction (µL)	
2	10x buffer
1.2	$MgCl_2$
0.5	dNTPs
0.1	Forward primer
0.1	Reverse primer
0.1	Taq
15	H2O

2.28 PCR Cycling Conditions

Thermocycler conditions plus predicted band sizes are indicated for each transgene used for these studies. Agarose percentages used to detect each transgene by gel electrophoresis is indicated for each transgene.

Kras	
Step #, Temperature	
1.	95°C, 15 min
2.	95°C, 30 sec
3.	60°C, 30 sec
4.	72°C, 1 min
5.	Go to step 2, 35X
6.	72°C, 5 min
7.	10°C, hold

Transgene = 600 bp, 2% gel

PDX	
Step #, Temperature	
1.	95°C, 15 min
2.	95°C, 30 sec
3.	58°C, 1 min
4.	72°C, 45 sec
5.	Go to step 2, 34X
6.	72°C, 10 min
7.	10°C, hold

Transgene = 400 bp, 2% gel

Pdx1-Cre (NCI)	
Step #, Temperature	
1.	95°C, 15 min
2.	95°C, 30 sec
3.	56°C, 30 sec
4.	72°C, 30 sec
5.	Go to step 2, 35X
6.	72°C, 10 min
7.	10°C, hold

Transgene = 650 bp,

TIP30 Touchdown	
Step #, Temperature	
1.	95°C, 15 min
2.	94°C, 20 sec
3.	65°C, 15 sec (-0.5°C/cycle)
4.	68°C, 10 sec
5.	Repeat steps 2-4 for 10 cycles
6.	94°C, 15 sec
7.	60°C, 15 sec
8.	72°C, 10 sec

9.	Repeat steps 6-8 for 28 cycles
10.	72°C, 10 min
11.	10°C, hold

Mutant = 300 bp
Heterozygote = 300 bp and 364 bp
Wild-type = 364 bp, 2% gel

tdTom	
Step #, Temperature	
1.	95°C, 15 min
2.	95°C, 30 sec
3.	61°C, 1 min
4.	72°C, 1 min
5.	Repeat steps 2-4, 35X
6.	72°C, 10 min
7.	10°C, hold

Mutant = 250 bp
Heterozygote = 250 bp and 330 bp
Wild-type = 330 bp, 1.5% gel

Kras G12D Conditional PCR	
Step #, Temperature	
1	95°C, 15 min
2	95°C, 30 sec
3	61°C, 30 sec
4	72°C, 45 sec
5	Go to step 2, 34X
6	72°C, 10 min
7	10°C, hold

Recombined (Mutant) = 650 bp
LSL Cassette = 500 bp
Wild-type = 622 bp, 3% gel

2.29 TIP30 Antibodies

The rabbit monoclonal anti-TIP30 antibody was purchased from Abcam (ab177961). It is raised against the C terminus and can detect isoforms 1 and 3 (27,049 daltons and 30, 131 daltons respectively). Note that the oriGene TA590574 Rabbit Polyclonal TIP30 antibody was tested and gave non-specific bands. The GeneTex GTX100119, Lot 40709 Rabbit polyclonal antibody also gave non-specific bands.

CHAPTER 3. DEVELOPING AN *IN VIVO* MODEL SYSTEM TO STUDY THE ROLE OF TIP30 LOSS ON PDAC PROGRESSION

3.1 Background and Rationale

Tat-**i**nteracting **p**rotein (30 kD), TIP30, is encoded by the gene *HTATIP2* (*CC3)* (Xiao et al., 1998, Shtivelman, 1997). TIP30 shares some properties with short-chain dehydrogenase reductases (SDRs), thereby placing it in the SDR family of oxioreductases (Omari et al., 2005). Some of these properties include an SDR fold and high affinity for coenzymes NADH and NADPH; however, the dimer formation of TIP30 differs slightly from that of typical SDRs. In addition, a substrate has not yet been identified for TIP30, nor has its function as an oxioreductase been proven (Omari et al., 2005). Based on reports in the literature, TIP30 has been identified as a metastasis suppressor with proapoptotic functions (Shtivelman, 1997; Xiao et al., 2000). Loss of TIP30 expression has been studied in the context of hepatocellular (Ito et al., 2003), lung (Li et al., 2013) and colorectal carcinoma (Chen et al., 2010). TGF-β-mediated silencing of TIP30 promotes metastasis in esophageal carcinoma (Bu et al., 2014). TIP30's role as a metastasis suppressor is linked to its proapoptotic properties. Through mechanisms of nuclear import inhibition of proteins with a primary nuclear localization signal (NLS) or an M9 transport signal, TIP30 can aid in exposing cells to cell-death signals (Xiao et al., 2000; King and Shtivelman, 2004; Shi et al., 2008). TIP30 loss has been associated with lymph node metastasis and low E-cadherin protein levels in human pancreatic ductal adenocarcinoma (hPDAC). In a study comprised of 106 PDAC cases, Guo et al. (2014) found a significant correlation between E-cadherin and

TIP30 expression. Low TIP30 expression was associated with a significant decrease in PDAC patient survival (Guo et al., 2014). Our laboratory recently published that microRNA (miR)-10b, a frequently upregulated miR in PDAC, targets TIP30 for degradation and that miR-10b suppression of TIP30 in pancreatic cancer cells (PCCs) results in prolonged downstream EGFR signaling and EGF- and TGF-β- mediated enhanced invasion (Ouyang et al., 2013). Given the relationship between miR-10b overexpression and TIP30 loss, and the poor survival outcomes in PDAC patients with low TIP30 levels (Guo et al., 2014)**,** we hypothesized that TIP30 loss contributes to the progression of PDAC and influences the metastatic potential of pancreatic cancer cells.

3.2 Results

3.2.1 *TIP30* Genetic Alterations in Human PDAC

To assess the role of TIP30 in human PDAC (hPDAC), we mined publically available databases and assessed The Cancer Genome Atlas (TCGA) whole exome sequencing data through cBioPortal (J. Gao et al., 2013; Cerami et al., 2012). We found that *HTATIP2* (gene for TIP30) was frequently altered in roughly 49% of hPDAC cases (UTSW cohort n=53/109) (Witkiewicz et al., 2015). The UTSW dataset consists of micro-dissected PDAC samples. According to Witkiewicz et al. (2015), microdissection enriches for tumor cells and mutational calling. These factors contribute to increased sequencing quality, which is imperative for improved accuracy in analysis of patient samples. In the UTSW cohort, 92% of PDAC cases contained a *KRAS* mutation. This observation closely aligns with reports of *KRAS* mutations in 93-95% of hPDAC. $KRAS^{G12D}$ is the most

frequent *KRAS* point mutation (Raphael et al., 2017; Almoguera et al., 1988; Rozenblum et al., 1997; Kern, 2000; Hruban et al., 2000).

The cBioPortal database uses the Genome Identification of Significant Targets in Cancer (GISTIC) algorithm to determine putative copy-number levels per gene. A GISTIC score of -2 indicates a deep loss or homozygous deletion, -1 is heterozygous loss (HETLOSS), 0 is diploid (WT), and anything greater than 2 is an amplification (GAIN/AMP); a score above 2 is considered a GAIN and a score above 3 is considered a high-level amplification (AMP) (J. Gao et al., 2013; Cerami et al., 2012). GISTIC scores allow for the identification of regions of significant amplification and deletion in chromosomal aberrations (reviewed in Beroukhim et al., 2007). Among 53 cases with *TIP30* alterations, 53% were copy-number deletions (n=28/53) while 47% (n=25/53) were copy-number gains (**Figure 6A**). We observed an overall 26% occurrence of *TIP30*-heterozygous loss (HETLOSS) in this cohort of PDAC patient samples. We found that among the cases with TIP30 loss, 86% (n=24/28) also had a *KRAS* mutation (**Figure 6A**).

To evaluate the effects of *TIP30* alteration on gene expression, we analyzed *TIP30* gene expression in PDAC by copy number variation. We obtained gene expression data from the TCGA Provisional dataset accessed through cBioPortal (J. Gao et al., 2013; Cerami et al., 2012). Copy number gain of *TIP30* led to a significant increase in *TIP30* mRNA expression levels ($p<0.001$, n=149). There was a decreasing trend in TIP30 expression levels for hPDAC cases with *TIP30*-copy-number loss, however this association was not significant (**Figure 6B**). In addition, expression levels in *TIP30* wild-type (WT) or diploid PDAC patient

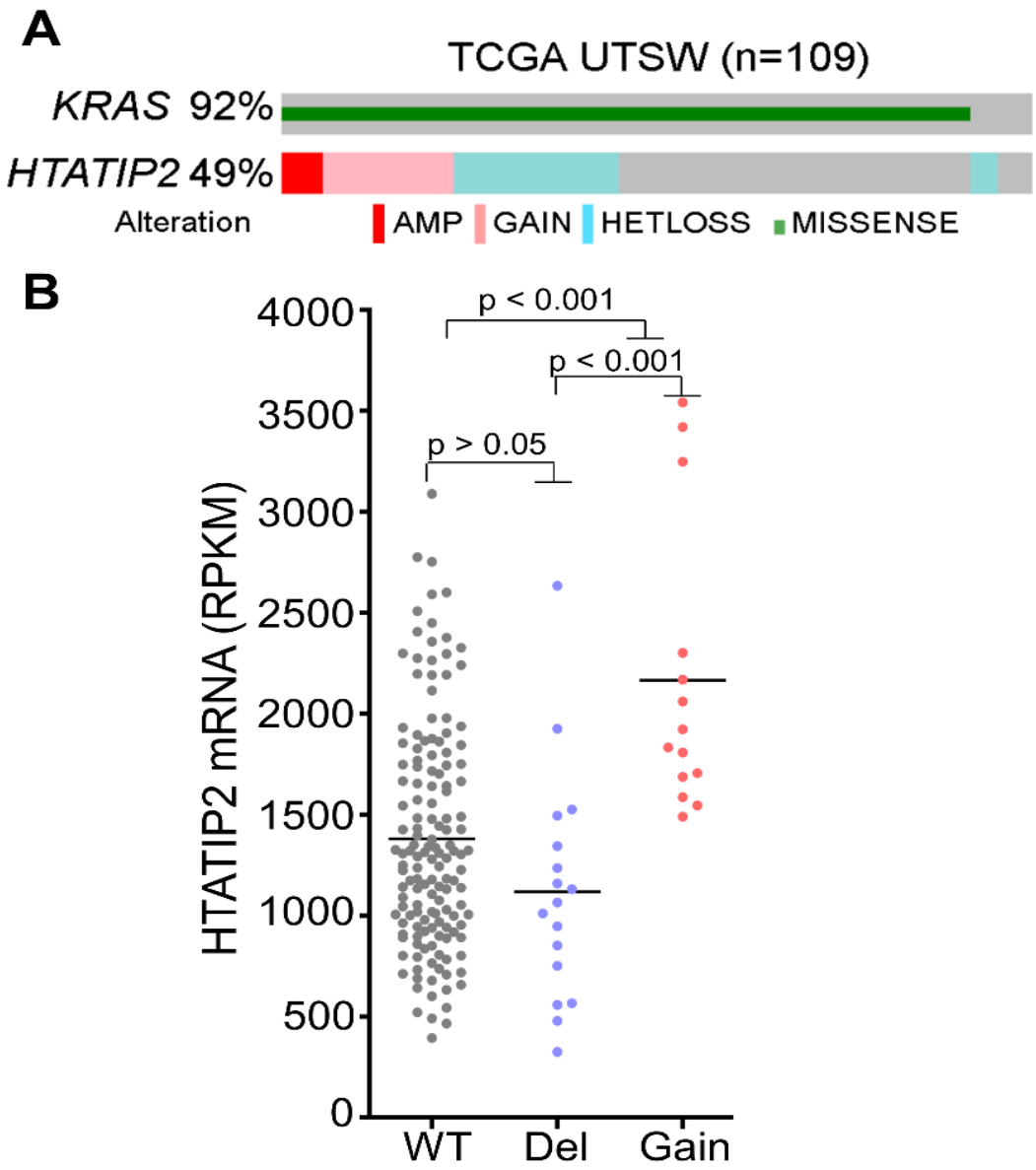

Figure 6. Alterations in *TIP30* copy number are associated with TIP30 gene expression in human PDAC

(A) University of Texas Southwestern database of copy number alterations in PDAC patient samples, n=109 (Witkiewicz et al., 2015) in cBioPortal (J. Gao et al., 2013; Cerami et al., 2012). Oncoprint was retrieved from http://www.cbioportal.org/ on November 29, 2017. *KRAS* point mutations are plotted against all *HTATIP2* (*TIP30*) genetic alterations. High-level amplification (AMP), low level gains (GAIN), heterozygous loss (HETLOSS), and point mutation (MISSENSE), no alteration (gray). **(B)** HTATIP2 mRNA expression as compared to matched copy number gain or loss (Del for shallow deletion) in human PDAC (hPDAC). RNA-seq data from TCGA Provisional, n=149. Data was accessed in cBioPortal on November 29, 2017. RPKM, reads per kilobase per million mapped reads measure of gene expression. hPDAC, human PDAC cases.

samples spanned a wide range: from 500 to 3,300 reads per kilobase per million (RPKM) mapped reads (**Figure 6B**). Lastly, hPDAC cases with *TIP30* loss had limited *TIP30* expression data.

3.2.2 *TIP30* Hypermethylation in Human PDAC

TIP30 promoter region methylation has been reported in both colorectal (Chen et al., 2010) and esophageal carcinoma (Dong et al., 2014). Methylation is another form of epigenetic alteration that can regulate gene expression and contribute to pancreatic carcinogenesis (McCleary-Wheeler et al., 2013). To assess if *TIP30* loss in human PDAC (hPDAC) cases occurred by means other than alteration of the genetic code itself, TIP30 DNA methylation data (Methylation450k) was obtained from the UCSC Xena browser database (Goldman et al., 2009) and accessed on November 11, 2018. *TIP30* was highly methylated at the promoter and 3'UTR regions in hPDAC cases (TCGA, PAAD, n=195) (**Figure 7A**). These data suggest that hypermethylation could also account for *TIP30* loss in human PDAC. The MethHC database (accessed on June 7, 2018) was used to further assess the relationship between the DNA methylation and *TIP30* mRNA expression in hPDAC cases (Huang et al., 2015). In a PAAD cohort of 91 hPDAC cases, *TIP30* expression inversely correlated with *TIP30* promoter methylation in matched hPDAC (n=91, r=-0.594, p=5.995E-15) (Huang et al., 2015) (**Figure 7B**), suggesting that high *TIP30* methylation associated with decreased *TIP30* expression. Three normal pancreas samples were present in the MethHC figure and had high TIP30 methylation and low *TIP30* expression levels (Huang et al., 2015, **Figure 7B**, green).

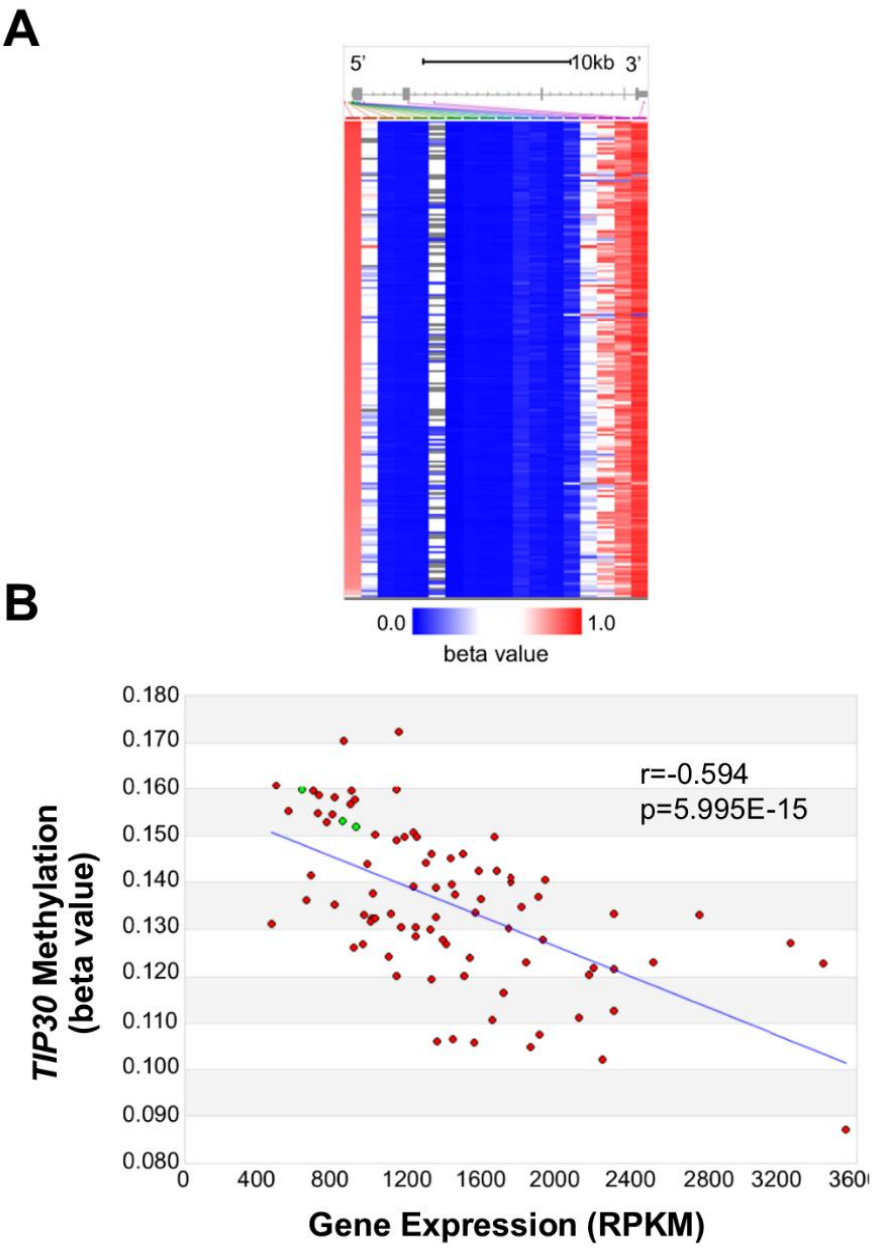

Figure 7. High *TIP30* methylation is linked to decreased TIP30 expression in human PDAC

(A) *TIP30* is hypermethylated in human PDAC cases. *HTATIP2* (*TIP30*) DNA methylation profile, by Methylation450K array in the TCGA pancreatic adenocarcinoma (PAAD) cohort, n=195. USCS Xena browser (Goldman et al., 2009) image was retrieved from https://xenabrowser.net on November 11, 2018. Beta values represent DNA methylation values. Methylation beta values of 0 (least methylated) to 1 (most methylated) are shown as a gradient of blue to red, respectively. **(B)** *HTATIP2* promoter methylation data in human PDAC (*TIP30* Methylation) is plotted against matched HTATIP2 (TIP30) gene expression levels (Gene Expression), PAAD cohort, n=91 (r=-0.594, p=5.995E-15). MethHC database (Huang et al., 2015) image was retrieved from methhc.mbc.nctu.edu.tw/php/index.php on June 7, 2018. Red, PDAC. Green, normal pancreas. *TIP30* methylation is represented in methylation beta value units. TIP30 gene expression is represented by reads per kilobase per million mapped reads (RPKM).

3.2.3 TIP30 Antagonist *MIR10B* is Frequently Amplified in Human PDAC

Studies in both pancreatic and esophageal cancer fields report that *TIP30* is a direct target of micro-RNA (miR)-10b (Ouyang et al., 2014; Dong et al., 2014). The miR-10b seed sequence has Watson-Crick complementarity to a region in *TIP30*'s 3'UTR; and miR-10b-overexpressing pancreatic and esophageal cancer cells have decreased *TIP30* mRNA levels (Ouyang, H., 2014; Dong et al., 2014). The non-coding gene *MIR10* is found in two variants in mammals and on two different chromosomes: 2q31.1 (*MIR10B*), and 17q21 (*MIR10A*). Both share similar seed sequences, differing by only one nucleotide in the mature strand, and have both similar and distinct targets (reviewed by Tehler et al., 2011). Since miR-10b is also one of the most frequently upregulated miRs in PDAC (Preis et al., 2011) and overexpression of miR-10a was also found to decrease TIP30 protein levels in pancreatic cancer cells (Ouyang et al., 2014), we hypothesized that both MIR10B and MIR10A are genetically altered in human PDAC (hPDAC). To assess the presence of *MIR10B* and *MIR10A* genetic alterations in hPDAC we mined TCGA data and found that both miRs are frequently altered in PDAC cases (**Figure 8A**). 43 of 109 PDAC cases without a *TIP30* alteration or with *TIP30* amplification or copy number gain alterations also have amplification or copy number gain of *MIR10B*, family member *MIR10A*, or both (n=10/109) (TCGA PDAC, UTSW). These findings suggest that hPDAC cases without TIP30 HETLOSS could attain decreased *TIP30* expression levels despite TIP30 wild-type status or positivity for TIP30 copy-number amplifications or gain. Thus, microRNA-dependent

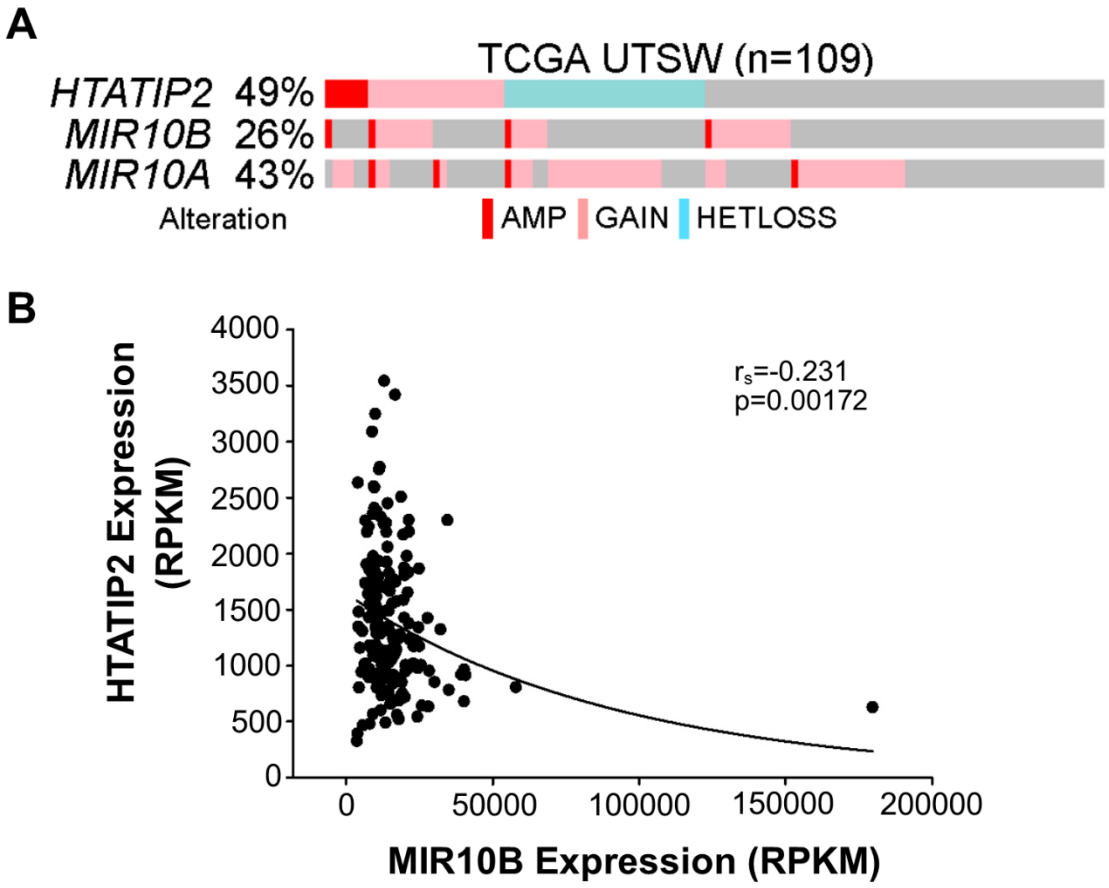

Figure 8. TCGA analysis of *MIR10B* alterations in hPDAC and correlation with TIP30 expression

(A) Oncoprint of TCGA *HTATIP2* (*TIP30*) copy number alterations (CNA), and *MIR10B*, and *MIR10A* copy number amplifications (AMP) and gains (GAIN) (UTSW, n=109, Witkiewicz et al., 2015). Image adapted from cBioPortal (J. Gao et al., 2013; Cerami et al., 2012) and retrieved from http://www.cbioportal.org/ on November 29, 2017. *MIR10B* and *MIR10A* copy number AMP and GAIN occur in hPDAC cases that are *HTATIP2* (*TIP30*)-wild-type or have *TIP30* copy number AMP, GAIN, or heterozygous loss (HETLOSS). PDAC cases with *MIR10B* and *MIR10A* HETLOSS are not depicted here. **(B)** Correlation between HTATIP2 (TIP30) expression and MIMAT0000254 (MIR10B) expression in hPDAC (TCGA provisional, n=182). Data was downloaded from the UCSC Xena browser database (Goldman et al., 2009) on July 7, 2018 (https://xenabrowser.net/). Exponential decay curve was best fit for the data, upon consultation with a biostatistician. Spearman coefficient: r=-0.231, p=0.00172. Gene expression values are represented by reads per kilobase per million mapped reads (RPKM).

mechanisms play an important role in epigenetic silencing of gene expression in pancreatic cancer (McCleary-Wheeler et al., 2013).

3.2.4 Co-occurrence of *TIP30* Copy Number Alterations with *MIR10B* and *MIR10A* Amplifications

In the UTSW dataset, the 87 hPDAC cases that were either diploid or amplified/gained for *TIP30* also had an amplification in either *MIR10A* or *MIR10B* (UTSW, n=109, **Figure 8A**). Since *TIP30* is a direct target of *MIR10B,* we assessed the relationship between *TIP30* copy number alterations (CNAs) and *MIR10B* amplification. We mined TCGA Provisional data and found that *TIP30* CNAs co-occur with amplification and gain of both *MIR10B* (TCGA Provisional, p=0.007), and *MIR10A* (p=0.015). To confirm the validity of the copy number alteration data, we assessed the MIR10A (MIMAT0000253) and MIR10B (MIMAT0000254) RNAseq data from Xena browser (Goldman et al., 2019, accessed on July 7, 2018). We compared gene expression values of MIR10A or B to matched *TIP30* gene expression values in human PDAC (hPDAC) cases. MIR10B expression was negatively correlated with TIP30 expression, in hPDAC (r=-0.231, p=0.00172 by Spearman's rank correlation coefficient; TCGA PAAD, n=182; **Figure 8B**). One hPDAC case was an extreme outlier with respect to MIR10B levels, as the RPKM was near 200,000; and the average RPKM for this dataset was closer to 15,000 (**Figure 8B**). This, however, did not affect the relationship between TIP30 and MIR10B expression (**Figure 9**). We conducted a Spearman Correlation on the data without the outlier, and a similar relationship between TIP30 and MIR10B

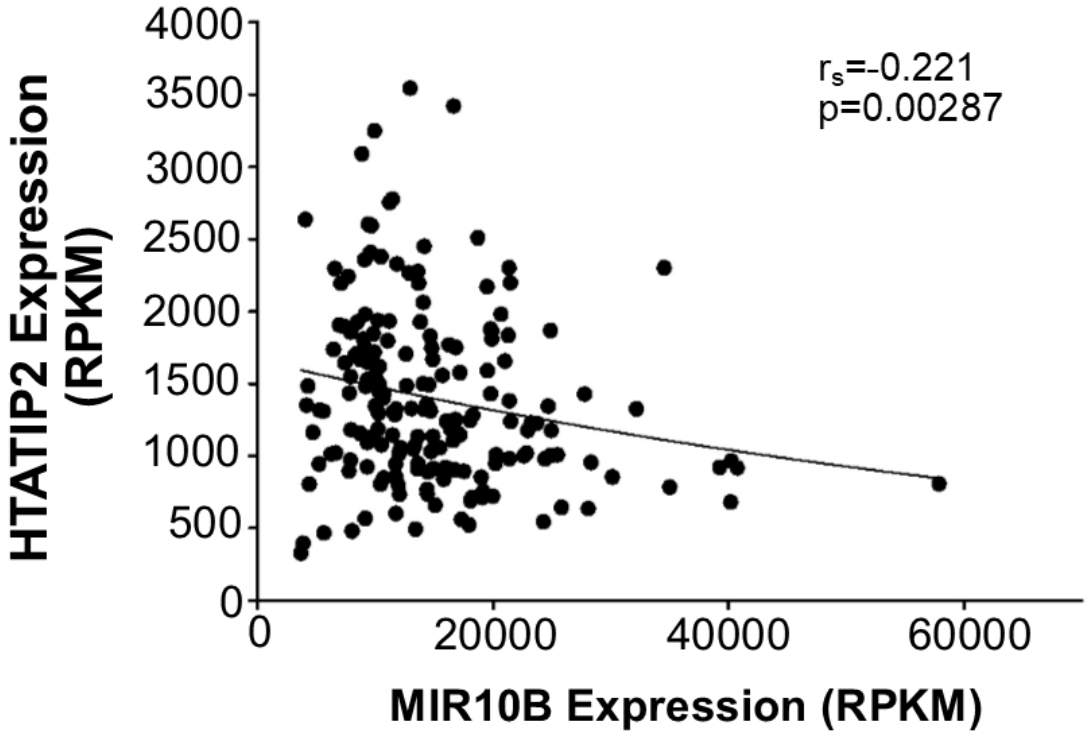

Figure 9. Relationship between MIR10B and TIP30 expression in human PDAC

Correlation between TIP30 (HTATIP2) expression and MIMAT0000254 (MIR10B) in human PDAC (hPDAC), as shown in Figure 8B, but without the outlier (TCGA provisional, n=181). Data was accessed on July 7, 2018 in UCSC Xena browser (Goldman et al., 2009), https://xenabrowser.net. Exponential decay curve was best fit for the data, upon consultation with a biostatistician. Spearman coefficient: r = -0.221, p=0.00287. Gene expression values are represented by reads per kilobase per million mapped reads (RPKM).

expression was observed (r=-0.221, p=0.00287, TCGA PAAD, n=181). The relationship between TIP30 and MIR10B expression levels was nonlinear; therefore an exponential decay curve was fit to the data (**Figure 8B**, **Figure 9**). Surprisingly, MIR10A and TIP30 expression data did not share a similar relationship. Human PDACs with high MIR10A expression levels also had high TIP30 expression levels (r=0.1468, p=0.048; TCGA PAAD, n=182).

3.2.5 Generation and Characterization of K30$^{+/-}$C and K30$^{-/-}$C Mice

To monitor and characterize *Tip30* loss in PDAC, we generated a novel K30C mouse which employs autochthonous, oncogenic *Kras*-driven murine PDAC (mPDAC) development. We crossed the well-established *LoxP-STOP-LoxP* (*LSL)-**K**ras^{G12D}* (**K**)*;Pancreatic duodenal homeobox 1* (*Pdx1)-**C**re* (**C**), genetically engineered mouse model (GEMM) ("KC", Hingorani et al., 2003) to full-body *Tip30*-deficient mice (Ito et al., 2003; Li et al., 2013) to generate KC mice with *Tip30*-deficiency (K30$^{+/-, -/-}$C). The KC mouse model of mPDAC closely resembles that of human PDAC (hPDAC) and has been well-characterized (Hingorani et al., 2003). In our studies, "KC" refers to the *LSL-Kras^{G12D}; Pdx1-Cre* mouse and not the *LSL-Kras^{G12D}*; *P48-Cre* mouse (Hingorani et al., 2003). KC pancreas ductal lesions progress through the full spectrum of pancreatic intraepithelial neoplasia as seen in hPDAC with a six months to one year latency of PDAC formation, and low frequency of metastases (Hingorani et al., 2003; reviewed in Hezel et al., 2006; Guerra and Barbacid, 2013). In their original study, Hingorani and colleagues (2003) reported that one *LSL-Kras^{G12D}; Pdx1-Cre* mouse presented with both liver and lung parenchyma and pleural metastasis at 6.25 months of age. *LSL-Kras^{G12D}*

mice harbor a point mutation in exon 2, the first *Kras* coding exon, at codon 12. This results in the amino acid substitution of glycine to an aspartic acid residue (G12D) in the endogenous *Kras* locus (Johnson et al., 2001; Jackson et al., 2001).

Pancreatic duodenal homeobox 1, Pdx1, previously known as IPF1, is a transcription factor necessary for the development of early pancreatic buds from the ventral foregut endoderm and is known to give rise to the alpha and beta cells of adult mouse islets (Offield et al., 1996). The *Pdx1* protein coding region is replaced by a Cre recombinase coding sequence (*Pdx1-Cre*, Gu et al., 2003). *Pdx1-Cre* directs a mosaic pattern of Cre-mediated recombination and excision of the *Lox*P-flanked transcription termination site (STOP sequence) in the pancreas tissue (Hingorani et al., 2003). The STOP sequence is upstream of the oncogenic *Kras* point mutation in the *LSL-Kras*^{G12D} cassette; this prevents the expression of oncogenic *Kras* in *LSL-Kras*^{G12D} mice without Cre. This system results in spatially controlled expression of mutant *Kras*^{G12D} in the pancreas epithelium (Jackson et al., 2001; Sauer, 1993; Sauer and Henderson, 1988; Hingorani et al., 2003) (**Figure 10A**).

The *Tip30*-deficient knock-out GEMM, first reported in 2003, is composed of a germline, insertion mutation for complete ablation of *Tip30* expression in the entire mouse (Ito et al., 2003). A targeting vector consisting of a 2.7-kb, *Hind*III-*Sac*I flanked *LacZ*-neomycin cassette replaces exons 2-3 of the *Tip30* genomic sequence, in-frame (Ito et al., 2003, **Figure 10B**). We detected this insertion just after the 25th nucleotide of exon 2, or 17 amino acids (aa) after the initiation start

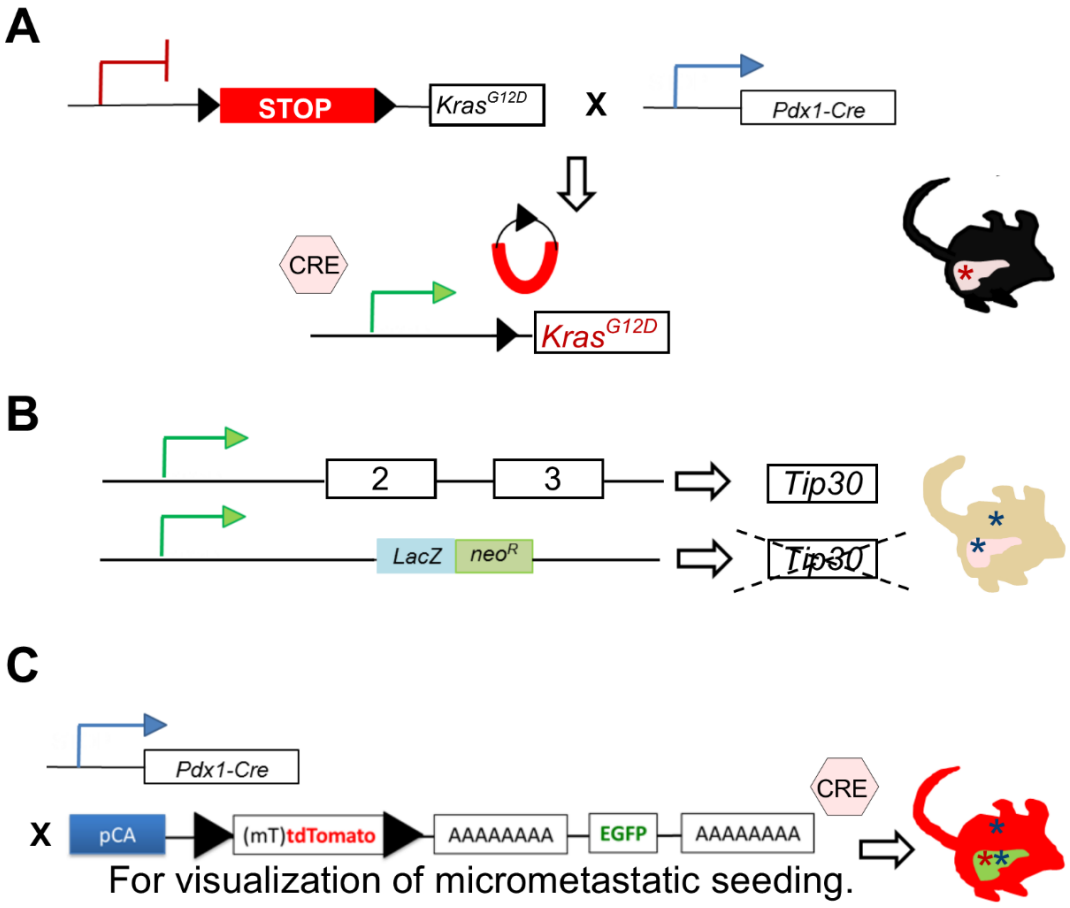

Figure 10. Schematic for generation of K30$^{+/+,\ +/-,\ -/-}$C and K30$^{+/+,\ +/-,\ -/-}$Ctd$^{+/-}$ or $^{-/-}$ mice

(A) KC mouse model (Hingorani et al., 2003). Cre recombinase ("CRE" pink hexagon), driven by the *Pancreatic duodenal homeobox 1* (*Pdx1*) promotor mediates excision of the STOP cassette flanked by *LoxP* sites. STOP cassette excision results in expression of oncogenic *Kras* (*Kras^{G12D}*). Red asterisk represents one copy of *Kras^{G12D}* in the pancreas. **(B)** *Tip30*-deficient mouse model (Ito et al., 2003, Li et al., 2013). Blue asterisk represents a full-body *Tip30*-deletion, including in the pancreas. A LacZ-neomycin resistant (neoR) cassette ablates exons 2-3 of *Tip30*. One wild-type allele and one mutant copy is depicted. **(C)** *LoxP-tdTomato-LoxP-EGFP* (Muzumdar et al., 2007) is dual-fluorescent reporter mouse. A *tdTomato* (*td$^{+/-}$ or* td$^{-/-}$) mouse and pancreas is red until *Pdx1*-Cre-mediated excision of the tdTomato cassette, at which point the pancreas tissue will fluoresce green. GEMMs in **A-B** were crossed to generate K30$^{+/+,\ +/-,}$ and $^{-/-}$C mice. GEMMs in **A-C** were crossed to generate K30$^{+/+,\ +/-,\ -/-}$Ctd$^{+/-}$ or $^{-/-}$ mice. pCA, chicken β-actin core promoter with a CMV enhancer.

site, and not at 10th amino acid as reported in Ito et al. (2003). *Tip30* is not essential for development in mice and *Tip30* loss alone did not result in primary tumors of the pancreas (Ito et al., 2003; Li et al., 2013). In 2003, Ito et al. reported that *Tip30*-deficient mice developed a high incidence of hepatocellular carcinoma at 18-20 months (Ito et al., 2003). In a 2013 study, the same group reported that 78-week-old *Tip30*-deficient mice had increased lung adenocarcinoma in a BALB/c background, as compared to wild-type controls (Li et al., 2013). The BALB/c mouse strain develops lung tumors at a high incidence and is sensitive to lung tumor formation (Li et al., 2013; Begley et al., 2012).

For our studies, we employed one copy of *Pdx1-Cre* (Gu et al., 2003) in our mouse model to mediate stochastic Cre recombinase expression. *Pdx1-Cre* drives *LoxP-STOP-LoxP* excision, and constitutive expression of one mutant *Kras* copy, $Kras^{G12D/+}$ (herein referred to as $Kras^{G12D}$) in the pancreas epithelium of KC mice (Hingorani et al., 2003). We generated mouse cohorts with *Tip30*-heterozygous ($K30^{+/-}C$), *Tip30*-null ($K30^{-/-}C$), and *Tip30*-wild-type ($K30^{+/+}C$) genotypes on a mixed BALB/c/B6/129SvJae noncongenic background. Littermate controls ($30^{+/-}$, or $30^{-/-}$, or wild-type) were generated internally or from within the same mouse colony as the experimental groups per The Jackson Laboratory recommendations. We also generated the following double mutant littermate controls: $K30^{+/-}$, $30^{+/-}C$, $K30^{-/-}$, and $30^{-/-}C$ mice (**Appendix C1**). Detection of successful recombination induced by *Pdx1*-driven Cre activity was achieved using a PCR method that differentiates between the wild-type *Kras* allele, the LSL cassette, and the recombined mutant allele that harbors the remaining *LoxP* site plus the *Kras* point

mutation. This method is known as the “Kras G12D Conditional PCR” method (Jacks, 2017) and is described further in section 2.4.1 of the Materials and Methods. We confirmed *Cre*-mediated excision-recombination of the conditional *LSL-Kras^{G12D}* allele, thus the presence of *Kras^{G12D}* in pancreata collected from an age-matched cohort of three-month-old K30C mice. 88% of the K30$^{+/+}$C, K30$^{+/-}$C, and K30$^{-/-}$C pancreata, assessed for recombination, tested positive for partial recombination (n=15/17). Only two out of the 17 samples tested for very low or undetectable recombination levels. DNA from the tail does not test positive for recombination (Hingorani et al., 2003). In addition to the pancreas, Hingorani et al. (2003, Supplemental) detected *LSL-Kras^{G12D}* recombination and *Cre* activity in genomic DNA from the stomach, duodenum, and mucocutaneous papillomas; however, the heart, lung, liver, spleen kidney, colon tissues, which were also assessed for recombination, tested negative (Hingorani et al., 2003, Supplemental). In our studies, we confirmed that DNA from K30C muscle biopsies were negative for recombination compared to pancreas tissues (**Figure 24**).

K30$^{+/+}$C, K30$^{+/-}$C, K30$^{-/-}$C, and control mice were born with near expected Mendelian genetic ratios (see section 2.1). We first determined *Tip30* status using tail genomic DNA from K30C mice. We collected a tail snip from each mouse in the cohort (TP30 mouse colony) and performed genotyping PCR for *LSL-Kras^{G12D}* (*Kras), Pdx1-Cre* (“PDX” or “Cre-Cre” primers see section 2.26), *and Tip30* mutant transgenes according to The Jackson Laboratory (see section **2.4**, **2.26-2.28**). The *Tip30* mutant PCR product was detected in one reaction, using primers that anneal to the *LacZ* sequence and an intronic region preceding Exon 2 of *Tip30* (“common”

primer), and produced a 300 base pair (bp) product. To detect a wild-type *Tip30* allele, the common primer plus a primer that anneals to the intronic region directly after Exon 2 of *Tip30* ("mutant' primer), was used in a separate reaction and produced a 364-bp product. The *Tip30* wild-type sequence was separated across the same agarose gel as the *Tip30* mutant DNA fragment. K30$^{+/+}$C and *Tip30* wild-type mice tested positive for only one 364-bp product. K30$^{+/-}$C and *Tip30*-heterozygous mice tested positive for both a wild-type and a mutant 300-bp product, and K30$^{-/-}$C and *Tip30*-null mice tested positive for only the 300-bp mutant product. Tail snip DNA from 55 mice in the colony was also genotyped for both *Pdx1* and *Cre* sequences simultaneously (Pdx1-Cre NCI, see section 2.26 for primer sequences) to validate that the *Cre*-positivity was coming from a *Pdx1-Cre* transgene, and not any other *Cre*. We confirmed that there were no other *Cre* transgenes in our mouse colony (other than *Pdx1-Cre*). Combined, these genotyping methods allowed us to group mice into three categories: K30$^{+/+}$C, K30$^{+/-}$C or K30$^{-/-}$C. K30C tail snip DNA tested positive for mutant *Kras^{G12D}* and *Cre* transgenes.

To further validate *Tip30* status, we subjected DNA extracted from an age-matched cohort K30$^{+/+}$C, K30$^{+/-}$C, and K30$^{-/-}$C mouse pancreas tissues to *Tip30* genotyping PCR as well as Kras G12D Conditional PCR (Jacks, 2017) to confirm successful *LSL-Kras^{G12D}* recombination and the presence of oncogenic *Kras* (**Appendix C2.A, B2.C)**. DNA from K30$^{+/+}$C mouse pancreata tested positive for one wild-type *Tip30* PCR product, while DNA from K30$^{+/-}$C and K30$^{-/-}$C mouse pancreata tested positive for both the wild-type and the mutant *Tip30* product, or

just the mutant product, respectively (**Appendix C2.A**). The cohort of mice with confirmed *Tip30* genotyping also exhibited partial *LSL-Kras^{G12D}* recombination in the pancreas (**Appendix C2.C**)**.** We evaluated a total of pancreas tissues from six different mice from each group and confirmed tail-genotyping results.

Two K30$^{+/-}$C mice in the study (TP576 and TP630) did not test positive for the *Tip30* mutant transgene by standard genotyping PCR and were initially placed in the K30$^{+/+}$C category. However, at five weeks, and three and a half months, respectively, these mice fell sick and exhibited a phenotype that was not observed by any other K30$^{+/+}$C mice in our colony. TP576 and TP630 pancreas tissues had decreased *Tip30* mRNA levels compared to K30$^{+/+}$C mice (not shown). Upon more thorough investigation and sequencing, we confirmed that TP576 and TP627 had a copy of the mutant allele. Insertion and deletion mutations were identified by sequencing using specific primers that annealed and amplified the mutated region. We confirmed the presence of the *LacZ* sequence in these two mice (not shown); therefore, we reassigned them to the K30$^{+/-}$C group.

To evaluate if the genetic alteration of *Tip30* copy number loss altered Tip30 gene expression in K30C mice, we isolated mRNA from pancreas tissues of age-matched K30C mice with validated *Kras^{G12D}* status. We assessed Tip30 mRNA levels using real-time quantitative reverse transcription (RT)-PCR and found that K30$^{+/-}$C pancreata exhibited a significant decrease in mean Tip30 expression levels when compared to K30$^{+/+}$C pancreata at exons 2-3 (n=6, p=0.007 by Student's t-test) (**Figure 11A**). Tip30 mRNA was not detectable (ND) in K30$^{-/-}$C pancreata (**Figure 11A**). We further confirmed the decrease in Tip30 pancreas

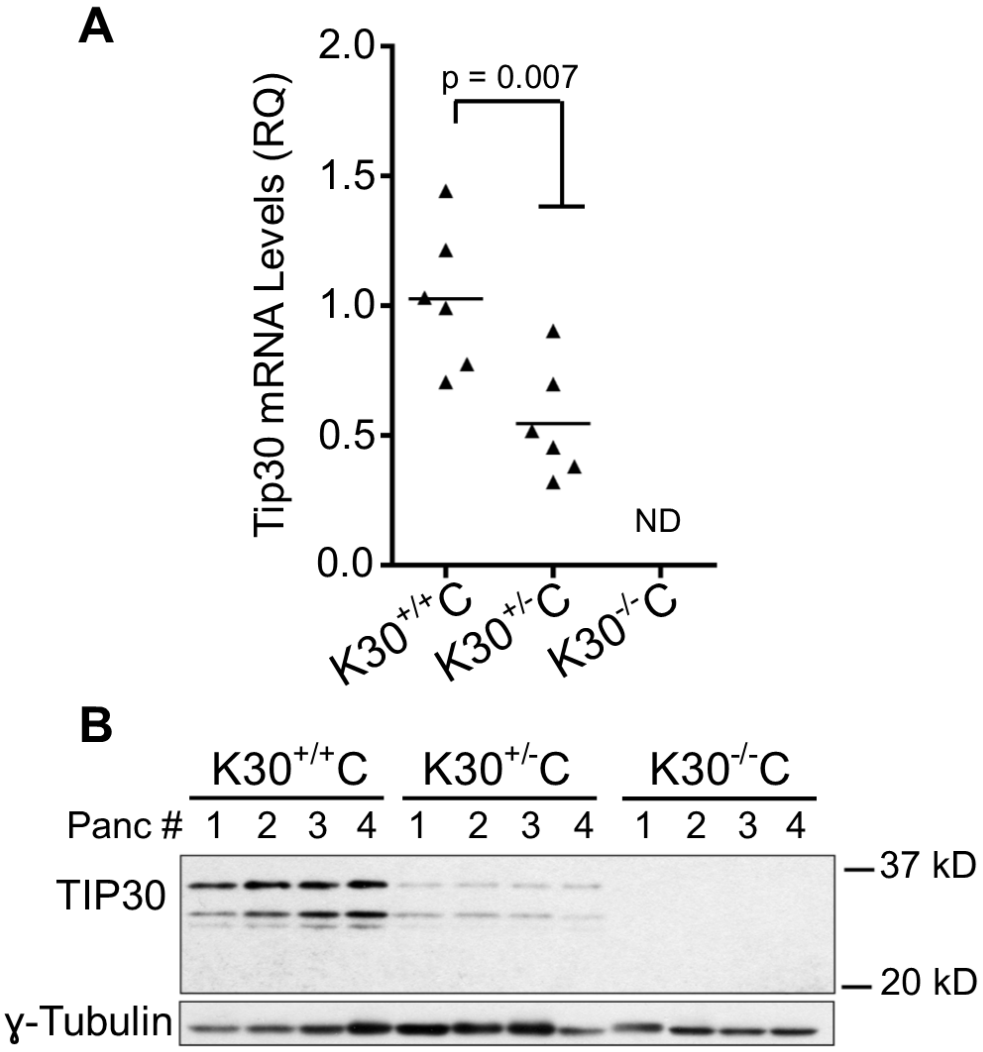

Figure 11. TIP30 levels are decreased in K30$^{+/-}$C and K30$^{-/-}$C pancreata

(A) Relative quantity of Tip30 exon 2-3 mRNA levels by qRT-PCR in murine pancreas tissues from an age-matched three-month-old K30$^{+/+}$C-TP578, TP579, TP580, TP197, TP228, TP581, K30$^{+/-}$C-TP431, TP452, TP468, TP470, TP473, TP684, and K30$^{-/-}$C -TP526, TP543, TP555, TP336, TP400, TP404, TP364 mice (n=6). Relative expression levels were calculated after normalization to internal loading control Rps6. Data is represented relative to K30$^{+/+}$C controls. RQ, Relative quantity. ND, not detected. **(B)** TIP30 protein levels in three-month-old pancreas tissues (Panc) from K30$^{+/+}$C-TP578, TP579, TP580, TP58, K30$^{+/-}$C-TP452, TP468, TP470, TP473, and K30$^{-/-}$C-TP364, TP526, TP543, TP555 mice (n=4). The TIP30 antibody used detects the two major isoforms of TIP30 (30 kD, and 27 kD). γ-Tubulin is the loading control.

tissue gene expression by analyzing Tip30 exon 6 mRNA levels (**Appendix C2.B**). Tip30 exon 6 mRNA levels were significantly decreased in pancreas tissues from $K30^{+/-}C$ mice (ages 2-3 months), when compared to $K30^{+/+}C$ controls (n=4, p=0.006, by one-way ANOVA and Tukey post-hoc test).Tip30 mRNA levels were negligible in $K30^{-/-}C$ mouse pancreata when compared to $K30^{+/+}C$ (n=4, p<0.001, **Appendix C2.B**). When compared to $K30^{+/-}C$ pancreata, $K30^{-/-}C$ mice also exhibited significantly decreased Tip30 exon 6 mRNA levels in pancreas tissues (n=4, p=0.025) (**Appendix C2.B**). In addition to mRNA analysis, we verified that TIP30 protein levels were also decreased in *Tip30*-deficient K30C mice. Western blotting analysis confirmed that pancreata from $K30^{+/-}C$ had decreased TIP30 protein levels, and that $K30^{-/-}C$ mice had undetectable levels of TIP30 (**Figure 11B**) suggesting that $K30^{-/-}C$ mice were *Tip30*-null. The decrease of TIP30 protein levels in the pancreas tissue of $K30^{+/-}C$ mice appeared to be more than half (**Figure 11B**).

To ensure that *Tip30* loss did not affect islet architecture, we compared immunohistochemistry immunofluorescent (IHC-IF) staining of amylase, glucagon, and insulin in pancreas tissues from three-month-old $K30^{+/+}C$ mice (n=4) to that of $K30^{+/-}C$ (n=4) and $K30^{-/-}C$ (n=2) mice (**Figure 12**). We examined five high-power fields per animal and observed expected distributions of amylase, glucagon, and insulin in the pancreas parenchyma in the analyzed mice from all three groups. We did not detect any notable alterations in the pancreas architecture of the endocrine and exocrine compartments. *Tip30*-deficient/KC groups had a few enlarged islets. We quantitated islet areas with Image J using 20X (high-power) images from five separate fields per mouse for four $K30^{+/+}C$ mice, four $K30^{+/-}C$

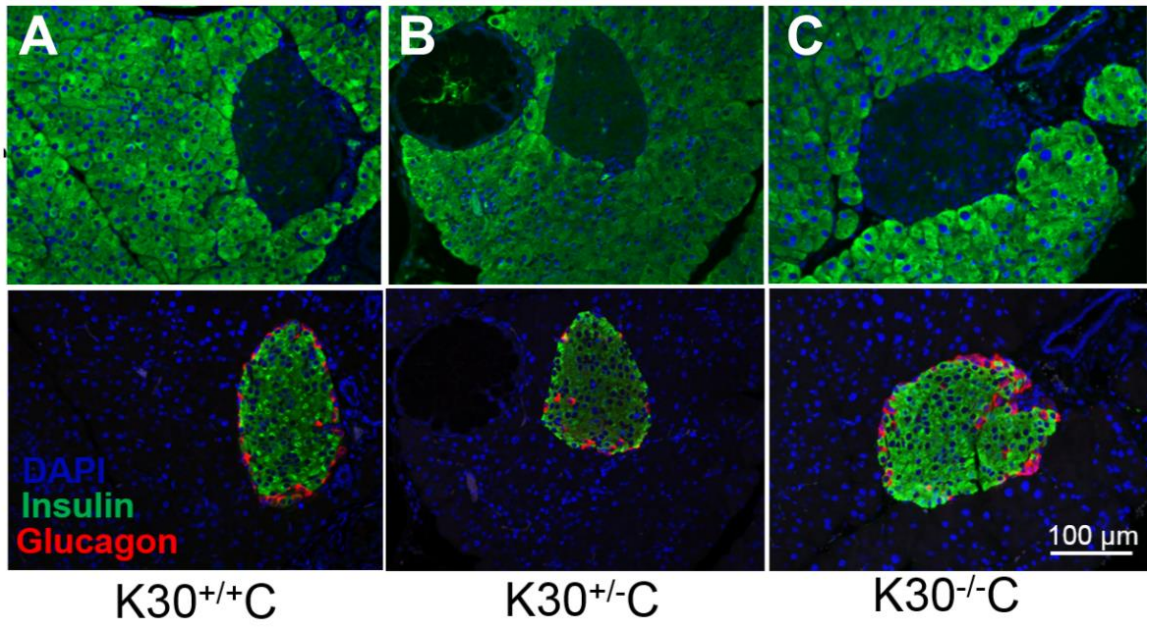

Figure 12. Loss of *Tip30* in the KC background did not alter the architecture of the endocrine and exocrine compartments

IHC-Immunofluorescence (IF) staining for amylase (green, top row), insulin (green, lower panel) and glucagon (red, lower panel), with DAPI nuclear stain (blue) in three-month-old pancreas tissue from $K30^{+/+}C$ (n=4), $K30^{+/-}C$ (n=4), $K30^{-/-}C$ (n=2) mice did not reveal any significant differences in insulin, glucagon, or amylase distribution between groups. A representative field from a stained section for $K30^{+/+}C$ (mouse ID TP579), $K30^{+/-}C$ (mouse ID TP431), and $K30^{-/-}C$ (mouse ID TP526) mice is shown. Scale bar: 100 µm. These images were evaluated with a pathologist.

mice, and two K30$^{-/-}$C mice. There was an increased trend in mean islet size from 0.375 (K30$^{+/+}$C) to 0.72 (K30$^{+/-}$C), and 0.72 (K30$^{-/-}$C), respectively. However, these quantitated differences were not significant; this could be due to small sample size.

3.2.6 Heterozygous-*Tip30* Loss Accelerated PDAC-Associated Death in K30C Mice

A series of experiments were initiated to evaluate *Tip30* genetic dose on PDAC formation in the KC background. We hypothesized that *Tip30* loss accelerates murine PDAC (mPDAC) progression, and leads to poor survival outcomes in *Tip30*-deficient, K30C mice. To assess the impact of *Tip30* loss on pancreas lesion progression, we first compared pancreas sections from three-month-old KC mice that were *Tip30*-heterozygous (K30$^{+/-}$C), *Tip30*-null (K30$^{-/-}$C), or *Tip30*-wild-type (K30$^{+/+}$C). Prior to necropsy, total body mass was recorded for each mouse. We observed no difference in mean total body mass between K30$^{+/+}$C and K30$^{+/-}$C mice. However, K30$^{-/-}$C mice weighed roughly five grams less than the other two groups of mice (n=7-10 mice per group), but this result was not statistically significant (**Appendix C3**). Mouse pancreas tissues were visually inspected at the time of necropsy and mice that were three months of age did not show any indication of tumor formation, other than an occasional large pancreata (**Appendix C3**).

Although pancreatic tumor formation was not detectable by gross observation at three months, we observed a decline in health in some of the *Tip30*-deficient K30C mice compared to controls and three-month-old K30$^{+/+}$C mice. *Tip30* copy-number loss was associated with an increase in morbidity-related

symptoms in K30C mice. Specifically, two of seven $K30^{+/-}C$ mice and four of ten $K30^{-/-}C$ mice presented with a hunched, scruffy coat, and difficulty breathing or "sick" status compared to one of the seven three-month-old $K30^{+/+}C$ mice, and were required to be euthanized at three months of age. We therefore hypothesized that the overall decline in health for *Tip30*-deficient K30C mice was a result of PDAC-associated neoplasia, undetectable by methods of gross observation.

We next utilized immunohistochemistry and light microscopy to further evaluate the pancreata of K30C mice. To assess the role of *Tip30* loss on mPDAC initiation and precursor lesion progression in K30C mice, we examined the histological sections from at least six mice per three-month-old $K30^{+/+}C$, $K30^{+/-}C$, and $K30^{-/-}C$ cohorts. To better visualize pancreatic cancer precursor lesion formation and PDAC we used an antibody specific to the pancreatic cancer cell epithelial marker cytokeratin 19 (CK-19). This staining was followed by a hematoxylin counterstain to discern pancreatic intraepithelial neoplasia (PanIN) lesion formation and PDAC from normal parenchyma. CK-19 marks the presence of pancreatic cancer cells in PDAC tissues (Jain et al., 2010; Preis et al., 2011).

We examined low-power and at least five high-power fields for each mouse and noted the abundance of CK-19 stain per field as well as any changes in pancreatic ductal architecture that were distinct from a normal duct. Since the KC mouse model utilizes both the genetic and histopathological progression of human PDAC we used the progression model illustrated in Figure 2 of Bardeesy and DePinho (2002) and Hezel et al. (2006) as a reference to identify normal pancreatic ducts from pancreatic precursor lesions such as PanIN and PDAC. We observed

an increase in CK-19-positve pancreatic precursor lesion formation in compound mutant *Tip30*-heterozygous KC mice ($K30^{+/-}C$), compared to both $K30^{+/+}C$ and $K30^{-/-}C$ mice in our three-month-old validated cohorts (**Figure 13A**). A total of six mice were evaluated per group and a representative field per mouse for four mice per group is included in **Figure 13A**.

Our initial hypothesis would suggest that $K30^{-/-}C$ mice will have similar or more advanced pathology than mice with monoallelic loss of *Tip30* ($K30^{+/-}C$). To our surprise, three-month-old $K30^{-/-}C$ mice presented with little to no lesion formation, by CK-19 staining. Our assessment of additional serial sections for the three-month-old cohorts did not appear to provide any evidence for additional lesions in $K30^{-/-}C$ mouse tissues that may have not been captured in the first section of tissue examined. Serial sectioning of 24 additional sections was performed by Rachael Topolski, a member of our laboratory. We stained section No. 11, 12 and 23, 24 for CK-19/hematoxylin stain, but found no major differences from our initial observations.

To assess PDAC formation due to KC background alone, we evaluated hematoxylin and eosin (H&E)-stained sections from $K30^{+/+}C$ mice at different time points with a pathologist. We used histopathological analysis of one section of pancreata collected at necropsy from $K30^{+/+}C$ mice aged two to six months to assess pancreas pathology. PanIN lesions and PDAC initiation were variable within age groups; however, we observed an increased grade of PanIN lesions as a function of age as well as complete penetrance of PDAC in $K30^{+/+}C$ mice by six months of age (n=2/2). One mouse out of 3 two-month-old $K30^{+/+}C$ mice presented

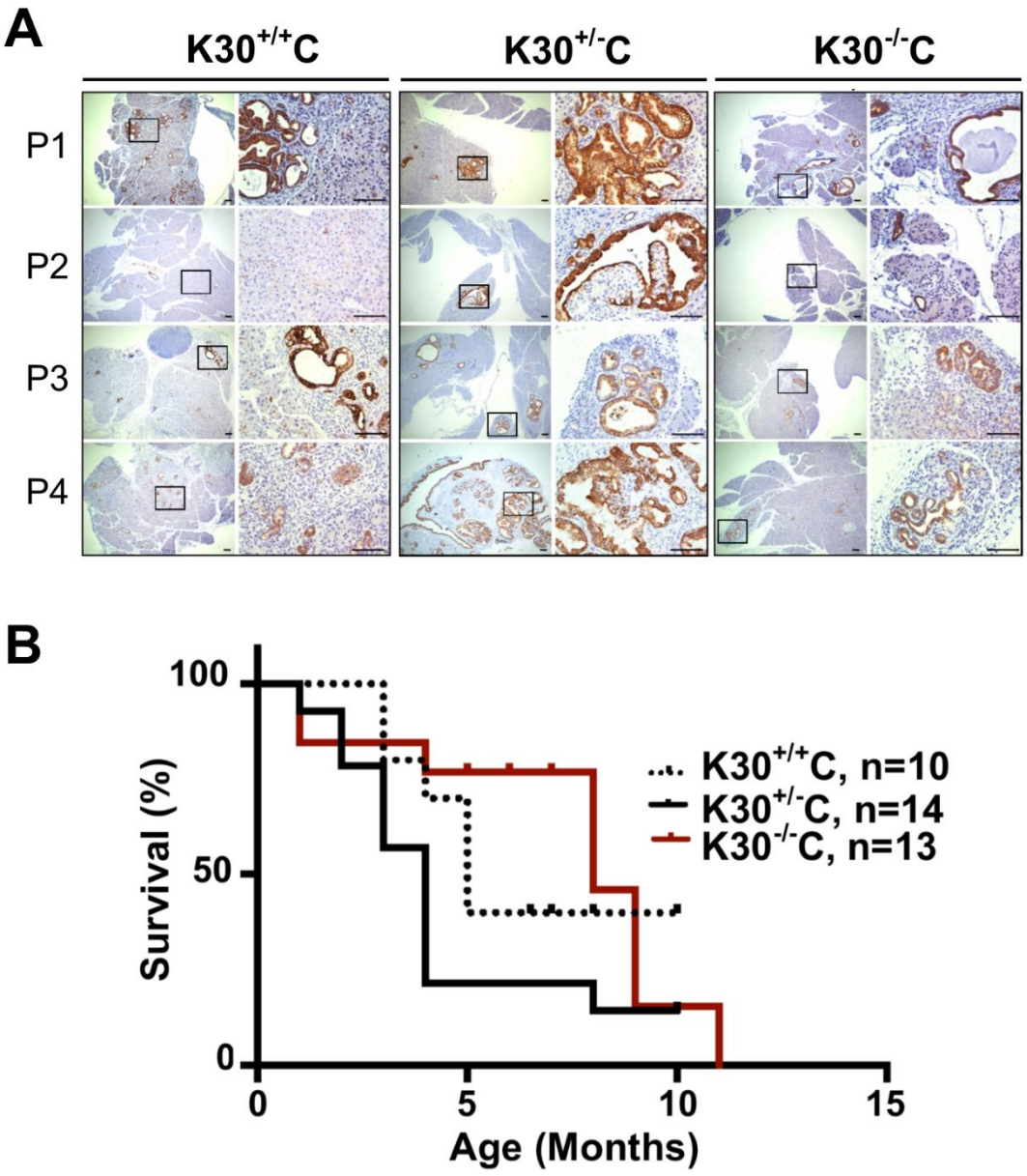

Figure 13. Survival analysis of CK-19-positive PDAC precursor lesions in the K30C mouse model

(A) CK-19 staining of pancreas specimen from three-month-old *Kras*^{G12D};*Pdx1-Cre*;*Tip30*$^{+/+, +/-,}$ or $^{-/-}$ (K30C) mice. A representative field of pancreas tissue is shown per mouse (P1-4), and pancreas lesions from four mice per genotype are shown, with low and high magnification (n=6). Five high-power fields were imaged per mouse: K30$^{+/+}$C (TP228, TP578, TP579, TP581), K30$^{+/-}$C (TP431, TP452, TP468, TP470, and K30$^{-/-}$C mice. Scale bars: 100 µm. **(B)** Survival curve (Kaplan-Meier) of the *Kras*^{G12D};*Pdx1-Cre*;*Tip30*$^{+/+}$ (K30$^{+/+}$C), *Kras*^{G12D};*Pdx1-Cre*;*Tip30*$^{+/-}$ (K30$^{+/-}$C), and *Kras*^{G12D};*Pdx1-Cre*;*Tip30*$^{-/-}$ (K30$^{-/-}$C) cohorts. Mice that were still alive at the conclusion of the study are represented as tick marks that appear on the Kaplan-Meier curves as "censored" (see Rich et al., 2010; Goel et al., 2010) observations. The total sample size in these Kaplan-Meir curves (including censored mice) are as follows: K30$^{+/+}$C: n=10, K30$^{+/-}$C: n=14, K30$^{-/-}$C: n=13. Log-rank, p=0.1149.

with the beginnings of PDAC, while the remaining two-month-old mice (n=2/3) presented with early PanIN lesions (PanIN-1B). At three months of age, 4 out of 7 $K30^{+/+}C$ mice examined had either a detectable PanIN-3 precursor lesion, the beginning of PDAC, or both. The PDAC histology for one of these mice took up the vast majority of the pancreas parenchyma (n=1/7). At four months, all $K30^{+/+}C$ mice presented with PanIN-3 (n=3/3), with cancer localized in the pancreatic duct detected in 1 of the 3 mice. In the five-month cohort, 3 out of 4 five-month-old $K30^{+/+}C$ mice presented with PanIN-2 and -3 lesions. Moreover, 2 out of 2 six-month-old $K30^{+/+}C$ mice presented with full-blown PDAC, with a focal area of lymph node metastasis in one of these two mice (TP177). Even though PDAC metastasis has been reported in a 6.25-month-old *Kras*^{G12D};*Pdx1-Cre* (KC) mouse by Hingorani et al. (2003), overall progression to PDAC in the KC mouse model is slow (Westphalen and Olive, 2003). Both six-month-old $K30^{+/+}C$ mice either had visible evidence of tumor formation (TP177) or a cystic appearing pancreatic tumor that was 15-20 mm in diameter (TP182). Because we did not expect to see PDAC cases in $K30^{+/+}C$ mice at six months, we genotyped for a panel of transgenes to exclude the possibility of additional GEMMs accidentally crossed into our model (**Appendix A**). We also submitted DNA samples, isolated from cell lines established from two different mouse pancreata per genotype ($K30^{+/+,\ +/-,}$ and $^{-/-}C$), for whole genome sequencing. We did not detect any transgene contamination or spontaneous mutations in our mouse model.

In Hingorani et al. (2003), PanIN-2 and PanIN-3 presentation was not abundant until *Kras*^{G12D};*Pdx1-Cre* (KC) mice reached nine months of age

(Hingorani et al., 2003); therefore, the PDAC progression observed in our $K30^{+/+}C$ mice occurred at a more advanced rate. Using the $K30^{+/+}C$ mice as our point of comparison, we next proceeded to further evaluate the increase in CK-19-positive lesions observed in $K30^{+/-}C$ mice and depicted in **Figure 13**. Following pathological analysis, we compiled a summary of the histological landscape and spectrum of PDAC precursor lesions in each group of K30C mice (**Table 2**). We visually scanned and examined entire mouse pancreas sections for each mouse in our three-month-old cohorts ($K30^{+/+}C$, $K30^{+/-}C$, $K30^{-/-}C$) at low and high power with a pathologist. At least seven mice per cohort were examined for microscopic evidence of preinvasive and invasive ductal PDAC. To determine the distribution of PDAC precursor lesions and PDAC between groups of K30C mice we evaluated high power images of CK-19 and H&E stains for at least five distinct focal areas per section. Areas of ductal atypia, hyperplasia, acinar to ductal metaplasia, focal areas of pancreatic intraepithelial neoplasia (PanIN), PDAC, and additional PDAC-associated disease were evaluated and noted in the report by our pathologist. For mice diagnosed with PanIN, further analysis of high powered fields were used to determine the highest grade of PanIN lesion per focal area. **Table 2** summarizes the pathology detected in the pancreas of each mouse, with the grade of PanIN lesion (from PanIN-1 to PanIN-3) indicated. If tissues appeared normal they were marked as such; and if PanIN lesion or PDAC was detected the occurrence (intensity level or density) was noted. For example, a distinction was made between PDAC that the pathologist noted was just beginning but was in too early stages to be diagnosed as such (half X in **Table 2** or level 0.5 intensity), moderate

Table 2. Histopathological detection and distribution of PDAC precursor lesions and PDAC-associated disease in three-month-old K30C mice

			Pancreas									
	Mouse ID	Age (Months)	Normal	Ductal Atypia/ Hyperplasia	ADMs	PanIN-1	PanIN-2	PanIN-3	PDAC	Inflam-mation	Reactive Lymph/Lymph Met	Lung/ Organs
$K30^{+/+}C$	TP197	3						X	XXXX			
	TP228	3		X				X		X		
	TP578	3		X		X				X		
	TP579	3							X			
	TP580	3		X						X		
	TP581	3				X	X	X	X	X		
	TP651	3			X		X					
$K30^{+/-}C$	TP223	3		X					X	X	X	
	TP431	3					X				X	X
	TP452	3					X	XX				X
	TP468	3					X	X				
	TP470	3						XXX	XXX		XX	
	TP473	3		X			X	XX		X		X
	TP684	3	X									
$K30^{-/-}C$	TP279	3							X			
	TP316	3						X		X		
	TP336	3		X								
	TP364	3		X					X	X		
	TP400	3	X									
	TP404	3			XX			X				
	TP526	3	X						X			
	TP543	3		X						X		
	TP555	3	X									
	TP569	3		X								

PDAC progression and PDAC-associated disease including lymph node spread in three-month-old K30C mice after consultation with a pathologist. Each X represents a focal area of lesion/s detected. One intact "X" represents incidence or one focal area for the entire tissue section (and =1) and indicates that the event occurred. Half of an X indicates that PDAC was reported to be beginning, but a definitive PDAC diagnosis could not be made. Half of an X (intensity level=0.5) is the lowest level of PDAC intensity observed in K30C mice. The number of X's represents the intensity or occurrence for the indicated lesion/pathology per mouse (and pancreas tissue section). An intensity level 4 (four "X"'s) represents the highest incidence of focal areas with lesions and the highest lesion intensity per mouse. PanIN, pancreatic intraepithelial neoplasia. Note the detection of affected organs (lungs) in $K30^{+/-}C$ mice compared to $K30^{+/+}C$ and $K30^{-/-}C$ mice (n=7-10). Lymph, lymph node. Lymph Met, lymph node metastasis.

PDAC, or full-blown PDAC (four X's in **Table 2** or level 4 intensity). For PanIN occurrence, if a mouse had three different focal areas of PanIN it was assigned three X's or a level 3 intensity value; two focal areas were assigned two X's or a level 2 intensity value, etc. For pancreas sections with less than five focal areas, the areas with highest grade lesions in the entire tissue section were assessed. A visual representation of average lesion and PDAC density and distribution, noted in **Table 2,** is presented in heat map form in **Figure 14.** Average lesion intensity in the heat map does not include individual mice that did not present with a focal lesion per indicated lesion category (ductal atypia, PanIN-1, PanIN-2, PanIN-3, PDAC, Inflammation, Lymph node involvement), except for the level 0 depiction. Level 0 or dark blue shading indicates that there were zero mice that had said lesion or pathology type (**Figure 14**). The majority of the pancreas sections used for **Table 2** were CK-19-stained (n=6), however hematoxylin and eosin (H&E) stained sections were also examined (**Table 2**). If a mouse had both an H&E section and a CK-19 section and a lesion was only detected in one of the two sections, then the mouse was observed to have had incidence of the reported lesion and the data was added to the summary in **Table 2.**

Based on our compiled observations, 71.4% of $K30^{+/-}C$ mice (n=6/7) had either a detectable PanIN-2, an abundance of PanIN-3 lesions or PDAC (n=2/7, **Table 2**). Comparatively, $K30^{+/+}C$ mice also presented with PanIN-2 to PDAC in at least one focal area at a rate of 71.4% incidence (n=5/7). However, in contrast to $K30^{+/-}C$ mice, $K30^{+/+}C$ (n=4/7) and $K30^{-/-}C$ (n=2/10) mice presented with a modest distribution of PanIN-2 and PanIN-3 lesions per mouse. The lesion density and

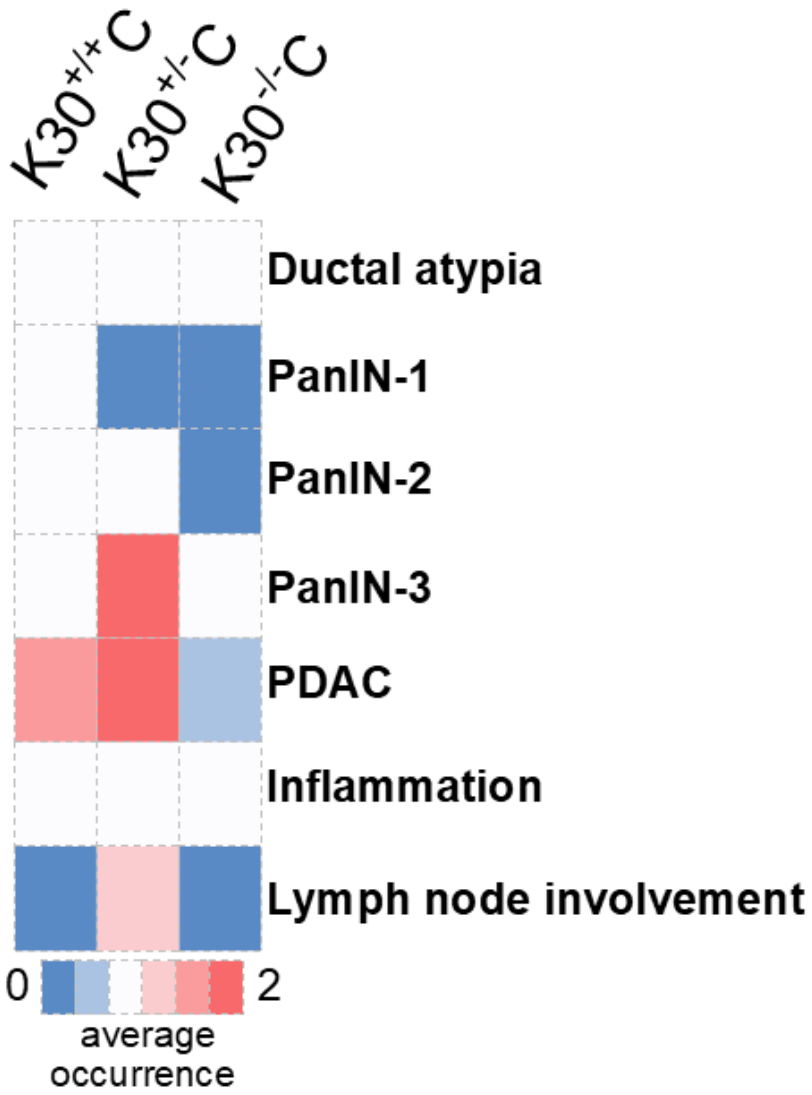

Figure 14. Representation of lesions identified per histopathological grade across the K30C mouse models at three months

$K30^{+/-}C$ mouse pancreatic tissue sections with at least one focal area of pathology exhibited the highest average occurrence of PanIN-3, PDAC, and invasive or metastatic PDAC to the lymph node (Lymph node involvement) as compared to $K30^{+/+}C$ and $K30^{-/-}C$ groups. Data represented in this heat map are a graphical representation of the average occurrence in pathology-positive $K30^{+/+,}$ $^{+/-,}$ and $^{-/-}C$ mice (mice in which an incidence was detected). Only mice with an occurrence were used to calculate average occurrence and lesion distribution/density (also referred to as intensity). An average occurrence of 0 (dark blue) indicates that there were no mice in that group with the indicated pathology. Average occurrence was calculated using the data in **Table 2**, where a pathologist noted focal area incidence as well as the level of lesion occurrence per mouse in three-month-old $K30^{+/+,}$ $^{+/-,}$ and $^{-/-}C$ groups (n=7-10). For this heat map, the scale of average occurrence ranges from lowest (0 or dark blue shading) to highest (2 or dark red shading). Mice with a noted intensity level of at least 0.5 (half an X in **Table 2**) were included in the averages represented in this heat map. The average values represented in the scale from lowest to highest are as follows: 0, 0.5, 1, 1.33, 1.67, and 2.

distribution is represented as an average in the heat map in **Figure 14**. The average occurrence of intensity of lesion per type is represented as lowest (dark blue or an average value of 0) to highest (dark red or an average value of 2) (**Figure 14**). Briefly, to calculate average intensity, mice with lesions per category in **Table 2** received a numerical value for each "X" or occurrence. Half of an "X" represents the lowest level of intensity observed and was assigned a value of 0.5. One "X" was assigned a value of 1, two "X"'s were assigned a value of 2, etc. These values were then averaged to represent the average lesion intensity for mice with at least one detectable lesion per indicated category. Lastly, a color scale was distributed across all of the averaged data for the three groups ($K30^{+/+, +/-,}$ and $^{-/-}$C).

While the percent incidence (development of a focal area) of PanIN-3 or PDAC did not differ between $K30^{+/+, +/-,}$ and $^{-/-}$C groups (**Table 2**), there was a striking difference in $K30^{+/-}$C lesion intensity for PanIN-3, PDAC, and lymph node involvement compared to $K30^{+/+}$C and $K30^{-/-}$C mice (**Table 2**, **Figure 14**). For K30C mice that presented with lesions, *Tip30*-heterozygous K30C mice had the highest level of PanIN-3 and PDAC (Figure 14). PanIN-3 lesions were more commonly found in patients diagnosed with PDAC (Konstantinidis et al., 2013). *Tip30*-heterozygous K30C mice also exhibited the most advanced PDAC-associated disease. Specifically, four $K30^{+/-}$C mice had moderate to high distribution of PanIN-2 to PDAC (n=4/7, **Table 2**); and two of those $K30^{+/-}$C mice (n=2/7) had either PDAC-associated lymph node invasion or metastasis when compared to $K30^{+/+}$C (n=0/7) and $K30^{-/-}$C (n=0/10) mice (**Figure 15-16**). Mice with

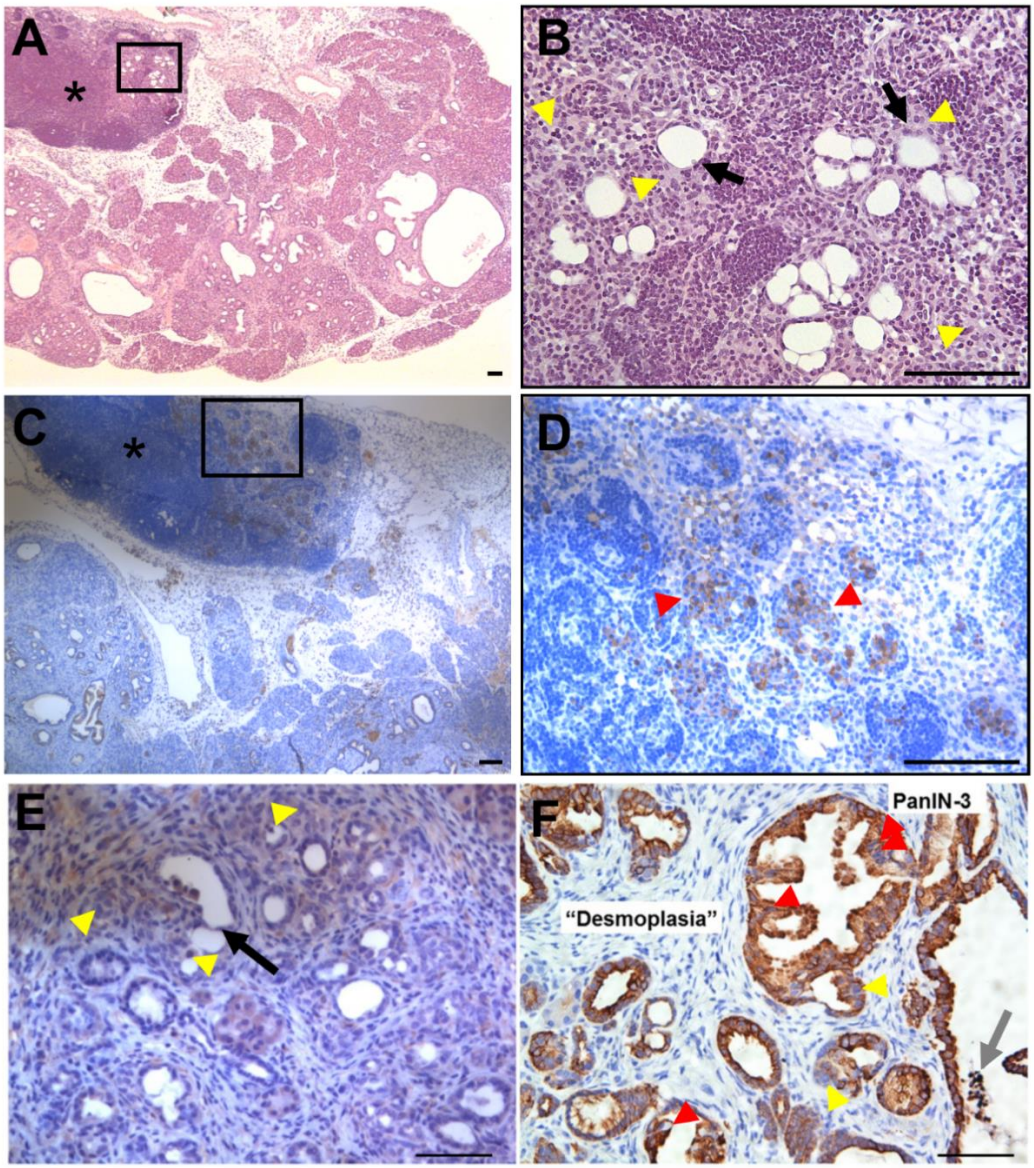

Figure 15. PDAC-associated lymph node metastasis was detected in a three-month-old K30$^{+/-}$C mouse

(A) Hematoxylin and eosin (H&E) staining of a pancreas section from a K30$^{+/-}$C mouse with more than 50% PDAC and lymph node metastasis at three months of age. Mouse ID is TP470. **(B)** Higher magnification of lymph node metastasis detected in **A**. Yellow arrow heads point to pancreatic cancer cell invasion in lymph node and black arrows point to a duct-like PDAC phenotype. **(C)** Representative image of cytokeratin-19 (CK-19) with hematoxylin counter-stain of TP470 pancreatic lesions and PDAC and CK-19-positive pancreatic cancer cells (PCCs) in pancreas and lymph node. **(D)** Higher magnification of lymph node region in **C**. Red arrow heads point to CK-19-positive PCCs. Lymph node is marked with asterisk. **(E)** Alpha-SMA stain with gland-gland presentation (black arrow) and PCC invasion (yellow arrow heads). **(F)** CK-19 stain of pancreas section with a noted pancreatic intraepithelial neoplasia (PanIN)-3 lesion and haphazard growth pattern (desmoplasia). Necrotic glandular debris (gray arrow), loss of nuclear polarity (red arrows), and nuclear irregularities (yellow arrow heads) were also observed. These images were evaluated with a pathologist and Hruban et al., 2006 was used as a reference. Mouse ID for this figure is TP470. Scale bars: 100 µm

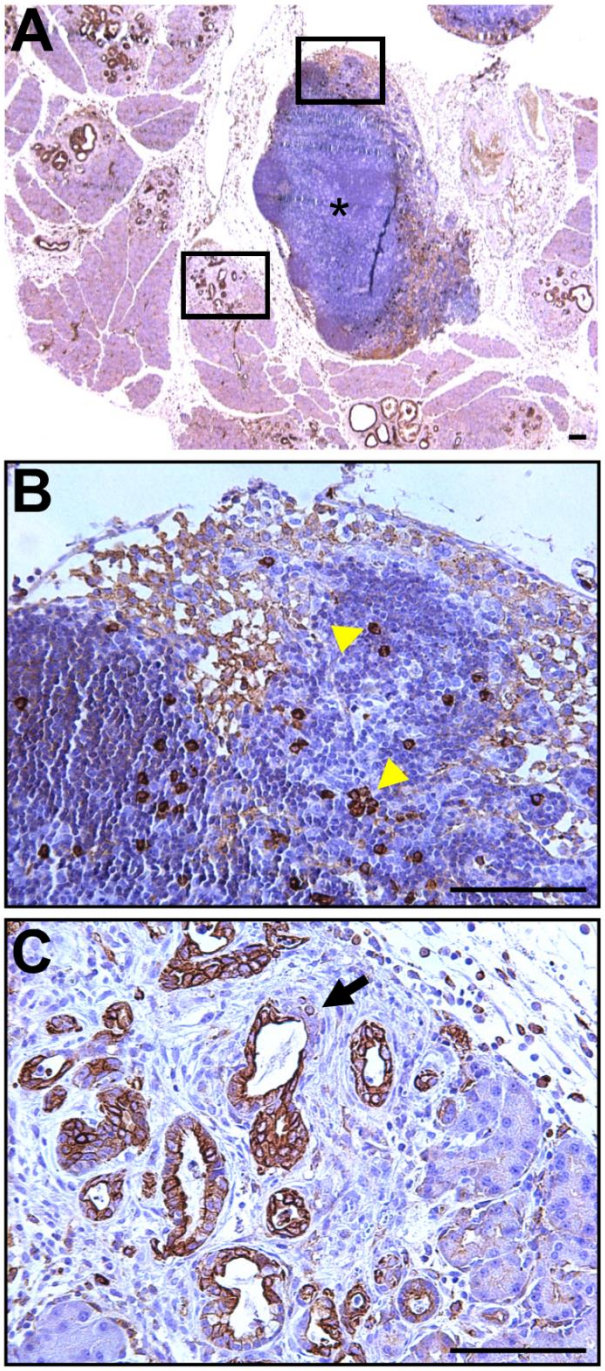

Figure 16. Early PDAC and lymph node invasion in a K30$^{+/-}$C mouse

(A) Representative low-power image of a CK-19 with hematoxylin counter-stained section of pancreas tissue from a three-month-old mouse with PDAC and lymph node invasion. Mouse ID is TP223**.** Lymph node is marked with asterisk. **(B)** Higher magnification of subcapsular lymph node invasion in **A**. Yellow arrow heads point to stained macrophages. **(C)** Higher magnification of PDAC focal area in **A**. Black arrow points to ductal differentiation. These images were evaluated with a pathologist. Scale bars: 100 µm.

detected inflammation in pancreas tissues had equal levels of inflammation across K30$^{+/+,\ +/-,}$ and $^{-/-}$C groups. There was a third K30$^{+/-}$C mouse in the three-month study for which a reactive lymph node was noted (**Table 2**-Mouse ID TP431). Although, examination of the pancreas section from mouse TP431 revealed only one focal area with a PanIN-2 lesion (**Table 2**, see **Figure 13**-K30$^{+/-}$C-P1), TP431 and another K30$^{+/-}$C mouse with detectable PanIN-3 (TP452) displayed strong mucin immunoreactivity in focal areas of high-grade PanIN formation by alcian blue stain (**Appendix C4.C-D**), as compared to K30$^{+/+}$C mice. Mucins are glycoproteins that are reported to enhance PDAC tumorigenesis and metastasis (Kaur et al., 2013). Whether the strong mucin staining observed in the precursor lesions of the two K30$^{+/-}$C mice was linked to lymph node involvement and metastatic disease cannot be stated with certainty. Additional staining of mouse pancreas sections from each group with quantitation, as well as assessing the mRNA and protein levels from these tissues would help determine the differences in mucin expression profiles between K30$^{+/+,+/-}$, and$^{-/-}$C mice, and the role of mucin in accelerating *Tip30*-heterozygous disease progression and metastasis in the K30C model.

We also examined additional K30C mice from as young as five weeks old to 11 months old but were limited by sample size to draw any definitive conclusions for PDAC progression or compare lesions between groups of K30C mice at additional timepoints. The pathologist did however detected an enlarged lymph node in the section of pancreas tissue from a five-month-old K30$^{+/-}$C mouse (TP573) in the examination. The pathologist noted that this particular lymph node was 20 times (20X) the size of a normal lymph node. This mouse had a detectable

PanIN-3 lesion and had focal areas that were approaching PDAC pathology. Further staining is required to accurately assess any metastatic disease in the lymph node by histological analysis for this mouse. A pancreatic cancer cell line was established from the pancreas of this TP573 mouse and used for further studies documented in this report (Table 4). More mouse pancreata will need to be examined and rigorously scored for a true quantitative assessment of differences in PDAC progression between $K30^{+/+}C$ and $K30^{+/-}C$ mice and substantiate a role for *Tip30*-heterozygous loss in accelerating the molecular landscape of PDAC in the K30C PDAC model. In summary, the advanced CK-19 positive lesions, abundance in PDAC precursor lesion in $K30^{+/-}C$ mice compared to other groups, and evidence of lymph node invasion and metastasis led us to interpret that monoallelic loss of *Tip30* accelerated pancreatic neoplasia in our K30C mouse model. Lesion density (the amount of lesions or focal areas of lesions reported per lesion or pathology type-"average occurrence" in **Figure 14**) and advanced PDAC-associated disease (detection of lymph node invasion or metastasis in a pancreas tissue section, **Table 2, Figure 14**) suggested that $K30^{+/-}C$ mice had advanced PDAC-associated disease progression when compared to $K30^{+/+}C$ and $K30^{-/-}C$ mice.

Surprisingly, according to the histopathological analysis and average occurrence, $K30^{-/-}C$ displayed the lowest level of PDAC intensity (**Figure 14**); this combined with the results from the survival analysis (**Figure 13B**) suggested that $K30^{-/-}C$ mice were protected at earlier timepoints (**Figure 14**). $K30^{-/-}C$ mice exhibited the highest overall median survival of the three K30C groups of mice:

eight months (n=10-14) as compared to five months ($K30^{+/+}C$) and four months ($K30^{+/-}C$). In addition, $K30^{-/-}C$ mice also exhibited the highest five-month survival (77%, n=13) compared to 40% in the $K30^{+/+}C$ group (n=10) and 21% in the $K30^{+/-}C$ group (n=14) of mice (**Figure 13B**). Therefore, predictably, the $K30^{-/-}C$ group of mice had the highest presentation of normal parenchyma or very low grade ductal atypia or hyperplasia in focal areas (n=7/10) compared to $K30^{+/-}C$ (n=3/7) and $K30^{+/+}C$ (n=3/7) at three months (by histopathological analysis). Based on the pathology analysis, the majority of $K30^{-/-}C$ mice also only presented with the beginning stages of PDAC and no further disease, suggesting a latency to PDAC formation in this group compared to the other K30C groups. We hypothesize that complete loss of *Tip30* protected K30C mice from PDAC disease progression at earlier timepoints. On the other hand, because 50% of $K30^{-/-}C$ mice exhibited PanIN-2-PDAC incidence (n=5/10), albeit at low levels of average occurrence, PDAC may have been initiated but the progression to clinical manifestation may have been delayed for reasons we could not explain in the scope of these studies.

In summary, the histopathological analysis reported in **Table 2** and average occurrence (**Figure 14**) in our K30C mouse models suggested that one copy loss of *Tip30* accelerated PDAC and PDAC-associated disease in a three-month-old cohort of K30C mice. Because phenotypic differences existed between K30C with monoallelic loss of *Tip30* and K30C mice that were *Tip30*-null we hypothesized that *Tip30* copy number or dose mediates disease progression in the K30C mouse model. Additional mice with a quantitative comparison of lesions between groups are needed to determine if the differences we observed between groups are

statistically significant. We could not explain the advanced progression to PDAC observed in K30$^{+/+}$C mice, however we predict that this advanced progression may have contributed to our inability to observe significant differences in PDAC incidence between our groups of mice. To address these concerns we need to compare equal numbers of mice at earlier time points (one to two months), in a pure, congenic background to minimize variability.

In our characterization of the *Tip30*-deficient K30C mouse models, we also assessed the role of *Tip30* loss in PDAC-associated survival. Decreased *Tip30* expression was linked to lymph node metastasis and poorer overall survival in a cohort of 106 chemotherapy and radiation therapy-naïve PDAC patients (Guo et al., 2014). We used the Kaplan-Meier estimate of survival to analyze non-breeder *Tip30*-deficient K30C mice (K30$^{+/-}$C and K30$^{-/-}$C), compared to K30$^{+/+}$C mice that were generated internally. 30$^{-/-}$ and 30$^{+/-}$ internal, littermate controls were also observed. Mice were monitored up to 12 months, except as indicated in section 2.23. Towards the end of data collection for the survival analysis, mice that could not be monitored for 12 full months, and were still alive at the end of the study were categorized by the statistical software as “censored” observations. We included in these subjects in our statistical analyses, and as tick marks on the survival curves in **Figure 13B** (see section 2.23 for more details). Time of death was noted when mice became moribund, were requested to be euthanized by veterinary staff, or were found dead.

Our survival analysis revealed that *Tip30*-heterozygous-KC mice (K30$^{+/-}$C) fell sick more rapidly, and early compared to other K30C groups. K30$^{+/-}$C mice

predominately fell sick between 5-16 weeks of age (**Figure 13B**) and exhibited a median overall survival of four months (n=14), as compared to eight months in $K30^{-/-}C$ mice (n=13, p=0.0788, Log-rank) (**Figure 13B**). In comparison to $K30^{+/+}C$ and $K30^{+/-}C$ groups, $K30^{-/-}C$ mice had the highest median survival, suggesting that the $K30^{-/-}C$ genotype was protective, before eight months of age. While *Tip30*-heterozygous-KC mice exhibited a trend for poor survival outcome (n=14), when compared to $K30^{+/+}C$ (n=10) who had a median survival of five months (n=10), and $K30^{-/-}C$ (n=13) mice, the differences in survival between all three groups did not reach statistical significance when assessed by Log-rank test (**Figure 13B**).

Pancreatic tumor development was not visible through gross observation and necropsy in both $K30^{+/-}C$ and $K30^{-/-}C$ mice until five and six months (**Figure 17B-C**, **Table 3**). Although there was a trend for an increase in tumor formation in $K30^{+/-}C$ and $K30^{-/-}C$ mice compared to $K30^{+/+}C$ mice at 5-6 months, the sample size was too small to reach any statistical significance. Interestingly, however, tumors varied in phenotype between both groups (**Figure 17-19**). By gross evaluation, $K30^{+/-}C$ mice presented with mostly pancreatic nodules (**Figure 17**), even at later time points of up to twelve months (**Figure 18A-B**). Later time points consist of our observation of three available mice: a $K30^{+/-}C$ mouse evaluated at twelve months (**Figure 18A-B**), ten months (**Figure 19**), and eight months (**Figure 19**). These data are limited due to an insufficient number of mice evaluated. In a six-month cohort, $K30^{+/-}C$ mice presented with increased detectable pancreatic nodules (n=4/7) as compared to $K30^{+/+}C$ (n=1/6) and $K30^{-/-}C$ (n=2/4) mice (**Table 3**). Overall, $K30^{+/-}C$ mice had firmer pancreatic tissue at younger ages compared

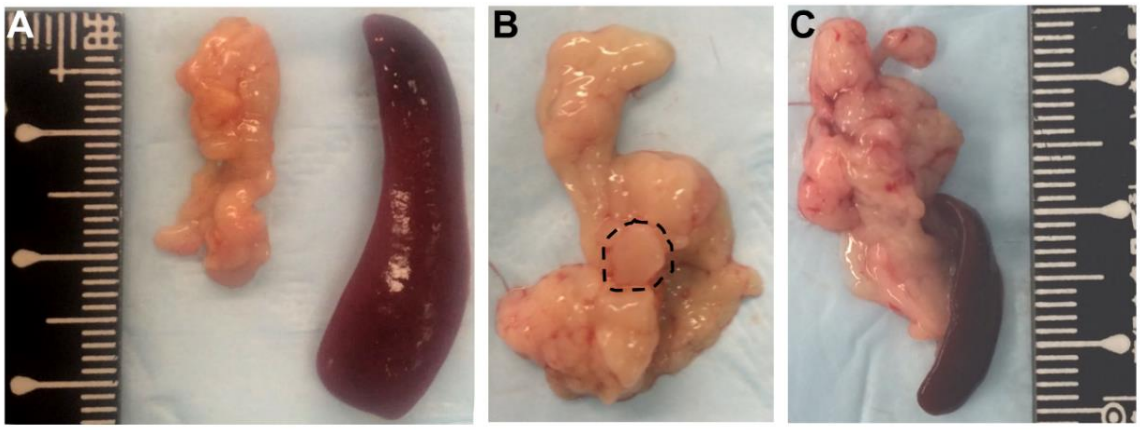

Figure 17. Pancreata from four- to five-month-old K30$^{+/-}$C mice and pancreatic nodule formation

(A) Pancreas and spleen from a four-month old female, TP622, imaged *ex vivo*. **(B)** Pancreas from a five-month old female, TP573, imaged *ex vivo*. Pancreatic nodule outlined with a black dashed circle, not shown to scale. **(C)** Pancreatic tumor formation in a five-month old female, TP544 with spleen still attached. Ruler in mm.

Table 3. Tumor presentation at necropsy in five to six-month-old K30C mice

		Tumor	Cyst*	% Tumor
5 MO	K30$^{+/+}$C	0/5	1/5	0%
	K30$^{+/-}$C	4/9	0	44%
	K30$^{-/-}$C	2/3	1/3	67%
6 MO	K30$^{+/+}$C	1/6	2/6	17%
	K30$^{+/-}$C	4/7	0	57%
	K30$^{-/-}$C	2/4	0	50%

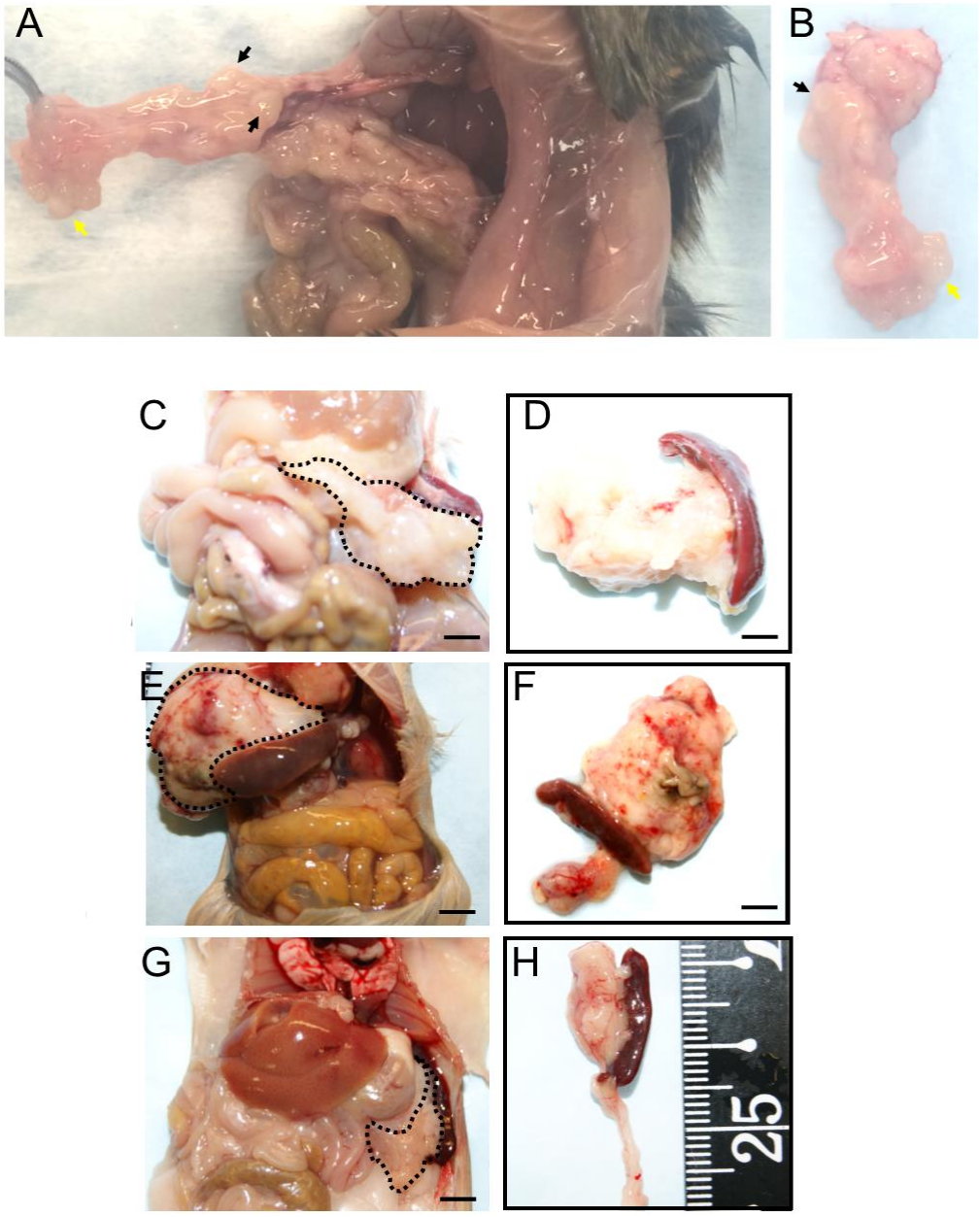

Figure 18. Frank tumor formation in *Tip30*-null K30C and K30Ctd$^{+/-}$ mice

(A) Pancreas *in situ* of 12-month-old K30$^{+/-}$C mouse, TP164. Black arrows point to nodule formation. Yellow arrows point to cystic region. **(B)** Pancreas from **A**, imaged *ex vivo*. **(C)** Pancreatic tumor (dotted line) in nine-month-old K30$^{-/-}$C mouse, TP889, *in situ*. **(D)** Pancreatic tumor from **C**, attached to spleen and imaged *ex vivo*. **(E)** Pancreatic tumor (dotted line) in ten-month-old K30$^{-/-}$C with tdTom-EGFP construct (K30$^{-/-}$Ctd$^{+/-}$, TP881). **(F)** Pancreatic tumor from **E**, attached to spleen and imaged *ex vivo*. **(G)** Normal pancreas tissue (dotted line) in 12-month-old K30$^{-/-}$ mouse, TP832. **(H)** Pancreas tissue from **G**, attached to spleen and imaged *ex vivo*. Scale bars: 5 mm. Ruler in mm.

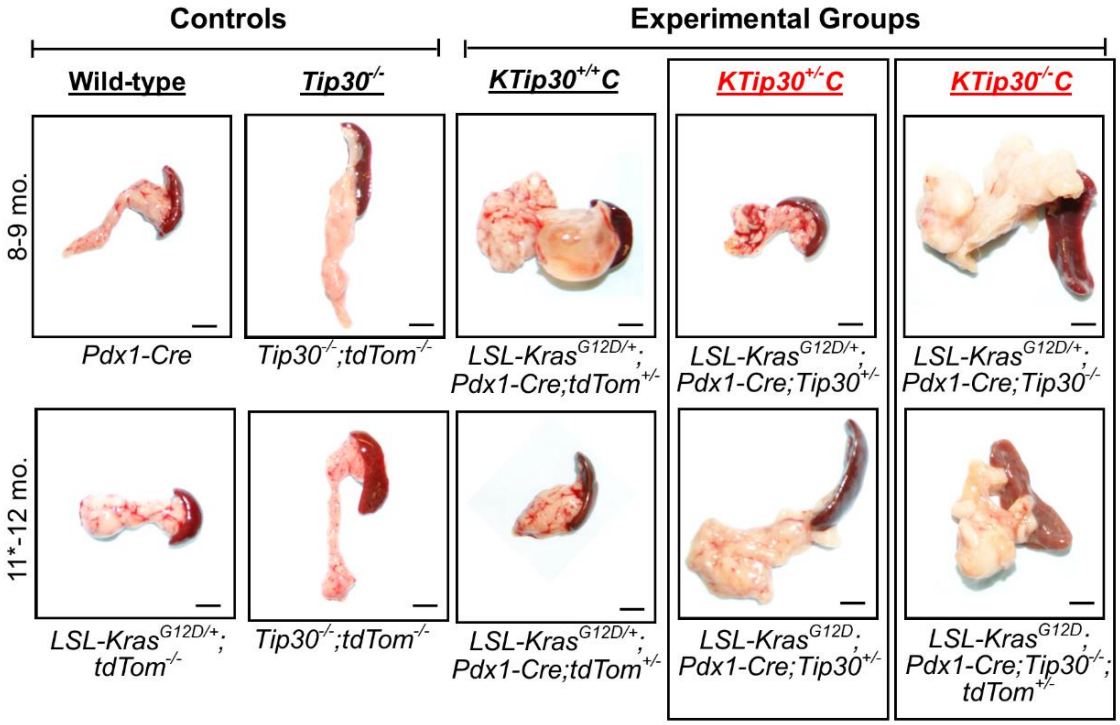

Figure 19. Complete deletion of *Tip30* results in increased incidence of gross pancreatic tumor formation with late presentation

Top Row: 8-9-month (mo.)-old pancreas tissue with spleen attached. Mouse ID, from left to right: E1908, TP890, TP942†, TP1004, TP889. Bottom Row: 11*-12-month (mo.)-old pancreas tissue with spleen attached, mouse ID from left to right: TP858, TP841, TP995, TP851, TP746. Scale bars: 5 mm. *TP851 is 10 months. †Cyst formation observed in some K30$^{+/+}$Ctd mice.

to K30$^{+/+}$C mice (n=1/5) and K30$^{-/-}$C (n=2/3) mice (**Figure 17**, **Table 3**). Although nodular-like in appearance, nodular areas were difficult to cut through at necropsy. These nodules may or may not be small tumors (approximately three mm in diameter). Focally nodular parenchyma has been reported in older KC mice (five months) by Hingorani et al. (in Figure 1D 2003). Of all mice observed in these studies including controls, only K30C with full *Tip30*-loss developed frank tumors that encompassed the entire pancreas tissue, albeit at later time points (**Figure 18-19**). We did not observe large, frank tumor formation in K30$^{+/-}$C mice. There was also a low penetrance of small pancreatic cysts or a cystic pancreas across the K30C mouse models as is indicated in **Table 3**.

3.2.7 K30$^{+/-}$C Mice Developed a High Incidence of Gross Pulmonary Lesions

One of our most striking observations from these studies was the presentation of pulmonary lesions in K30$^{+/-}$C mice (**Figure 20**). Seven of these mice were reported sick with difficulty breathing (n=7), and thus were included in the survival analysis. We examined the lungs of 31 K30$^{+/-}$C, 20 K30$^{-/-}$C and 17 K30$^{+/+}$C mice ranging between the ages of 5 and 44 weeks old for tumor incidence (**Appendix C5**). Not only did K30$^{+/-}$C mice have decreased overall median survival when compared to K30$^{+/+}$C and K30$^{-/-}$C mice, 42% of K30$^{+/-}$C mice (n=13/31) exhibited an incidence of pulmonary lesions and abnormalities as early as five weeks and as late as eight months compared to 0% K30$^{+/+}$C mice (n=0/17, p=0.002) and 10% K30$^{-/-}$C mice (n=2/20) (**Figure 20**, **Appendix C5-C6**). Chi-square analysis was performed on all three groups of K30C mice and a significant

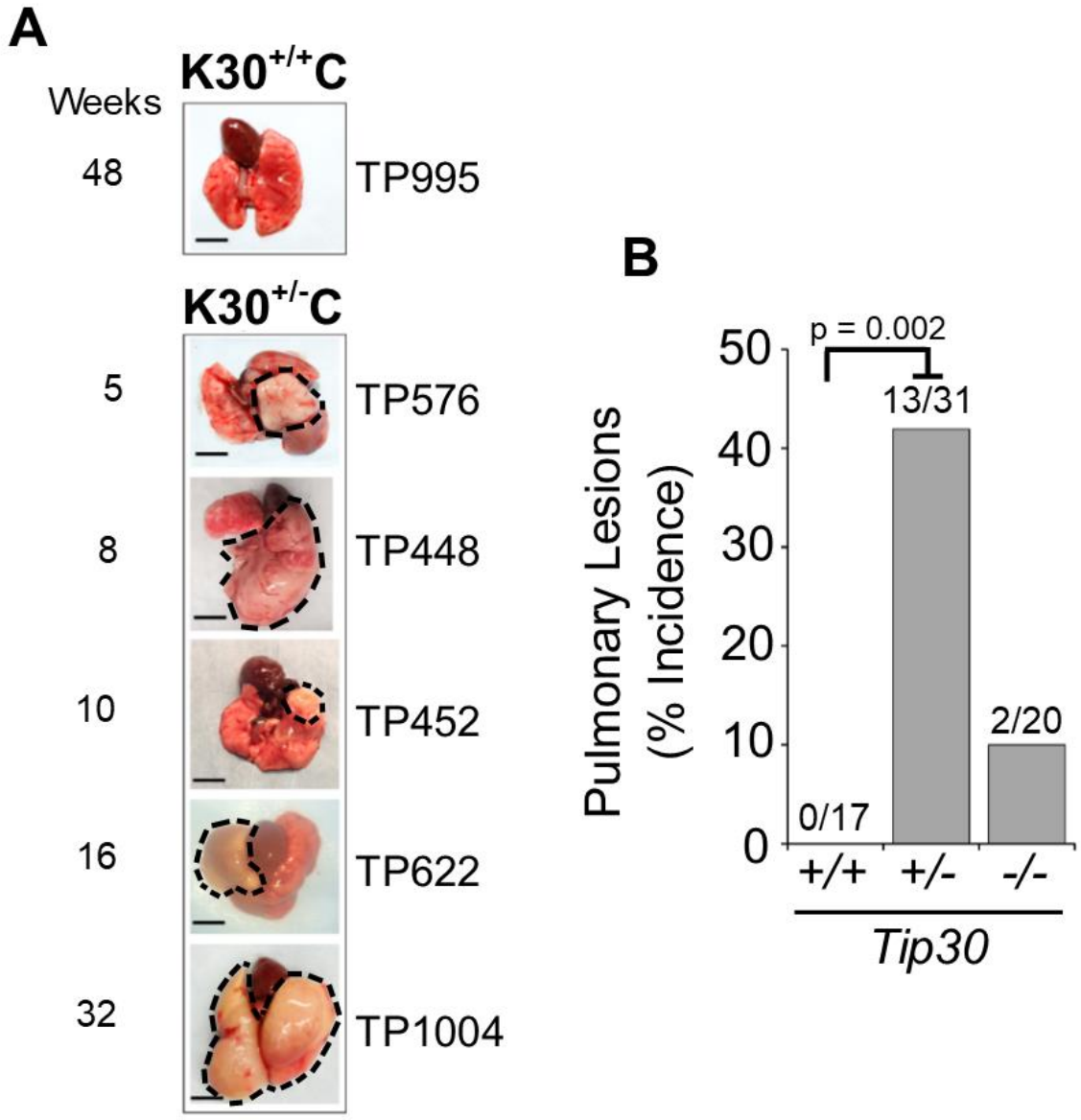

Figure 20. *Tip30*-heterozyous K30C mice developed increased incidence of gross pulmonary abnormalities

(A) Pulmonary lesions in lung tissues from five-week-old to thirty-two-week-old $K30^{+/-}C$ mice. Dashed region outlines the observed lesion formation. The apex of the lung is oriented to the bottom in these images, with the heart still attached to lung tissues. Scale bars: 5 mm. Lung images shown are from: $K30^{+/+}Ctd^{+/-}$-TP995 healthy lung control, and $K30^{+/+}C$-TP576, -TP448, -TP452, -TP622, and -TP1004 mice. Seven additional mice with pulmonary lesions were imaged. **(B)** Percent incidence of pulmonary lesion formation in K30C mouse model. Number of mice with gross pulmonary lesions observed over total number of mice assessed per group. +/+, $K30^{+/+}C$; +/-, $K30^{+/-}C$; -/-, $K30^{-/-}C$ mice. Chi-square p=0.001. Followed by Fisher exact test with Bonferroni correction. p=0.002 for +/+ vs. +/-. Other two-group comparisons had no significant difference.

difference in lesion incidence was determined (p=0.001, n=17-31) (**Figure 20**). This was followed by a Fisher exact test and Bonferroni correction which confirmed that the incidence of pulmonary lesions observed in $K30^{+/-}C$ mice was significant as compared to $K30^{+/+}C$ controls (p=0.002, n=17-31).

Tip30 deficiency has been reported to accelerate spontaneous lung tumor development in 78-week-old BALB/c mice (Li et al., 2013) and the BALB/c genetic background is prone to lung tumors at high frequency (Begley et al., 2012; Li et al., 2013). However, in contrast to Li et al. (2003), 92% of the $K30^{+/-}C$ mice that presented with this phenotype were 24 weeks old or less (n=12/13 mice). Also, 9 of 13 $K30^{+/-}C$ mice with pulmonary lesions were only 8-16 weeks-old. Therefore, to exclude the possibility that *Tip30*-deficiency alone caused pulmonary lesion formation, and to confirm that the phenomenon we observed appeared only *Tip30*-deficient K30C mice, a total of 6 *Tip30*-heterozygous ($30^{+/-}$) and 22 *Tip30*-null ($30^{-/-}$) littermate controls with and without *LSL-Kras*^{G12D} or *Pdx1-Cre* transgenes, but not both, were evaluated. In addition, 6 wild-type controls ranging from five weeks to six months in age were also examined. These animals did not present with pulmonary lesions or visible signs of disease at necropsy (see list of genotypes in **Appendix C1**).

These data combined suggested that *Tip30*-heterozygous loss and *Kras*^{G12D} driven to the pancreas epithelium resulted in preferential pulmonary involvement. Pulmonary lesions were at least five millimeters in diameter, with some that encompassed an entire lobe or both lobes of the lung tissue (**Figure 20, Appendix C6**). Mice that presented with a pulmonary lesion were mostly affected

in the right lobe. In K30$^{+/-}$C mice that developed pulmonary lesions, there were almost equal numbers of males and females (n=7 M; n=6 F), suggesting that pulmonary lesion development was not sex-dependent. Based on the increased pancreas pathology in the K30$^{+/-}$C group detected in the three month cohort we hypothesized that our unique observation of increased pulmonary lesions in K30$^{+/-}$C mice were linked to PDAC-associated disease, and metastatic disease.

The high incidence of visible pulmonary pathology in K30$^{+/-}$C mice led us to re-examine the pancreas tissues in these mice as only one of these mice presented with a visibly detectable pancreatic tumor (five-month-old TP647, within the head of the pancreas). We performed a histological assessment of an H&E stained pancreas section from nine *Tip30*-heterozygous-KC mice that demonstrated visible lung lesions. We hypothesized that the pulmonary lesions were associated with pancreatic lesions that could only be detected by histological examination. Our analyses with the aid of our pathologist revealed a range of pancreatic lesions and pathology ranging from ductal atypia, chronic inflammation, to PanIN-3 precursor lesions, in eight out of nine pulmonary lesion-positive K30$^{+/-}$C mice (**Figure 21**). These observations support the hypothesis that the pancreas pathology induced by the KC background, and observed in K30$^{+/+}$C mice alone at slightly longer latency may have cooperated with full-body *Tip30*-heterozygous loss to accelerate disease progression in K30$^{+/-}$C mice.

Pancreatic cancer cell (PCC) dissemination has been reported to precede pancreatic tumor formation and detection of PDAC by rigorous histological analysis (Rhim et al., 2012). We, therefore, hypothesized that pulmonary lesions in K30$^{+/-}$

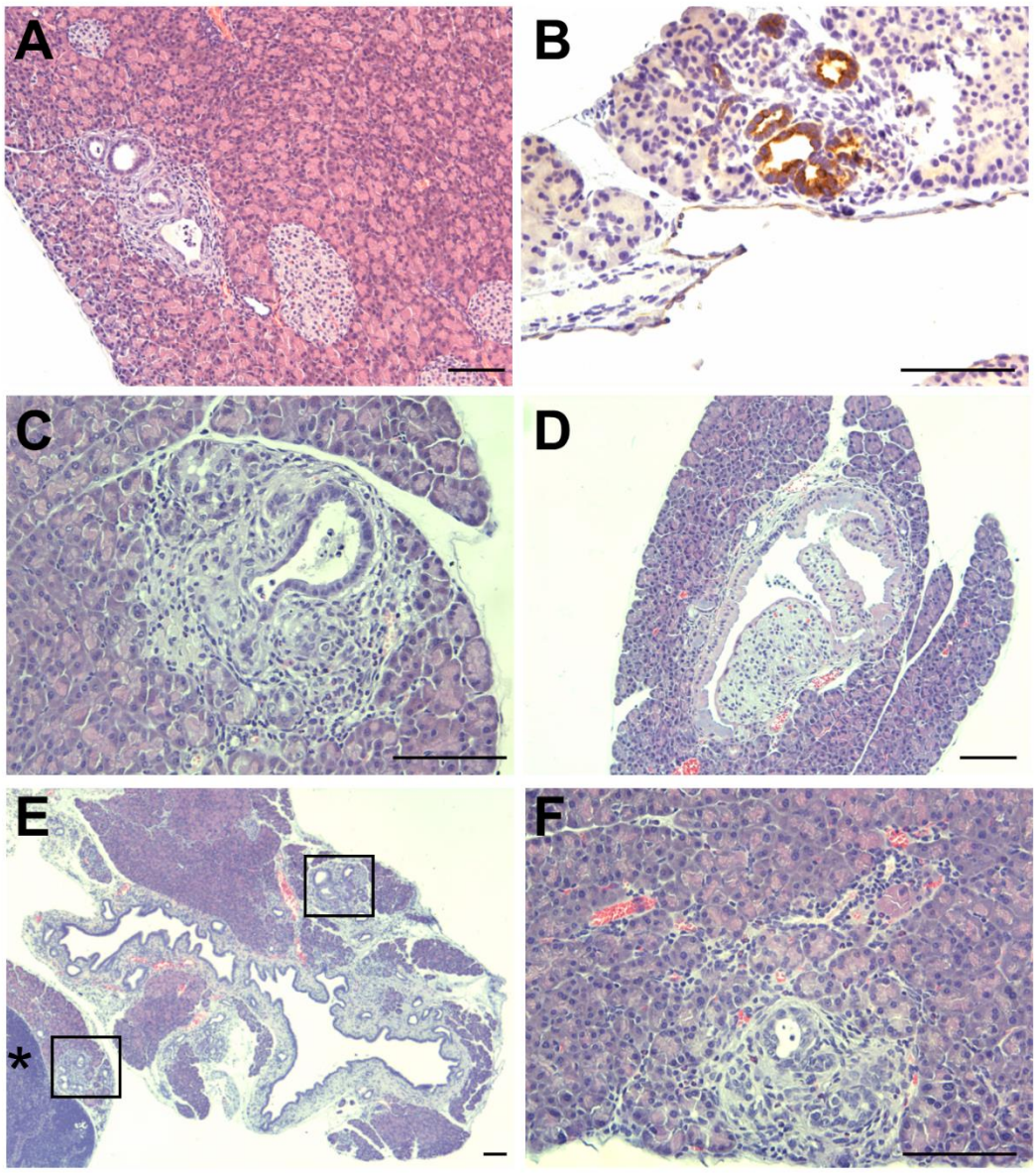

Figure 21. K30$^{+/-}$C mice with pulmonary lesions presented with microscopic pancreatic ductal atypia and PDAC precursor lesions

(A) Hematoxylin and Eosin (H&E) staining of five-week-old mouse ID TP576. Ductal atypia. **(B)** CK-19 stain of TP576. **(C)** H&E stain of eight-week-old mouse ID TP448. Beginning of a pancreatic intraepithelial neoplasia (PanIN)-3 lesion. **(D)** H&E stain of 12-week-old mouse ID TP452. Marked hyperplasia. (**E-F**) Loss of polarity and nuclear atypia in low **(E)** and high **(F)** power images of H&E stained section of 16-week-old mouse ID TP627. Scale bars: 100 µm. Squares indicate focal areas with lesions. Asterisk indicates lymph node.

C mice were a result of PCC metastasis. To detect PCC metastasis to the lung we examined one H&E-stained lung tissue section each from 11 of the 13 $K30^{+/-}$C mice which presented with visible pulmonary lesions for evidence of PCC metastatic lesions. Surprisingly, we were not able to detect PDAC metastasis in these lung sections. Instead, pulmonary-lesion-positive $K30^{+/-}$C mice had a 45% incidence of lung adenocarcinoma (n=5/11) (**Figure 22C-D**). H&E sections from pulmonary tissues of both $K30^{-/-}$C and $K30^{+/+}$C mice were also examined, and 16% of $K30^{-/-}$C mice (n=1/9) exhibited pulmonary histology similar to lung adenocarcinoma that was identified in the $K30^{+/-}$C group. This mouse also happened to have a pulmonary lesion by gross observation (**Appendix C6.E**). Lung adenocarcinoma was not detected by histological analysis in $K30^{+/+}$C mice aged two-three months (n=7) (**Figure 22**). Pulmonary tissues from two $30^{-/-}$ control mice were also assessed by pathology and were histologically negative for lung adenocarcinoma. Histopathological analysis revealed a higher incidence of thymic, follicular, or mantle zone lymphoma when assessing the spleen, and kidney, in addition to detectable lymphoma in the lungs of some subjects (**Figure 22D**). This included early lymphoma and lymphoma in n=3/7 $K30^{+/+}$C mice, in all 12 $K30^{+/-}$C mice with gross pulmonary lesions, and n=2/7 $K30^{-/-}$C mice. Lymphoma assessment was based on H&E sections of spleen, kidney, and pulmonary tissues. Incidences of lymphoma were also detected in $30^{-/-}$C control mice. The histopathological analysis of six lungs from two- to three-month-old $K30^{-/-}$C mice came back normal. Amongst three-month-old mice, we observed three with extramedullary hematopoiesis (EMH), myelodysplastic syndrome

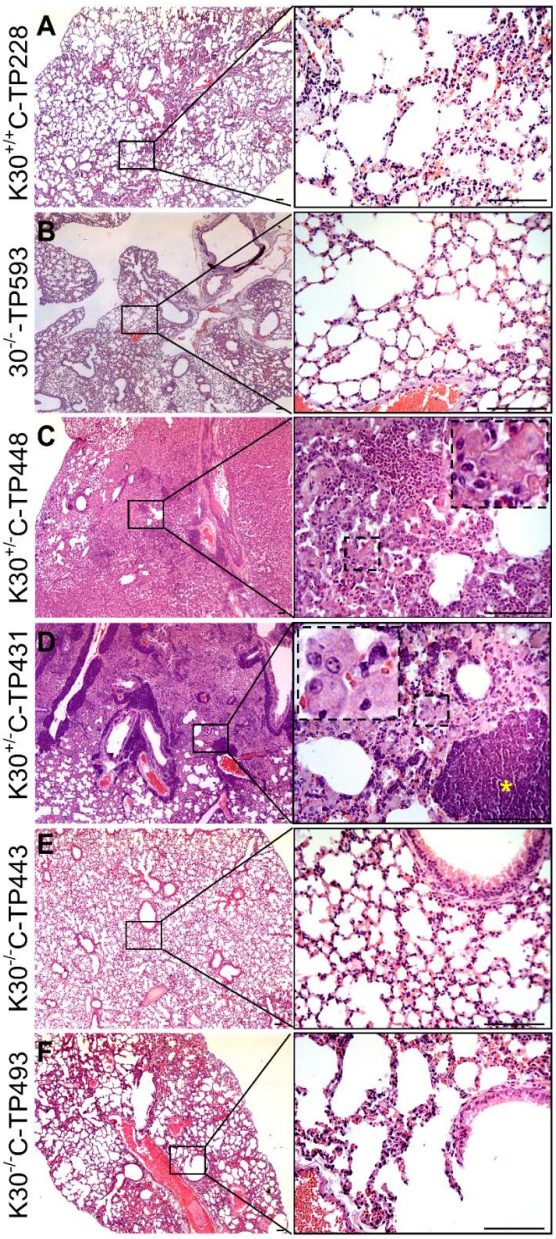

Figure 22.*Tip30*-heterozygosity increases lung adenocarcinoma incidence in pulmonary lesion-positive K30$^{+/-}$C mice

(A) Representative normal mouse lung tissue section stained for H&E from a *Tip30*-wild-type K30$^{+/+}$C mouse. Areas of trachea and alveolar ducts (higher magnification) are visible. **(B)** Representative lung tissue section of 30$^{-/-}$ control mice (n=2) in the K30C cohort. **(C-D)** H&E staining of lung adenocarcinoma with some darker areas of lymphoma detected in representative images of two 2-3-month-old K30$^{+/-}$C mice. **(C)** Low and high power of lung adenocarcinoma with high inflammation detected in a two-month-old K30$^{+/-}$C-TP448 mouse. **(D)** Lung adenocarcinoma and lymphoma presentation in a three-month-old K30$^{+/-}$C-TP431 mouse with inset magnifying abundant macrophage infiltration. **(E-F)** Representative fields of two-month old K30$^{-/-}$C mouse pulmonary tissue sections, and lung tissues from the K30$^{-/-}$C cohort that were negative for pulmonary lesion formation by gross observation. Scale bars: 100 µm. Low power image (2.5X) on the left, and high power insert (20X) on the right is presented for each subject.

(MDS), with small germinal centers in the spleen. Follicular lymphoma was detected in some spleen as well. Additional staining to distinguish lung adenocarcinoma from PDAC metastasis would help strengthen these studies.

3.2.8 Pancreatic Cancer Cell Dissemination to Lung Tissues in K30$^{+/-}$C mice

The observation of early pulmonary lesions in K30$^{+/-}$C mice with detectable lung adenocarcinoma without PDAC metastasis by histological analysis was surprising. Because *Kras^{G12D};Pdx1-Cre* (KC) mice do not test positive for *LSL-Kras^{G12D}* recombination in the lungs or liver (Hingorani et al., 2003, Supplemental), *Pdx1*-Cre leakage to the lung tissues was unlikely. Added to this, 17 K30$^{+/+}$C (aged of 2-6 months) did not present with the pulmonary lesion phenotype (**Appendix C5**). In particular, pulmonary lesion incidence was significantly increased in K30C mice that had one copy loss of *Tip30.* (K30$^{+/-}$C) with p=0.001 by chi square statistic (**Figure 20B**). In a separate article, Li et al. (2013) reported an increased incidence of lung tumors and lung adenocarcinoma in 78-week-old *Tip30*-deficient mice on the BALB/c background, a mouse strain that is more susceptible to lung tumor formation (Li et al., 2013; Begley et al., 2012). A total of *Tip30*-deficient mice (aged 1-12 months) with either a *LSL-Kras^{G12D}*, a *Pdx1-Cre*, neither, or both transgenes were examined by gross observation (**Appendix C1**). However, we did not observe the pulmonary lesion phenotype in *Tip30*-deficient mice alone (30$^{+/-}$ or 30$^{-/-}$) in our studies (**Appendix C1**); and not only did we observe a significant preferential incidence in pulmonary lesions based on *Tip30* copy number (**Figure 20B**), the time to pulmonary lesion incidence occurred early compared to the Li et

al. (2003) report, at an average of three months (when examined up to 12 months, see **Appendix C5**).

Due to the high abundance of PDAC-associated lesions and PDAC-associated lymph node invasion and metastases detected in the cohort of $K30^{+/-}C$ mice compared to the other two groups of K30C mice and the occurrence of an affected lung phenotype as early as 5 weeks, we hypothesized that the pulmonary lesions had resulted from a PDAC metastatic seeding event. In a recent study, Rhim et al. (2012) reported that pancreatic cancer cell dissemination precedes histopathological detection of PDAC (Rhim et al., 2012). Rhim et al. (2012) found that mutant PDAC cells entered the circulation before PDAC detection by rigorous histopathological analysis (analysis of multiple sections throughout the entire tissue). We therefore hypothesized that one copy loss of *Tip30* accelerated pancreatic cancer cells seeding to the lungs in our $K30^{+/-}C$ mouse model, and that metastasis had evaded detection by histopathological analysis.

We sought to evaluate the pulmonary tissues of $K30^{+/-}C$ mice with lesions for $Kras^{G12D}$-positive pancreatic cancer cells. We used the Kras G12D Conditional PCR method from The Jacks Lab (Jacks, 2007) to examine the DNA from the pancreas, pulmonary lesion, and adjacent normal, healthy lung tissue of $K30^{+/-}C$ mice. Here, we hypothesized that lung lesion formation was a secondary event that occurred in response to pancreatic cancer cell seeding of the lung tissues of $K30^{+/-}C$ mice. We hypothesized that the lung lesions were PDAC-associated and would be positive for a population of $Kras^{G12D}$-positive PCCs that could then be identified by the recombined allele and insertion of one *Lox*P site (650 bp). To test

this hypothesis, we biopsied the pulmonary tissue lesions as well as neighboring, observably healthy ("adjacent-normal"). Gross examination was used to determine whether the tissue region was abnormal or normal. This matched sampling method allowed us to compare affected areas versus adjacent-normal lung tissues within $K30^{+/-}C$ mice. We used Kras G12D Conditional PCR (Jacks, 2017) to assess the presence of mutant *Kras* in DNA extracted from the biopsied tissues, as well as snap-frozen pancreas and muscle tissues, as available. Genomic DNA from $K30^{+/+}C$, $K30^{+/-}C$, and $K30^{-/-}C$ mouse pancreata tested positive for recombination and therefore, they were considered to be $Kras^{G12D}$-positive. Presence of $Kras^{G12D}$ in the pancreas gave rise to $Kras^{G12D}$-positive pancreatic cancer cells isolated from the pancreas epithelium, confirmed by fluorescence-activated cell sorting (FACS) of GFP-positive cells (**Appendix C7**). Pancreatic cancer cells were labeled with GFP, germline, after the incorporation of the dual fluorescent reporter mouse tdTomato-EGFP (Muzumdar et al., 2007, **Figure 10**) into the K30C mouse model, and pure GFP populations as well as PCCs derived from the pancreas tissues of K30C mice were fully recombined for $Kras^{G12D}$ (**Figure 23B**).

In addition to 1-*Lox*P-$Kras^{G12D}$-positive pancreas tissue and PCC DNA (**Figure 24**, **Figure 23B**), DNA from the pulmonary lesions of $K30^{+/-}C$ pulmonary lesion-positive mice was positive for oncogenic *Kras* (by recombined 1-*Lox*P-$Kras^{G12D}$, n=3/3, **Figure 24**). Two out of three $K30^{+/-}C$ mice with a pulmonary lesion visible by gross examination had undetectable $Kras^{G12D}$ in biopsied, healthy-appearing lung tissue using the same method. Adjacent normal lung tissue DNA in 5-week-old TP576 and 2-month old TP448 was negative for the *1-LoxP-*$Kras^{G12D}$

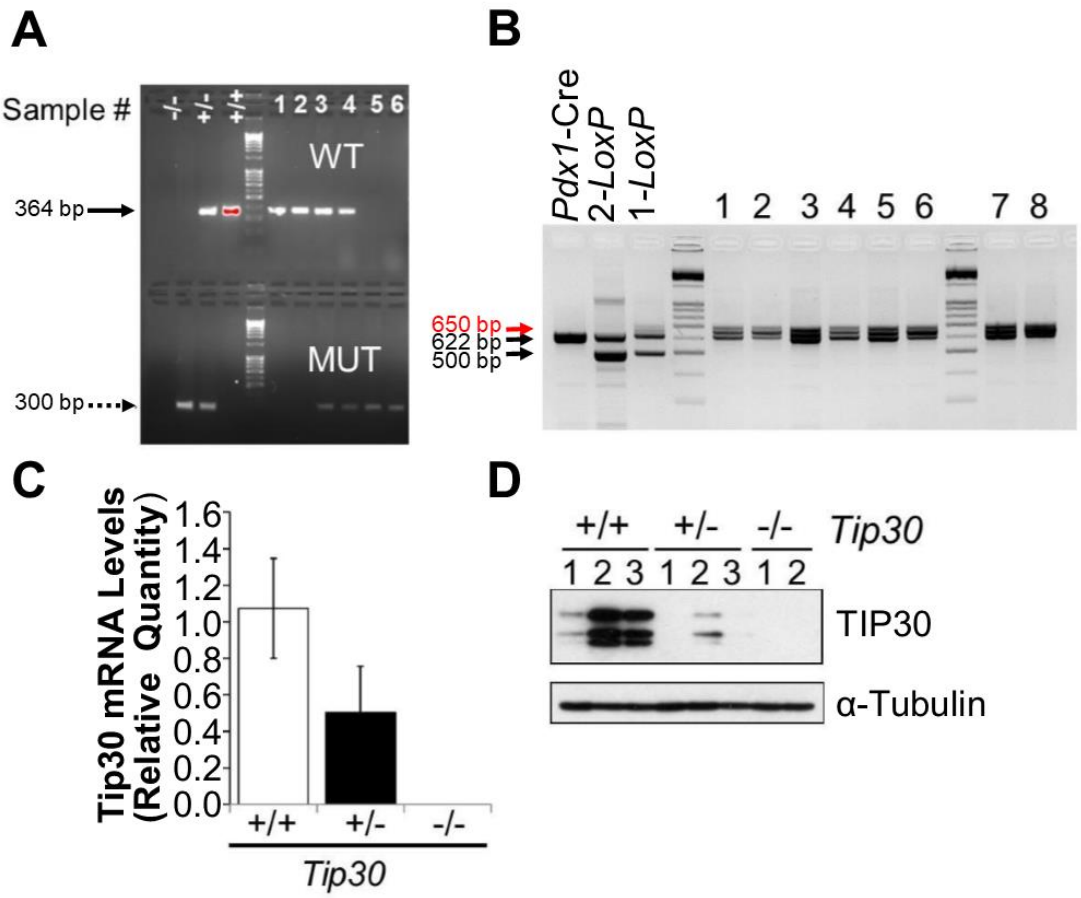

Figure 23. Characterization of PCCs from K30C and K30Ctd$^{+/-}$ models of murine PDAC

(A) Genotyping PCR for *Tip30* wild-type allele (top band, WT) and *Tip30* mutant allele (bottom band, MUT) in separate PCR reactions, using genomic DNA extracted from the following mPCCs: TP711 (1), TP715 (2), TP573 (3), TP647 (4), TP592-1 (5), and TP889 (6). First three lanes represent *Tip30* $^{-/-,\ +/-,}$ and $^{+/+}$ tail DNA genotyping controls. Ladder, 10 kB. **(B)** Recombination efficiency of mPCCs and presence of oncogenic *Kras*, as assessed by Kras G12D Conditional PCR (Jacks, 2017) for cell line DNA and controls from pancreas tissues. *Pdx1*-Cre, DNA from a control mouse pancreata positive for wild-type *Kras* allele only at 622 bp. 2-*Lox*P, DNA from a control mouse pancreata positive for both a 622-bp product and an unrecombined *LSL-Kras^{G12D}* allele at 500-bp. 1-*Lox*P, DNA from a mouse pancreata positive for the 622 bp, 500 bp, and recombined 1-*LoxP-Kras^{G12D}* (650 bp) products. Samples #1-6 are as described in **A**. TP151-GFP (7), and TP912-Lu-GFP (8). Ladder, 10 kB. **(C)** Relative Tip30 mRNA levels from murine PCCs (mPCCs) with wild-type (TP151-GFP, TP711, TP715: +/+), heterozygous loss (TP573, TP647, TP852-GFP: +/-), or complete loss (TP592-1, TP735-GFP, TP892-GFP: -/-) of *Tip30*. Three cell lines per group were normalized to an internal Rps6 loading control and to the mean of three *Tip30* WT mPCC lines (+/+). Data represent the means ± SEM of three cell lines per group. Student's t-test for +/+ vs. +/-, p=0.1889. Cell line IDs correspond to mouse ID's from which cell lines were derived. "-GFP" indicates the cell line was isolated from a K30Ctd$^{+/-}$ mouse and was sorted by GFP using flow cytometry. (**D**) Two to three mPCCs each from different K30C and K30Ctd$^{+/-}$ mice were assessed for TIP30 protein levels. TP151-GFP, TP711, TP715 (+/+); TP573, TP647, TP852-GFP (+/-), and TP592, and TP735-GFP (-/-). 20 µg of protein was separated over 15% SDS-PAGE. This experiment was repeated three different times (technically) with two different aliquots of the same antibody. The TIP30 antibody ab177961 from Abcam detects two major isoforms (27 and 30 kD) of TIP30. α-Tubulin is the loading control.

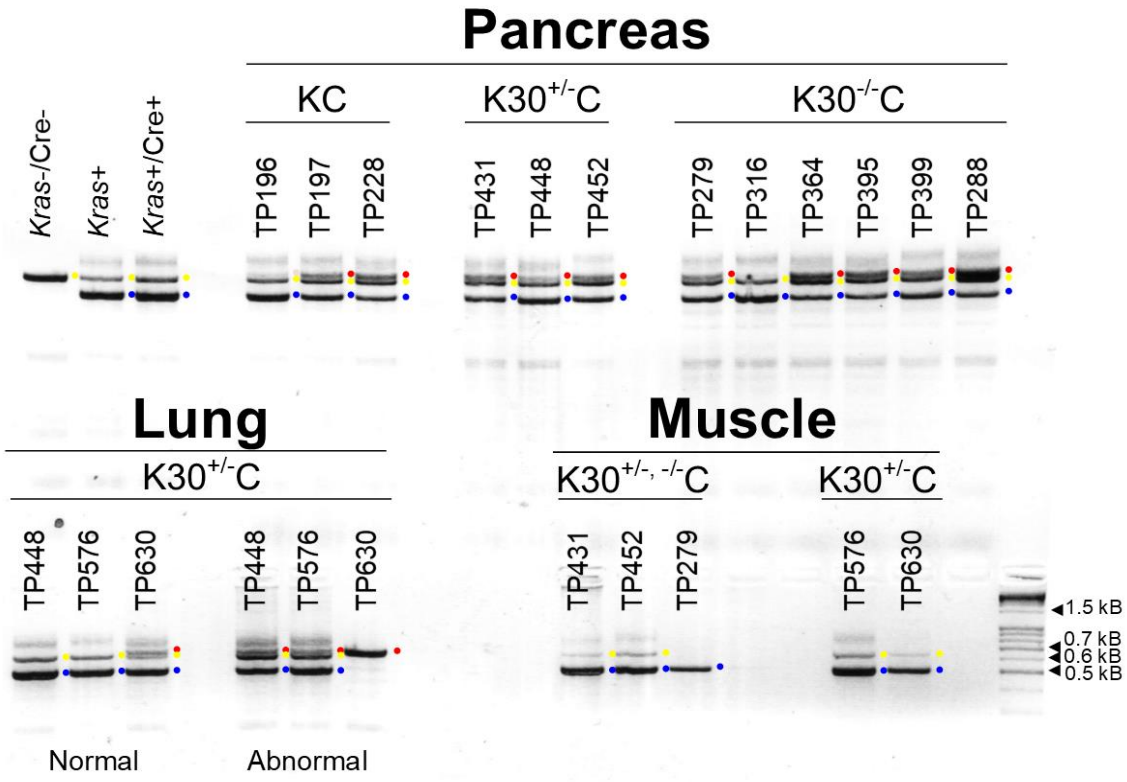

Figure 24. Pancreas tissues and abnormal pulmonary lesions, but not adjacent normal lung tissue*, from K30$^{+/-}$C mice tested positive for *Kras^{G12D}*-recombined PCC DNA

Kras G12D PCR of DNA from the pancreas and muscle tissues of K30$^{+/+;\ +/-;\ \text{or}\ -/-}$ C mice, and both abnormal lung and healthy (normal) lung tissue biopsies from K30$^{+/-}$C mice with pulmonary lesion presentation was used to detect the presence of 1-*LoxP*-*Kras^{G12D}*-positive PCC DNA using the Kras G12D Conditional PCR method (Jacks, 2017). The first control is a negative control, from pancreas tissue of a mouse negative for both the *LSL*-*Kras^{G12D}* and the *Pdx1*-Cre transgenes (TP418, *Kras*-/Cre-), and the second a positive control from a mouse with one copy of the *LSL*-*Kras^{G12D}* transgene (*Kras*+), and as expected, no recombination event. The *Kras*+/Cre+ control (TP228) appears not to be positive for *LSL*-*Kras^{G12D}* recombination, although originally genotyped as a K30$^{+/+}$C mouse at weaning. Recombined 1-*Lox*P allele, 650 bp (red dot); wild-type *Kras*, 622 bp (yellow dot); unrecombined 2-*Lox*P, 500 bp (blue dot). Ladder, 10 kB. *3.5-month-old TP630 mouse tested positive for recombined 1-*Lox*P DNA in the biopsy of adjacent normal lung tissue. Muscle tissue served as negative internal controls and tested negative for recombination or PCC DNA. Normal lung tissue appeared healthy and were free of lesions by gross observation.

PCR product (**Figure 24**). A third 500-bp PCR product in this analysis confirmed the presence of unrecombined *LoxP-STOP-LoxP* construct, which we interpreted as DNA from lung cells of the pulmonary tissues. All three groups ($K30^{+/+}C$, $K30^{+/-}C$, and $K30^{-/-}C$) tested negative for recombination in muscle tissues, while $K30^{-/-}C$ and $K30^{+/+}C$ groups tested positive for partial recombination in the pancreas (**Figure 24**).

The third $K30^{+/-}C$ mouse (mouse ID TP630) exhibited a phenomenon known as loss of heterozygosity (LOH) of the wild-type *Kras* allele. Mouse ID TP630 had a larger pulmonary lesion than the other two mice in this analysis, possibly because it was older: 14 weeks of age compared to 8 weeks (TP448) and 5 weeks (TP576) of age. This may or may not have contributed to a more advanced diseae state in this region of affected tissue. We were not able to detect wild-type *Kras* by PCR in this mouse's pulmonary lesion, but both the adjacent normal lung and pancreas tissue biopsies in this mouse retained detectable levels of the wild-type *Kras* allele by this PCR method (**Figure 24**, see **Appendix C8**). Copy number loss of one *KRAS* allele with a mutation in the second allele is seen in 35% of hPDAC cases according to TCGA data (n=100/109, UTSW), accessed through cBioPortal on November 14, 2018 (J. Gao et al., 2013; Cerami et al., 2012). In addition, we were able to detect *1-LoxP-Kras*^{G12D} in the adjacent normal lung tissue biopsy of TP630. Note that DNA from the muscle tissue did not test positive for recombination. In addition, DNA sampled from mouse pancreata of control mice that lacked the *Pdx1-Cre* transgene but were positive for the *LSL-Kras*^{G12D} allele. Ductal atypia was detected in a pancreas section of this mouse by

histopathological analysis. These findings suggested that, for this mouse, although the adjacent-normal tissue was visibly lesion-free, the tissue still maintained some pancreatic cancer cells that were undetectable by gross examination. In total, two out of three of mice with pulmonary lesions and 1-*Lox*P-Kras^{G12D} positive DNA were confirmed to have detectable lung adenocarcinoma by pathological evaluation (two-month-old TP448 in **Figure 22C**, and four-month-old TP630). Combined the advanced histopathology observed in the pancreas tissues of K30$^{+/-}$C mice, and the similarity in *Kras*^{G12D}-recombined DNA from the PCCs and pancreas tissues in our mouse models (**Figure 23B** and **Figure 24**, **Appendix C2.C**) with the DNA from the pulmonary lesions but not adjacent normal lung tissues (n=2, **Figure 24**), these additional findings supported that PCC had seeded the lungs of K30$^{+/-}$C mice. However, we understand that more substantiation is needed to confidently state that a recombination event did not occur during embryogenesis in the pulmonary tissues of K30$^{+/-}$C mice and contributed to the results obtained from our observations**.**

To further evaluate if *Tip30*-heterozygosity enhanced metastatic pulmonary seeding in KC mice, we crossed the dual-fluorescent membranous tomato/membranous enhanced GFP (mT/mG) Cre reporter mouse (Muzumdar et al., 2007) into our model (K30Ctd$^{+/-}$). EGFP-labeling of the pancreas epithelium was driven *Pdx1*-Cre excision of the *LoxP-tdTomato-LoxP* cassette. This resulted in GFP-positive pancreas tissues (**Figure 25**) and allowed us to sort PCCs for GFP-positivity by flow cytometry (**Appendix C7(A)-(B)**). One allele of *LoxP-tdTomato-LoxP-EGFP* (herein “td”) is sufficient for adequate GFP fluorescence

(Muzumdar et al., 2007). When using the same imaging settings, td$^{+/-}$ and td$^{-/-}$ mice did not exhibit any distinguishable differences in phenotype or fluorescence. PCCs derived from GFP-fluorescent pancreata and distant organ seeding (disseminated or metastatic PCCs) were confirmed to have the *Kras^{G12D}* mutation by the "Kras G12D Conditional PCR" method (Jacks, 2017) (see **Figure 24B**, Lane No. 7).

To confirm *Pdx1-Cre*-specific GFP-targeting, we imaged the internal organs, both *in situ* and *ex vivo,* of *Tip30*-deficient; td$^{+/-}$ mice with and without *Pdx1-Cre* using the same light box fluorescent imaging settings. Compound mutant *Tip30*-deficient;*Pdx1-Cre*-negative;td$^{+/-}$ mice were always RFP-positive (**Figure 25A-B**). While *Tip30$^{+/-}$* and *Tip30$^{-/-}$*;td+/- mice that were positive for the *Pdx1-Cre* transgene exhibited green-fluorescent pancreas tissues (**Figure 25C-D**). The pulmonary lesion that developed in a three-month-old K30$^{+/-}$Ctd$^{+/-}$ mouse did not fluoresce (green) as an entire mass, and we were unable to detect GFP-positive PCCs in the lesion by fluorescence light box imaging (n=1/5). We interpreted these data as support for no off-target *Pdx1*-Cre recombination in the lung tissues of both K30$^{+/+,}$ $^{+/-,}$ or $^{-/-}$C mice and K30$^{+/-}$C-mouse pulmonary lesions.

One two-month-old K30$^{+/-}$C mouse (mouse ID TP852) in our study was reported as sick but did not present with a pulmonary lesion. Although the lungs appeared healthy by gross observation (similar to that of K30$^{+/+}$C control mouse ID TP995 in **Figure 20A**), we were able to visibly detect micrometastatic seeding, clustered predominately in the superior and middle lobes of the right lung near the trachea (**Appendix C9)** by GFP imaging. The pathologist diagnosed K30$^{+/-}$Ctd$^{+/-}$-

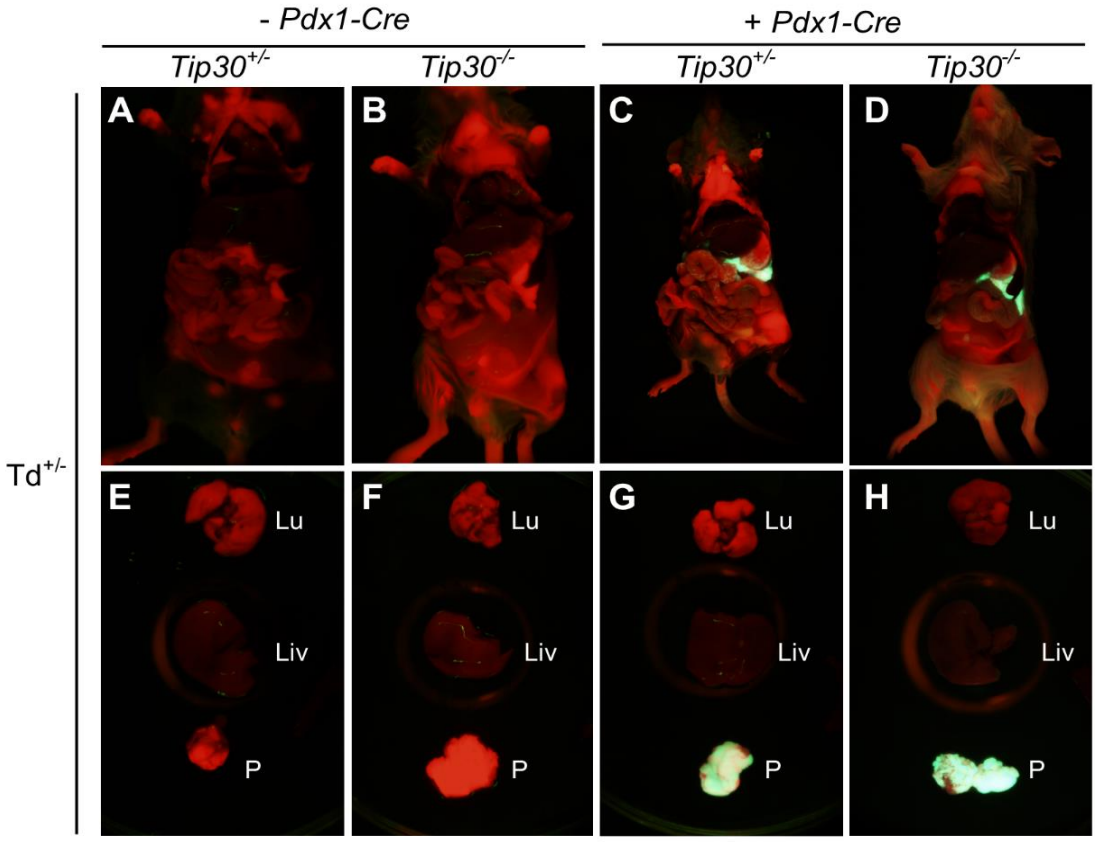

Figure 25. *Pdx1-Cre*-driven EGFP labeling using the dual *LoxP-tdTomato-LoxP-EGFP* reporter mouse

(A-B) *Tip30*-deficient control mice without the *Pdx1-Cre* transgene present negative for EGFP labeling of pancreas tissue by *in situ* GFP/RFP imaging. **(A)** Five-month-old, *Tip30*-heterozygous ($30^{+/-}td^{+/-}$) mouse (TP666). **(B)** Representative image (TP693) of three, three-month-old $30^{-/-}td^{+/-}$ *Tip30*$^{-/-}$ mice imaged. **(C-D**) *Pdx1*-Cre drives EGFP labeling to the pancreas epithelium in *Tip30*-deficient mice. **(C)** Representative image (TP690) of two, three-month-old, *Tip30*-heterozygous;*Pdx1-Cre* ($30^{+/-}Ctd^{+/-}$) mice imaged *in situ*. **(D)** Representative image (TP704) of two, three-month old $30^{-/-}Ctd^{+/-}$ mice. (**E-H**) Lung (Lu), liver (Liv) and pancreas (P) tissues imaged *ex vivo*.

TP852 with chronic ductal inflammation of the pancreas, after examining a histological section of pancreas tissue from this mouse.

GFP-positive pancreatic cancer cells (PCCs) from both pancreas and lung tissues were cultured and successfully expanded from $K30^{+/-}Ctd^{+/-}$-TP852 (**Figure 26**). By day four, in culture, metastatic PCCs appeared disorganized in morphology (with elongated projections) and exhibited a disproportionate cytoplasmic to nuclear ratio and a strong GFP signal that lined the nuclear membrane (**Figure 26D**). By Day 11, GFP-positivity was uniform throughout GFP-positive metastatic PCCs. The presence of supporting cells, that were GFP-negative, could also be visualized in culture by Day 11 (**Figure 26E**). Without GFP-labeling (**Figure 26E**, bottom panel) these disseminated PCCs would have been indistinguishable from the surrounding cells in culture (**Figure 26E**, brightfield). DNA and cellular analysis suggested the presence of two different populations of cells in the lung tissues: those that were recombined and *Kras*^{G12D} positive, as well as cells that were not recombined and *Kras* wild-type only. TP852-pancreatic and -lung-metastatic (lung met) PCCs were sorted for GFP-positivity using fluorescence-activated cell sorting (FACS) (**Appendix C7(B)**). GFP-negative cells were sorted into a separate pool, however the cell sorting may have not resulted in a pure population as is indicated in **Figure 26F**. In culture, the GFP-negative pool of cells presented with GFP cells over time, suggesting that there may have been limitations in sorting a pure negative population.

Genomic DNA was extracted from the GFP-positive lung met PCCs (TP852-Lu-GFP) and assessed for recombined 1-*Lox*P-*Kras*^{G12D}. Similar to our

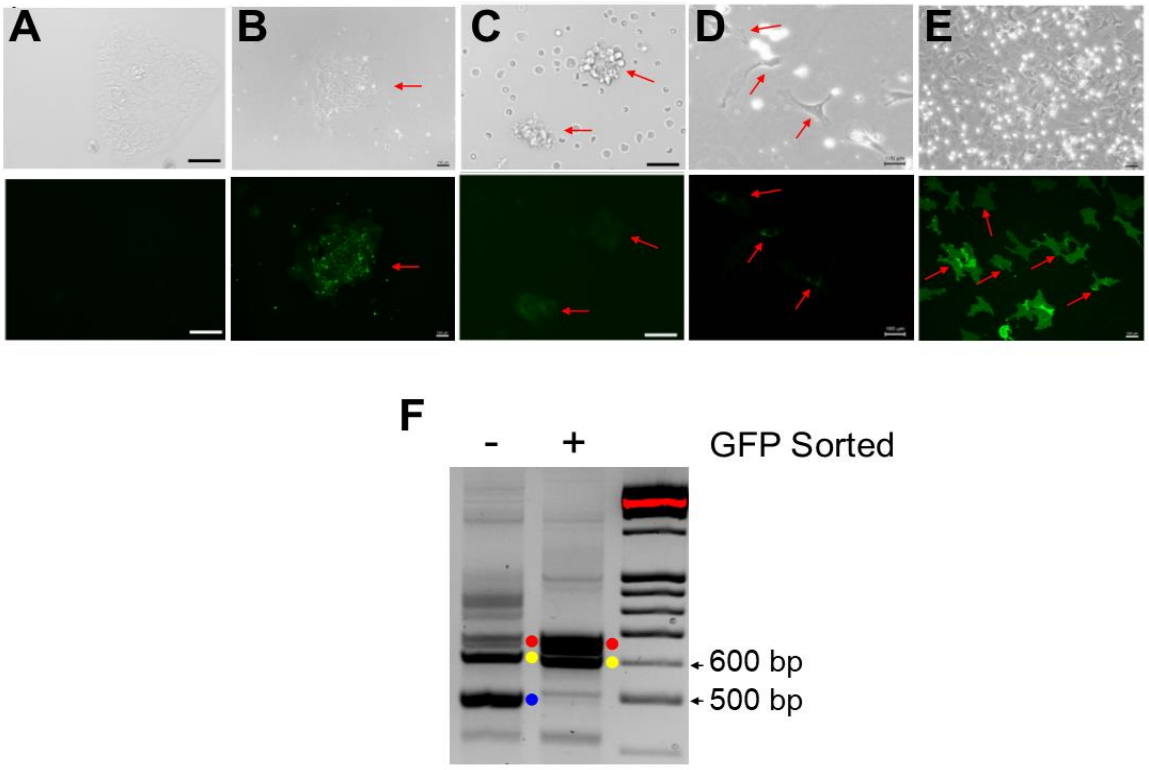

Figure 26. GFP-positive PCCs isolated from the pulmonary tissue of a two-month-old K30$^{+/-}$C mouse are fully recombined for *Kras*^{G12D}

(A) Negative control for GFP imaging using PCCs negative for *LoxP-tdTomato-LoxP-EGFP* transgene. **(B)** Cells cultured from pancreas of two-month-old K30$^{+/-}$Ctd$^{+/-}$ mouse (TP852), Day 11 in culture. **(C-E)** Cells cultured from lung of mouse TP852, shown at Day 0 **(C)**, Day 4 **(D)**, and Day 11 **(E)** in culture, respectively. Red arrows indicate GFP positive metastatic PCCs. Scale bars: 100 µm in **A-E**. Fields were imaged in both brightfield (top) and GFP (below). **(F)** Fluorescence-activated cell sorting of mixed cell population shown in **E**, followed by Kras G12D Conditional PCR (Jacks, 2017) of GFP-positive sorted cells (+) and GFP-negative sorted cells (-). GFP-positive sorted cell population was fully recombined (red dot, recombined 1-*Lox*P-*Kras*^{G12D} allele at 650 bp). Yellow dot, wild-type *Kras* allele at 622 bp; blue dot, Unrecombined 2-*Lox*P at 500 bp. 10 kB ladder.

observations in primary PCCs isolated from pancreas tissues (**Figure 23B**), $K30^{+/-}$ $Ctd^{+/-}$-TP852-Lu-GFP-positive sorted cells had fully recombined 1-*LoxP-Kras*^{G12D} transgene DNA (**Figure 26F**). TP852-Lu-GFP [GFP positive] metastatic PCCs therefore tested positive (fully recombined) for oncogenic *Kras* suggesting that they indeed had originated from the pancreas tissue (**Figure 26F**). These data support that oncogenic *Kras* PCCs with *Tip30* heterozygous are capable of seeding the lungs of *Tip30*-heterozygous KC mice. These seeding event may contribute to the early lung adenocarcinoma observed in our model system. We recognize that more mice will need to be analyzed to substantiate these interpretations.

Cells were also isolated from the pancreas and lung tissues of a three-month-old $K30^{+/+}Ctd^{+/-}$ mouse (TP912) (**Appendix C7(A)**). TP912 was not expected to have GFP positive cells in the lungs as the mouse was not sick, nor did it have any GFP-positive cells visible by fluorescent imaging. We hoped to use these cells as a negative control for mechanistic studies of metastatic PCCs that had seeded the lungs in $K30^{+/-}$C mice. However, in culture of cells isolated from the lung tissue, a population of GFP-positive cells were visualized and subjected to fluorescence-activated cell sorting. Gating these cells to a GFP-negative pancreatic cancer cell line (**Appendix C7(A)**, Neg Ctrl) revealed that the cells indeed were GFP-positive (**Appendix C7(A),** Neg Ctrl vs. TP912-Lung). The mixed population of cells from TP912-Lung tested positive for both recombined *1-Lox*P-*Kras*^{G12D} and unrecombined *LSL* DNA. This suggested that PCCs that had seeded the lung yet were not detectable by gross observation or visualization with

light box GFP imaging co-existed with a population of lung cells in K30$^{+/+}$C mouse ID TP912 lung tissue. The GFP-positive cell line from the lung of TP912 was called TP912-Lu-GFP. An H&E-stained pancreas section of the TP912 mouse was evaluated by our pathologist, and a PanIN-3 lesion with microinvasion and carcinoma *in situ* was detected. Kras G12D Conditional PCR (Jacks, 2017) to detect oncogenic *Kras* revealed that the sorted TP912-Lu-GFP cells were comprised of fully recombined 1-*LoxP*-*Kras*^{G12D} DNA (**Figure 23B**, lane 8). In addition, DNA from TP912-Lu-GFP cell was also sent for whole genome sequencing (the average read depth was 31X). Our analysis of the TP912-Lu-GFP sequence confirmed that these cells were negative for the *Tip30* Exon 2-3 deletion. Our sequencing analysis also confirmed that the *Rb1*, *Tp53*, and *Smad4* gene sequences were wild-type in these cells; therefore we considered this mouse to be a true K30$^{+/+}$C mouse.

3.2.9 Complete Loss of *Tip30* Enhanced Hepatic Seeding, Frank Tumor Formation, and Late Onset of Metastatic Burden in K30$^{-/-}$C Mice

In contrast to the phenotype observed in K30$^{+/-}$C mice, K30$^{-/-}$C mice developed classical, dense PDAC tumors (**Figure 18, Figure 19**). K30$^{-/-}$Ctd$^{+/-}$-TP735 (mouse ID TP735) presented with this phenotype at three months. However, the other K30$^{-/-}$C mice did not present with this phenotype until at least nine months (K30$^{-/-}$C, n=1; and K30$^{-/-}$Ctd$^{+/-}$, n=2). Not only could the pancreatic tumors be unmistakably identified, histological assessment with a pathologist confirmed the following pathology: cystic adenocarcinoma of the pancreas, moderately differentiated PDAC, PDAC with detection of a broken membrane, and

moderately differentiated PDAC plus fibrosarcoma (spindeloid tumor) for the H&E sections from K30$^{-/-}$C tumors aged six to eleven months old. Sarcomatoid histology is reported to be a less common subtype of PDAC (Hezel et al., 2006). Since the heterozygous loss of *Tip30* resulted in increased pulmonary metastatic seeding and increased secondary pulmonary lesion formation, we hypothesized that total loss of *Tip30* also enhances early PDAC metastasis that may bypass detection by gross assessment. We assessed H&E stains of liver and lung tissues from three-month-old K30$^{-/-}$C mice but did not detect any indication of liver or lung metastatic lesions by histology. Therefore we proceeded to evaluate a cohort of K30C mice that were also positive the dual fluorescent tdTomato-EGFP reporter (Muzumdar et al., 2007). The addition of this transgene (*Lox*P-tdTomato-*Lox*P-EGFP) results in enhanced green fluorescent expression in the pancreas epithelium only in the presence of *Pdx1*-mediated Cre recombinase (**Figure 25**). Mice that are positive for this transgene (td$^{+/-}$ or td$^{-/-}$) but negative for *Pdx1*-Cre express tomato, a red fluorescence, in their pancreas tissues (**Figure 25A-B**).

In an attempt to detect the presence or absence of any micrometastatic seeding organs from three-month-old K30$^{+/+}$Ctd$^{+/-}$ (n=3), K30$^{+/-}$Ctd$^{+/-}$ (n=5) and K30$^{-/-}$Ctd$^{+/-}$ (n=4) mice were examined and imaged using a GFP/RFP light box imaging system, both *in situ* and *ex vivo* (**Figure 27**). This is described in more detail in section 2.15. Micrometastatic seeding was identified by groups of dotted clusters that ranged in size (**Figure 27B**, white arrow). Micrometastatic seeding to the liver was observed in 75% of three-month-old K30$^{-/-}$Ctd$^{+/-}$ mice compared to 0

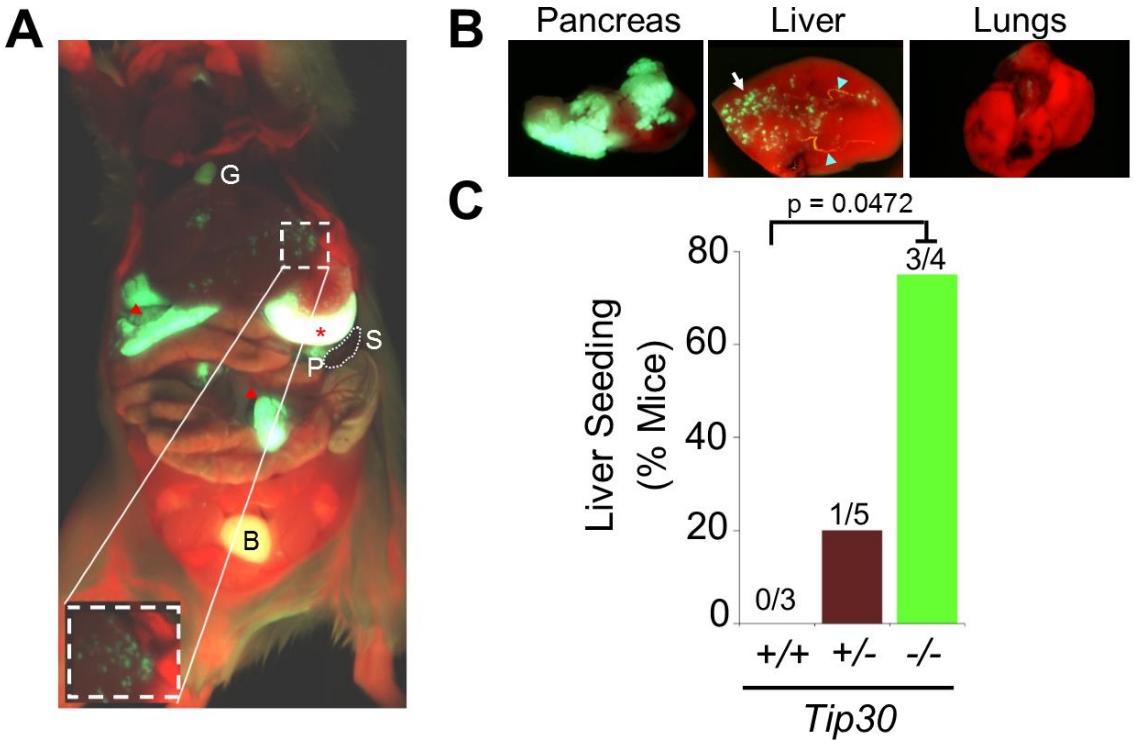

Figure 27. Complete loss of *Tip30* enhances micrometastatic seeding to the liver in a novel mPDAC model ($K30^{-/-}Ctd^{+/-}$)

(A) Whole body dual GFP/RFP light box imaging of a $K30^{-/-}Ctd^{+/-}$ mouse (TP703). 60% Brightness and 50% contrast was used in this image for better visualization. White dashed box and inset represents one area of micrometastatic seeding detected. Dotted oval outlines the spleen (S), which is attached to the GFP-positive pancreas (P). Both the gallbladder (G) and bladder (B) autofluoresce. The stomach (red asterisk) and the small intestine (red arrowheads) are GFP-positive. **(B)** GFP/RFP light box imaging of pancreas, liver, and lungs from mouse in **A**, *ex vivo*. White arrow points to example of micrometastatic seeding. Blue arrowheads point to examples of autofluorescence from imaging. **(C)** Quantitation of mice observed with liver micrometastatic seeding: $K30^{+/+}Ctd^{+/-}$ (+/+), $K30^{+/-}Ctd^{+/-}$-TP733 (+/-), and $K30^{-/-}Ctd^{+/-}$-TP703, TP735, TP771 (-/-). Chi-square test for trend, p=0.0315. n=3-5, as indicated. $K30^{+/+}Ctd^{+/-}$ vs. $K30^{-/-}Ctd^{+/-}$ p=0.0472.

out of 3 $K30^{+/+}Ctd^{+/-}$ (p=0.0472 by Chi-square test for trend, n=3/4), after an overall significance was detected between the three groups. The incidence of micrometastatic seeding detected in the liver of 1 out of 5 $K30^{+/-}Ctd^{+/-}$ mice was not significant when compared to micrometastatic seeding to the liver of $K30^{-/-}Ctd^{+/-}$ mice (**Figure 27C**). Due to the small sample size, the Chi-square result may not be valid. There were limitations in GFP-imaging and autofluorescence at image-capture; i.e., the gallbladder was found to autofluoresce under this imaging modality. Autofluoresence is distinguished by jagged streaks of light (**Figure 27B**, blue arrows). The duodenum and stomach were GFP-positive, as were other areas of the small intestine (**Figure 27A** vs. **Appendix C10**); we also observed this to be the case in $K30^{+/+}Ctd^{+/-}$ or $^{-/-}$ mice (**Figure 25** vs. **Appendix C10**). We isolated cell lines from the liver and the pancreas tissues of a three-month-old $K30^{-/-}C\ td^{+/-}$ mouse (mouse ID TP735) with micrometastatic seeding in the liver (detected by GFP imaging). We then sorted both the primary and metastatic PCCs (TP735-LM-GFP PCCs) using FACS to confirm the presence of GFP-positive PCCs in the liver of $K30^{-/-}C$ mice with micrometastatic seeding (**Appendix C7(B)**). We also froze sections from these tissues that appeared to contain GFP-positive micrometastases, as well as pancreas, lung, and liver from control mice that were GFP-negative, in optimal cutting temperature (OCT) compound for future studies. One $K30^{-/-}Ctd^{+/-}$ mouse presented with GFP positivity past the caecum and in the colon or large intestine (mouse ID TP746, see **Appendix C11**). The *Pdx1-Cre;LSL-Kras*^{G12D} model has been reported to result in lesions of the

gastrointestinal epithelium including the stomach and small bowel, but not in the lung, heart, liver, spleen, or kidney (Hingorani et al., 2003).

Macrometastases usually develop soon after dissemination (Nguyen et al., 2009). For this reason, we followed K30$^{-/-}$C mice to later time points and observed mice for grossly visible metastases. Three to five-month-old K30$^{-/-}$Ctd$^{+/-}$ mice did not show any signs of metastasis by histological analysis, not even those that were positive for micrometastases by light box GFP/RFP imaging or positive for GFP-sorted-*Kras*^{G12D} PCCs isolated from the liver. In contrast, the three K30$^{-/-}$C mice that developed frank tumor presentation by nine to eleven months of age also presented with liver nodules (**Figure 28A**) and lesions or full-blown lymph node metastases visible by gross observation (**Figure 29**). A total of five mice between the ages of 9-11 months, from both K30C and K30Ctd cohorts, were available for these analyses.

We confirmed that *Tip30* loss led to PCC liver metastases in two cases. The pancreatic tumors in these mice measured as big as ~45 mm in diameter. Nine-month-old K30$^{-/-}$C-TP889 (mouse ID TP889) (**Figure 18C-D**, **Figure 19**) presented with gross hepatic nodule formation (**Figure 28A**).Age-matched and littermate K30$^{+/+}$C and *Tip30*-deficient control mice did not exhibit this phenotype (**Figure 28B-C**). Severe, gross lymph node metastasis and metastatic burden to the liver was also observed in ten-month-old K30$^{-/-}$Ctd$^{+/-}$-TP881 (Mouse ID #881) (**Figure 29**). Histopathological analysis confirmed that the gross liver nodules observed in TP889 were sites of PDAC metastases (**Figure 28A, D-**Fields 1-3), with evidence of necrosis (**Figure 28D**-Field 4). A third mouse, in this late-aged group, only

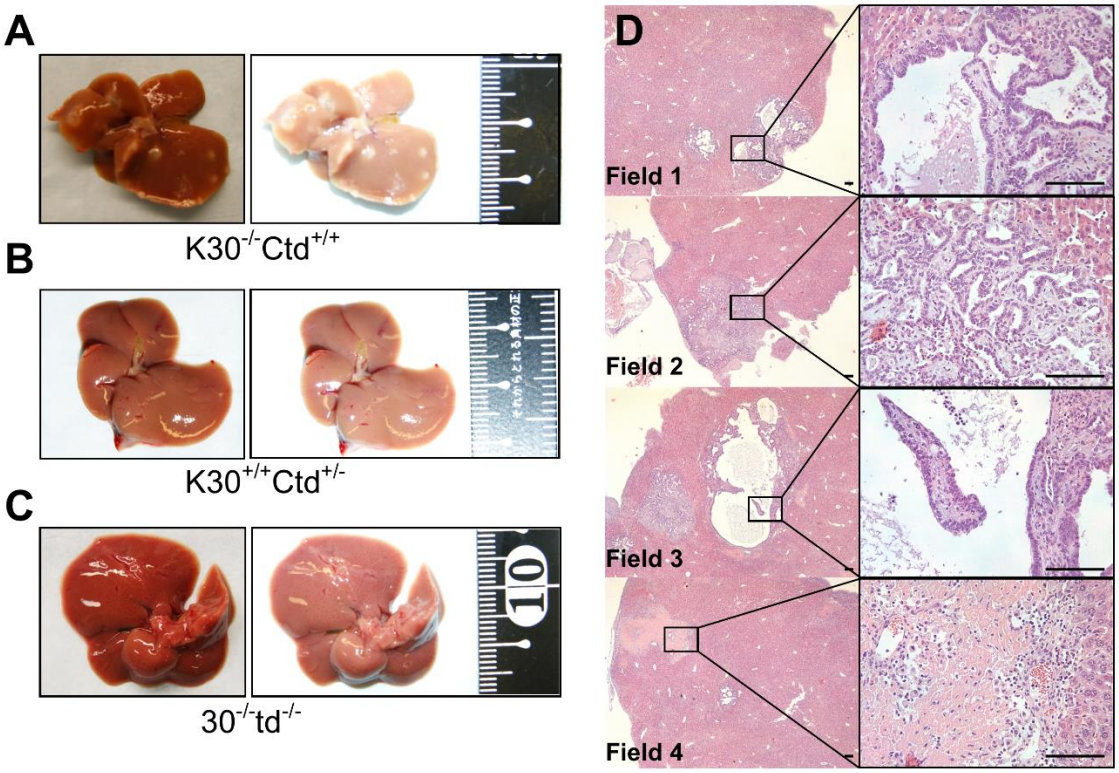

Figure 28. PDAC hepatic metastasis in a *Tip30*-null K30C mouse

(A) Gross liver nodule formation observed in a nine-month-old $K30^{-/-}Ctd^{+/+}$ mouse (TP889), imaged *ex vivo* compared to disease-free livers from age and sex-matched **(B)** $K30^{+/+}Ctd^{+/-}$ (TP942) and **(C)** $30^{-/-}td^{+/-}$ (TP890) mice. TP890 was also a littermate control. Ruler in mm. Images in the second column of **A-C** were taken with a flash setting. **(D)** Three different fields from an H&E stain of $K30^{-/-}Ctd^{+/+}$-TP889 liver tissue. Field 3 represents a necrotic lesion. Histopathological analysis and PDAC-associated macrometastatic lesions were confirmed with our pathologist. Scale bars: 100 µm.

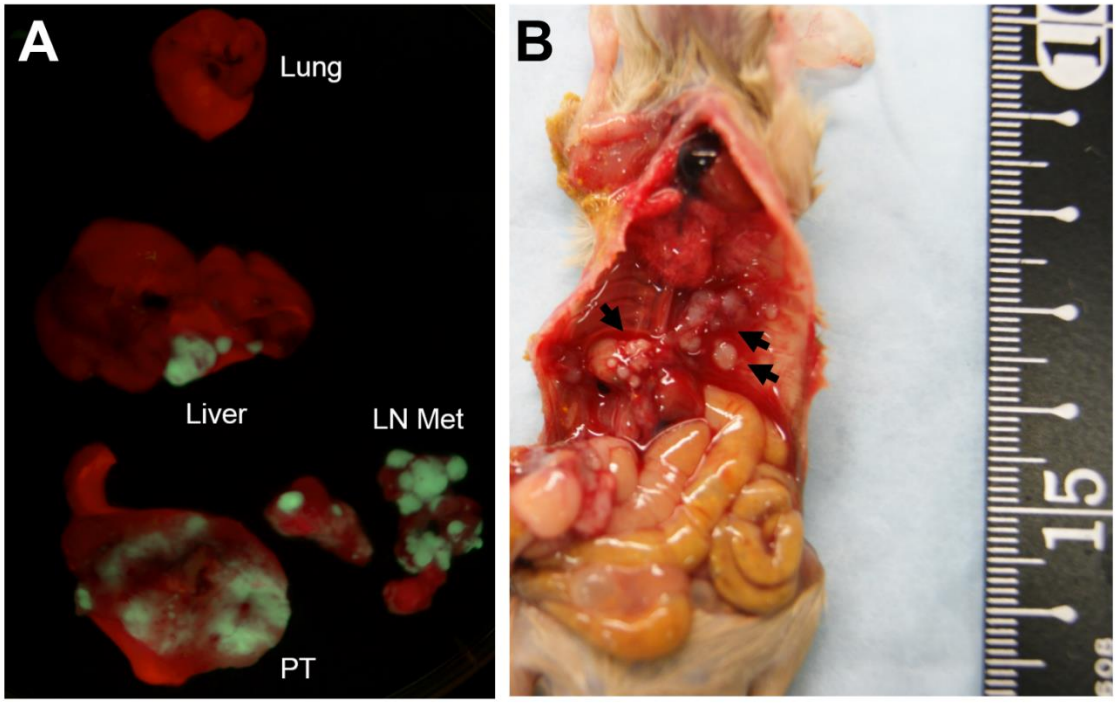

Figure 29. Representative image of PDAC tumor and subsequent metastatic burden in liver and lymph nodes of a K30$^{-/-}$Ctd$^{+/-}$ mouse

(A) GFP positivity in pancreatic tumor (PT) is surrounded by larger tdTomato-positive stromal reaction. GFP-positive mass and nodules were detected on the liver. Lungs were free of GFP-positivity. **(B)** Lymph node metastasis lines inner cavity (black arrows). Mouse ID is TP881. Lymph nodes (LN Met), and PDAC tumor (PT) attached to the spleen (S). These images were examined by our pathologist.

developed micrometastatic seeding to the liver but did not present with observable gross nodule formation or liver metastasis (**Appendix C11**). Histopathological analysis of a section of liver tissue instead identified lymphoma, even though this mouse had a ~10 mm in diameter pancreatic tumor (**Figure 19**-TP746 pancreatic tumor); and PDAC with necrosis was identified by histology (not shown). These preliminary observations in our PDAC mouse model suggested that total loss of *Tip30* resulted in pancreatic cancer cell liver metastasis. Consistent with our observations of the $K30^{-/-}Ctd^{+/-}$ model, pulmonary tissue from TP881 was negative for full-GFP positivity, metastatic nodules, or pulmonary lesion formation by gross observation (**Figure 29**).

We also observed an abnormal large cyst formation (measuring 10-22 mm in diameter) in four $K30^{+/+}Ctd^{+/-}$ mice (see **Figure 19**, TP942), while $30^{-/-}Ctd^{+/-}$ or $30^{+/-}Ctd^{+/-}$ and wild-type controls ($30^{+/+}Ctd^{+/-}$) did not exhibit this phenotype. In addition, GFP positivity and visual representation of potential $Kras^{G12D}$ recombination in *Pdx1-Cre;LSL-*$Kras^{G12D}$*;LoxP-tdTomato-LoxP-EGFP* mice extended further into the small intestines than was visible in *Pdx1-Cre;LoxP-tdTomato-LoxP-EGFP* mice (**Appendix C10, Figure 25**). The pathology of the pancreatic lesions and tumors observed in the $K30^{+/-}C$ and $K30^{-/-}C$, respectively, were different from the pancreatic cysts observed in $K30^{+/+}Ctd^{+/-}$ mice. $K30^{+/+}Ctd^{+/-}$ pancreata seemed normal otherwise and mesh-like, without the presence of a tumor (**Figure 19**). These fluid-filled cysts may resemble more closely the part of a mucinous cystic neoplastic (MCN) lesion containing nonhemorrhagic fluid, as

reported by de Wilde et al. (2012). However, additional analyses are needed to confirm their identity.

3.3 Summary

In this study, we generated and characterized a mouse model of PDAC with *Tip30*-heterozygous ($K30^{+/-}C$) and -homozygous loss ($K30^{-/-}C$) to investigate if *Tip30* loss accelerates pancreatic cancer in a murine model of PDAC (mPDAC). *Tip30*-heterozygous loss enhanced PDAC-associated disease and lesion progression in a cohort of three-month-old mice K30C, compared to *Tip30*-wild-type and *Tip30*-null K30C mice. $K30^{+/-}C$ mice presented with a gross pancreatic tumor pathology mostly in the form of pancreatic nodules, even at later ages, compared to classical pancreatic tumor presentation in older $K30^{-/-}C$ mice (9-11 months). A preponderance of CK-19-positive pancreas lesions, advanced disease stage diagnosed by lymph node invasion and metastasis, and poorer survival outcome across a cohort of age-matched mice led to the observation that heterozygous-loss of *Tip30* contributed to the increased distribution of PDAC precursor lesions and advanced disease. Analysis of TCGA data of human PDAC cases revealed that *HTATIP2* heterozygous loss occurred in 26% of hPDAC cases (UTSW, n=109) and that decreased TIP30 expression also results from *TIP30* promoter methylation or increased expression of MIR10B in hPDAC.

The findings from our first hypothesis on *Tip30* loss in PDAC tumor formation and progression then led us to investigate the role of *Tip30* loss in enhancing metastatic burden in this murine K30C PDAC model (**Figure 30**). Indeed, we found evidence of pancreatic cancer cell seeding in the lungs of $K30^{+/-}$

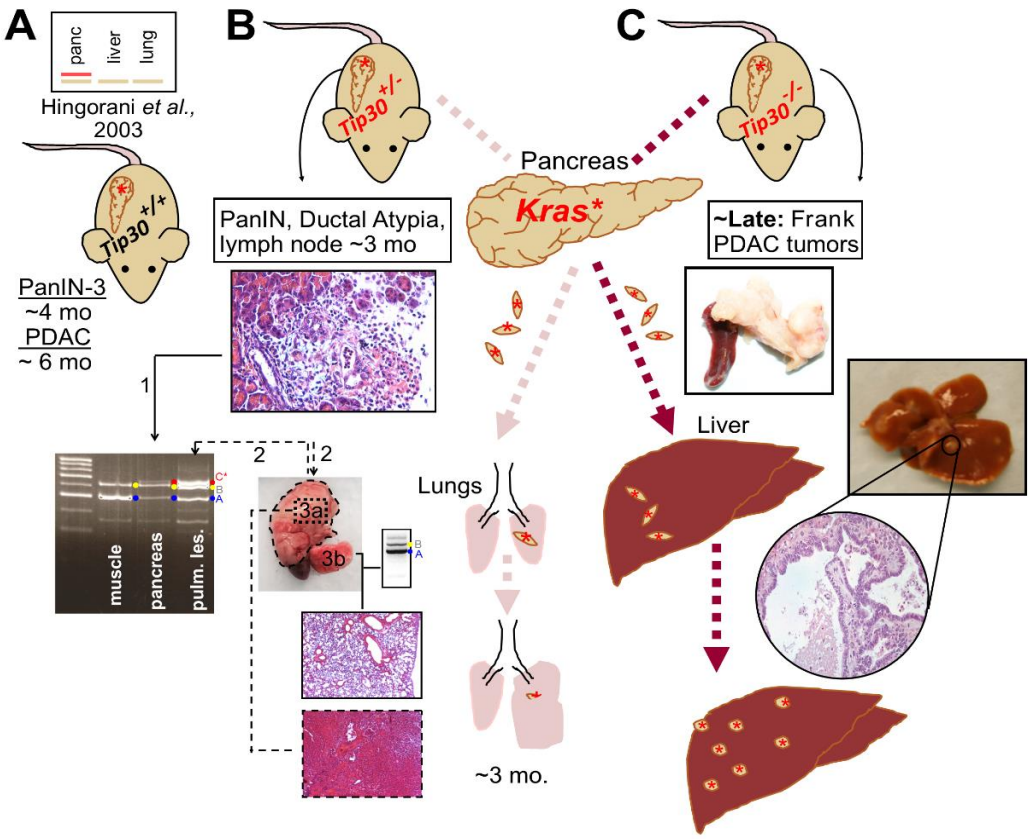

Figure 30. Summary and schematic of *Tip30*-copy-loss-mediated, organ-specific dissemination and metastasis in a murine model of PDAC

(A) In KC mice described in Hingorani et al. (2003), *Pdx1*-Cre drives a conditional *Kras*^{G12D} mutation to the pancreas epithelium (red *), with no trace in the pulmonary or hepatic tissues as detected by Kras G12D Conditional PCR in Hingorani et al. (2003). In this study, K30$^{+/+}$C mice were generated in the same background (BALB/c/B6/129SvJae mixed background) as the *Tip30*-deficient K30C mice under investigation. We observed shorter latency to PDAC than was reported by Hingorani et al. (2003). **(B)** In a three-month cohort, K30$^{+/-}$C mice exhibited more pronounced pancreas precursor lesions and PDAC by histology with evidence of lymph node invasion and metastasis (n=2/7). Additionally, 42% of K30$^{+/-}$C mice developed early pulmonary lesions (3a), and had poor survival outcome. Biopsies from the pulmonary lesions tested positive for the presence of PCCs via a PCR assay to detect the recombined mutant *Kras* allele and remaining *LoxP* site that was introduced in the pancreas epithelium, (dotted line and "2"). Matched adjacent normal pulmonary tissue (3b) tested negative for recombination and greatly positive for the unrecombined PCR product (n=2). Evaluation of H&E sections by a pathologist confirmed lung adenocarcinoma in 5 out 12 lung sections from mice with pulmonary lesions. These preliminary results suggested that pancreatic cancer cells seeded the lung in *Tip30*-heterozygous KC mice, and a *Tip30*-heterozygous pulmonary/immune environment may have contributed to early progression of lung adenocarcinoma and other abnormalities in the lung. **(C)** *Tip30*-null mice developed micrometastatic seeding to the liver when crossed with KC mice (K30$^{-/-}$Ctd) at a higher frequency compared to K30$^{+/-}$Ctd mice, at three months (n=3/4). Hepatic metastatic nodule formation was visualized grossly in two 9-10-month-old K30$^{-/-}$C mice. PDAC metastatic lesions by H&E stain shown in circle. K30$^{-/-}$C mice developed frank pancreatic tumors that were dense and encompassed the entire pancreas tissue.

C mice and in the liver of K30$^{-/-}$C mice by utilizing a tdTomato-EGFP reporter mouse in our studies that allowed for GFP labeling, and further identification, a sorting of *1-LoxP-Kras^{G12D}* pancreatic cancer cells. We also used the method of "Kras G12D Conditional PCR" method developed by The Jacks Lab (Jacks, 2017) to identify PCCs in the affected lung tissues of K30C mice with heterozygous but not in the adjacent normal lung tissue (n=2). K30C mice with one copy loss and homozygous loss of *Tip30* had increased disease burden in affected secondary tissues, the lungs, and the liver, respectively, which presented in the form of either gross pulmonary lesions and lung adenocarcinoma (in K30$^{+/-}$C) or liver metastases (in K30$^{-/-}$C) (**Figure 30**). Pancreas tissues, primary PCCs, metastatic sites, and corresponding metastatic PCCs isolated from the observed metastatic sites were confirmed to be positive for *1-LoxP-Kras^{G12D}* DNA and were therefore confirmed to be pancreatic cancer cells. Lastly, the massive pancreatic tumor formation in nine to eleven-month-old K30$^{-/-}$C mice that had not been previously observed in the KC mouse model (Hingorani et al., 2003), support our hypothesis that *Tip30* copy loss accelerates PDAC and metastatic organotropism in the K30C model.

CHAPTER 4. CHARACTERIZATION OF TIP30-DEFICIENT MURINE PANCREATIC CANCER CELLS FROM K30C AND K30Ctd MICE

4.1 Background and Rationale

Investigating the role of *Tip30* loss in an autochthonous PDAC model (K30C) revealed differences in the phenotype and time to tumor formation, as well as preferential differences in organ-specific-pancreatic-cancer cell (PCC) dissemination and metastasis between *Tip30*-heterozygous K30C mice ($K30^{+/-}C$) and *Tip30*-null K30C mice ($K30^{-/-}C$). $K30^{+/-}C$ mice presented with PCC seeding of pulmonary tissues and $K30^{-/-}C$ mice presented with PCC hepatic metastases. We next sought to understand underlying mechanistic differences in *Tip30* copy number loss on pancreatic cancer cell activity and their contribution to PDAC tumorigenicity. We isolated cell lines from the pancreas tissues of K30C mice as well as from organs observed to be burdened with metastatic disease or seeding to test the hypothesis that loss of TIP30 in pancreatic cancer cells alters PCC growth kinetics, the expression of cell growth and survival proteins in PCCs, and epithelial-mesenchymal transition (EMT). Reports of *Tip30* loss resulting in a growth advantage in mouse embryonic fibroblasts (MEFs) (Ito et al., 2003) led us to predict that any cell, especially a cancerous cell, with a loss in *Tip30* would have a growth advantage.

To begin investigating the role of *Tip30* copy number loss in PCC growth kinetics, we first performed *in vitro* assays to assess two-dimensional and three-dimensional growth in *Tip30*-heterozygous and *Tip30*-null PCCs, compared to *Tip30*-wild-type PCCs. In addition, we performed biochemical assays to

investigate the role of *Tip30* loss on EGFR levels in murine PCCs. siRNA knockdown of *Tip30* prevented the fusion of a Rab5/ACSL4/endophillinB/TIP30 complex, slowing EGFR trafficking; and in internalization studies deleting *Tip30* in primary hepatocytes (*Tip30*$^{-/-}$) led increased EGF-EGFR complex colocalization (Zhang et al., 2011). To add to this, TIP30-knockdown delayed EGFR degradation in a human hepatocellular cell line (Zhang et al., 2011). Few studies have focused on the role of *Tip30* loss in pancreatic cancer. In 2003, Ouyang et al. reported that overexpression of TIP30 antagonist, miR-10b, in human pancreatic cancer cells, increased the levels of EMT-associated gene expression and EGF-stimulated invasion. The authors also reported that silencing *Tip30* by siRNA resulted in sustained EGFR signaling (Ouyang et al., 2013). How *Tip30* gene dose mediates pancreatic cancer cell function and activity have not yet been reported.

4.2 Results

4.2.1 Generation of Primary and Metastatic Pancreatic Cancer Cell Lines from K30C and K30CtdTom-EGFP (K30Ctd) Mouse Models

To evaluate mechanistic changes in *Tip30*-heterozygous and -null pancreatic cancer cells (PCCs), we established cell lines from both K30C and K30Ctd$^{+/-}$ mouse pancreata and metastatic lesions. PCCs and metastatic PCCs from K30Ctd$^{+/-}$ mice were labeled (-GFP PCCs) after flow sorting for GFP positivity (**Appendix C7(A)-(B)**). Cell lines were isolated from mice with visible pancreatic or metastatic pathology at sacrifice (**Table 4**). In the case of K30$^{+/+}$C controls, where a detectable tumor or seeding was not visible by gross examination, cell

Table 4. Tissues used to establish pancreatic cancer cell lines (PCCs)

Genotype	**Mouse ID**	**Age (mo)**	**Pancreas Description**	**Pathology Report (Pancreas)**
$K30^{+/+}$Ctd+/-	TP151	3	Tumor & Cystic	Cyst, PanIN-3, Reactive lymph node
$K30^{+/+}$C	TP711	4	Small Cyst	PanIN-3
$K30^{+/+}$C	TP715	4	-	PanIN-3
$K30^{+/-}Ctd^{+/-}$	TP852	2	-	Chronic ductal inflammation
$K30^{+/-}$C	TP573	5	Meshy, pancreatic nodules	PanIN-3, Enlarged lymph node (20X), approaching adenocarcinoma
$K30^{+/-}$C	TP647	5	Meshy, with pancreatic nodule, small tumor in head of pancreas.	PanIN, inflammation
$K30^{-/-}C^{td+/-}$	TP735	3	Dense tumor	Adenocarcinoma
$K30^{-/-}$C	TP592	6	Cystic pancreas, large tumor	Broken basement membrane
$K30^{-/-}$C $td^{+/+}$	TP889	9	Dense, firm, gross	Cystic adenocarcinoma

Age in months (mo). 20X, twenty times greater than normal.

lines were established from tissues, as available, for a basis of comparison between *Tip30*-wild-type and -deficient PCCs or metastatic (met) PCCs. Two *Tip30* wild-type PCC lines were established from four-month-old $K30^{+/+}C$ mice, with PanIN-3 pancreatic histopathology. The third cell line was established from a three-month- old $K30^{+/+}Ctd^{+/-}$ mouse in which a tumor was grossly visible, and PanIN-3 and a reactive lymph node detectable by histopathological evaluation (**Table 4**). Differences between the K30C and K30Ctd tomato mouse models in regards to PDAC tumor development have not yet been investigated. We validated *Tip30* genotyping, presence of the engineered oncogenic *Kras* mutation (Jacks, 2017), and TIP30 protein levels in K30C and K30Ctd (GFP) PCCs (**Figure 23**). We observed nearly 100% *LSL-Kras*^{G12D} recombination in primary pancreatic cancer cells established from these models, including sorted GFP PCCs (n=3 per group, $K30^{+/+}C$, $K30^{+/-}C$, or $K30^{-/-}C$ with or without tdTomato-EGFP) (a representative analysis is shown **Figure 23B**), thereby suggesting that the cells isolated from pancreas tissues were indeed PCCs and positive for mutant *Kras*. These interpretations stemmed from visualizing complete loss of the 500-bp PCR product that detects the unrecombined *LSL* cassette, by methods of gel electrophoresis. After successful GFP sorting, metastatic PCCs also followed the pattern of 100% recombination efficiency observed in primary PCCs (**Figure 23B**, **Figure 26F**).

Additionally, whole genome sequencing was performed on mPCCs. With assistance from Dr. Francis Enane (IU School of Medicine), *Tip30* was confirmed to be intact at exons 2-3 by sequencing analysis. *Rb1*, *Tp53*, and *Smad4* were

also confirmed to be wild-type in K30$^{+/+}$C PCCs, including the TP912-Lung-GFP sample. The K30$^{+/+}$Ctd$^{+/-}$ cell line TP151-GFP exhibited lower TIP30 protein levels compared to the other two cell lines from K30$^{+/+}$C mice without the tdTomato construct. Similar variability was observed in the K30$^{+/-}$C group; however, overall TIP30 protein levels of K30$^{+/-}$C PCCs were still less than that of K30$^{+/+}$C PCCs by an average of 50% (**Figure 23D**). Similar variability was observed in PCC Tip30 mRNA levels. Tip30 mRNA levels in a GFP cell line from each K30C group followed the same trend as Tip30 mRNA levels in pancreas tissues and in cell lines from K30C mice. However, compared to cell lines isolated from K30C mice without the tdTomato construct, cell lines established from K30Ctd mice had the lowest Tip30 mRNA levels of all three cell lines for both the K30$^{+/+}$Ctd and the K30$^{+/-}$Ctd group (see TIP30 protein level differences in K30$^{+/+}$Ctd PCCs in **Figure 23D**). It is conceivable that the heterogeneity observed from mouse-to-mouse in our studies could also be observed on a cellular level. Additional cell lines from both groups of mice, and preferably at least three from each model could help account for the variability coming from the EGFP construct. Cell lines were CK-19 positive but were also positive for smooth muscle actin (α-SMA), a mesenchymal cell marker (**Figure 31-32**).

K30$^{+/-}$C mice with visible pulmonary lesions or lung seeding by GFP (TP852) were used to establish pulmonary metastatic PCCs (-Lung PCCs). K30$^{-/-}$C mice with visible liver nodules or visible hepatic micrometastatic seeding detected by fluorescence light box imaging were used in establishing metastatic liver PCCs (-LM PCCs) from the hepatic tissues of TP889 and TP735 mice. TP735-

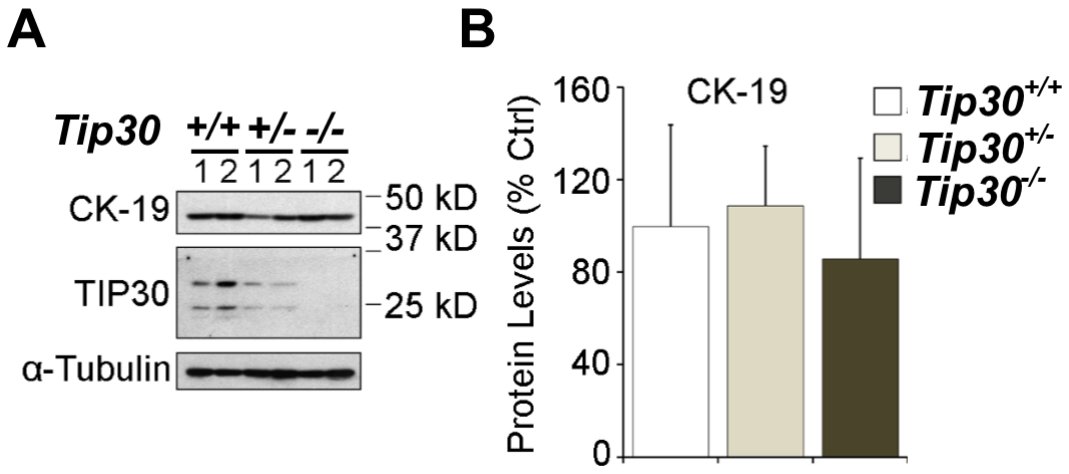

Figure 31. Primary K30C PCCs did not show marked differences in CK-19 protein levels

(A) Representative immunoblot of basal CK-19 levels in mPCCs from K30C and K30Ctd$^{+/-}$ GEMMs with wild-type (+/+, TP711. TP715), heterozygous (+/-, TP673, TP647), and homozygous (-/-. TP592-1, TP889) loss of *Tip30* (n=2 shown, repeated three different times per cell line except for GFP cell lines, performed once). CK-19 protein levels were assessed for a total of three independent PCCs per group (*Tip30*$^{+/+}$-TP151-GFP, -TP711, -TP715 PCCs; *Tip30*$^{+/-}$-TP573, -TP647, -TP852-GFP PCCs; and *Tip30*$^{-/-}$-TP592-1, -TP889, -TP735-GFP PCCs). **(B)** Data represent the densitometry means ± SEM of three cell lines per group: *Tip30*$^{+/+}$-TP151-GFP, -TP711, -TP715 PCCs; *Tip30*$^{+/-}$-TP573, -TP647, -TP852-GFP PCCs; and *Tip30*$^{-/-}$-TP592-1, -TP889, -TP735-GFP PCCs. Protein levels were normalized to loading control (α-Tubulin) and K30$^{+/+}$C PCC levels (+/+). One-way ANOVA followed by Tukey post-hoc test performed on n=3; no significant difference found between groups.

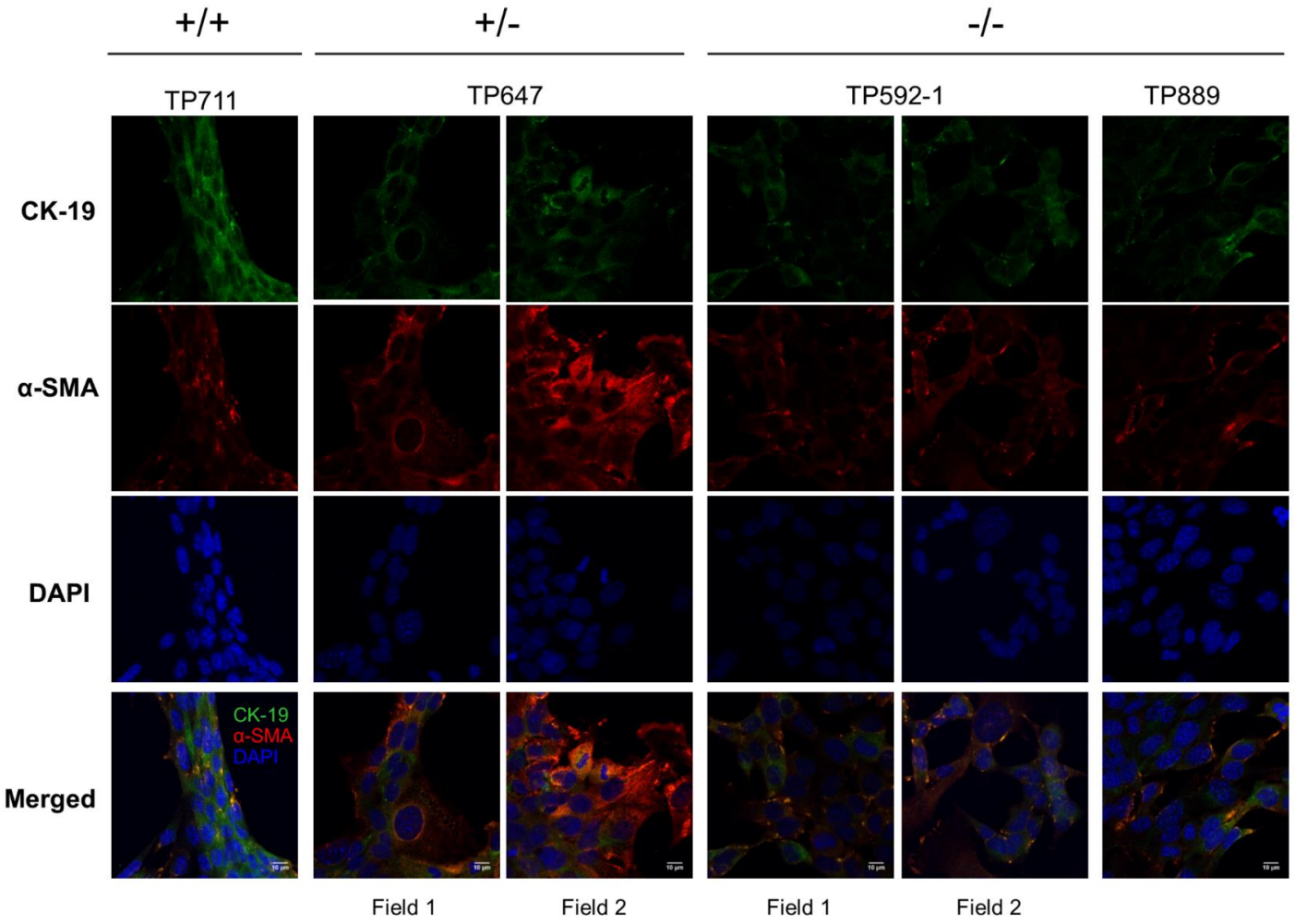

Figure 32. Detection of epithelial and mesenchymal marker levels in K30C PCCs by immunofluorescence

+/+, *Tip30*-wild-type. +/-, *Tip30*-heterozygous. -/-, *Tip30*-null.

LM-GFP PCCs were assessed for *Kras*^{G12D} recombination after flow sorting (**Appendix C7(B)**) and were found to have similar, fully recombined DNA (not shown) as both primary PCCs and as is shown for the lung metastatic PCCs in **Figure 26F**. These observation further strengthened the hypothesis that loss in *Tip30* copy number mediated pancreatic cancer cell dissemination and seeding of pulmonary tissues on our model. The resemblance in genetic characterization between primary PCCs, liver- and lung metastatic PCCs supported the hypothesis that the cells and DNA isolated from the pulmonary tissue and positive for oncogenic *Kras* were PCCs that originated from the pancreas.

4.2.2 *Tip30*-Deficienct mPCCs have increased Two- and Three-Dimensional Growth Properties

Puck et al. (1956) first described the clonogenic assay to assess the ability of cancer cells to form colonies after seeding. We performed two-dimensional (2D) clonogenic and three-dimensional (3D) growth assays to assess differences in growth of K30$^{+/-}$C or K30$^{-/-}$C PCCs compared to K30$^{+/+}$C PCCs (**Figures 33-34**). Murine PCCs (mPCCs) exhibited an average trend for increased growth, that correlated with copy number loss of *Tip30* (**Figure 34A**). While TIP30 protein and mRNA (individual mRNA levels not shown) levels were markedly lower in TP151-GFP PCCs than in that of TP711, and TP715 K30$^{+/+}$C PCCs (**Figure 23D**), this difference did not translate to a growth advantage in 2D or 3D (**Figure 33A**, **Figure 34A**).

Metastatic PCCs from the liver of K30$^{-/-}$C mice exhibited increased two-dimensional colony growth forming areas when compared to metastatic PCCs

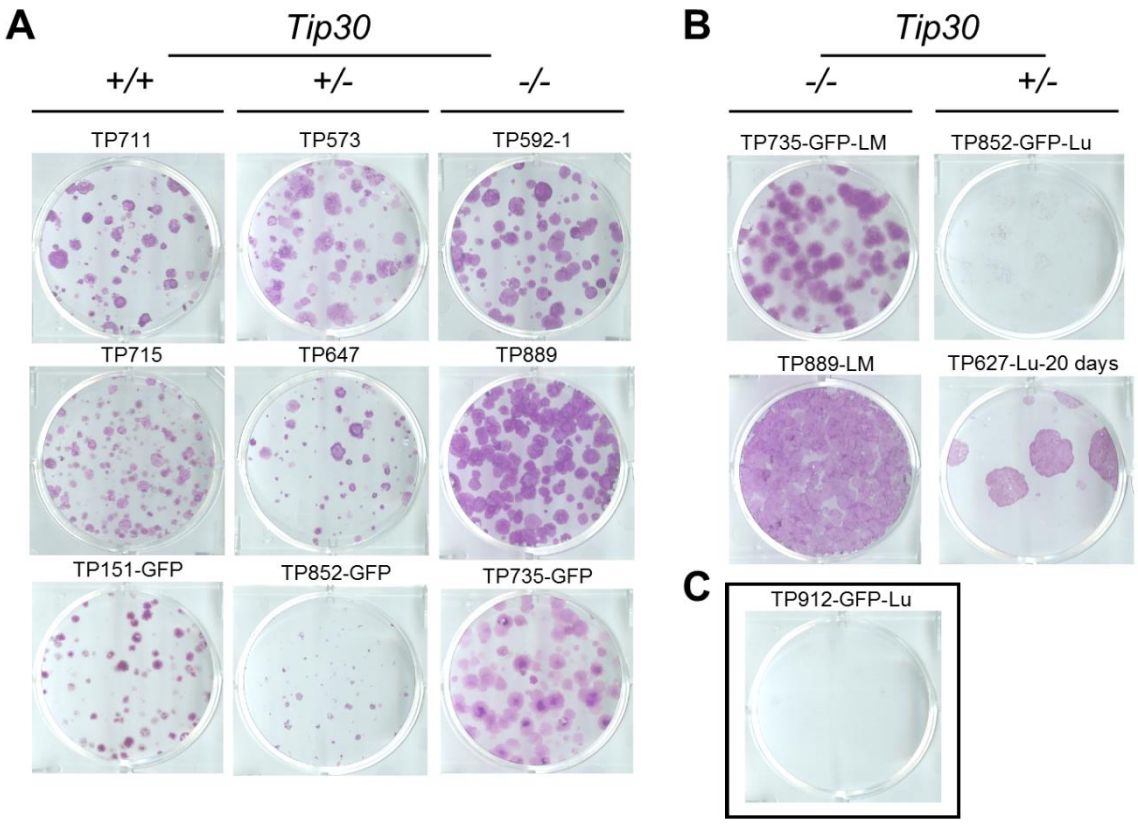

Figure 33. Complete loss of *Tip30* enhances colony formation for murine pancreatic cancer cells *in vitro*

(A) Two-dimensional growth of murine pancreatic cancer cells (mPCCs) with two *Tip30*-wild-type alleles (+/+), *Tip30*-heterozygous loss (+/-), and *Tip30*-homozygous loss (-/-) was assessed using a clonogenic growth assay (n=3, per group). Colony formation was monitored for 7-8 days. mPCCs were derived from K30C and K30Ctd$^{+/-}$ GEMMs. One representative image per cell line is shown. Experiments were repeated three separate times except for TP735-GFP and TP852-GFP cell lines (performed two separate times), and in duplicate. **(B)** PCCs established from metastatic lesions of the liver (-LM) or metastatic seeding or gross lesions of the lung (-Lu) for TP852-GFP and TP627 respectively. Growth was assessed after 7-8 days, except for TP627-Lu, which was allowed to grow for 20 days to monitor if K30$^{+/-}$C lung metastatic PCCs were capable of colony formation. Experiments were repeated three separate times except for TP852-GFP-Lu (twice), and TP627-Lu-20 days (once). Brightness of scanned images were adjusted to 70% with a contrast (50%). **(C)**TP912-GFP-Lu is from a K30$^{+/+}$Ctd$^{+/-}$ mouse, and serves as a metastatic PCC control. Colony formation was assessed after 7-8 days.

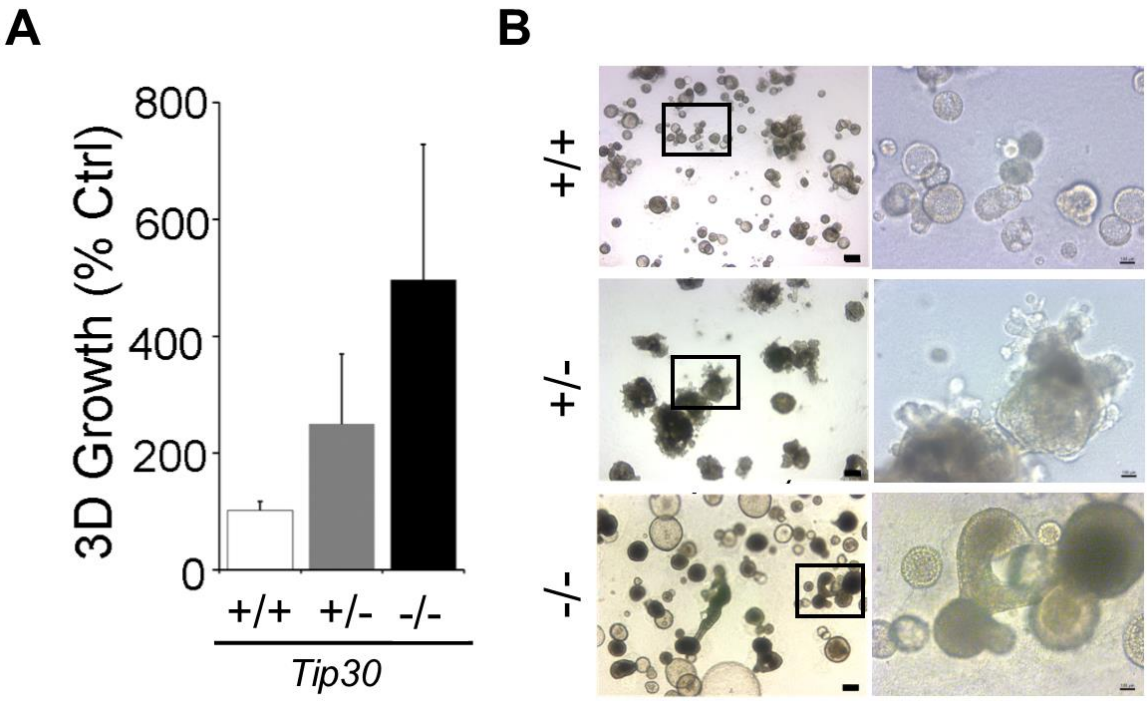

Figure 34. *Tip30*-deficiency accelerates 3D anchorage-independent growth in pancreatic cancer cells

(A) In a three-dimensional growth assay that utilizes 3% matrigel (Sempere et al., 2011), murine pancreatic cancer cells (mPCCs) exhibited a trend of increasing 3D colony formation and growth with decreasing *Tip30* copy number. 3D growth was assessed after 17-18 days in culture, and total colony areas were quantitated after MTT incorporation in ImageJ. Data represent the means ± SEM of three cell lines per group ($K30^{+/+}$C-TP151-GFP, -TP711, -TP715 PCCs; $K30^{+/-}$C-TP573, -TP647, -TP852-GFP PCCs; and $K30^{-/-}$C-TP592-1, -TP889, -TP735-GFP PCCs). **(B)** A representative brightfield image of mPCCs with either wild-type *Tip30* (+/+), hetloss of *Tip30* (+/-), or *Tip30*-null (-/-) genotype status at low and high power. The following cell lines are represented: TP711 (+/+), TP573 (+/-), and TP889 (-/-) PCCs (in 3D). Scale bars: 100 µm.

isolated from the lungs of K30$^{+/-}$C mice (**Figure 33B**). *Tip30*-heterozygous lung metastatic (met) PCCs eventually formed colonies in 2D when the growth period reached 20 days in culture. Finally, while GFP-positive PCCs, isolated from the lungs of a three-month-old K30$^{+/+}$C mouse (TP912)-intended for use as a control-expanded in culture, these cells did not form 2D colonies (**Figure 33B**).

Anchorage-independent growth is a well-established hallmark of carcinogenesis and one of the three tests used to establish tumorigenicity (Borowicz et al., 2014; Shin et al., 1975; Mori et al., 2009). With regards to physiological relevance, there are limitations for growing cells in 2D and on plastic. Growth in 3D culture systems is considered to provide more biologically relevant information (Edmondson et al., 2014). We performed three-dimensional growth assays using primary pancreatic cancer cells (n=3) to confirm our 2D observations. *Tip30* loss gave murine PCCs (mPCCs) a growth advantage in our 3D culture system. This assay consisted of a 3% matrigel (a gelatinous collagen IV/laminin-rich medium) suspension where 3D colonies would develop, that rested over a layer of 1% soft-agar solution (Sempere et al., 2011). Growth kinetics varied between cell lines within both *Tip30*-heterozygous and *Tip30*-null mPCC groups. We observed a trend for increased 3D colony formation in *Tip30*-deficient and -null mPCCs after 17-18 days. *Tip30*-null mPCCs formed double the 3D colony areas of *Tip30*-deficient (*Tip30*$^{+/-}$) mPCCs. The colony areas of *Tip30*-null PCCs doubled that of *Tip30*-heterozygous PCCs. A similar trend in *Tip30* copy number loss and growth has been reported in immortalized mouse embryonic fibroblast cells (Ito et al., 2003). In addition, while *Tip30*-null mPCC 3D colonies were larger or more

abundant when compared to *Tip30*-wild-type PCCs, both of these groups shared a similar phenotype. 3D colonies that formed from either *Tip30*-wild-type or -null mPCCs formed very smooth spheres that were sometimes hollow. In contrast, mPCCs with heterozygous loss of *Tip30* had a striking phenotypical difference in colony formation when compared to both *Tip30*-null and -wild-type PCCs. In 3D growth conditions, these $K30^{+/-}C$ PCCs had an invasive-like phenotype (**Figure 34A, B**). *Tip30*-heterozygous PCCs formed disorganized and aggressive-looking 3D colonies, with multiple budding events, or protrusions, extending from a primary colony (**Figure 34B**). mPCCs from $K30^{+/-}C$ genotype, with one copy loss of *Tip30*, may therefore have enhanced invasive properties, but additional assays would need to be conducted to confirm this hypothesis.

Tip30-null TP735-GFP PCCs exhibited a seven-fold increase in growth in 3D ($p=0.0008$) when compared to *Tip30*-wild-type-TP151-GFP ($K30^{+/+}Ctd^{+/-}$) PCCs (**Figure 35A-B**) suggesting that complete *Tip30* loss led to increased growth capacity of mPCCs. TP735-GFP PCCs formed colonies that were composed of elongated and spindle-like cells compared to $K30^{+/+}Ctd^{+/-}$ PCC line TP151-GFP (**Figure 35C**). This difference between the two cell lines was only visible in 3D culture, and both cell lines shared a similar phenotypic morphology in 2D culture (**Figure 35C**). These studies highlight the importance of assessing growth in 3D when evaluating PCC growth potential and the impact of tumor and metastasis suppressor loss in PCCs. Although PCC growth *in vivo* is the ultimate evaluation of tumorigenicity and would confirm the metastatic potential of *Tip30*-null compared to *Tip30*-heterozygous mPCCs.

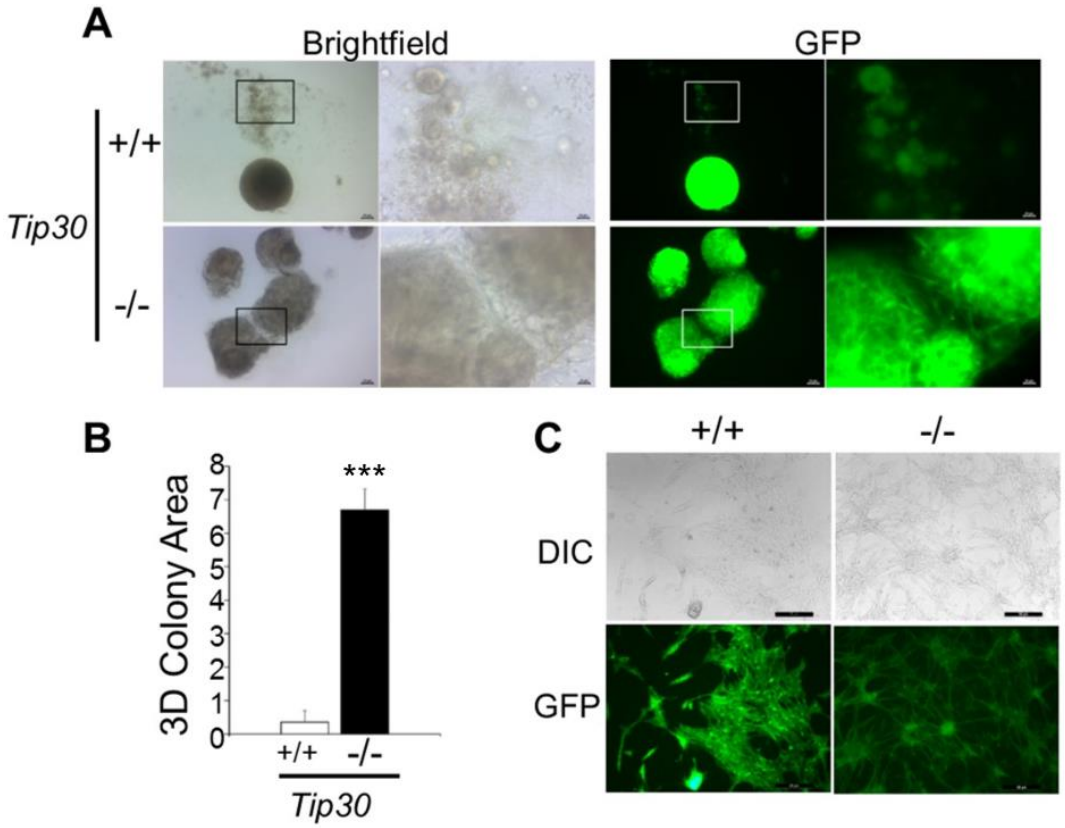

Figure 35. *Tip30*$^{-/-}$-GFP-positive mPCC growth in 3D culture as compared to *Tip30*$^{+/+}$-GFP PCCs

(A) A representative image of 3D Growth of K30$^{-/-}$Ctd$^{+/-}$ mPCCs (TP735-GFP) compared to K30$^{+/+}$Ctd$^{+/-}$ (TP151-GFP) PCCs at low and high power. Visualization by GFP imaging in right panel. Scale bars: 25 µm. **(B)** Quantitation (by ImageJ) of MTT incorporation and total colony areas for three independent experiments represented in **A**. Colonies formed over 16-17 days in a three-dimensional growth assay. Data represent the means ± SEM of three independent experiments, normalized to *Tip30*$^{+/+}$ control PCCs. Student's two-tailed t-test was performed, p=0.0008. (**C**) GFP+ PCCs exhibit similarities in cell morphology in two-dimensional growth culture conditions. Brightness was set to 60% and Contrast to 70% in the TP735-GFP 2D GFP image (-/-, GFP) to allow for better visualization of morphology. Both DIC images were adjusted to a Brightness of 60% and 70%, for +/+, and -/- respectively with a contrast change from 50% to 70% of the original image in Microsoft Publisher. Scale bars: 50 µm.

The increase in 2D and 3D growth forming areas of *Tip30*-deficient PCCs led us to hypothesize that *Tip30* copy number loss influenced PCC proliferation. *Tip30* has been reported to regulate c-Myc, a transcription factor encoded by the *c-MYC* oncogene that regulates cell proliferation (Miller et al., 2012), expression in mammary glands by interacting with the estrogen receptor α-interacting coactivator CIA (Jiang et al., 2004). *Tip30*-deficiency was found to enhance c-Myc transcription, while overexpression of *Tip30* was found to repress it (Jiang et al., 2004). To understand if differences in c-Myc transcript levels played a role in *Tip30*-deficient PCC proliferation, c-Myc transcript levels were assessed in murine pancreatic cancer cell lines isolated from the pancreas tissues of K30$^{+/+,\ +/-,}$ and $^{-/-}$C mice (n=3 per group). Interestingly, *Tip30*-heterozygous PCCs (*Tip30*$^{+/-}$) exhibited a 50% trend of decrease in c-Myc levels when compared to *Tip30*-wild-type (*Tip30*$^{+/+}$) and *Tip30*-null (*Tip30*$^{-/-}$) PCCs, suggesting that the enhanced growth kinetics observed in*Tip30*-deficient PCC may have occurred independent of c-Myc. However, this interpretation cannot be substantiated without further analyses; since, these results did not reach statistical significance (n=3, **Figure 36**). This could be due to the heterogeneity between cell lines and a need for increased sampling of c-Myc levels in more than three cell lines.

4.2.3 Increased EGFR Protein and mRNA Levels in PCCs with *Tip30*-Heterozygous Loss

EGFR overexpression is reported characteristic of hPDAC (Korc et al., 1992). Additionally, EGFR pathway upregulation has been shown to precede

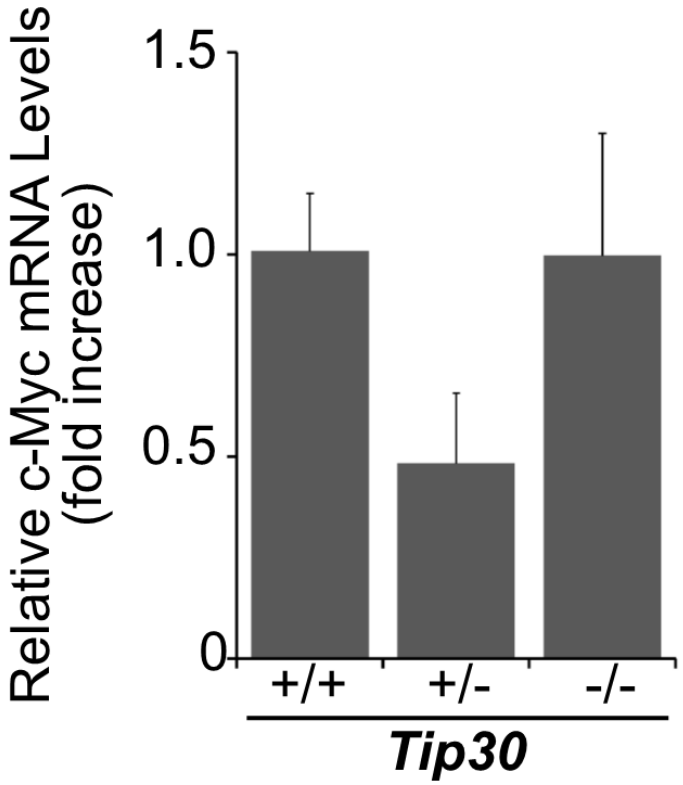

Figure 36. c-Myc mRNA expression levels in K30C murine PCCs

Relative quantity of c-Myc in K30C PCCs, after qRT-PCR is shown. c-Myc levels were normalized to β-actin, and *Tip30*-wild-type (+/+) pancreatic cancer cells (PCCs). Data represent the means ± SEM of three cell lines per group ($K30^{+/+}$C-TP151-GFP, -TP711, -TP715 PCCs; $K30^{+/-}$C-TP573, -TP647, -TP852-GFP PCCs; and $K30^{-/-}$C-TP592-1, -TP889, -TP735-GFP PCCs). A one-way ANOVA followed by Tukey post-hoc test for n=3 was performed. Data did not reach statistical significance. +/+, *Tip30*-wild-type; +/-, *Tip30*-heterozygous; -/-, *Tip30*-null.

tumorigenesis in *Kras*-mutant mice (Ardito et al., 2012). TIP30 loss was reported to increase EGF-EGFR complex formation in the early endosome in hepatocellular carcinoma cells (Zhang, 2011). TIP30 loss has also led to alveolar epithelial type II (AT2) cell expansion, increased EGFR in lung tissues and tumors, and the increased expression of downstream signaling proteins pERK1/2 and pAKT in *TIP30*-deficient human lung adenocarcinoma cells (Li et al., 2013). We therefore decided to interrogate the presence of EGFR in pancreatic cancer cells (PCCs) with genetic loss of *Tip30*. We hypothesized that *Tip30*-loss would alter EGFR protein levels, and expected to see an inverse relationship between EGFR protein levels and *Tip30* copy number loss. Three validated murine pancreatic cancer cell lines isolated from K30C pancreatic tumors, with either a *Tip30*-wild-type, *Tip30*-heterozygous, or *Tip30*-null genetic background (**Table 4**), were utilized to examine EGFR protein levels.

Interestingly, only the *Tip30*-heterozygous PCCs exhibited increased EGFR protein levels (**Figure 37A-B**). *Tip30*-heterozygous PCCs had a seven-fold increase in EGFR compared to *Tip30*-wild-type PCCs; and EGFR levels in *Tip30*-null PCCs compared to *Tip30*-heterozygous PCCs were decreased significantly (p=0.046). *Tip30*-heterozygosity also resulted in a 70% increase in Egfr transcript levels (did not reach statistical significance) while PCCs with complete loss of *Tip30* exhibited a 50% decrease in Egfr mRNA levels (n=3, p=0.01 by one-way ANOVA) when compared to $Tip30^{+/-}$ PCCs (**Figure 37C**). We also used confocal microscopy imaging to assess the localization of EGFR in $K30^{+/-}$C PCCs and to confirm our biochemical observations of EGFR protein levels. Compared to

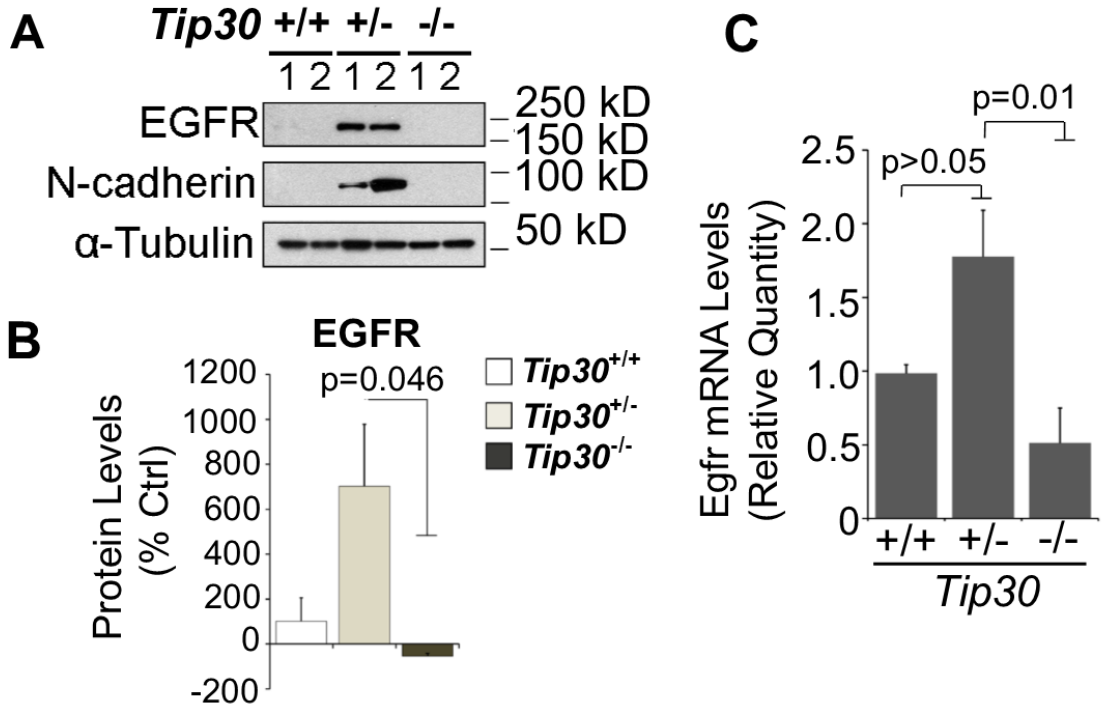

Figure 37. *Tip30*-heterozygous PCCs have increased EGFR protein and transcript levels

(A) Representative immunoblot of basal EGFR and N-cadherin levels in mPCCs from K30C and K30Ctd$^{+/-}$ GEMMs with wild-type (+/+), heterozygous (+/-), and homozygous (+/-) loss of *Tip30* (n=2 shown). Experiment was repeated three different times per cell line except for GFP cell lines, (performed once). **(B)** Densitometry quantitation of EGFR levels in **A**. Data represent the densitometry means ± SEM of three independent cell lines per group: K30$^{+/+}$C-TP151-GFP, -TP711, -TP715 PCCs; K30$^{+/-}$C-TP573, -TP647, -TP852-GFP PCCs; and K30$^{-/-}$C-TP592-1, -TP889, -TP735-GFP PCCs. Protein levels were normalized to loading control (α-Tubulin, and K30$^{+/+}$C PCC levels (+/+). One-way ANOVA followed by Tukey post-hoc test performed on three biological replicates per group (three different cell lines per group). $p<0.05$ was considered statistically significant. **(C)** Relative Egfr transcript levels in K30C PCCs. Egfr mRNA levels were normalized to β-actin. Data represent the means ± SEM of three cell lines per group. One-way ANOVA followed by Tukey post-hoc test for n=3 cell lines per group (see list in **B**). $p<0.05$ was considered statistically significant. +/+, *Tip30* wild-type; +/-, *Tip30*-heterozygous; -/-, *Tip30*-null.

$K30^{+/+}C$ and $K30^{-/-}C$ PCCs, EGFR levels were highest in $K30^{+/-}C$ PCCs (n=2). Thirty minutes of 1 nM EGF treatment resulted in a change of EGFR distribution from cytosolic to perinuclear in $K30^{+/-}C$ PCC line TP573 (from mouse ID TP573) (**Figure 38**). The cell line with the lowest EGFR protein level in the $K30^{+/-}C$ group (TP852-GFP) had an increase in HER2 and HER3 levels. Other than this observation in that single cell line, genetic loss of *Tip30* did not seem to significantly alter HER2 and HER3 levels (data not shown).

4.2.4 N-Cadherin and E-Cadherin Protein Levels in *Tip30*-Deficient mPCCs Rely on Tip30 Gene Dose

Epithelial cell migration is known to require the loss of cell polarity and cell-cell adhesion properties, as well as an acquisition of mesenchymal properties including upregulation of mesenchymal-cell like markers (Padua and Massagué, 2009; Voon et al., 2017). The process whereby cells shift towards a more migratory and invasive state and express marker levels associated with their altered state is known as epithelial-mesenchymal transition or EMT (Nieto et al., 2016). Circulating pancreatic cancer cells that are N-cadherin-positive harbor a mesenchymal and invasive phenotype and show low E-cadherin levels (Rhim et al., 2012). Although both E-cadherin-positive and -negative cells from mice with pancreatic intraepithelial neoplasia (PanIN) were capable of forming pancreatic tumors in mice in a study by Rhim et al., E-cadherin-low PanIN cells that had undergone EMT displayed an advantage in tumor-initiation (Rhim et al., 2012). We sought to investigate if loss in *Tip30* gene copy number resulted in pancreatic cancer cells

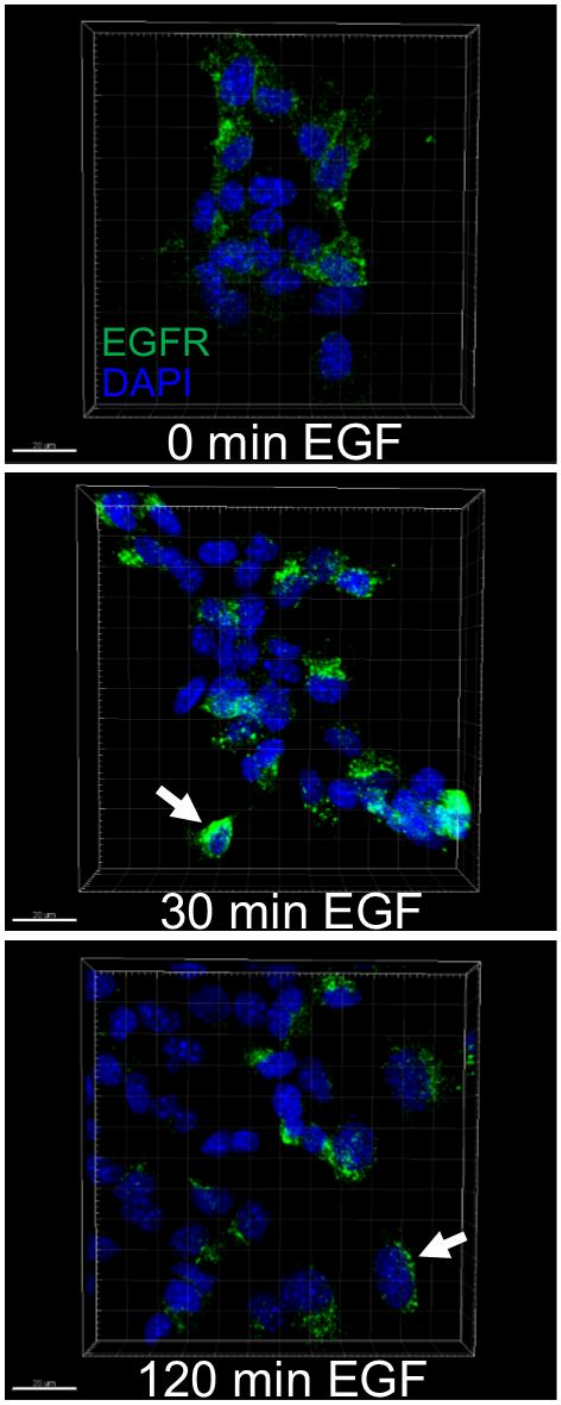

Figure 38. Perinuclear EGFR accumulation as a consequence of EGF treatment in a cell line isolated from the *Tip30*-heterozygous K30C mouse

$K30^{+/-}$C-TP573 PCCs were treated with 1 nM EGF after serum starvation overnight for the indicated time points (0-120 minutes of EGF treatment). EGFR distribution (green) is shown with DAPI nuclear stain (blue). White arrows point to perinuclear localization. Scale bars: 20 μm.

that were more EMT-like, characterized by increased N-cadherin and decreased E-cadherin levels.

Interestingly, similar to the EGFR observations, we found that N-cadherin levels were increased in $K30^{+/-}C$ PCCs (n=2, **Figure 37A**). The N-cadherin levels in the third $K30^{+/-}C$ cell line, TP852-GFP, were undetectable precluding quantitative presentation of the data. However, in the *Tip30*-null mPCC lines analyzed (n=3), N-cadherin protein levels were lower when compared to $K30^{+/-}C$ PCCs (**Figure 37A**). We note that these latter observations are from just two $K30^{+/-}C$ cell lines. Additionally, two liver-met PCC lines from $K30^{-/-}C$ mice exhibited lower N-cadherin levels compared to metastatic PCCs from the lung (not shown). In addition to low N-cadherin levels, *Tip30*-null PCCs exhibited a six-fold decrease in E-cadherin protein levels when compared to *Tip30*-heterozygous PCCs (p=0.054, **Figure 39**) and *Tip30*-wild-type PCCs (p=0.058). There was no significant difference in CK-19 levels in mPCCs between each group (**Figure 31**).

4.2.5 Overexpression of microRNA-10b Increased Basal EGFR and AKT Levels in Human AsPC-1 Pancreatic Cancer Cells

MicroRNA (miR)-10b is an antagonist of TIP30 in pancreatic and esophageal cancer cells (Ouyang et al., 2014; Dong et al., 2014). Furthermore, miR-10b overexpression in human pancreatic cancer cells (hPCCs) lowers Tip30 mRNA levels by half when compared to control (Ouyang et al., 2013) similar to the levels seen in the pancreas tissues and PCCs from $K30^{+/-}C$ mice (**Figure 11A**, **Figure 23C**). To confirm the finding that *Tip30*-heterozygosity was the cause of

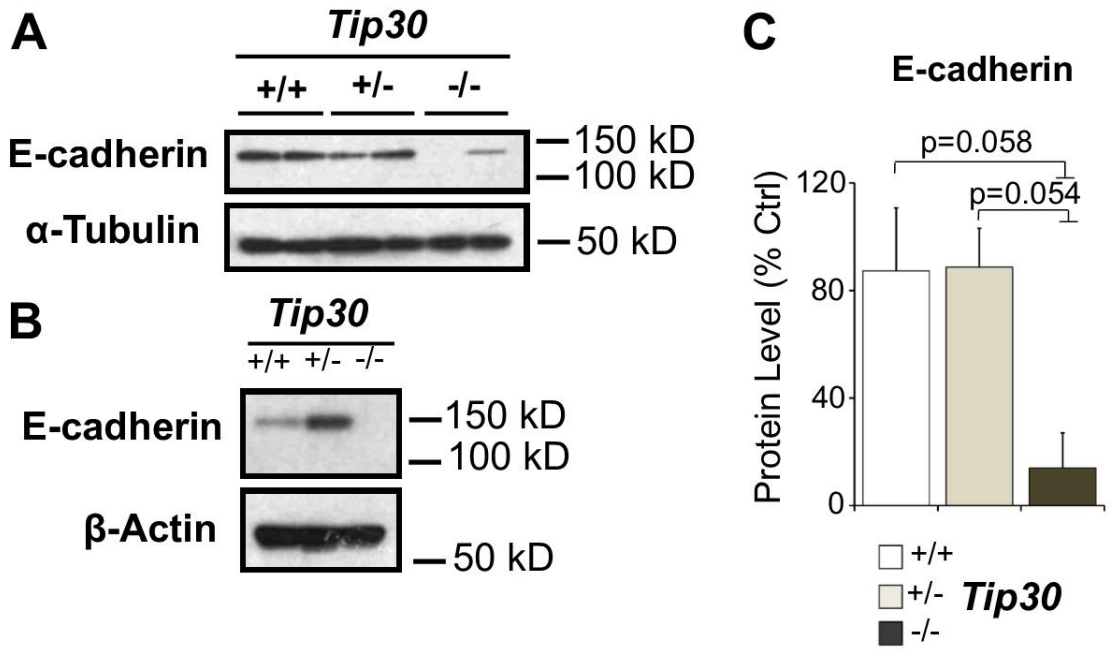

Figure 39. *Tip30*-null PCCs have decreased E-cadherin protein levels

(A) Representative immunoblot of basal E-cadherin levels from two different mPCC lines obtained from two $K30^{+/+,\ +/-,}$ and $^{-/-}$ C mice. **(B)** Representative immunoblot of basal E-cadherin levels for three technical replicates of one GFP cell line from a $K30^{+/+,\ +/-,}$ and $^{-/-}$ $Ctd^{+/-}$ mouse. **(C)** Densitometries of protein levels in **A-B** were normalized to respective loading controls and to mean $K30^{+/+}$C PCC E-cadherin protein levels (Ctrl). Data represent the densitometry means ± SEM of three independent cell lines per group: $K30^{+/+}$C-TP151-GFP, -TP711, -TP715 PCCs; $K30^{+/-}$C-TP573, -TP647, -TP852-GFP PCCs; and $K30^{-/-}$C-TP592-1, -TP889, -TP735-GFP PCCs. One-way ANOVA followed by Tukey post-hoc test was performed. $p<0.05$ was considered significant for n=3 (three separate PCC lines from each group of $K30^{+/+,\ +/-,}$ and $^{-/-}$C or $td^{+/-}$ mice). Wild-type (+/+), heterozygous (+/-), and homozygous (+/-) loss of *Tip30.*

increased basal EGFR levels, we evaluated basal EGFR protein levels and downstream effectors, in a human PDAC cell line (AsPC-1) engineered to overexpress miR-10b (AsPC-1-miR-10b-OX-GFP). This cell line was established in the Korc laboratory (Methods 2.16). AsPC-1-miR-10b-OX-GFP human PCCs (hPCCs) were confirmed to exhibit an eight-fold increase in miR-10b microRNA levels ($p=0.012$, $n=3$), when compared to control (AsPC-1-GFP-C), (**Figure 40**). Three independent experiments were performed, and miR-10b levels were normalized to the internal loading control RNU6B.

MicroRNA (miR)-10b-overexpressing AsPC-1 cells were probed for phosphorylated and total EGFR and AKT, using an antibody specific for EGFR and with no cross-reactivity with other ErbB family members and a pan AKT antibody after 0, 10, 30 minutes (min) or 24 hours (hr) EGF treatment (**Figure 41**). AKT (or protein kinase B) is a serine/threonine protein kinase involved in regulating cell survival (Pap and Cooper, 1998). A subset of PDAC tumors are reported to have high levels of AKT2 (Yamamoto et al., 2004). At basal conditions, miR-10b overexpression increased both total and phosphorylated EGFR and AKT levels (**Figure 41**). Total AKT levels remained relatively consistent between untreated and 10-min to 24-hr, EGF-treated conditions in AsPC-1-miR-10b-OX-GFP compared to control hPCCs (**Figure 41**). A similar trend of increasing phosphorylated-EGFR (pEGFR) and phosphorylated-AKT (pAKT) levels was observed in both AsPC-1-miR-10b-OX-GFP and control AsPC-1-GFP-C hPCCs treated with EGF (**Figure 41**). However, increase in the phosphorylated protein levels were slightly more pronounced in AsPC-1-miR-10b-OX-GFP cells (n=3, not

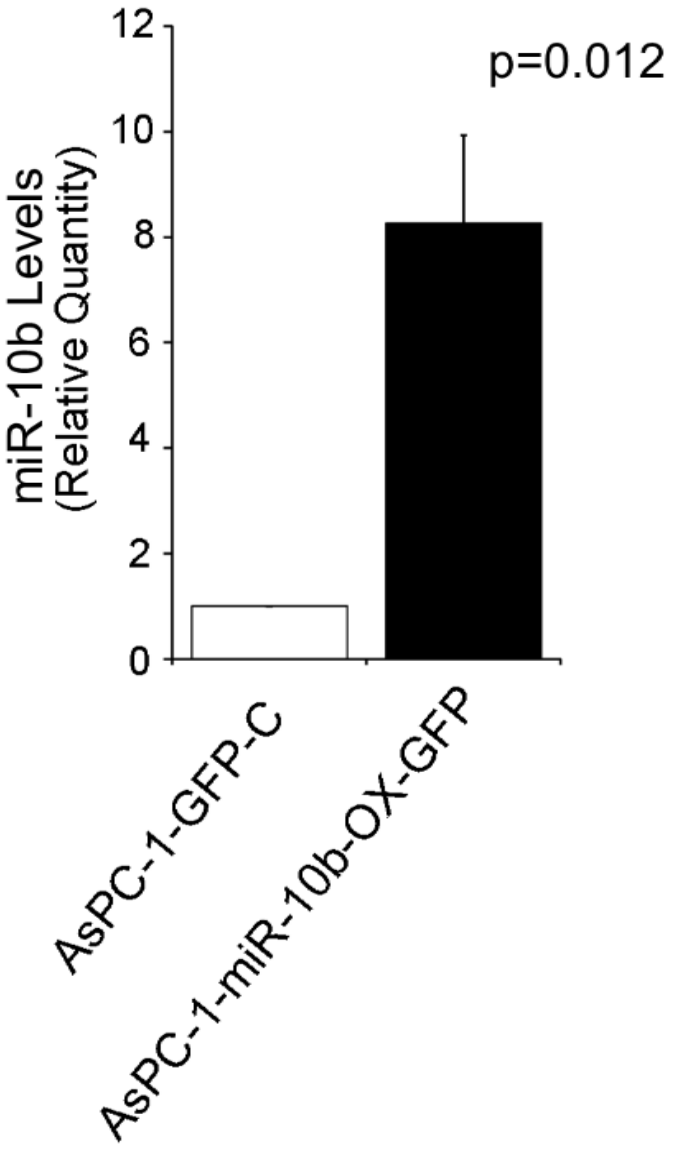

Figure 40. miR-10b levels in human AsPC-1 PCCs with miR-10b-overexpression

qRT-PCR was used to assess the microRNA (miR)-10b levels in miR-10b-overexpressing human AsPC-1 cells (AsPC-1-miR-10b-OX-GFP) as compared to control (AsPC-1-GFP-C). CT values were obtained and normalized to RNU6B per experiment, and the fold increase is depicted. Data represent the mean ± SEM of three independent experiments. Student's two-tailed t-test was used for statistical significance. $p<0.05$ was considered statistically significant.

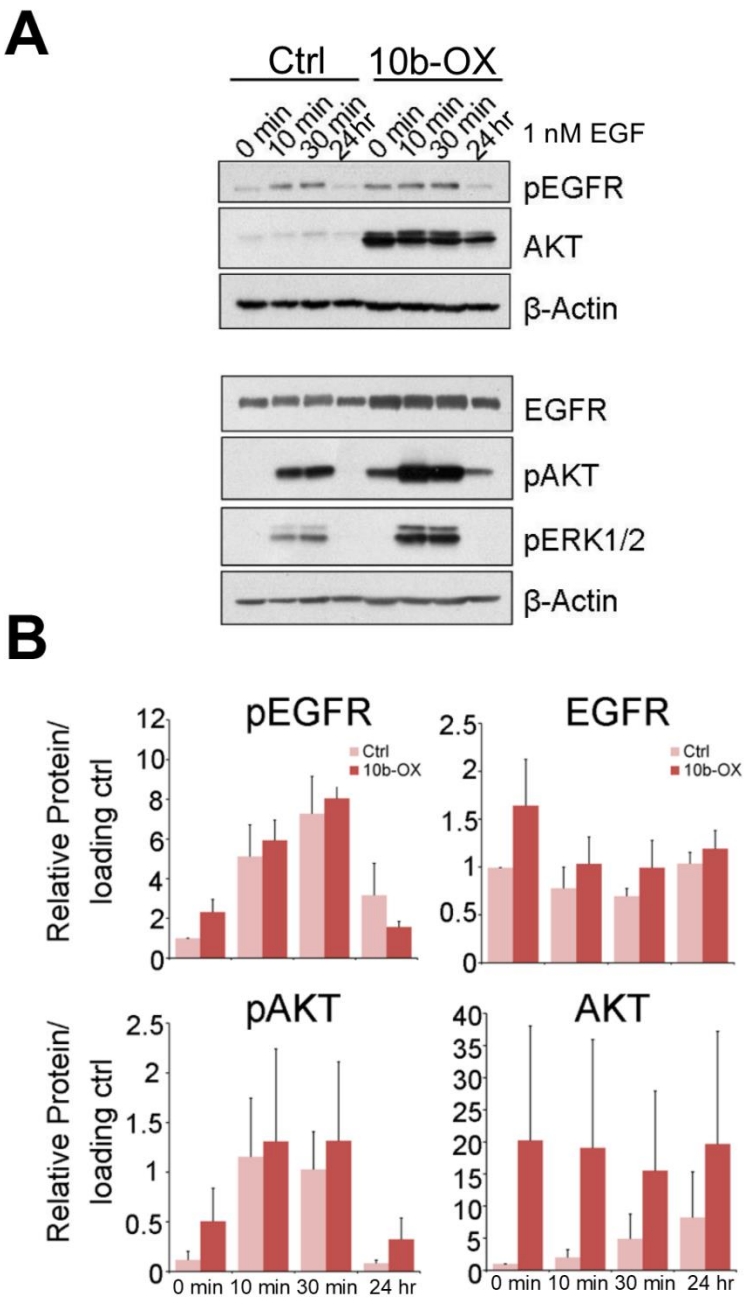

Figure 41. Basal EGFR and AKT protein levels are increased in AsPC-1 pancreatic cancer cells overexpressing miR-10b

(A) AsPC-1-miR-10b-OX-GFP (10b-OX) or AsPC-1-GFP-C (Ctrl) PCCs were treated with 0, 10, 30 minutes (min), or 24 hours (hr) 1 nM EGF after 24 hr serum-starvation (low-serum conditions) and were examined for phosphorylated (p) and total EGFR, AKT, and pERK1/2 protein levels and β-actin loading control. A representative immunoblot (of at least three independent experiments) is shown. **(B)** Data represent the densitometry means ± SEM of three to four experiments shown in **A**. pAKT and AKT densitometries are from four independent experiments. Protein levels were normalized to loading controls and then to the 0 min-Ctrl for pEGFR, EGFR, and AKT. pAKT levels were normalized to loading control only.

statistically significant). An increase in pERK1/2 was also observed in miR-10b-overexpressing AsPC-1 cells after 10-30 minutes of EGF treatment (**Figure 41**).

4.3 Summary

Tip30-deficient immortalized mouse embryonic fibroblasts were reported to increase in cell number with each copy number loss of *Tip30* in a 2D growth assay (Xiao et al., 2003); therefore, we investigated whether the loss of TIP30 could lead to accelerated 2D and 3D murine PCC (mPCC) growth kinetics. Due to the role of TIP30 in EMT and metastasis (Zhu et al., 2015; Zhao et al., 2007; Shtivelman, 1997), we also predicted that in addition to enhancing proliferation, loss of *Tip30* could lead to alterations in expression of EMT markers and an invasive phenotype in PCCs. To this end, we observed that *Tip30* loss accelerated the colony growth formation both *in vitro* and in a three-dimensional culture system of primary oncogenic-*Kras* PCCs isolated from K30C pancreas tissues. Differences in *Tip30* copy number resulted in differences in mPCC-accelerated growth and colony morphology in 3D. In addition, metastatic *Tip30-null* PCCs isolated from the liver had a growth advantage in 2D (**Figure 33B**, n=2) and 3D when compared to *Tip30*-heterozygous PCCs isolated from pulmonary tissues of $K30^{+/-}C$ mice (not shown). $K30^{+/-}C$ metastatic PCCs took longer to form visible colonies in 2D when compared to $K30^{-/-}C$ metastatic PCCs (**Figure 33B**). Interestingly, EGFR levels were increased seven-fold in *Tip30*-heterozygous PCCs compared to *Tip30*-wild-type PCCs (**Figure 37B**, n=3). *Tip30*-null PCCs had low levels of basal EGFR protein compared to both *Tip30*-heterozygous and wild-type PCCs; however the decrease in EGFR was only significant when compared to *Tip30*-heterozygous PCCs

(p=0.046 by one-way ANOVA, n=3, **Figure 37B**). This trend for increased EGFR was also observed at the mRNA level, and by assessing localization by confocal microscopy.

Lastly, we found that both basal EGFR and AKT levels were increased in a human pancreatic cancer cell line, AsPC-1, overexpressing miR-10b. These findings further support our observation that *Tip30*-heterozygosity (or partial loss) increased basal EGFR levels in pancreatic cancer cells. Immunofluorescence studies confirmed that *Tip30* status did not result in a striking difference in CK-19 levels between mPCCs. Immunofluorescence studies did reveal, however, the presence of alpha-SMA in these PCCs, especially those with heterozygous-*Tip30* loss. However further quantitation and western analyses would need to be done, as not all mesenchymal-like markers were observed to be increased in this study (data not shown). While N-cadherin was found to be increased in *Tip30*-heterozygous mPCCs, Vimentin levels were not consistently increased when compared to *Tip30*-wild-type mPCCs. There were also no significant differences detected in p53 protein levels (data not shown). *Tip30*$^{+/-}$ mPCCs exhibited increased N-cadherin (n=2) with no change in E-cadherin when compared to *Tip30*-wild-type PCCs. In contrast *Tip30*$^{-/-}$ mPCCs exhibited low N-cadherin and E-cadherin levels (**Figure 37A vs Figure 39C**). These results suggest copy loss of *Tip30* results in an epithelial-mesenchymal hybrid phenotype, which recently has been described in cancer (Pastushenko et al., 2018).

CHAPTER 5. DISCUSSION

Pancreatic Ductal Adenocarcinoma (PDAC) makes up the majority of pancreatic cancers and has a poor prognosis. This outcome is due in large part to its highly metastatic nature. Metastatic disease accounts for 90% of all cancer deaths (Chaffer and Weinberg, 2011). The current standard of care for PDAC is FOLFIRINOX or gemcitabine plus nab-paclitaxel. However, these therapeutic regimens have not made a significant impact in the overall five-year survival of PDAC over the past 40 years. 91-92% of patients diagnosed with PDAC die from this disease (Siegel et al., 2018). Factors influencing this poor outcome include late presentation at advanced stages of the disease, and therapeutic resistance.

Tip30, also known as *Htatip2,* was originally identified as a metastasis suppressor in non-small cell lung cancer (NSCLC) and a proapoptotic factor (Shtivelman, 1997). We found TIP30 to be genetically altered in human PDAC in our analysis of TCGA data in cBioPortal (Witkiewicz et al., 2015; J. Gao et al., 2013; Cerami et al., 2012). In our studies, we have generated a unique mouse model to study pancreatic cancer progression, and have found that the genetic dose of *Tip30* mediates organ-specific PDAC metastasis. This study is the first report of the characterization of a *Tip30*-deficient mouse model with autochthonous PDAC, driven by conditional expression of oncogenic *Kras* to the pancreas epithelium (K30C). Other than a recent paper describing epithelial plasticity in metastatic organotropism in pancreatic cancer (Reichert et al., 2018), this is the first study to explore the hypothesis that *Tip30*-copy-number-loss guides an organ-specific PDAC metastatic seeding event. Our findings show that $Kras^{G12D}$-positive

pancreatic cancer cells (PCCs) seeded the lungs of K30$^{+/-}$C mice as early as five weeks, and K30$^{-/-}$C liver tissues as early as three months. In K30$^{+/-}$C mice, this early seeding event accelerated inflammation and secondary lesion formation in pulmonary tissues. The observed phenomenon is hypothesized to be *Kras*^{G12D}-dependent because *Tip30*-heterozygous (ages two months to six months, n=6) and *Tip30*-null (ages one month to 12 months, n=21) mice, alone, did not fall sick nor develop any lung lesions, pancreas nodules, or tumors at necropsy. *Tip30*-deficient mice alone also did not exhibited any evidence of micrometastic seeding to distant organs when assessed in the dual-fluorescent reporter mouse background.

While our observations are novel, there are inherent limitations due to the noncongenic background of the mice. Whether a full-body versus a conditional *Tip30* genetic ablation contributed to unexpected variability in the data collected obtained remains unknown. This variability included acceleration of disease in the K30$^{+/+}$C background and the additional phenomenon of lung adenocarcinoma in combination with a PCC seeding event. While these events did not confound the overall conclusions, they must be taken into account for future studies that should aim to delineate the mechanism for PDAC organotropism and why PCC seeding to the lung predominated in KC mice with heterozygous-loss of *Tip30*. Further studies on genetic differences in metastatic cells that seed the lung versus the liver in the K30C model could provide further insight on therapeutic targets for PDAC patients with *TIP30* alterations.

5.1 Early Metastatic Seeding in PDAC Precedes PDAC Detection

The observed pancreatic cancer cell (PCC) pulmonary seeding in K30$^{+/-}$C mice, and micrometastatic liver-seeding in three-month-old K30$^{+/-}$C mice, before detection of PDAC tumor at necropsy, demonstrates the challenges involved in PDAC detection. In a report by Rhim et al. (2012), PCC dissemination preceded detection of pancreatic ductal adenocarcinoma by histological analysis (Rhim et al., 2012). Similar to the Rhim et al. (2012) study, our histopathological analyses did not reveal PDAC at such early time points. However, K30$^{+/-}$C mice with pulmonary lesions did exhibit some pancreas pathology and PDAC-associated disease that ranged from ductal atypia to PanIN-3. In PDAC patients, there is no correlation between metastatic presentation and tumor size (Alteri et al., 2017; Hidalgo, 2010; Haeno et al., 2012); therefore, we would expect similar variability in mPDAC models. Also, disease reoccurrence is linked to early metastatic events that sometimes do not appear at initial diagnosis (Pantel et al., 2008). Metastasis evolution studies point to two different models to explain metastatic occurrence: a linear progression model (late dissemination) and a parallel progression model (early dissemination) (Turajlic and Swanton, 2016). The parallel progression model, which assumes that dissemination is more than a one-time occurrence and that the clones responsible for establishing metastases seed long before primary tumor detection in the clinic, more closely fits our findings (Turajlic and Swanton, 2016).

We hypothesized that PCCs seed the lung tissues of *Tip30*-heterozygous K30$^{+/-}$C mice early, as *Tip30*-heterozygous-KC mice presented with increased

incidence of grossly visible lung lesions as early as five-eight weeks. For KC mice that were *Tip30*-null, both frank tumor presentation and metastatic nodule formation, an indication of macrometastasis and the last stage of a tumor cell's metastatic colonization process (Obenauf and Massagué, 2015), was observed at later time points (nine to eleven months) with pancreatic tumors as big as 15 mm in diameter. A horizontal transfer of information via exosomes is one mechanism that could explain our observation of early micrometastatic seeding in the liver of three-month-old K30$^{-/-}$C mice with an overall low incidence of PDAC. One PDAC study shows that the formation of the liver pre-metastic niche occurs before PDAC lesion formation and is due to pancreatic cancer exosome uptake by hepatic stellate cells (Costa-Silva et al., 2015). Further research is required to determine if exosomes play a significant role in our model. Of all groups evaluated for our studies, the K30$^{+/-}$C group became moribund early and had the poorest survival outcome, although differences did not reach statistical significance. At necropsy, 42% of K30$^{+/-}$C mice (n=13/31) had large pulmonary lesions of varying size and phenotype. While we did not expect these lesions to be lung adenocarcinoma, the finding that 45% (n=5/11) of abnormal lung tissues assessed by histopathological analysis had detectable lung adenocarcinoma could be explained by the BALB/c mouse strain. Previous investigators reported an increased incidence of pulmonary tumors and lung adenocarcinoma in *Tip30*-deficient BALB/c mice compared to *Tip30*-wild-type mice, albeit at 78 weeks of age (Ito et al., 2013).

The concept that tumor size does not have to correlate with a tumor's tendency to metastasize was explored in a candidate metastasis suppressor

Caveolin-1 (Cav1) study using bone marrow-derived dendritic cells (BMDCs) in a breast cancer model (Celus et al., 2017). Investigators reported that mice reconstituted with bone marrow from WT or Cav1 knock-out (Cav1KO) mice exhibited no difference in primary tumor growth or weight; however, mice reconstituted with Cav1KO marrow had a two-fold increase in lung metastases compared to WT-marrow mice (Celus et al., 2017). In contrast, and alignment with original models for tumor-metastasis dogma, investigators have shown that pancreatic cancer cells acquire the genetic mutations necessary for metastasis later in evolution and after the development of the primary-tumor-initiating cell (Yachida et al., 2010).

In our model system, we detected pancreatic cancer cell seeding as early as two months in the lung, and three months in the liver, of K30C mice with heterozygous and homozygous loss of *Tip30*, respectively. It is important to note that the cell tracing/tracking technique, via the dual-fluorescent tdTomato-EGFP mouse introduced in this model, enabled the detection of these early metastatic seeding events. Also, bright-field analysis of a field of metastatic *Tip30*$^{+/-}$PCCs in culture confirmed that GFP-positive and GFP-negative cells were indistinguishable. We suspect that the PCCs that seeded the lung were dormant and did not colonize. Successful colonization requires malignant evolution of either the disseminated cell population or the tumor microenvironment (Nguyen et al., 2009). Use of lineage tracing or a dual method of detection will be critical to identify early metastatic seeding events in PDAC. Studying disseminated cells that have successfully seeded a target organ early will help uncover differences for why

PCCs seed the lung versus the liver. They may also shed insight into the switch that allows a dormant tumor cell to become competent for colonization. The dormancy switch is not yet understood in pancreatic cancer.

5.2 PDAC Liver vs. Lung Metastasis: PDAC Metastatic Organotropism

We found that PCCs in K30$^{+/-}$C mice predominately seeded the lung while PCCs in K30$^{-/-}$C mice seeded the liver. To understand the role of *Tip30* dose in mediating organ-specific metastasis, we first considered reported cases of PDAC metastases to the liver versus the lung in PDAC patients. In a review article by Yachida and Iacobuzio-Donahue, pulmonary and abdominal lymph node metastasis is most common in one-third of patients that do not have hepatic metastases at autopsy (Yachida and Iacobuzio-Donahue, 2007). Both the liver and lung are sites of relapse for pancreatic cancer (reviewed by Nguyen et al., 2009). In a recent study hPDAC patients with more poorly differentiated tumors were found to associate with liver- over lung-metastasis recurrence; and the cohort of PDAC patients with lung recurrence had increased lymph node metastases (Sahin et al., 2018). Lymph node spread varies in humans diagnosed with Stage IV pancreatic cancer (Alteri et al., 2017; Hidalgo, 2010). How these data are impacted by limitations in detection is not clear. Interestingly, in our studies the group of mice with more poorly differentiated PDAC (K30$^{-/-}$C) exhibited increased incidence of liver metastasis. In contrast, *Tip30*-heterozygous-KC mice were the only group of K30C mice that presented with an incidence of either lymph node invasion or lymph node metastasis in a three-month cohort. However, associations between

genotype and our observation of early lymph node metastasis are limited by small sample size and experimental design.

Bypass of liver metastases in PDAC patients can be attributed to hepatofugal portosystemic shunting due to obstruction of the splenic vein or to aggressive features of the primary carcinoma as is reviewed in Yachida and Iacobuzio-Donahue (2007). The results presented herein, including 1) poorer survival outcome in K30$^{+/-}$C mice, 2) detection of increased K30$^{+/-}$C lymph node invasion or metastasis after evaluation of pancreas histology in an age-matched cohort, and 3) lack of symmetry and an invadopodia-like protrusions in 3D cultures of *Tip30*$^{+/-}$ PCCs, support our interpretations that *Tip30* hetloss induces an aggressive subtype of tumorigenesis and PDAC-associated lesions when coupled with oncogenic *Kras*. Our *in vitro* findings also support an aggressive K30$^{+/-}$C-pancreatic cancer cell (PCC)-phenotype; however, studies are still needed to confirm the invasive potential of primary and metastatic *Tip30*$^{+/-}$ PCCs. Assessment of more cell lines per group would also strengthen our study.

Prior and more recent studies on PCC dissemination and metastasis, using genetically engineered mouse models (GEMMs) of PDAC, recapitulate the phenomenon of PCC metastases to both the liver and lungs (Rhim et al., 2012; Reichert et al., 2018). According to findings from Reichert and colleagues (2018), the cause for liver versus lung organotropism in the mPDAC model evaluated was related to epithelial plasticity and the loss of one versus two copies of *p120catenin* (*p120ctn*). In these studies, mono-allelic loss of *p120ctn*, a stabilizer of E-cadherin, mediated *Kras*^{G12D}-driven liver metastasis (Reichert et al., 2018). While we did not

assess epithelial cell marker stability, we observed that *Tip30*-null PCCs had markedly decreased levels of E-cadherin, further supporting a role for E-cadherin in mediating PDAC metastasis to the liver. However, we note that there was no significant difference in E-cadherin protein levels between *Tip30*-wild-type and *Tip30*-heterozygous PCCs.

Marked phenotypic differences between *Tip30*-deficient and *Tip30*-null PDAC tissues by gross and microscopic evaluation supported our *Tip30*-dose dependent metastatic organotropism interpretations. Pancreata from KC mice with one-copy-loss of *Tip30* were phenotypically different from KC-*Tip30*-null mouse pancreata. In $K30^{+/-}C$ mice with pancreatic nodule presentation that appeared to be multifocal, we identified ductal atypia and advanced PDAC precursor lesions, commonly pancreatic intraepithelial neoplasia (PanIN). These observations are in line with theories that describe cancer origins as multicentric: microscopically related but growing independently before coalescing into a single tumor (Slaughter et al., 1953). While oncogenic *Kras* appeared to drive disease progression in the K30C model, *Tip30* copy number loss enhanced pancreatic tumorigenesis. In contrast, $K30^{-/-}C$ mice did not have a more advanced lesion distribution in the group of mice assessed. Pancreatic tumor presentation was detected late (nine-eleven months) in these mice. Overall, $K30^{-/-}C$ mice lived longer than $K30^{+/-}C$ mice, but this difference allowed for an increased opportunity for larger pancreatic tumor mass formation. Tumors from late $K30^{-/-}C$ mice looked like classic PDAC tumors and these tumors were not difficult to discern from normal pancreas at necropsy.

Our results suggested that *Tip30* gene dosage mediates organotropic differences observed in PCC seeding of distant organs.

In our studies, we based our conclusions on the data as a whole; however, it is important to note that even within groups there were differences between mice. These differences within each group did not permit differences between groups to reach statistical difference, despite examining considerable numbers of animals per group. PDAC tumors are very heterogeneous; and each human patient has a unique tumor blueprint in addition to commonalities when compared to patients with other tumors. The K30C mice in our studies displayed a similar heterogeneous tumor landscape. While pancreatic nodules predominated in $K30^{+/-}C$ mice and frank PDAC tumor formation or liver metastasis in $K30^{-/-}C$ mice, not all mice developed nodules or liver metastasis. Whether these differences were the result of differences in TIP30 protein levels between animals within each group or other epigenetic changes that affected gene expression is unknown. For example, in the *Tip30*-heterozygous group, there was a variation in Tip30 mRNA levels between mice, but analysis of protein levels from the pancreata of the same mice did not mirror these differences. The significance of those variations on impacting the results is not well understood. Also, whole genome sequencing on PCC lines isolated from at least two separate mice from each group did not reveal any differences in the *Tip30* coding region or additional mutations at the genetic level. Moreover, functional activity assays would need to be done to fully understand these differences.

5.3 Accelerated Pulmonary Seeding of Pancreatic Cancer Cells (PCCs) in K30$^{+/-}$C Mice

Ito et al. (2003) demonstrated that 18-20-month-old *Tip30*-deficient mice developed increased tumor prevalence, with a slightly higher incidence observed in *Tip30*-heterozygotes. Alternately, Li et al. (2013) reported a 33% incidence of lung adenocarcinoma in *Tip30*-null mice at 19.5-months. In our studies, we confirmed an increased pathology affecting both pancreas and pulmonary tissues in mice heterozygous for *Tip30* compared to *Tip30*-null mice in the KC background. When we introduced the oncogenic *Kras* murine mouse model of PDAC (KC) into the *Tip30*-deficient background (K30C), we observed increased pancreas pathology as well as more advanced disease in both K30$^{+/-}$C and K30$^{-/-}$C mice as compared to the K30$^{+/+}$C group. While *Tip30*-null/KC mice developed frank tumors at 9 to 11 months and earlier signs of micrometastatic seeding to the liver, K30$^{+/-}$C mice had a phenotype that appeared similar to the Li et al.(2013) study, but at an accelerated rate (an average of 3 months compared to 19.5 months). Our data support that this increased pathology is the result of PCC dissemination and seeding to pulmonary tissues in K30$^{+/-}$C mice.

Two methods were used in this study to evaluate PCC seeding to the lungs of K30$^{+/-}$C mice. First, the “Kras G12D Conditional PCR” method (Jacks, 2017) which differentiates a wild-type *Kras* allele, a *LSL-Kras*^{G12D} transgene, and a recombined 1-*Lox*P-*Kras*^{G12D} PCR product (Jacks, 2017; Hingorani et al., 2003) in pancreas tissues from transgenic mice. The presence of oncogenic *Kras* in the endogenous *Kras* locus, driven by the tissue-specific promoter *Pdx1*, to the

pancreas, was used to identify PCCs in both primary pancreatic tumors and metastatic sites, including lung tissue biopsies using this method. The second method utilized GFP-labeling through the incorporation of a dual-fluorescent reporter mouse, also driven by *Pdx1-Cre*. This confirmed the presence of GFP-positive PCCs in the lung tissue of a K30$^{+/-}$C mouse. These GFP-positive cells were isolated, sorted, and were found to be positive for oncogenic *Kras* by 1-*LoxP*-*Kras*^{G12D}-positivity. Our findings suggest that PCCs with oncogenic *Kras* elicit an activity (to promote malignant transformation) that likely synergizes with the microenvironment where copy-loss of one *Tip30* allele persists. This combination of events is therefore most likely responsible for the accelerated formation of lung adenocarcinoma after PCC dissemination to lung tissues because we observed the lung lesion/adenocarcinoma phenomenon on average of 13 months earlier than previously reported. The lung adenocarcinoma may have been selected for and outcompeted PCC macrometastases, which would have been detected by histological analysis (as it was observed for K30$^{-/-}$C-TP889). We hypothesize that our observations *in vivo* may be linked to the increased EGFR levels observed in K30$^{+/-}$C primary PCCs.

Results from the original study on the KC mouse model (Hingorani et al., 2003) suggest that nonspecific recombination of oncogenic *Kras* in pulmonary tissues is highly unlikely. Whole-body GFP imaging and GFP localization after *Pdx1-Cre* mediated recombination supported the specificity of GFP labeling to pancreas tissues. Why only one-copy of *Tip30* loss resulted in significant pulmonary lesion formation in our model is unclear. Lung tissues from K30$^{+/-}$C mice

with grossly visible pulmonary lesions were abundant with inflammation and macrophage infiltration. Alveolar macrophages are the first line of defense against pathogens that come in contact with the lung (Rubins, 2003); therefore, an inflammation storm may have occurred in response to a PCC seeding event in our studies. This environment may not have been permissive for true colonization of the PCCs, which would explain the lack of detectable macrometastases by gross observation or histology.

We used Kras G12D Conditional PCR (Jacks, 2017) combined with a method for visual tracking of PCCs by GFP-labeling (after confirming *Pdx1-Cre*-specific GFP-fluorescent pancreas tissues as depicted in **Figure 25**) to detect pancreatic cancer cells that had disseminated to distant organs. The source of GFP-labeling utilized was the *LoxP-tdTomato-LoxP-EGFP* reporter mouse (Muzumdar et al., 2007) or "td" after *Pdx1*-Cre mediated excision of the tdTomato cassette. We were able to, therefore, track micrometastatic seeding in compound mutant K30Ctd mice. Hingorani and colleagues (2003, Supplemental) originally evaluated *Pdx1-Cre* for driving the pancreas-specific expression of oncogenic *Kras* in KC mice. Hingorani et al. (2003, Supplemental) did not detect *Pdx1*-Cre activity or recombination in the lungs nor the liver of KC mice.

The significant increase in pulmonary lesions in young $K30^{+/-}C$ mice compared to other groups suggested that *Pdx1*-Cre activity did not lead to recombination in lung tissues, in the K30C model. This observed phenotype also appeared to be specific to K30C mice with heterozygous loss of *Tip30*, considering 13 out of 31 $K30^{+/-}C$ mice were affected compared to only 2 out of 20 $K30^{-/-}C$ mice.

Therefore, we hypothesized that pancreatic cancer cells seeded the lung and created a microenvironment that promoted lung adenocarcinoma due to *Tip30*-heterozygosity. The surrounding lung cells may have become transformed and resulted in lung adenocarcinoma selection and outgrowth, over a pancreatic cancer metastatic event. After the PCCs disseminated to the lung, they may have been unable to colonize and form detectable metastases if the environment was not favorable for growth proliferation or if their proliferative growth properties were not sufficient to allow for metastasis. Metastastic colonization at distant tissues is an inefficient process (reviewed by Gay and Malanchi, 2017). The metastatic niche or microenvironment must be permissive or else disseminated tumor cells can exist in a state of dormancy (Gay and Malanchi, 2007; Chambers et al., 2002). Additionally, studies show that the organ microenvironment can influence cancer cell gene-expression patterns (reviewed by Chambers et al., 2002).

Although we uncovered pancreatic cancer cell dissemination to the lung tissues of $K30^{+/-}C$ mice, it was not clear if the migration and dissemination of the pancreatic cancer cells caused a change in the pulmonary environment or if *Tip30*-heterozygous loss in the lung primed the pulmonary environment for pulmonary lesion formation. It would be interesting to evaluate if the latter resulted in a specific molecular landscape that attracted pancreatic cancer cells. When cancer cells seed a site, they have a potential to exert their malignant growth signature on and transform surrounding cells via the field effect. A field effect, referred to initially as “field characterization” in a 1953 study, refers to the preconditioning and influence that a cell has on its environment (Slaughter et al., 1953). These influences can

manifest in the form of irreversible changes in a particular cell's environment. In cancer, this concept helps discern between individual, original cancer cells and the once-unaffected peripheral cells that incorporate cancer-inducing alterations based on their proximity and location (Slaughter et al., 1953). Reports of non-cell autonomous effects of mutant KRAS have previously been published (Bao et al., 2017; Beckler et al., 2012; Grabocka and Bar-Sagi, 2016). In the study by Beckler et al. (2012), investigators reported that exosomes released from *KRAS*^{G13D}-mutant colorectal cancer (CRC) cells were internalized by isogenically-matched wild-type *KRAS* colorectal cancer cells and resulted in the enhanced three-dimensional growth in soft agar of both *KRAS* WT CRC cells and rat intestinal epithelial cells (Beckler et al., 2013). Therefore, mutant KRAS was transferred from mutant cells to wild-type cells via exosomes (Beckler et al., 2013). In addition, according to TCGA, genetic alterations in which one allele of *KRAS* is lost and the second allele mutated is common in human PDAC (J. Gao et al., 2013; Cerami et al., 2012). Our studies support the idea that the metastatic seeding event observed was an oncogenic *Kras*-driven event, as metastasis was not observed in mice that did not have the *Kras*^{G12D} mutation.

The absence of recombined DNA in the normal lung tissue biopsies and the presence of GFP-positive cells in the lung tissue of the K30$^{+/-}$C-TP852 mouse at two months led us to hypothesize that PCCs were seeding the lungs. The absence of conditional *LSL-Kras*^{G12D} allele recombination in the lung and liver tissues of the KC model, as reported by Hingorani et al. (2013, Supplemental), supported our interpretations of this metastatic seeding phenomenon. Further investigation is

needed to study whether pulmonary *Tip30*-heterozygosity resulted in increased metastatic lung-seeding or if *Tip30*-heterozygosity synergized with *Tip30*-heterozygous PCC activity, which then resulted in accelerated secondary lesion formation. The ratio of GFP-positive to GFP-negative cells visualized in culture may be representative of the distribution of PCCs and lung cells in the pulmonary lesion; predictably, it would be a high lung cell-to-PCC ratio. Also, the presence of two populations of cells also became evident in the DNA analysis of GFP-positive versus GFP-negative sorted cells, cultured from the lung lesion of the $K30^{+/-}Ctd^{+/-}$-TP852 mouse.

Since our observations were in mice whose average ages were three months, the likelihood for an off-target recombination event in the lung tissues of KC mice was low (Hingorani et al., 2003, Supplemental). Accelerated lung lesion formation, in the *Tip30*-heterozygous K30C model, was probably driven by paracrine or autocrine signaling between the disseminated PCCs and surrounding alveolar cells or lung resident cells (Obenauf and Massagué, 2015). An accelerated metastatic seeding event to pulmonary tissues, in our observations, was supported by the identification of pancreatic lesions in the pancreas tissues and detectable lymph node invasion and metastasis as early as three months in $K30^{+/-}$C mice. PDAC patients with lymph node metastasis have a poorer prognosis (Kanda et al., 2011). Also, mice overexpressing the lymphangiogenic growth factor VEGF in the pancreas islets, develop lymph node metastases while VEGFC-deficient mice do not (reviewed by Stacker et al., 2002). While the KC model alone typically results in a long latency to tumor development with a low frequency of

metastasis, metastases to both the lung and liver were nevertheless reported (Hingorani et al., 2003). Therefore, metastasis is a plausible phenomenon in GEMMs that utilize the KC mouse model. In our hands, we observed an accelerated progression to PDAC for $K30^{+/+}C$ mice alone, compared to what was reported in the literature, and were able to confirm no interference of contaminating transgenes based on validation studies (**Appendix A**). $K30^{+/+}C$ mice presented with tumors at six months, and PDAC was detected in n=2/2 of these mice by histopathological analysis.

Future experiments are needed to determine whether the PCCs isolated from $K30^{+/-}C$ lungs or $Kras^{G12D}$-positive DNA found in biopsied pulmonary lesions in $K30^{+/-}C$ mice are not of pulmonary origin. These studies, and additional staining for pancreatic cancer cell markers in the lung tissue, will further confirm that these cells are of pancreatic origin. Testing for the presence of bone morphogenetic protein 7 (BMP7), a protein involved in the dormancy of metastatic prostate cancer cells, may also shed light on the state of disseminated PCCs in the lung (Kobayashi et al., 2011). In a review on organ-specific metastasis, BMPs secreted by lung resident cells resulted in breast cancer cell differentiation and dormancy (Obenauf and Massagué, 2015). However, as evident by the data in our studies, disseminated pancreatic cancer cell presentation might not evolve into a classic colonization or macrometastatic event, both of which are easily detected by gross observation. It is possible, however, that TP852 may have fallen sick at two months due to complications unrelated to PDAC seeing that PDAC had not yet developed in this mouse, and PDAC precursor lesions were not detected.

In addition, one K30$^{+/-}$C mouse had 1-*LoxP-Kras*^{G12D} positive DNA in a pulmonary region that appeared healthy and not yet affected. The third mouse without any symptoms and of the KC genotype was also found to have GFP/1-*LoxP-Kras*^{G12D}-positive PCCs in a culture of cells isolated from its lung. Even in the pancreas, recombination is not 100% efficient, as reported in Hingorani et al. (2003). This is a limitation of the *Pdx1* promoter, and was observed in pancreas tissues from K30C mice by the Kras G12D Conditional PCR analysis (see Pancreas in **Figure 24, Appendix C2.C**).

5.4 Copy Number Loss of Tumor Suppressor *Tip30*: Translational Relevance and Therapeutic Potential

We expected to see the poorest survival outcomes in K30C mice that were *Tip30*-null. However, our findings were inconsistent with that expectation. Instead, complete loss of *Tip30* was protective, allowing prolonged survival and bypass of detectable disease by gross evaluation at earlier time points (three months). The initial differences in survival outcome observed (in KC mice with heterozygous loss in *Tip30* compared to homozygous loss) led us to initially hypothesize that *Tip30* was functioning as a haploinsufficent tumor suppressor in our model. Further, monoallelic loss of *Tip30* would result in the poorest disease outcome, similar to Beclin 1 (Qu et al., 2003). *In vivo*, tumor-initiating cells could have been compensating for *Tip30*$^{-/-}$ loss resulting in slowed disease progression to PDAC. Although we did not characterize the tumor microenvironment during PDAC initiation in our model, we suspect that there may be enhanced fibroblast and pancreatic stellate cell activation and recruitment based on our observation of

dense, fibrotic tumors with marked desmoplasia in the K30$^{-/-}$C group. Both pancreatic stellate cells (Bachem et al., 2004) and activated cancer associated fibroblasts or CAFs (reviewed in Wang et al, 2017) contribute to extracellular matrix (ECM) deposition and remodeling; studies have also demonstrated that CAFs are the only cell type required to initiate tumor growth (reviewed in Wang et al., 2017). At this time we cannot explain why two-copy loss of *Tip30* resulted in frank PDAC tumor development in K30$^{-/-}$C mice as compared to the other K30C groups, but we did confirm that PCCs from *Tip30*-null K30$^{-/-}$C PDAC tumors had a two-dimensional and three-dimensional growth advantage. Further studies are needed to understand the mechanism. An alternative hypothesis is that complete loss of *Tip30* eventually leads to the activation of EGFR-independent tumor growth promoting mechanisms. Further studies are needed to evaluate these proposed claims.

K30$^{+/-}$C mice had an average 50% decrease in pancreatic Tip30 mRNA level as compared to age-matched controls; and whole genome sequences of two *Tip30*$^{+/-}$ PCCs isolated from K30$^{+/-}$C mice displayed an intact wild-type *Tip30* sequence (data not shown). However, the difference in TIP30 protein levels between the two groups appeared to be greater than a 50% decrease. While the explanation for this differential was not clear, it may contribute to the poor survival and early disease outcome observed in K30$^{+/-}$C mice, as compared to K30$^{-/-}$C mice. Perhaps, the complete loss of *Tip30* leads to one pathway in our mPDAC model while loss of one copy induces a post-translational modification that results in aberrant TIP30 protein function.

We observed that decrease in *Tip30*-gene dose led to an associated increase in pancreatic cancer cell growth in 2D and 3D growth. A similar trend in growth was reported by Ito et al. (2003) for *Tip30*$^{+/+}$, *Tip30*$^{+/-}$, *Tip30*$^{-/-}$ immortalized mouse embryonic fibroblasts (MEFs). However, we did not observe a gene dosage effect when analyzing EGFR and N-cadherin protein levels. Instead, one copy loss of *Tip30* led to increased EGFR levels in cell lines derived from our model, while loss of both copies of *Tip30* did not significantly impact EGFR levels when compared to *Tip30*-wild-type PCCs. Lack of detectable EGFR levels in *Tip30*-null PCCs may have been due to a negative feedback loop after complete loss of TIP30. A compensatory pathway may have triggered this feedback loop after the complete loss of Tip30 gene expression. Also, loss of both copies of *TIP30* may not be a biologically occurring event in PDAC. These ideas would also further investigation to confirm the role of TIP30.

Interestingly, monoallelic deletions (*TIP30-HETLOSS*) make up all *TIP30*-copy number loss alterations in human PDAC cases (hPDACs) (Witkiewicz et al., 2015). The Cancer Genome Atlas (TCGA) does not show any hPDAC cases with homozygous deletions in *TIP30* in either the UTSW or the TCGA Provisional datasets (Witkiewicz et al., 2015; J. Gao et al., 2013; Cerami et al., 2012). Therefore the K30$^{-/-}$C observations in our studies may be due to the microenvironmental selective pressure of our genetically engineered mouse model (see review by Ben-David et al., 2018). Comparatively, we do not know if *TIP30*-HETLOSS PDAC cases have an epigenetic modification that negatively affects the remaining wild-type allele. Hypermethylation of the second allele could lead to total

loss of *TIP30*. While there are instances of missense mutations in *TIP30* across various cancers, a genetic alteration of homozygous deletion in *TIP30* is uncommon (J. Gao et al., 2013; Cerami et al., 2012). For instance, in a cohort of 963 breast cancer patient samples sequenced and reported in the TCGA Provisional database in cBioPortal, there were only two cases of *TIP30* homozygous deletion (J. Gao et al., 2013; Cerami et al., 2012). Complete loss of *Tip30*, plus oncogenic *Kras*-driven PDAC initiation in our model may have selected for tumor formation and the pathology we observed in $K30^{-/-}C$ mice.

Because a subset of PDAC patients exhibit heterozygous loss, according to TCGA data (Witkiewicz et al., 2015) our observations and findings have a potential for translational relevance. This group of *TIP30*-deficient patients may benefit from therapies that target *TIP30* loss; however, the data obtained from TCGA first needs to be validated. Although the RPKM (reads per kilobase per million mapped reads) measure is widely used and accepted for high-throughput sequencing data interpretation, there are some in the field who do not consider it to be an accurate measure of relative molar RNA concentration (Wagner et al., 2012). On the other hand, although the TCGA data from our studies were not validated, microarrays were conducted in a cohort of 106 PDAC patient samples from the Pancreas Disease Center of Changhai Hospital, and a scoring system determined that while 50.9% of PDAC cases in the cohort were TIP30-high, TIP30-low patient samples were associated with lymph node metastasis (Guo et al., 2014). Therefore, pancreatic cancers with *TIP30* loss may represent a unique subclass which requires novel therapeutic strategies.

5.5 EGFR-KRAS Signaling Axis, Kras-Induced Aggressiveness in the K30$^{+/-}$C Model

In one K30$^{+/-}$C mouse, the genomic DNA from the pulmonary lesion tissue biopsy tested positive for full recombination of the conditional *LSL-Kras^{G12D}* allele with loss of the wild-type *Kras* allele. One thought in response to such an observation is that a loss of heterozygosity occurred. Loss of the wild-type *Kras* allele, also known as “loss of heterozygosity (LOH) at *Kras*”, has been reported to promote metastasis in the *p16flox/flox;LSL-Kras^{G12D};Pdx1-Cre* mouse model, and was found in cell lines derived from metastases compared to matched primary tumors (Qiu et al., 2011). The investigators confirmed that this LOH phenomenon had occurred *in vivo* (Qiu et al., 2011).

In the case of esophageal squamous cell carcinoma (ESCC), although decreased *TIP30* expression was not reported to be associated with increased tumor size, it did significantly correlate with lymph node metastasis and differentiation (Dong et al., 2014). After mining TCGA data, we did not find a significant association between *TIP30* copy number loss and PDAC survival in hPDAC cases (Witkiewicz et al., 2015). Patients with low TIP30 levels may not have had a poorer survival outcome when compared to PDAC patients with high TIP30 levels. It is possible that the limited number of available patient samples in the dataset, including PDAC patients with normal levels of TIP30, and disease-free controls (or limitations in sample quality) skewed survival results. Any treatment that patients may or may not have received before tumor sequencing may also play a role in survival outcome. In the Li et al. (2013) study, *TIP30*-low-

expressing lung adenocarcinoma patients had a higher median survival compared to *TIP30*-high-expressing lung adenocarcinoma patients; the investigators attributed this result to *TIP30*-low patients having a better response to EGFR-targeted therapy (Li et al., 2013). *Tip30* loss is reported to sustain EGFR signaling (Zhang et al., 2010; Li et al., 2013; Zhang et al., 2011). Whether *Tip30* loss cooperates with Kras activity has not yet been studied. KC mice are reported to have increased GTP-bound Ras protein levels in the pancreas when compared to littermate controls (Hingorani et al., 2003). The functional relevance of the *Kras* mutation for both the $Kras^{G12D/+}$ and $Tip30^{-/-}$ or $Tip30^{+/-}$ genotypes in our mouse models can be assessed using a Ras activity assay. Ras activity has been linked to metastatic outcome in PDAC (Muzumdar et al., 2017); therefore, these additional studies could reveal the function or mechanism behind some of our novel observations in *Tip30*-deficient K30C mice.

EGFR has been an attractive target in cancer research due to the increased EGFR expression in various tumors have, including PDAC (Korc et al., 1992; Navas et al.; 2012; Fjällskog et al., 2003; Tobita et al., 2003). To add to this, oncogenic *Kras*-driven PanIN lesions and PDAC is dependent on EGFR signaling (Navas et al., 2012). In our studies, we found that mPCCs positive for mutant *Kras* with *Tip30*-heterozygosity resulted in a seven-fold increase in EGFR protein levels when compared with mPCCs with mutant *Kras* alone. The human pancreatic cancer cell line, AsPC-1, also exhibited an increase in basal EGFR levels with miR-10b overexpression. miR-10b directly represses TIP30 mRNA (Ouyang et al., 2014, Dong et al., 2014). Constitutive EGFR overexpression leads to neoplasia,

and EGFR ablation in the KC mouse model abolishes pancreatic transformation (reviewed by Crawford et al., 2019). EGFR has been proposed to be required for the initial Kras loading of GTP or that it activates the protein product of the remaining wild-type *Kras* allele (Crawford et al., 2019). In 2007, a large randomized phase III clinical trial for the EGFR inhibitor erlotinib plus gemcitabine modestly improved median survival of PDAC patients when compared to gemcitabine alone, with p=0.038 (Moore et al., 2007). Other EGFR inhibitors or combinatorial therapies targeting EGFR and insulin growth factor receptor (IGFR) have had mixed efficacy in clinical trials. For instance cetuximab plus gemcitabine did not lead to statistical significance in overall survival (Philip et al., 2009), while gefitinib plus gemcitabine had promising results for patients with PTEN expression (Fountzilas et al., 2008). While one study linked an increase in EGFR with PDAC liver metastasis, another study reports that PDACs with family member ERBB2 or HER2 overexpression lacked liver metastases and were associated instead with lung and brain metastasis (Chou et al., 2013). In a clinical trial for HER2 overexpressing metastatic pancreatic cancer patients, targeting HER2 overexpression with trastuzumab plus chemotherapeutic capecitabine did not lead to improvements in median overall survival (Harder et al., 2012). One limitation of the study was the small patient sample and patients with HER2 expression (reviewed by Adamska et al., 2017), however the investigators do not recommend HER2 targeting to treat metastatic PDAC. In a cohort of 469 PDAC patients, the prevalence of a *HER* amplification was 2% (Chou et al., 2013). Overexpression of HER2 was observed in one out of three *Tip30*-heterozygous K30C cell lines.

Protein levels in this cell line were low when compared to the other two cell lines from that group, however both EGFR and HER2 levels were elevated when compared to *Tip30*-wild-type and *Tip30*-null PCCs. Study into the circumstances that lead to an increase in EGFR levels versus HER2 levels could provide further insight into TIP30's mechanism of action in PDAC. Also, the subset of PDAC patients with *TIP30* heterozygous loss may be more responsive to EGFR or HER2 targeted therapy.

5.6 Questions of Leakiness and *Pdx1*-Cre Specificity

Pancreatic duodenal homeobox 1 (*Pdx1*) is expressed in the pancreas epithelium and is required for pancreas development and differentiation as early as embryonic day 8.5; *Pdx1* is also expressed in regions that will give rise to the duodenum and stomach (Green et al., 1992; Offield, 1996; Gu et al., 2003; Gannon et al., 2001; reviewed in Babu et al., 2007). In the field of pancreatic cancer modeling, *Pdx1*-Cre is not known to have off-target effects in the lung or liver (Magnuson and Osipovich, 2014). However, limitations exist in all model systems. For instance *LSL-Kras^{G12D}; Pdx1-Cre* mice were reported to have mucocutaneous papillomas in addition to intestinal metaplasia as early as two months (Hingorani et al., 2003). *LSL-Kras^{G12D};Pdx1-Cre* mice are reported to develop sporadic mucocutaneous papillomas, intestinal metaplasia, and hyperplastic polyps of the duodenum (Hingorani et al., 2003, p.441). These observations still raise questions about more precise control in experimental models and suspicions of leakiness in mouse model systems. For this reason, we generated controls from within the colony for these studies. Also, the organotropic metastases observed in these

studies did not appear at random, but was linked to the genetic dose of *Tip30*. Although unlikely, we acknowledge the possibility of leakiness in all experiments that utilize genetically engineered mouse models. To combat these concerns, other *in vivo* model systems use a two-step control of conditional expression to minimize leakiness and off-target effects (Collins et al., 2012; Feil et al., 2009; reviewed in Herreros-Villanueva et al., 2012). Since hPDAC is a disease of the adult pancreas, conditional aberrant expression in adult mouse pancreas tissues may not only address issues of leakiness but may also be more relevant. In addition, use of an orthotopic model whereby labeled pancreatic cancer cells are directly injected into the pancreas may serve as another alternative to more confidently link metastatic seeding in distant organs with primary tumor formation.

While the use of a beta-galactosidase reporter to assess *Pdx1-Cre* expression in all tissues was not performed in these studies, recombination-based lineage tracing has been shown previously (Kawaguchi et al, 2002; Gu et al., 2002; Hingorani et al., 2003). Both *Pdx1* localization and *Pdx1*-Cre activity has been thoroughly investigated (Offield et al., 1996; Gu et al., 2002; Kawaguchi et al, 2002; Hingorani et al., 2003); and KC mouse model (Hingorani et al., 2003) is commonly used for murine PDAC studies (Guerra and Barbacid, 2013). For instance, through the use of a LacZ-PDX1 fusion allele, *Pdx1* was first detected at embryonic day E8.5 (Offield et al., 1996). At E9.5, it was visible in the dorsal and ventral pancreatic buds and the duodenal endoderm (Offield et al., 1996). At E18.5, just before birth, *Pdx1* expression was reported to be restricted to the developing pancreatic islet (Offield et al., 1996). *Pdx1*-null embryos lack islet differentiation and mature

pancreatic beta cells and acinar cells (Offield et al., 1996). Perinatal stages had similar boundaries and expression levels of PDX1 (Offield et al., 1996). *In situ* hybridization studies by Gu et al. (2002), in mesenchymal, endothelial, and smooth muscle cells, revealed human placental alkaline phosphatase (HPAP) reporter expression in pancreas acini, islets and ducts in four and eight-week-old *Pdx1*-Cre/Z/AP reporter mice as well as in a tamoxifen-induced Cre mouse model system, with Cre induction at E9.5 (Gu et al, 2002). Consequently, there is no literature precedent for extra-pancreatic/duodenal expression of PDX1.

To date, there have been no reports in the literature of *Pdx1* expression or *Pdx1-Cre* activity in tissues in the liver or lung in *LSL-Kras^{G12D}; Pdx1-Cre* mice (reviewed by McKinnon and Docherty, 2011; Hingorani et al., 2003). In Hingorani et al. (2003, Supplemental) recombination was not detected in lung or liver tissues in KC mice by a PCR method to detect the recombined *Kras^{G12D}* allele. Nevertheless, we cannot exclude the possibility that a recombination event early in embryogenesis occurred in a progenitor cell of developing liver or lung with a different fate than that of the pancreas. The pre-pancreatic ventral foregut endoderm, the lung bud, the trachea, and the hepatic diverticulum all are derived from the ventral foregut endoderm (Serls et al., 2005). However, pancreas-, liver-, and lung-specific genes are required for hepatic and lung bud development (Serls et al., 2005). In addition to the expression of specific transcription factors, growth factors, such as the fibroblast growth factor (FGF), and their concentration thresholds determine cell fate (Serls et al., 2005). In theory, it would only take one molecule of Cre recombinase expression to result in a recombination event in a

cell fated to become lung tissue, leading to a source of oncogenic *Kras* in the lung. Reports of *Pdx1-Cre* leakage to the brain do exist (Song et al., 2010).

5.7 Limitations in Detection by Histology

In addition to the discussion in section 5.1, it is possible that histological evaluation alone may not be sufficient to detect PDAC metastasis or metastatic pancreatic cancer cells. We only examined one slice of lung tissue, and even so, sites of metastasis can easily be missed during sectioning and slide preparation. Further staining with a more rigorous panel of markers and examination of lung sections for GFP-labeled pancreatic cancer cells would allow for more thorough characterization of the lung microenvironment.

5.8 Whole-Body *Tip30*-Deficiency

We cannot exclude the possibility that *Tip30*-deficiency in the lung contributed to lung adenocarcinoma formation or even to metastatic seeding because the *Tip30*-deficient K30C mouse used in these studies had a whole-body *Tip30*-deficiency. *Tip30*-deficient mice alone did not show any signs of pulmonary lesions in our model, and in the literature lung adenocarcinoma and gross lesion formation did not occur until 19-20 months (Li et al., 2013). The BALB/c background is known to have a propensity to develop lung tumors and adenocarcinoma; according to the Mouse Tumor Biology (MTB) Database there are at least six separate reports of the BALB/c strain developing a high incidence of lung adenocarcinoma (Begley et al., 2012). In addition multiple reports have documented BALB/c mice developing an increased incidence of lung adenoma (Begley et al., 2012). MTB is based out of Jackson Laboratory and is a National

Institutes of Health (NIH)-driven and continuously updated repository of tumor biology data (Begley et al., 2012). Both studies documenting the *Tip30*-deficient mouse model (Ito et al., 2003; Li et al., 2013) did not report any incidence of pancreatic tumor formation, however we recognize that studies in a conditional *Tip30*-deficient mouse model would be more clinically relevant for studies of PDAC. It is even plausible that without a whole-body deficiency in *Tip30*, pancreatic cancer cells may be limited in their metastatic potential.

5.9 Strain Effect on Tumor Incidence: The Importance of a Congenic Background

Mouse strain and genetic background influence phenotype in studies that utilize transgenic mouse models (Berghe et al., 2015; Gerlai, 1996; Simpson et al., 1997). Therefore, either the use of one strain for backcrossing to create a purer background or generation of controls from within the mouse colony under investigation is recommended. Investigators commonly backcross transgenic mice ten generations to attain a congenic background, i.e., backcrossing ten generations to the C57BL/6J mouse strain (Berghe et al., 2015). Ten generations of backcrossing results in a 0.1% chance that the locus from the donor strain remains (Lusis et al., 2007). For mice made of multiple strains (i.e., more than four, and referred to as “stock” by The Jackson Laboratory), there is no method to detect the sequence percentage of all strains involved (e.g., on four different loci). In an attempt to select for the strain of interest, there remains a chance of transfer of the donor strain with each crossing. Where there is an influence of an additional strain, there is a chance for an influence on phenotype. In mouse models for cancer

research, where certain strains have been reported to be contaminated or led to an increased incidence of tissue-specific tumor formation, this circumstance could contribute to variability in results or even novel-appearing findings. There is a risk for phenotypes that may or may not be attributed to the gene of interest. For example, the *Tip30*-deficient mouse in the C57BL/6 background showed an increase in tumors of the liver at 18-20 months (Ito et al., 2003), while the *Tip30*-deficient mouse in the BALB/c background had an increase in lung tumors at 19.5 months (Li et al., 2013). Lung tumors are known to occur at a high rate in BALB/c mice as they are reported to be more susceptible to adenocarcinoma of the lung (Begley et al., 2012; Li et al., 2013).

Attaining background purity takes time, can be costly and challenging; however, doing so could prevent variations in research outcomes, lead to increased reproducibility, and potentially allow for smaller sample sizes to reach definitive conclusions in research studies. Pure genetic background, which can be achieved by after ten generations of backcrosses is reported to minimize variability in tumor penetrance, disease onset kinetics, lesion phenotype, and propensity for metastasis (Lee et al., 2016). Although a congenic background is exceptionally close to a pure background, in transferring a mutation of interest from one mouse background to another the region that flanks the selected gene will always remain donor material (Lusis et al., 2007). These genes in these flanking regions are termed “passengers” and can influence traits of interest (Lusis et al., 2007).

The mice generated for these studies were the result of crosses between mice on a background of three or more different strains, including three different

sources of strain 129 (129P2), 129S4 and other strains of 129. The genetic variation in the 129 strain is well documented and results in phenotypic differences (Simpson, 1997; Threadgill, 1997). The 129 strain is also associated with a light tan chinchilla color, which we also observed after a few interbreedings of *Tip30*-deficient mice. Although the original coat color of the mice should have been white (95% BALB/c background), this phenotype points to the impact that a small 5% in the genetic background can have when selected for accidentally through crosses. Crossbreeding the B6;129-Kras2tm4Tyj (*Kras*^{G12D}/+ or *Kras*^{G12D} mice) strain with B6.FVB-Tg(Ipf1-cre)1Tuv mice has resulted in vulvar and periauricular papilloma presentation in as many as 40% of progeny (Gades, 2008). We also observed rectal and vulvar masses in our studies. Phenotypic variability also highlights the need for increased sample size to meet statistical significance. Indeed, the phenotypic results in the mice that developed tumors were so variable that even when using our results as preliminary data to perform a power analysis for future, the number of mice needed was unpractical.

Lymphoma is the most common tumor in GEMMs, and BALB/c background is highly susceptible to lung adenomas (Percy and Barthold, 2008; Ward, 2006). Lymphoma prevalence in the B6;129 strain can also be found through the MTB Database (Begley et al., 2012). The background of the *Tip30*-deficient mouse model that was used to generate each group of mice in this colony consisted of roughly 5% of the 129P2(B6) background that is referenced in Ward, 2006, according to The Jackson Laboratory. This small percentage is enough to contribute and pass on strain-related predispositions. One limitation of using mice

from a stock strain is that these mice consist of more than four different strains, according to Jackson Laboratory. Therefore identification of all of the strains present in one's experimental group of mice is difficult to discern. It is important to note that a near pure genetic background, which can be achieved after ten generations of backcrosses, can minimize variability in tumor penetrance, disease onset kinetics, lesion phenotype, and propensity for metastasis (Lee et al., 2016). These data on the influence of genetic background on tumor penetrance are well documented for mouse models of mammary (Guy et al., 1992; Lifsted et al., 1998) and colon cancers (Beckwith et al., 2005; Mahler and Leiter, 2002; Bristol et al., 2000) and are beginning to be mentioned for GEMM research of pancreatic cancer (Lee et al., 2016).

CHAPTER 6. CONCLUSION AND FUTURE DIRECTIONS

We hypothesized that loss of *Tip30* would result in poor PDAC prognosis based on evidence of TIP30's proapoptotic and metastasis suppressive functions. Here we describe a novel genetically engineered mouse model (GEMM) of PDAC where we employed previously established mouse models, KC (Hingorani et al., 2003), and the *Tip30*-deficient mouse (Xiao et al., 2003) to generate a novel K30C mouse model to study PDAC. Our results in this murine model of PDAC support a tumor- and metastasis- suppressive role for *Tip30* in PDAC progression. Based on our observations, we concluded that *Tip30*-heterozygous pancreatic cancer cells (PCCs) had more aggressive features than do *Tip30*-wild-type and *Tip30*-null PCCs. We report a pattern of preferential metastasis of pancreatic cancer cells (PCC's) to lung or liver tissue mediated by single *Tip30* genetic loss.

In conclusion, we found that *Tip30* loss and heterozygosity accelerated organ-specific pancreatic cancer cell (PCC) metastasis. We observed a delayed onset of frank PDAC tumor formation in KC mice that were *Tip30*-null with an increased prevalence of micrometastatic seeding compared to $K30^{+/-}C$ heterozygous mice, KC (n=3), or *Tip30*-null control mice (n=22). We concluded that the $K30^{+/-}C$ group of mice had more aggressive pancreas lesions by histopathological analysis in a three-month cohort when compared to $K30^{+/+}C$ and $K30^{-/-}C$ mice, and increased distribution of PanIN-2/3 lesions and PDAC. Just as phenotypic differences were observed in pancreata of $K30^{+/-}C$ versus $K30^{-/-}C$ mice, differences between PCCs isolated from pancreas tissues from both groups were visible in 3D cell cultures. Although PCCs from $K30^{+/-}C$ mice had a more

aggressive phenotype and increased EGFR levels compared to PCCs from KC and K30$^{-/-}$C mice, they had less proliferative potential and less 2D and 3D colony area formation when compared to *Tip30*-null PCCs. The trend of increase in growth with increasing *Tip30* copy number loss was first reported by Ito and colleagues and in immortalized mouse embryonic fibroblasts (MEFs) (Ito et al., 2003). We expected a dose-dependent increase in EGFR levels as *Tip30* copy number decreased. However, we observed that only the K30$^{+/-}$C PCCs had increased EGFR levels. Our finding that EGFR levels were increased only in PCCs with both oncogenic *Kras* and *Tip30*-heterozygous loss was novel; this increase in EGFR did not appear to have an impact on proliferation in two-dimensional or three-dimensional growth culture conditions. In regards to epithelial-mesenchymal transition (EMT), we observed that *Tip30*-null PCCs had decreased E-cadherin protein levels without an increase in N-cadherin. It would be interesting to investigate if the metastatic PCCs that seeded the liver had increased levels of E-cadherin and underwent the reverse of EMT, mesenchymal-epithelial transition (MET) to regain epithelial properties. Future RNA sequencing studies comparing the gene expression between *Tip30*-heterozygous and *Tip30*-null primary and metastatic PCCs would likely reveal gene-dose dependent effects of *Tip30* on signaling pathways.

In addition, lung lesions and lung adenocarcinomas (as early as five and eight weeks in predominately K30$^{+/-}$C mice, n=13/31, compared to the reports of presentation of such events at 78 weeks from the original *Tip30*-deficient mouse model and predominately in *Tip30*$^{-/-}$ mice), alerted us to a different phenomenon

than previously published. It is possibly that what we observed in our model was due to the addition of the PDAC-initiating *Kras*^{G12D} mutation that was conditionally targeted to the pancreas epithelium during embryogenesis. Heterozygous loss of *Tip30* resulted in lung or pulmonary seeding of pancreatic cancer cells in KC mice as detected by *LoxP-Kras*^{G12D} DNA by PCR and tracking of GFP+ cells. On the other hand, homozygous loss of *Tip30* resulted in liver micrometastatic seeding as detected by GFP analysis, and increased incidence of liver metastasis in KC mice compared to K30$^{+/+}$C and K30$^{+/-}$C mice. Interestingly, *Tip30*-null PCCs had increased two-dimensional and three-dimensional growth properties when compared to both wild-type and *Tip30*-heterozygous PCCs. *In vivo*, *Tip30*-null K30C mice were able to grow larger PDAC tumors, as *Tip30*-heterozygous K30C mice succumbed to disease early. Later time points revealed *Tip30*-dosage-mediated differences in pancreatic tumor phenotype.

DNA from the lung lesions tested positive for *LSL-Kras*^{G12D} recombination, further suggesting that the advanced pulmonary lesions observed as early five weeks, although secondary events, were a result of PCCs migrating from the pancreas. Experiments using a GFP-sorted cell line established from a two-month-old KC mouse with *Tip30* hetloss (TP852) further supported that pancreatic cancer cells migrate to the lung. Micrometastatic seeding to the lung of this mouse was visible, but very faintly. It is possible that in mice with more advanced pulmonary lesions, an increased infiltration of immune cells resulted in increased pathology and masked the visibility of GFP-positive PCCs. Gross pulmonary lesions were observed in one of five three-month-old K30$^{+/-}$Ctd$^{+/-}$ mice. However, GFP-positive

micrometastatic seeding was not visible by gross observation upon further analysis and the lesion was not GFP-positive. This was in contrast to the micrometastatic seeding visible in the two-month-old K30$^{+/-}$Ctd$^{+/-}$ mouse. The lung tissue of K30$^{+/-}$ Ctd$^{+/-}$-TP852 was not assessed for the presence or absence of microscopic PDAC metastasis lesions. However, the presence of metastatic lesions would have preceded gross nodule formation based on what was observed in the liver of *Tip30*-null mice. A 12-month-old *Tip30*-heterozygous KC mouse did develop a visible lung nodule; however, the histology for that tissue was not assessed. One three-month-old KC mouse from the TP30 colony also had GFP-positive and oncogenic-*Kras* positive PCCs cultured from lung tissue. GFP-positivity was visible only in culture. Future studies can assess micrometastatic seeding in all lung tissues and the capacity for colonization and macrometastatic outgrowth versus dormancy. More importantly, analysis of additional mice with conditional *Kras*^{G12D} and *Tip30* mutations or of an orthotopic model mirroring the system used for these studies will be necessary to further elucidate the role of *Tip30* gene dose on PCC organotropic metastasis.

Future directions would involve looking at lung tissues at earlier time points to detect total GFP+ PCCs to evaluate if metastatic seeding preceded the lesion formation we observed in pulmonary tissues. For example, an orthotopic study whereby fluorescently-labeled K30$^{+/-}$C PCCs are injected orthotopically into the pancreas tissues of syngeneic or nude mice would allow for an alternative approach to monitor *Tip30*-deficient PCC metastatic seeding. We could also use this model to observe if lung metastasis still occurs in the event of *Tip30* wild-type

lung tissues. This design would allow for the analysis of far fewer animals and would also shed insight to the differences in the phenotype of tumors that we originally observed in K30$^{+/-}$C mice compared to K30$^{-/-}$C mice. The following experiments could then uncover the mechanism of action for *Tip30* copy loss in PDAC metastatic organotropism:

1. RNAsequencing of *Tip30*$^{+/-}$ and *Tip30*$^{-/-}$ PCCs to uncover specific signaling pathways involved in mediating PDAC.
2. Analysis of human PDAC tissue samples to validate TCGA databases of genetic alterations, and TIP30 gene expression both at mRNA and protein levels.
3. Migration and invasion assays to understand the role of increased EGFR levels in *Tip30*$^{+/-}$ PCCs in mediating PDAC metastasis to the lung.
4. Analysis of *Tip30*$^{+/-}$ PCCs with increased EGFR levels for sensitivity to EGFR inhibition.

Also, if *Tip30*$^{+/-}$ metastatic PCCs isolated from the lung are more migratory than primary PCCs, and if this is due to increased EGFR activity, then targeting EGFR in combination with therapeutic regimens to treat PDAC may help better target or prevent metastatic disease in the subset of PDAC patients with *TIP30*-heterozygous loss.

How and why differences in *Tip30* gene dose mediate organ-specific PDAC metastasis requires further investigation. We predict that the immune system is heavily involved in the observations from our studies, and impacted by the heterozygous loss of *Tip30*. Chemokines and chemokine receptors are reported

to play a role in organ-specific metastasis by recruiting lymphocytes and haematopoietic cells to certain organs (Chambers et al., 2002). K30$^{+/-}$C mice with pulmonary lesions had an abundance of inflammation noted during histopathological evaluation. Therefore, further studies on the role of the immune response and the tumor microenvironment in the context of *Tip30* loss would be beneficial in order to understand if *Tip30* loss allows for PCC evasion of the immune response, as observed with the increase in macrophage infiltration in the lung tissues of the K30$^{+/-}$C mice.

In summary, we have generated and characterized a novel model of mPDAC and found that *Tip30*-deficiency, when coupled with the pancreas-specific oncogenic *Kras*^{G12D} background, enhanced the overall tumor progression of K30$^{+/-}$C and K30$^{-/-}$C mice and influenced organ-specific metastatic seeding. The genetic and phenotypic differences observed in K30C mice with either heterozygous or complete loss of *Tip30* were translated in *in vitro* systems. We observed a trend of increased pancreatic cancer cell growth with increasing *Tip30* copy loss, as well as increased levels of the epidermal growth factor receptor (EGFR) in primary PCCs derived from our most aggressive model. Our findings of enhanced basal EGFR using murine PCCs isolated from K30C mice were replicated using a human PDAC cell line that was genetically engineered to overexpress microRNA (miR)-10b. miR-10b directly targets TIP30 mRNA for degradation (Ouyang, 2013; Dong et al., 2014). In these analyses, we also observed increase in downstream signaling markers, including AKT and phosphorylated ERK1/2, both of which play an important role in cell survival (Amaravadi and Thompson, 2005; Mebratu and

Tesfaigzi, 2010). Overall, these observations were further supported by the subset of patients with *TIP30* hetloss according to data from The Cancer Genome Atlas (Witkiewicz et al., 2015). The findings from these studies combined with the available literature suggest that it would be useful to assess these patients' metastatic status, and explore if TIP30 or its downstream targets can be investigated for therapies designed to target metastasis. Additionally, as a vast majority of cancers, including PDAC, have amplifications in *TIP30* according to TCGA (J. Gao et al., 2013; Cerami et al., 2012), it would be equally important to understand the role of TIP30 overexpression in PDAC, in the context of wild-type miR-10b levels. Gene dose-dependent effects of TIP30 uncovered in this study illustrates complexities involved in pancreatic cancer progression and the difficulty in establishing a linear relationship between genomic aberrations, disease progression, and potentially therapeutic response.

APPENDICES

APPENDIX A. GENOTYPING FOR ADDITIONAL MOUSE MODELS

mp53	Genotype	PCR
TP151	KC	8/4/2017
TP177	KC	1/23/2015
TP177	KC	4/17/2015
TP180	KC	1/23/2015
TP180	KC	4/17/2015
TP182	KC	1/23/2015
TP182	KC	4/17/2015
TP184	KC	1/23/2015
TP184	KC	4/17/2015
TP196	KC	10/31/2014
TP197	KC	10/31/2014
TP578	KC	10/12/2016
TP579	KC	10/12/2016
TP580	KC	10/12/2016
TP581	KC	10/12/2016
TP711-Re	KC	12/9/2016
TP713-Re	KC	12/9/2016
TP715-Re	KC	12/9/2016
TP912	KC	8/11/2017
TP431	$K30^{+/-}C$	4/1/2016
TP448	$K30^{+/-}C$	4/1/2016
TP452	$K30^{+/-}C$	4/1/2016
TP473-Re	$K30^{+/-}C$	4/1/2016
TP477	$K30^{+/-}C$	4/1/2016
TP555	$K30^{-/-}C$	4/1/2016
TP573	$K30^{+/-}C$	4/1/2016
TP576	$K30^{+/-}C$	4/1/2016
TP609	$K30^{+/-}C$	4/1/2016
TP622	$K30^{+/-}C$	4/1/2016
TP627	$K30^{+/-}C$	4/1/2016
TP630	$K30^{+/-}C$	4/1/2016
TP881	$K30^{-/-}C$	8/11/2017
TP368	$K30^{-/-}$	4/1/2016
TP392	$KT30^{+/-}$	4/1/2016

Rb	Genotype	PCR
TP151	KC	8/3/2017
TP151 PCCs	KC	8/25/2017
TP177	KC	1/23/2015
TP180	KC	1/23/2015
TP182	KC	1/23/2015
TP184	KC	1/23/2015
TP196	KC	11/10/2014
TP197	KC	11/10/2014
TP503	KC	5/23/2018
TP545	KC	6/6/2018
TP577	KC	6/6/2018
TP578	KC	10/12/2016
TP579	KC	10/12/2016
TP580	KC	10/12/2016
TP581	KC	10/12/2016
TP711-Re	KC	12/9/2016
TP711 PCCs	KC	8/25/2017
TP713-Re	KC	12/9/2016
TP715-Re	KC	12/9/2016
TP715 PCCs	KC	8/25/2017
TP834	KC	9/8/2016
TP881	KC	8/11/2017
TP912	KC	8/11/2017
TP1016-Re	KC	6/28/2017
TP431	$K30^{+/-}C$	4/6/2016
TP448	$K30^{+/-}C$	4/6/2016
TP609	$K30^{+/-}C$	4/6/2016
TP622	$K30^{+/-}C$	4/6/2016
TP627	$K30^{+/-}C$	4/6/2016
TP630	$K30^{+/-}C$	4/6/2016

Bmal	Genotype	PCR
TP177	KC	1/23/2015

TP450-Re	$K30^{+/-}$	4/1/2016
TP502-Re	$30^{+/-}C$	4/1/2016

miR-155	Genotype	PCR
TP912	KC	8/11/2017
TP881	$K30^{-/-}C$	8/11/2017

miR-21 (OX (eGFP), KO (TK, CK)	Genotype	PCR
TP151	KC	8/4/2017
TP177	KC	8/4/2017
TP180	KC	8/4/2017
TP182	KC	8/4/2017
TP184	KC	8/4/2017
TP503	KC	8/4/2017
TP545	KC	8/4/2017
TP577	KC	8/4/2017
TP711-Re	KC	8/4/2017
TP713-Re	KC	8/4/2017
TP715-Re	KC	8/4/2017
TP912	KC	8/4/2017
TP592	$K30^{-/-}C$	8/4/2017
TP647	$K30^{+/-}C$	8/4/2017
TP852	$K30^{+/-}C$	8/4/2017
TP892	$K30^{-/-}C$	8/4/2017

Agr2	Genotype	PCR
TP477	$K30^{+/-}C$	11/18/2015
TP576-Re	$K30^{+/-}C$	11/18/2015
TP711	KC	12/9/2016
TP713	KC	12/9/2016
TP715	KC	12/9/2016

Smad4L/L	Genotype	PCR
TP151	KC	3/30/2017
TP177	KC	3/30/2017
TP180	KC	1/23/2015
TP182	KC	1/23/2015
TP184	KC	1/23/2015
TP711-Re	KC	12/9/2016
TP713-Re	KC	12/9/2016
TP715-Re	KC	12/9/2016

tet-Smad7	Genotype	PCR
TP711-Re	KC	12/9/2016
TP713-Re	KC	12/9/2016
TP715-Re	KC	12/9/2016

Smad7	Genotype	PCR
TP711-Re	KC	12/8/2016
TP713-Re	KC	12/8/2016
TP715-Re	KC	12/8/2016

Ink4a	Genotype	PCR
TP177	KC	1/23/2015
TP180	KC	1/23/2015
TP182	KC	1/23/2015
TP184	KC	1/23/2015
TP711-Re	KC	12/9/2016
TP713-Re	KC	12/9/2016
TP715-Re	KC	12/9/2016

HER3	Genotype	PCR
TP151	KC	8/21/2017
TP578	KC	3/23/2018
TP579	KC	3/23/2018
TP580	KC	3/23/2018
TP581	KC	3/23/2018
TP711-Re	KC	12/30/2016
TP713-Re	KC	12/30/2016
TP715-Re	KC	12/30/2016
TP912	KC	8/21/2017
TP1016	KC	8/21/2017

TP180	KC	3/30/2017
TP182	KC	3/30/2017
TP184	KC	3/30/2017
TP711-Re	KC	3/30/2017
TP713-Re	KC	3/30/2017
TP715-Re	KC	3/30/2017
TP834-Re	KC	3/30/2017
TP860-Re	KC	3/30/2017
TP864-Re	KC	3/30/2017
TP912	KC	3/30/2017
TP431	$K30^{+/-}C$	3/30/2017
TP448	$K30^{+/-}C$	3/30/2017
TP609	$K30^{+/-}C$	3/30/2017

Syndecan 4	Genotype	PCR
TP711-Re	KC	12/9/2016
TP713-Re	KC	12/9/2016
TP715-Re	KC	12/9/2016

TP431	$K30^{+/-}C$	3/23/2018
TP452	$K30^{+/-}C$	3/23/2018
TP468	$K30^{+/-}C$	3/23/2018
TP473	$K30^{+/-}C$	3/23/2018
TP526	$K30^{-/-}C$	3/23/2018
TP543	$K30^{-/-}C$	3/23/2018
TP555	$K30^{-/-}C$	3/23/2018
TP569	$K30^{-/-}C$	3/23/2018

p16	Genotype	PCR
TP151 PCCs	KC	8/25/2017
TP177	KC	1/23/2015
TP180	KC	1/23/2015
TP182	KC	1/23/2015
TP184	KC	1/23/2015
TP711-Re	KC	12/9/2016
TP711 PCCs	KC	8/25/2017
TP713-Re	KC	12/9/2016
TP715-Re	KC	12/9/2016
TP715 PCCs	KC	8/25/2017
TP912 PCCs	KC	8/25/2017
TP576-panc	$K30^{+/-}C$	3/29/2016
TP630-panc	$K30^{+/-}C$	3/29/2016
TP630-Lu	$K30^{+/-}C$	3/29/2016

This testing was to ensure that other transgenes in the lab were not mixed into the mice of TP30 Colony. Date of genotyping (testing) is listed under "PCR". Updated 12/1/18. Tail DNA, unless otherwise indicated. Key: Re, tail sample collected at endpoint; PCCs-pancreatic cancer cells; Lu, Lung.

Primers, Reaction Components, and Thermocycler Conditions

NCOA5
(S. Gao et al., 2013)

Ncoa5 WT: GACCGTTATCTGAGGGTGGA
Ncoa5 Mutant (neo): GCCAGAGGCCACTTGTGTAG
Ncoa5 Common (C): TTCACCTGCAACCTTCTCCT

2 µL 10X
1 µL $MgCl_2$

0.5 µL dNTPs
0.1 µL Common Primer
0.1 µL Ncoa5 WT (or Ncoa5 MT (neo)-separate reaction)
0.1 µL Taq
15.2 µL ddH2O

Cycling (Step #, Temperature)

1. 95°C, 15 min
2. 95°C, 30 sec
3. 57°C, 1 min
4. 72°C, 1 min
5. Repeat steps 2-4 for 35 cycles.
6. 72°C, 10 min
7. 10°C, hold

$Ncoa5^{+/-}$ = 324-bp band in both M and WT reactions

MMTV-Neu

(Jackson Laboratory, Stock #00237; Zhang et al., 2010)

MMTV-Neu Reverse (R): TTTCCTGCAGCAGCCTACGC
MMTV-Neu Forward (F): CGGAACCCACATCAGGCC
MMTV-Neu IPC*-F: CAAATGTTGCTTGTCTGGTG
MMTV-Neu IPC-R: GTCAGTCGAGTGCACAGTTT
*Internal Positive Control

1.8 µL 10X
1 µL $MgCl_2$
0.5 µL dNTPs
0.1 µL Forward primer
0.1 µL Reverse primer
0.1 µL IPC-F
0.1 µL IPC-R
0.1 µL Taq
15.2 µL ddH2O

Cycling (Step #, Temperature)

1. 95°C, 15 min
2. 95°C, 30 sec
3. 60°C, 30 sec*
4. 72°C, 35 sec, repeat steps 2-4 for 12 cycles.
5. 95°C, 15 min
6. 58°C, 30 sec
7. 72°C, 35 sec, repeat steps 5-7 for 25 cycles.
8. 72°C, 10 min
9. 10°C, hold

*Decrease -0.5°C/cycle

IPC = 324 bp
Transgene = 600 bp

IL6
(Jackson Laboratory, Stock #002650; S. Gao et al., 2013)

IL6 Common (C):	TTCCATCCAGTTGCCTTCTTGG
IL6 WT Reverse (R):	TTCTCATTTCCACGATTTCCCAG
IL6 MT Reverse (R):	CCGGAGAACCTGCGTGCAATCC

1.8 µL	10X
1 µL	$MgCl_2$
0.5 µL	dNTPs
0.2 µL	Common Primer
0.1 µL	Ncoa5 WT
0.1 µL	Ncoa5 MT (neo)
0.1 µL	Taq
15.2 µL	ddH2O

Cycling (Step #, Temperature)

1. 95 °C 15 min
2. 95 °C 30 sec
3. 62 °C 1 min
4. 72 °C 1 min
5. Repeat steps 2-4 for 35 cycles.
6. 72 °C 10 min
7. 10 °C, hold

M band (380 bp)
WT band (174 bp)

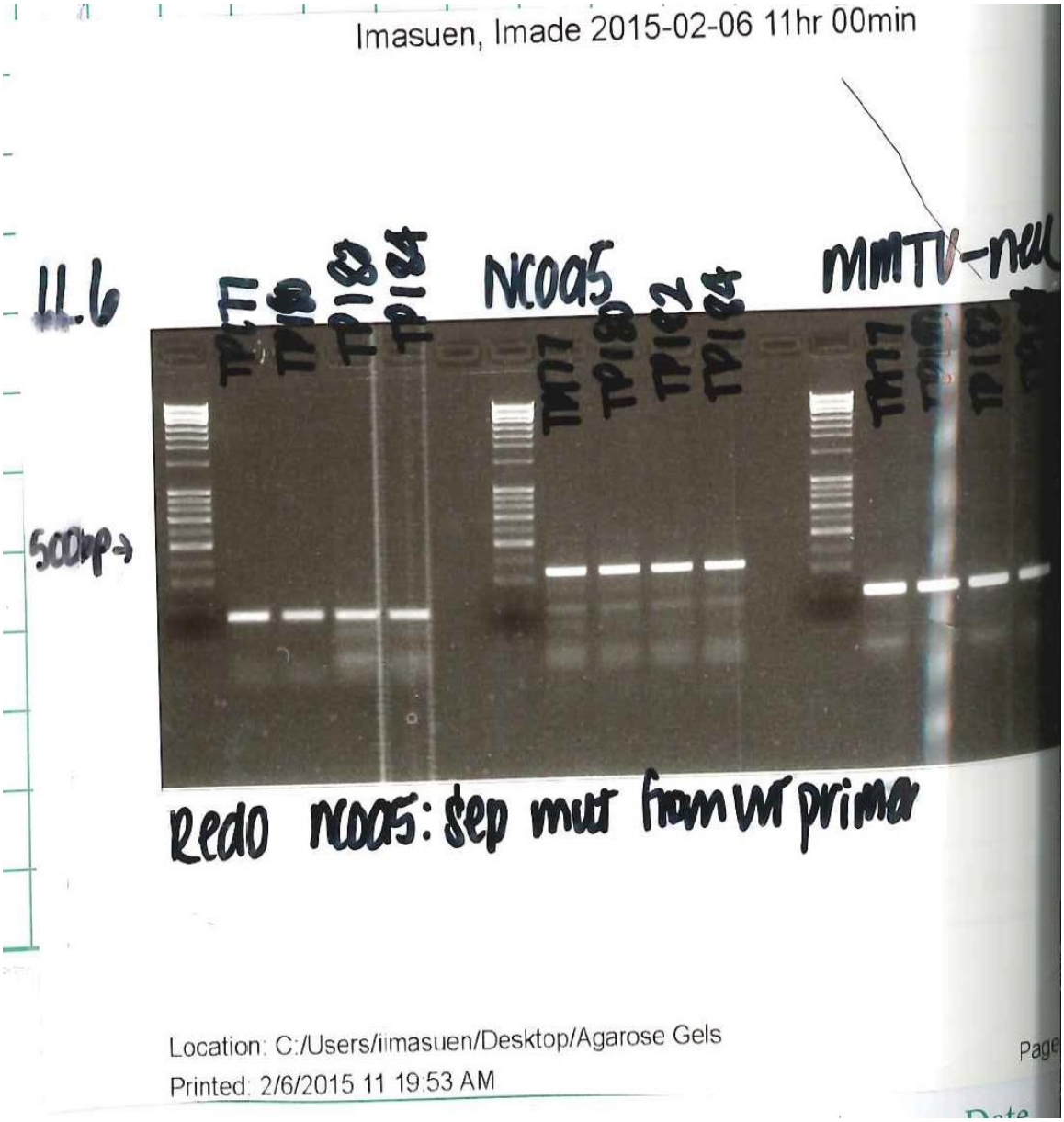

10 kB Ladder. IL6: WT (174 bp band only); MMTV-Neu: Negative

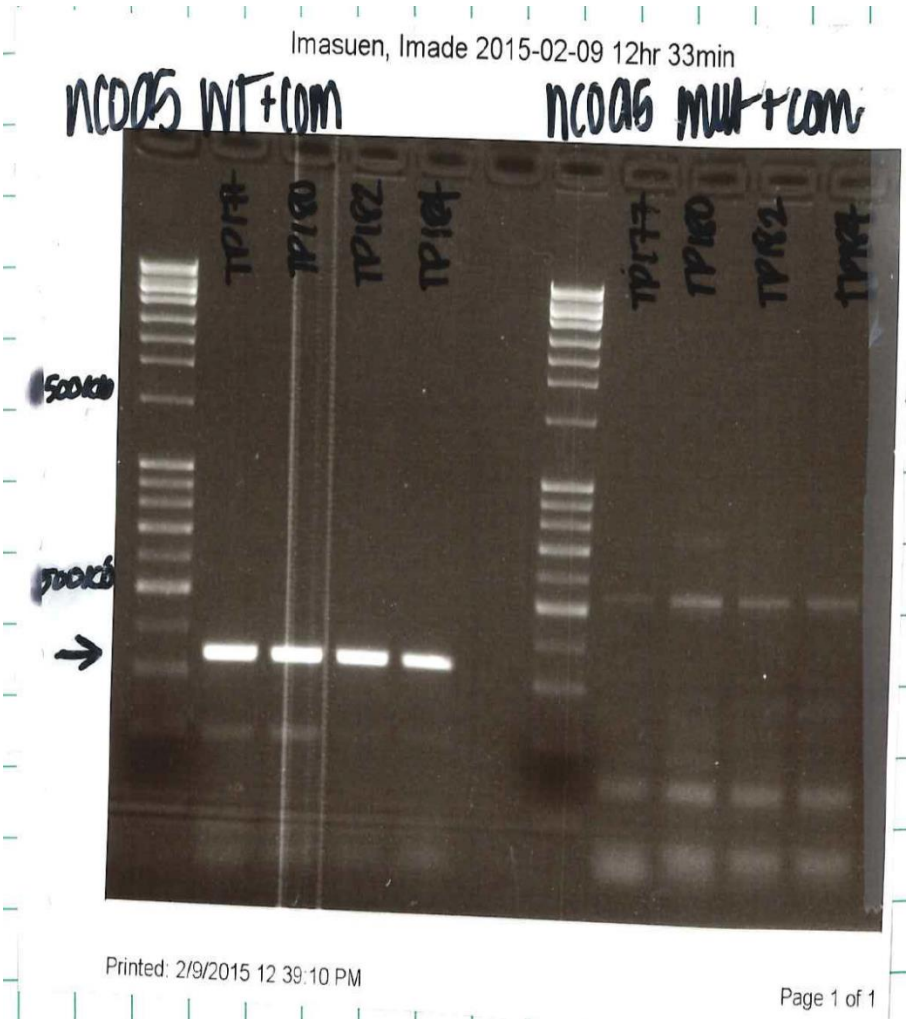

10 kB Ladder. Ncoa5: WT (324-bp band in WT reaction only)

Bmal

(The Jackson Laboratory 007668)
Bmal FP: ACT GGA AGT AAC TTT ATC AAA CTG
Bmal RP: CTG ACC AAC TTG CTA ACA ATT A

2 µL	10X
1.2 µL	$MgCl_2$
0.5 µL	dNTPs
0.1 µL	Common Primer
0.1 µL	Ncoa5 WT
0.1 µL	Taq
15.2 µL	ddH2O

Cycling (Step #, Temperature)

1. 95 °C, 15 min
2. 95 °C, 30 sec
3. 60 °C, 30 sec

4. 72 °C, 30 sec
5. Repeat steps 2-4 for 36 cycles.
6. 72 °C 5 min
7. 10 °C, hold

M band (431 bp)
Heterozygote (both 327 bp and 431 bp)
WT band (327 bp)

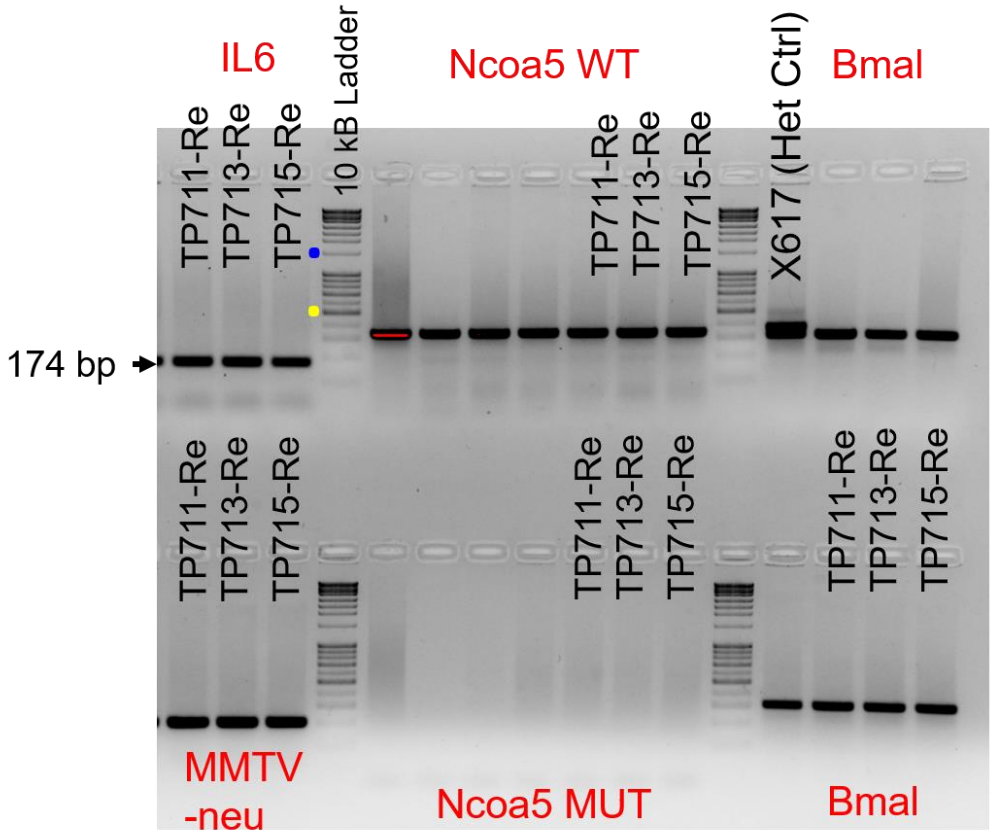

File name: “Imasuen-Williams, Imade 2016-12-09 14hr 10min IL6, MMTV-Neu, Ncoa5, Bmal”. **IL6:** KO model-Mice show defects in responses to various viruses and in inflammatory responses to tissue damage or infection (https://www.jax.org/strain/002650). Mut=380 bp, Het=380 bp and 174 bp, WT=174 bp. Only a WT band was detected in the tail DNA from these K30$^{+/+}$C mice. **MMTV-neu**: Transgene= ~600bp, Internal positive control = 200bp. No MMTV-neu transgene detected. Bmal: Only the lower, WT band was detected compared to a heterozygous control (Het). 10 kB ladder. Blue dot represents 1500 bp mark, yellow dot represents 500 bp mark.

1.5% gel, 10 kB ladder, 1) Het ctrl tail DNA from mouse ID X617, 2) $K30^{+/+}$C-TP177, 3) $K30^{+/+}$C-TP180, 4) $K30^{+/+}$C-TP182, 5) $K30^{+/+}$C-TP184

p16

1 (P3): AGGAGTCCTGGCCCTAGAAA*
2 (P4): CCAAAGGCAAACTTCTCAGC
*Against the lac Z-tagged mutant allele Cdkn2a via Blast

2 µL	10X
1.2 µL	$MgCl_2$
0.5 µL	dNTPs
0.1 µL	Forward primer
0.1 µL	Reverse primer
0.1 µL	Taq
15 µL	ddH2O

Cycling (Step #, Temperature)

1. 95 °C, 15 min
2. 95 °C, 30 sec
3. 60 °C, 30 sec
4. 72 °C, 40 sec
5. Repeat steps 2-4 for 35 cycles.
6. 72 °C, 2 min
7. 10 °C, hold

Double band: L/+

Upper: L/L
Lower: WT

2% gel, 10 kb ladder. K30+/+C (TP711. TP713, and TP715) mice and tail DNA tested negative for the p16 transgene, as compared to the positive control.

mp53 (R172H)

T35: CTTGGAGACATAGCCACACTG
T36: AGCTAGCCACCATGGCTTGAGTAAGTCTGCA

2 µL	10X
1 µL	$MgCl_2$
0.5 µL	dNTPs
0.25 µL	Forward primer
0.25 µL	Reverse primer
0.1 µL	Taq
14.9 µL	ddH2O

Cycling (Step #, Temperature)

1. 95 °C, 15 min
2. 95 °C, 30 sec
3. 56 °C, 1 min
4. 72 °C, 1 min
5. Repeat steps 2-4 for 35 cycles.
6. 72 °C, 2 min
7. 10 °C, hold

M band (positive)
WT (negative)

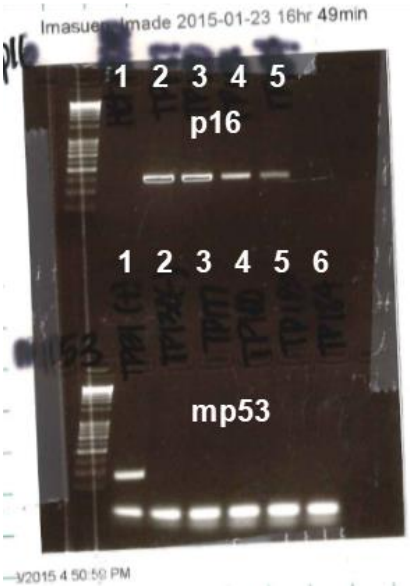

2% gel, 10 kB ladder, p16 genotyping PCR: 1) Het ctrl tail DNA from mouse ID PD220 (did not show), 2) K30$^{+/+}$C-TP177, 3) K30$^{+/+}$C-TP180, 4) K30$^{+/+}$C-TP182, 5) K30$^{+/+}$C-TP184; mp53 genotyping PCR: 1) positive (+) ctrl tail DNA from mouse ID TP131, 2) negative (-) Ctrl-Tail TP130, 3) K30$^{+/+}$C-TP177, 4) K30$^{+/+}$C-TP180, 5) K30$^{+/+}$C-TP182, 6) K30$^{+/+}$C-TP184

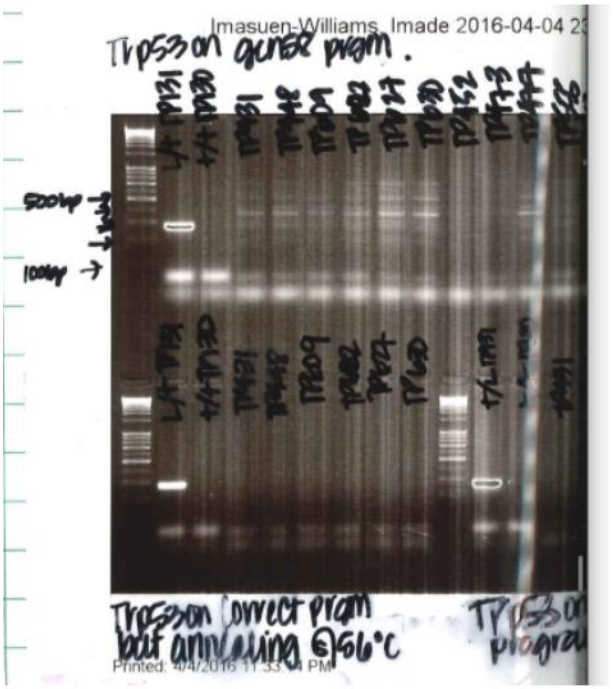

2% gel, 10 kB ladder. Positive control (L/+) from mouse ID TP131, negative control (+/+) from mouse ID TP130. K30$^{+/-}$C mice (TP431, TP448, TP609, TP622, TP627, TP630, TP452, TP573, and TP477) tested negative for the mp53 transgene. K30$^{/-}$C mouse TP555 tested negative for mp53.

Rb

R007: GGC GTG TGC CAT CAA TG
R008: AAC TCA AGG GAG ACC TG

2 µL	10X
1 µL	$MgCl_2$
0.5 µL	dNTPs
0.25 µL	Forward primer
0.25 µL	Reverse primer
0.1 µL	Taq
13.9 µL	ddH2O

+ 2 µL Tail DNA

Cycling (Step #, Temperature)

1. 95 °C, 15 min
2. 95 °C, 30 sec
3. 60 °C, 30 sec
4. 72 °C, 1 min
5. Repeat steps 2-4 for 35 cycles.
6. 72 °C, 5 min
7. 10 °C, hold

L/L (Upper band)-650 bp
L/+ (Double band)-650 and 600 bp
+/+ or WT (Lower band)-600 bp

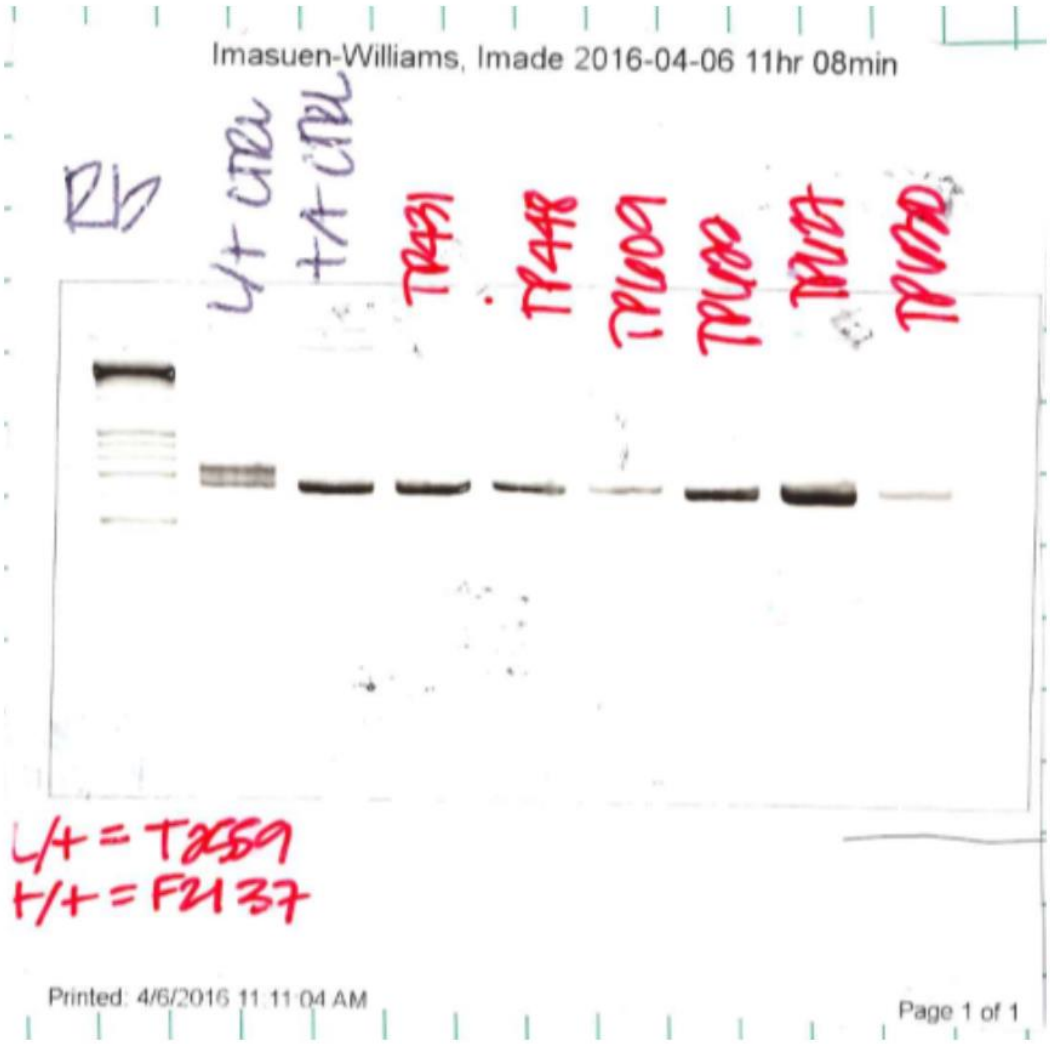

3% gel, 10 kB ladder, positive (L/+) and negative (+/+) controls from mouse ID's as indicated (T2559, and F2137). K30$^{+/-}$C mice TP431, TP609, TP622, TP627, TP630 test negative for the Rb mutant transgene.

3% gel, 10 kB ladder, $K30^{+/+}$ $Ctd^{+/-}$-TP912 and TP881-$K30^{-/-}Ctd^{+/-}$ were negative for the Rb transgene. Controls are indicated.

miR-155 (KO)

Wild type Forward: GTG CTG CAA ACC AGG AAG G
Wild type Reverse: CTG GTT GAA TCA TTG AAG ATG G
Mutant: CGG CAA ACG ACT GTC CTG GCC G

2 µL	10X
1 µL	$MgCl_2$
0.5 µL	dNTPs
0.5 µL	WTF Primer
0.5 µL	WTR Primer
0.5 µL	MT Primer
0.1 µL	Taq
15.2 µL	ddH2O

+ 2 µL Tail DNA

-/- (Upper band)
+/- (Double band)
+/+ or WT (Lower band)

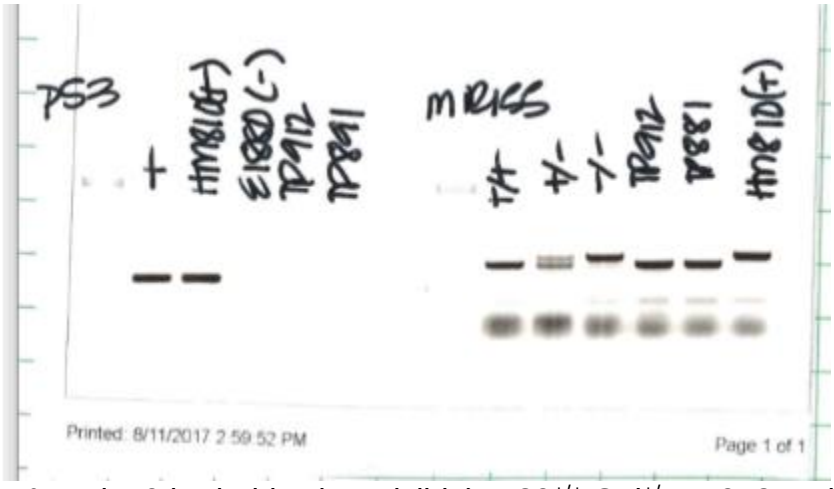

1.5% gel, 10 kB ladder (not visible), K30$^{+/+}$ Ctd$^{+/-}$-TP912 and TP881-K30$^{-/-}$Ctd$^{+/-}$ were negative for the miR-155 transgene. Controls are indicated.

<u>miR-21</u>

2 µL	10X
1.2 µL	$MgCl_2$
0.5 µL	dNTPs
0.1 µL	Forward primer
0.1 µL	Reverse primer
0.1 µL	Taq
15 µL	ddH2O

miR-21 conditional (CK)
miR-21-conditional-Forward: GCTTACTTCTCTCTGTGATTTCTGTG
miR-21-conditional-Reverse: GGTGGTACAGCCATGCGATGTCACGAC

Cycling (Step #, Temperature)
1. 95 °C, 15 min
2. 95 °C, 30 sec
3. 60 °C, 30 sec
4. 72 °C, 30 sec
5. Repeat steps 2-4 for 35 cycles.
6. 72 °C, 2 min
7. 10 °C, hold

L/L (Upper band)
L/+ (Double band)
+/+ or WT (Lower band)

miR-21 KO (TK)
miR-21-straightKO F: CCGGCTTTAACAGGTG
miR-21-straightKO R: GATACTGCTGCTGTTACCAAG

Cycling (Step #, Temperature)

8. 95 °C, 15 min
9. 95 °C, 30 sec
10. 62.3 °C, 30 sec
11. 72 °C, 1 min
12. Repeat steps 2-4 for 38 cycles.
13. 72 °C, 5 min
14. 10 °C, hold

-/- (Lower band)
+/- (Double band)
+/+ or WT (Upper band)

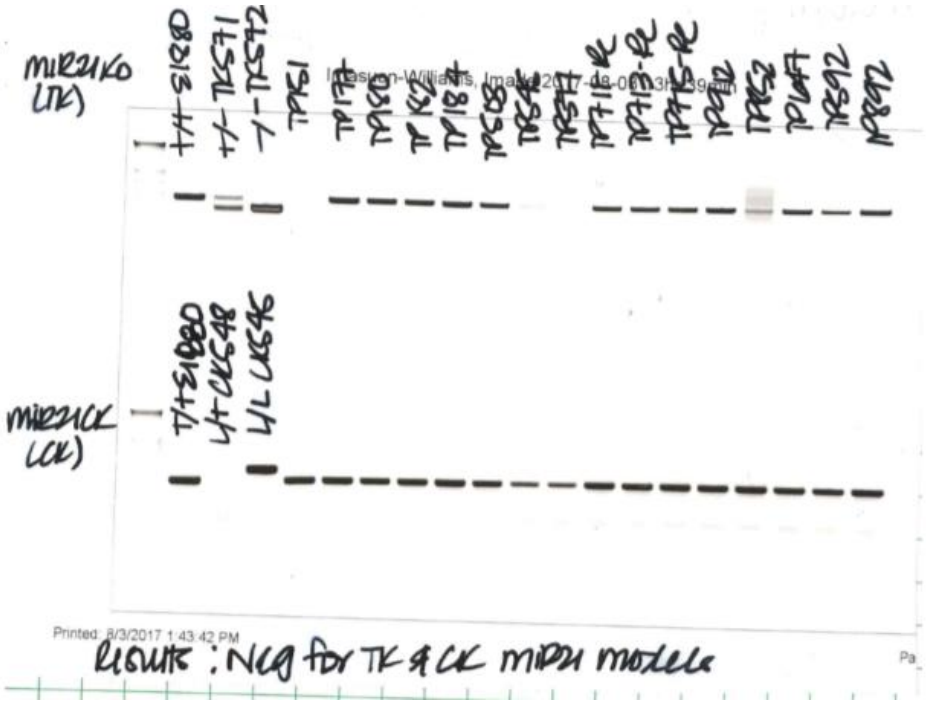

2% gel, 10 kB ladder. K30 were genotyped for the miR-21 transgenes as indicated above. The miR-21 transgene was not detected in any of the mice tested. Three tail DNA samples were low in DNA. $K30^{+/+}$C-TP151, -TP177, -TP180. -TP182, -TP184, -TP503, -TP545, -TP577, -TP711-Re, -TP713-Re, -TP715-Re, -TP912; $K30^{+/-}$C-TP852, -TP647; $K30^{-/-}$C-TP592, -TP892.

Agr2

flox1: ATCCAACAAGCATCCACTGA
flox2: CTTTGGCCAAGGTACCAGAA
flox3: CTGGATCTAATTTGTGCTGAAT

2 µL	10X
1.2 µL	$MgCl_2$
0.5 µL	dNTPs

0.1 µL Forward primer
0.1 µL Reverse primer
0.1 µL Taq
14.9 µL ddH2O

Cycling (Step #, Temperature)

1. 95 °C, 15 min
2. 94 °C, 30 sec
3. 58 °C, 1 min
4. 72 °C, 1 min
5. Repeat steps 2-4 for 35 cycles.
6. 72 °C, 5 min
7. 10 °C, hold

-/- (Upper band)
+/- (Double band)
+/+ or WT (Lower band)

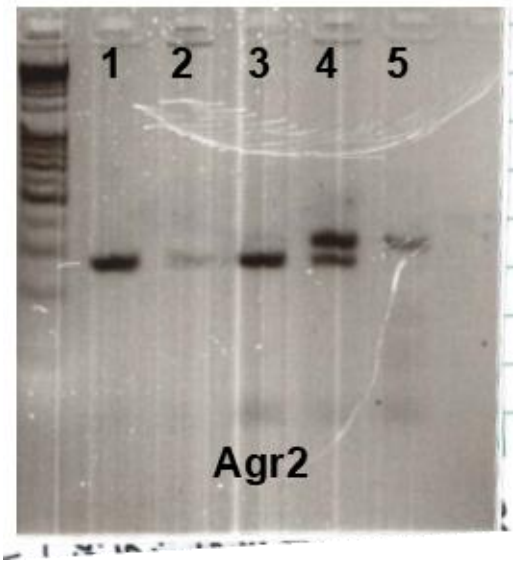

3% gel, 10 kB ladder, 1) K30$^{+/-}$C-TP477, 2) K30$^{+/-}$C-TP576, 3) -/- ctrl tail from mouse ID U1403, 4) +/- ctrl tail from mouse ID U1420, 5) -/- ctrl tail from mouse ID U1480. TP477 and TP576 are negative for the Agr2 transgene.

tet-Smad7

Tet_S7FP ATCCACGCTGTTTTGACCTC
Tet_S7RP GAGCGCAGATCGTTTGGT

Final Concentration
1X Buffer
1.5 mM $MgCl_2$
0.25 mM dNTPs

0.5 µM Forward primer
0.5 µM Reverse primer
0.025U/µL Taq

Cycling (Step #, Temperature)

1. 95 °C, 15 min
2. 95 °C, 30 sec
3. 60 °C, 1 min
4. 72 °C, 1 min
5. Repeat steps 2-4 for 34 cycles.
6. 72 °C, 2 min
7. 10 °C, hold

Smad7

EGFP mut_FP: AAGTTCATCTGCACCACCG
EGFP mut_RP: TCCTTGAAGAAGATGGTGCG (R):

Final Concentration
1X Buffer
1.5 mM $MgCl_2$
0.375 mM dNTPs
0.6 µM Forward primer
0.6 µM Reverse primer
0.025U/µL Taq

Cycling (Step #, Temperature)

1. 95 °C, 15 min
2. 95 °C, 30 sec
3. 55 °C, 45 sec
4. 72 °C, 1 min
5. Repeat steps 2-4 for 34 cycles.
6. 72 °C, 10 min
7. 10 °C, hold

M band (380 bp)
WT band (174 bp)

Ink4a

Forward: CCAAGTGTGCAAACCCAGGCTCC
Reverse: TTGTTGGCCCAGTGATGCCGACATC

2 µL	10X
1.2 µL	$MgCl_2$
0.5 µL	dNTPs

0.1 µL	Forward primer
0.1 µL	Reverse primer
0.1 µL	Taq
15 µL	ddH2O

L/L (Upper band): 200 bp
L/+ (Double band)
+/+ or WT (Lower band)

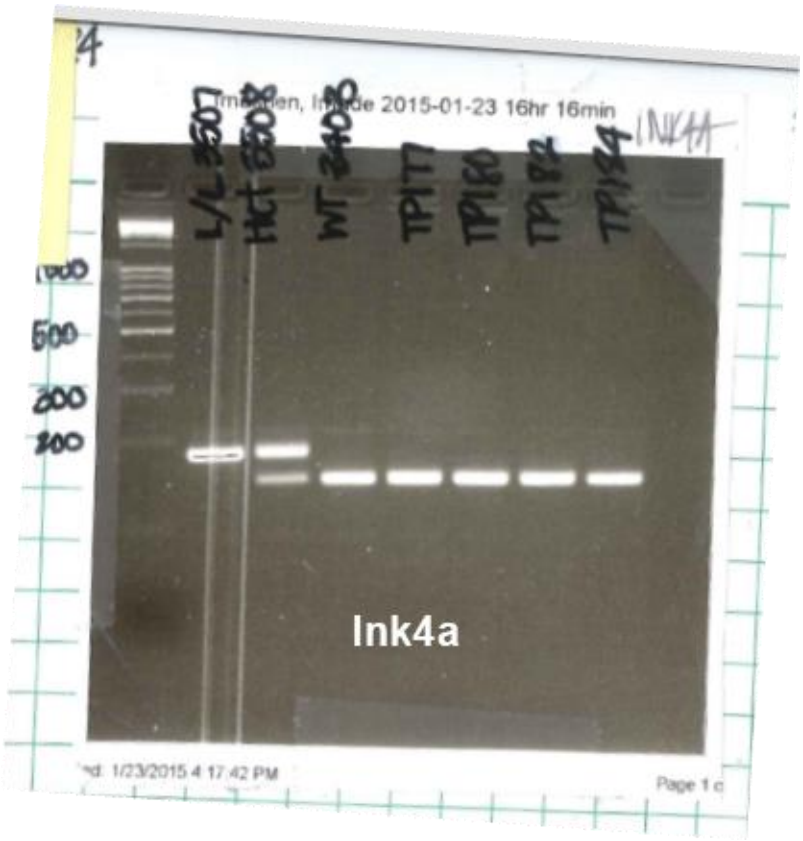

3% gel, 10 kB ladder, positive L/L ctrl tail DNA from mouse ID 3507, L/+ ctrl tail DNA from mouse ID 3508, K30$^{+/+}$C-TP177, -TP180, -TP182, and -TP184 tail DNA.

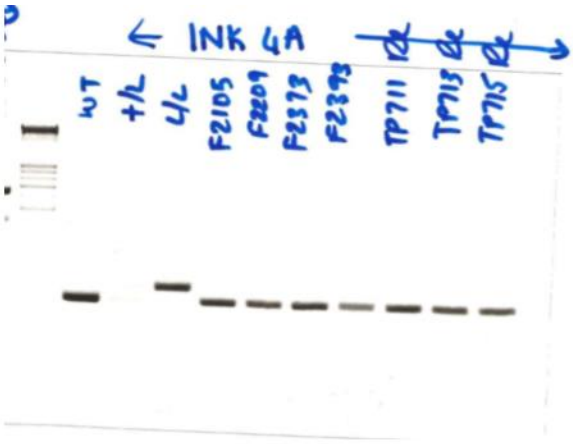

3% gel, 10 kB ladder. K30$^{+/+}$C mice (TP711, TP713, TP715) are negative for the Ink4a transgene, as compared to the positive (L/L) control.

HER3*

SDR3: CACTGCAGGAAGGAGAGGTC
CCL1: GCTATACGAAGTTATTCGAGGC

2 µL	10X
1.2 µL	$MgCl_2$
0.5 µL	dNTPs
0.1 µL	Forward primer
0.1 µL	Reverse primer
0.1 µL	Taq
15 µL	ddH2O

Cycling (Step #, Temperature)

1. 95 °C, 15 min
2. 94 °C, 30 sec
3. 64 °C, 30 sec
4. 72 °C, 1 min
5. Repeat steps 2-4 for 35 cycles.
6. 72 °C, 1 min
7. 10 °C, hold

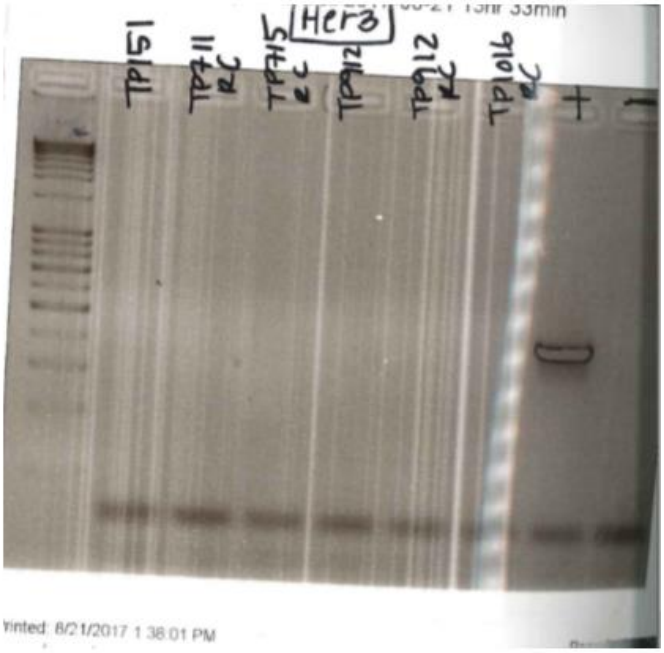

2 % gel, 10 kB ladder. Tail DNA from K30$^{+/+}$C mice (TP151, TP711, TP715, TP912, and TP1016) does not test positive for the HER3 transgene as compared to the positive control.

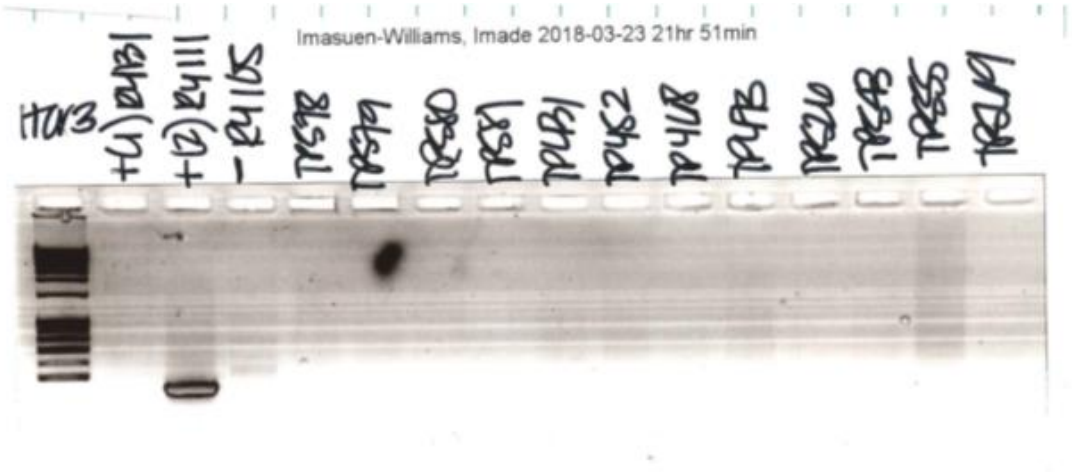

2% gel, 10 kB ladder. Tail DNA from K30$^{+/+}$C mice (TP578, TP579, TP580, TP581), K30$^{+/-}$C mice (TP431, TP452, TP468, TP473), and K30$^{-/-}$C mice (TP526, TP543, TP555, TP569) does not test positive for the HER3 transgene as compared to positive (R4111) and negative (R4105) controls.

Smad4L/L
(The Bardeesy Lab, Bardeesy et al., 2006b

DPC6: GGGAACAGAGCACAGGCCTCTGTGACAG
DPC9: TTCACTGTGTAGCCCCGCCTGTCCTGGA

2.5 µL	10X, 15 mM $MgCl_2$
0 µL	$MgCl_2$
0.5 µL	dNTPs
1.25 µL	20 µM DPC6
1.25 µL	20 µM DPC9
0.13 µL	Taq
18.37 µL	ddH2O

Cycling (Step #, Temperature)

1. 95 °C, 15 min
2. 95 °C, 30 sec
3. 60 °C, 1 min
4. 72 °C, 1 min
5. Repeat steps 2-4 for 33 cycles.
6. 72 °C, 10 min
7. 10 °C, hold

M band (400 bp)
WT band (350 bp)

Smad transgene
(The Bardeesy Lab)

SM3: TGCTCTGAGCTCACAATTCTCCT
DPC9:TTCACTGTGTAGCCCCGCCTGTCCTGGA

2.5 µL	10X, 15 mM $MgCl_2$
0 µL	$MgCl_2$
0.5 µL	dNTPs
1.25 µL	20 µM SM3
1.25 µL	20 µM DPC9
0.13 µL	Taq
18.37 µL	ddH2O

Cycling (Step #, Temperature)

1. 95 °C, 15 min
2. 95 °C, 30 sec
3. 60 °C, 1 min
4. 72 °C, 1 min
5. Repeat steps 2-4 for 33 cycles.
6. 72 °C, 10 min
7. 10 °C, hold

200 bp band = Presence of null allele
No band = Absence of null allele

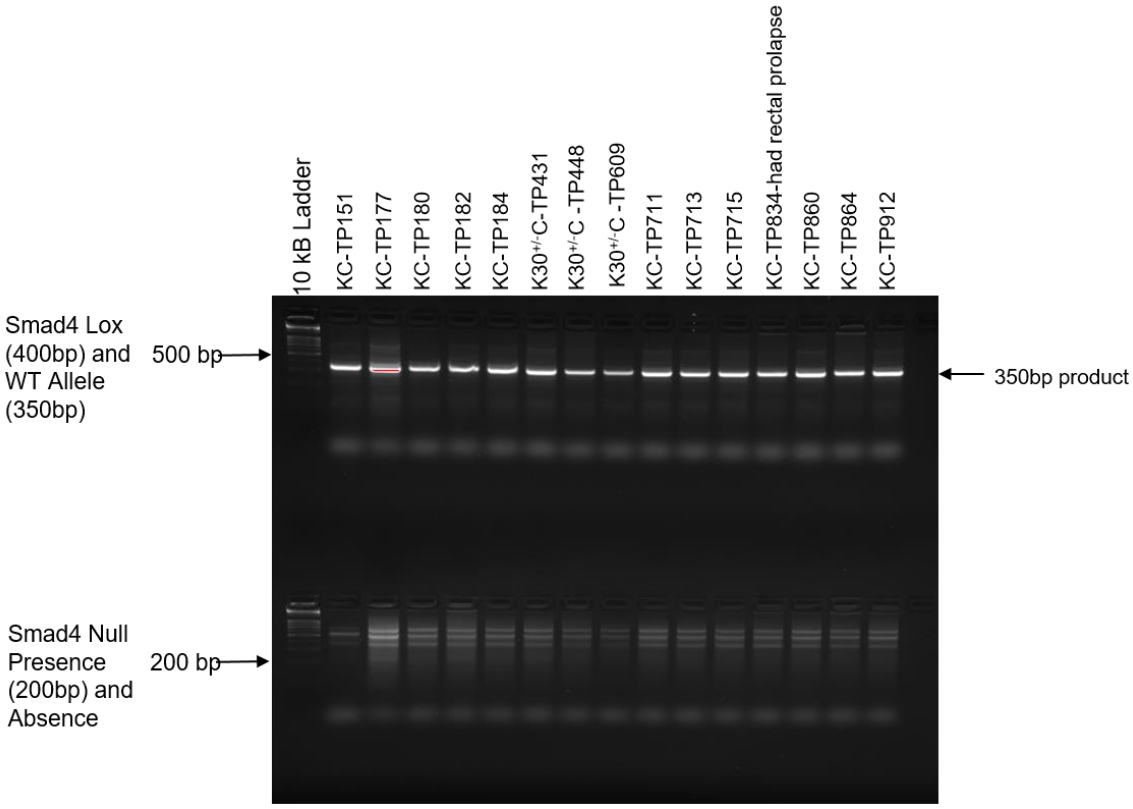

3% gel. To confirm that the KC mice from TP colony were not Smad4-mutant (Bardeesy et al., 2006), DNA was subjected to two genotyping PCR reactions to assess presence or absence of the Smad4 transgene. **Results:** In the top PCR reaction, only a wild-type 350 bp PCR product is present, and no 400bp product in addition, indicating that all of these mice from the TP colony have WT Smad4. In the bottom PCR reaction there is absence of a 200bp PCR product supporting the findings in the top PCR reaction. Tail DNA was used. 4/4/17 IIW.

Syndecan-4

Sdc4 Primer 1: CCCTTCCCTGAAGTGATTGA
Sdc4 Primer 2: GACACTGAGCACACCTCGAA
Neomycin Primer 3: AGACAATCGGCTGCTCTGAT
Neomycin Primer 4: ATACTTTCTCGGCAGGAGCA

2 µL	10X
0.8 µL	$MgCl_2$
0.5 µL	dNTPs
0.1 µL	neo 3
0.1 µL	neo 4
0.1 µL	Taq
15.4 µL	ddH2O
2 µL	10X
1.2 µL	$MgCl_2$

0.5 µL	dNTPs
0.1 µL	Sdc4 Primer 1 (WT)
0.1 µL	Sdc4 Primer 2 (WT)
0.1 µL	Taq
15 µL	ddH2O

Neomycin: 261 bp
Sdc4: 593 bp

APPENDIX B. MURINE PANCREATIC CANCER CELL LINE AUTHENTICATION AND VALIDATION

Cell Line ID	Genotype	Sex	Age (Months)	Date	Passage Number	Generation C57BL/6
TP151-GFP-D7	$K30^{+/+}Ctd^{+/-}$	F	3	2/17/2017	18-1	0
TP151-GFP-F5	$K30^{+/+}Ctd^{+/-}$	F	3	2/17/2017	19-2	0
TP711-C2	$K30^{+/+}C$	M	4	2/17/2017	8	2
TP711-D5	$K30^{+/+}C$	M	4	2/17/2017	8	2
TP715-B6	$K30^{+/+}C$	F	4	2/17/2017	7	2
TP715-E2	$K30^{+/+}C$	F	4	2/17/2017	7	2
TP573-D5	$K30^{+/-}C$	F	5	2/17/2017	28-22	0
TP573-E4	$K30^{+/-}C$	F	5	2/17/2017	30-24-1	0
TP647-E5	$K30^{+/-}C$	F	5	2/17/2017	12	2
TP647-G5	$K30^{+/-}C$	F	5	2/17/2017	12	2
TP852-GFP-C5	$K30^{+/-}C^{+/-}$	M	2	6/1/2017	9	3
TP852-GFP-D4	$K30^{+/-}C^{+/-}$	M	2	6/1/2017	9	3
TP592-1-D7	$K30^{-/-}C$	F	6	2/17/2017	14	0
TP592-3-E4	$K30^{-/-}C$	F	6	2/17/2017	21-1	0
TP735-GFP-E8	$K30^{-/-}C^{+/-}$	M	3	2/17/2017	21-1	0
TP735-GFP-F6	$K30^{-/-}C^{+/-}$	M	3	2/17/2017	21-1	0
TP892-GFP-G2*	†$K30^{-/-}C^{+/-}$	F	1	6/1/2017	9	3
TP892-GFP-G4	†$K30^{-/-}C^{+/-}$	F	1	6/1/2017	9	3

Single cell clones (SSCs) from murine pancreatic cancer cell lines isolated from pancreas tissues (TP mouse colony) were authenticated by IDEXX BioResearch (Columbia, MO, USA). Date of completed authentication report for Single Cell Clone (SCC)-pancreatic cancer cell lines is indicated. IDEXX BioResearch Case # 5352-2017 (Received: 2/10/2017, Completed: 2/17/2017) and 161651-2017 (Received: 5/25/2017, Completed: 6/1/2017) *Incorrect ID on original report (Case # 16151-2017). †Mouse TP892 was produced from two parents with the *Pdx1-Cre* transgene by accident, whether it received two copies has not been validated

APPENDIX C. SUPPLEMENTAL TABLES AND FIGURES

CONTENTS

C1. List of non-tdTomato K30C control mice necropsied, examined and collected

Non-tdTomato (K30C)		
***Tip30*$^{+/+}$**		**Genotype**
TP1043	5-wk-old F	K30+/+
TP1045	5-wk-old M	30+/+C
TP602	2-month-old F	30+/+
TP596	2-month-old M	30+/+
TP632	3-month-old M	30+/+C
TP629	3-month-old M	30+/+C
***Tip30*$^{+/-}$**		**Genotype**
TP463	2-month-old F	30+/-
TP428	4-month-old F	30+/-C
TP437	4-month-old F	K30+/-
TP357	5-month-old M	30+/-C
TP604	5-month-old M	K30+/-
TP520	6-month-old M	30+/-C
***Tip30*$^{-/-}$**		**Genotype**
TP319	1-month-old M	K30-/-
TP353	1-month-old F	30-/-
TP487	1-month-old M	30-/-C
TP816	1-month-old M	30-/-
TP511	2-month-old F	30-/-C
TP513	2-month-old F	K30-/-
TP518	2-month-old M	30-/-C
TP595	3-month-old M	30-/-
TP528	3-month-old F	30-/-C
TP546	3-month-old M	30-/-
TP247	4-month-old M	30-/-
TP301	4-month-old M	30-/-C
TP299	4-month-old M	K30-/-
TP497	4-month-old F	30-/-
TP588	4-month-old M	30-/-
TP593	4-month-old M	30-/-
TP356	5-month-old M	30-/-C
TP635	5-month-old F	30-/-
TP366	6-month-old F	K30-/-
TP488	6-month-old M	K30-/-
TP487	6-month-old M	30-/-
TP832	12-month old F	K30-/-

Controls Collected for TP30 Project (Tissues). TP427 Ear Tag is the mouse that is the first of the new PDX (NCI).

C2. *Tip30* Genotyping, additional mRNA validation of *Tip30* loss, and *LSL-Kras*^{G12D} recombination in K30C pancreata

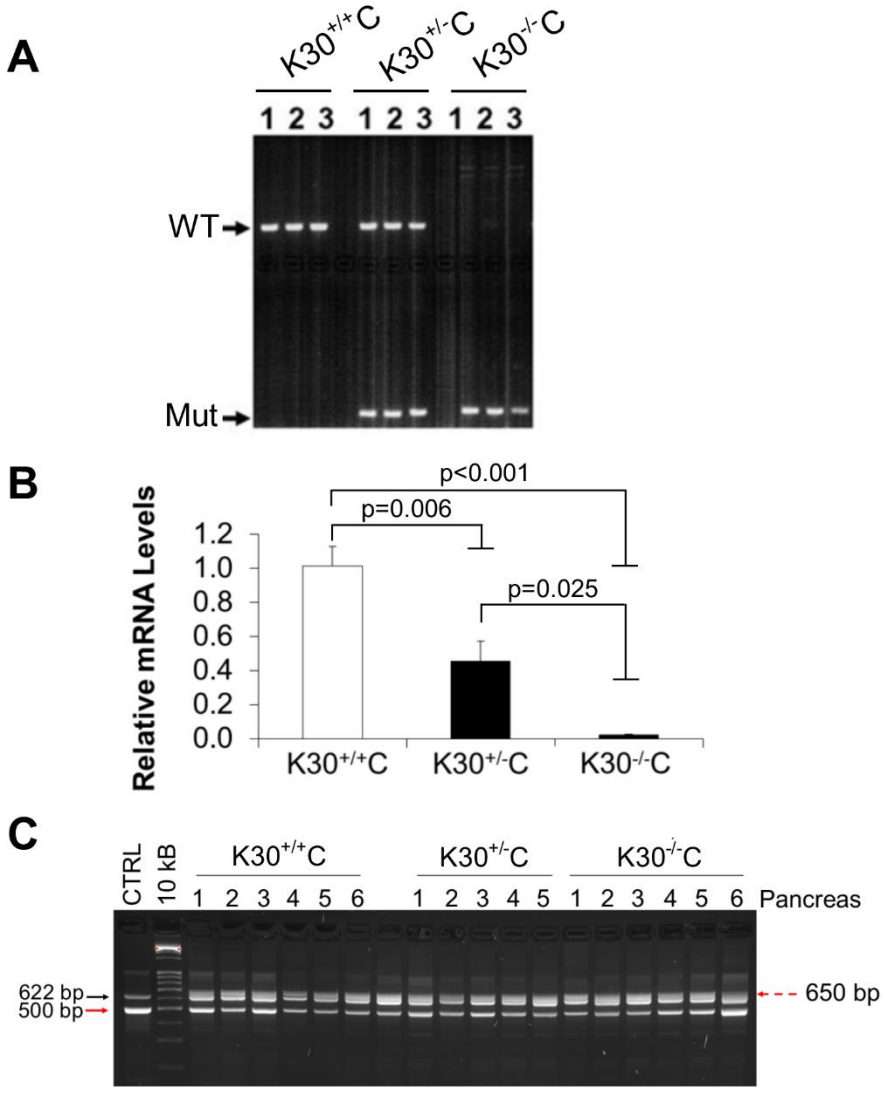

(A) DNA from K30C mouse pancreata was analyzed for wild-type (WT) and *Tip30* mutant (Mut) alleles by genotyping PCR for *Tip30*. n=3 per group is shown. **(B)** mRNA from K30C pancreas tissues was analyzed for Tip30 exon 6 transcript levels, n=4 (2-3 month old KC-TP578, TP579, TP580, TP503; K30$^{+/-}$C-TP431, TP452, TP473, TP448; and K30-/-C-TP526, TP543, TP555, and TP493). One-way ANOVA followed by Tukey post-hoc test was performed and p<0.05 was considered significant. **(C)** Kras G12D Conditional (Jacks, 2017) using 200 ng genomic DNA isolated from pancreata of three-month-old K30$^{+/+}$C, K30$^{+/-}$C, K30$^{-/-}$C mice confirmed recombination and presence of oncogenic *Kras*. CTRL, *Pdx1-Cre*-negative control; 10 kB ladder. Red dashed arrow, recombined 1-*Lox*P-*Kras*^{G12D} allele (650 bp). Black solid arrow, wild-type *Kras* allele (622 bp). Red solid arrow, unrecombined 2-*Lox*P allele (500 bp). K30$^{+/+}$C-TP197, TP228, TP578, TP579, TP580, TP581 mice; K30$^{+/-}$C-TP431, TP452, TP468, TP470, and TP684; K30$^{-/-}$C-TP364, TP336, TP400, TP404, TP526, TP543, and TP555. (Unlabeled sample belongs with last group but was loaded out of place.)

C3. Gross examination of three-month old K30C mice

	Mouse	Sick (Y/N)	Weight (g)	Visible pancreas lesions (Y/N)	Visible Lung Le-sion (Y/N)	Additional Gross Path.
$K30^{+/+}C$	TP197	N	24	N, Large	N	-
	TP228	Scruffy	14	N	N	Face mass
	TP580	N	30	N	N	-
	TP578	N	32	N	N	-
	TP579	N	28	N	N	-
	TP581	N	28	N	N	Eye mass
	TP651	N	30	N	N	-
AVG WEIGHT:						**26 g**
$K30^{+/-}C$	TP223	N	26	N	N	-
	TP431	Scruffy/Dif Breathing	20	N	Y, Enlarged lung	-
	TP452	Hunchy/ Scruffy	31	N	Y, Large lung lesion	-
	TP468*	N	31	N, Large	N	-
	TP470	N	22	N	N	Prolapsed rec-tum, Eye mass
	TP473	N	31	N	N	Large spleen
	TP684	N	26	N	N	-
AVG WEIGHT:						**27 g**
$K30^{-/-}C$	TP279	N	26	N	N	Ear mass
	TP316	N	24	N	N	-
	TP336	Y	10	N	N	-
	TP364	Y, Hunchy	18	N	N	-
	TP400	Y	15	N	N	-
	TP404	Y, Hunchy	17	N	N	-
	TP526	N	22	N	N	-
	TP543	N	30	N	N	-
	TP555	N	28	N	N	-
	TP569	N	25	N	N	-
AVG WEIGHT:						**21.5 g**

Total body mass (Weight) just before necropsy is noted in grams (g).

C4. Strong alcian blue staining of mucinous K30$^{+/-}$C pancreas lesions

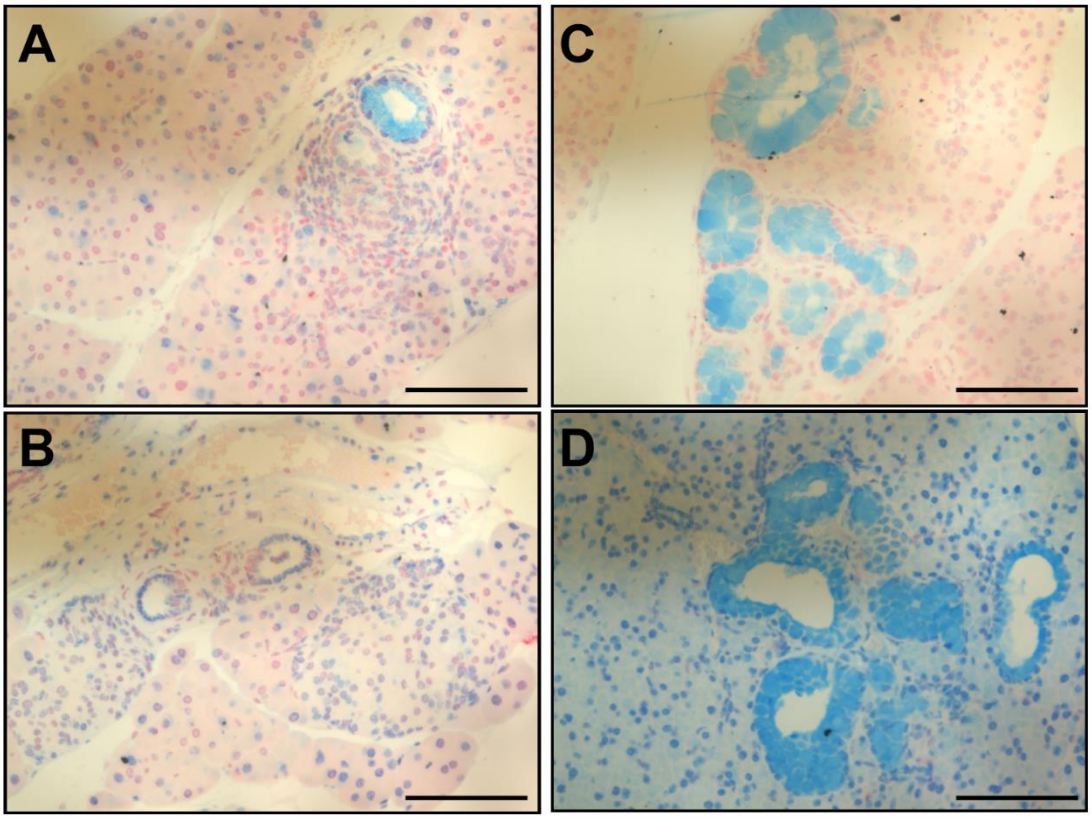

(A-B) K30$^{+/+}$C mice: TP578 (**A**) and TP579 (**B**). **(C-D)** Representative images from two K30$^{+/-}$C mice: TP452 (**C**) TP431 (**D**). Scale bars: 100 μm.

C5. Pulmonary lesion incidence in K30C cohorts

Genotype	Mouse ID	Age (Months)	Sex	Pulmonary Lesion (+)
$K30^{+/+}C$	TP503	2	F	
$K30^{+/+}C$	TP545	2	F	
$K30^{+/+}C$	TP577	3	M	
$K30^{+/+}C$	TP578	3	M	
$K30^{+/+}C$	TP579	3	M	
$K30^{+/+}C$	TP580	3	M	
$K30^{+/+}C$	TP581	3	M	
$K30^{+/+}C$	TP584	4	M	
$K30^{+/+}C$	TP711	4	F	
$K30^{+/+}C$	TP713	4	M	
$K30^{+/+}C$	TP715	4	M	
$K30^{+/+}C$	TP597	5	F	
$K30^{+/+}C$	TP625	5	M	
$K30^{+/+}C$	TP1163	5	F	
$K30^{+/+}C$	TP1053	5	F	
$K30^{+/+}C$	TP652	6	F	
$K30^{+/+}C$	TP1062	6	F	
$K30^{+/-}C$	TP576	1.25	M	+
$K30^{+/-}C$	TP440	2	F	
$K30^{+/-}C$	TP448	2	F	+
$K30^{+/-}C$	TP455	2	F	
$K30^{+/-}C$	TP476	2	M	
$K30^{+/-}C$	TP682	2	M	+
$K30^{+/-}C$	TP718	2	M	
$K30^{+/-}C$	TP431	3	M	+
$K30^{+/-}C$	TP452	3	M	+
$K30^{+/-}C$	TP468*	3	M	
$K30^{+/-}C$	TP470	3	F	

K30$^{+/-}$C	TP473	3	M	
K30$^{+/-}$C	TP684	3	M	
K30$^{+/-}$C	TP775	3	M	
K30$^{+/-}$C	TP477	4	F	±
K30$^{+/-}$C	TP478	4	F	
K30$^{+/-}$C	TP498	4	F	
K30$^{+/-}$C	TP500	4	F	
K30$^{+/-}$C	TP609^	4	F	±
K30$^{+/-}$C	TP622*	4	F	±
K30$^{+/-}$C	TP627	4	F	±
K30$^{+/-}$C	TP630	4	M	+
K30$^{+/-}$C	TP544	5	F	
K30$^{+/-}$C	TP573	5	F	
K30$^{+/-}$C	TP647	5	F	±
K30$^{+/-}$C	TP686	5	F	
K30$^{+/-}$C	TP752	5	M	±
K30$^{+/-}$C	TP1061	5	F	
K30$^{+/-}$C	TP623	6	F	
K30$^{+/-}$C	TP1004	8	M	±
K30$^{+/-}$C	TP851*	10	F	
K30$^{+/-}$Ctd$^{+/-}$	TP852	2	M	±
K30$^{+/-}$Ctd$^{+/-}$	TP728	3	M	±
K30$^{-/-}$C	TP843	1	F	
K30$^{-/-}$C	TP443	2	F	
K30$^{-/-}$C	TP493	2	M	
K30$^{-/-}$C	TP516	2	M	
K30$^{-/-}$C	TP519	2	M	
K30$^{-/-}$C	TP526	3	M	
K30$^{-/-}$C	TP543	3	M	
K30$^{-/-}$C	TP555	3	M	+
K30$^{-/-}$C	TP569	3	F	
K30$^{-/-}$C	TP716	4	F	

K30$^{-/-}$C	TP717	4	F	
K30$^{-/-}$C	TP587	4	M	
K30$^{-/-}$C	TP590	4	M	
K30$^{-/-}$C	TP634	5	M	±
K30$^{-/-}$C	TP592	6	F	
K30$^{-/-}$C	TP812	8	F	
K30$^{-/-}$C	TP880	8	F	
K30$^{-/-}$C	TP813	9	F	
K30$^{-/-}$C	TP889	9	M	
K30$^{-/-}$C	TP853	11	M	

±, subjects that were imaged.

C6. *Tip30*-deficiency induces early onset pulmonary abnormalities and lesions in K30C mice

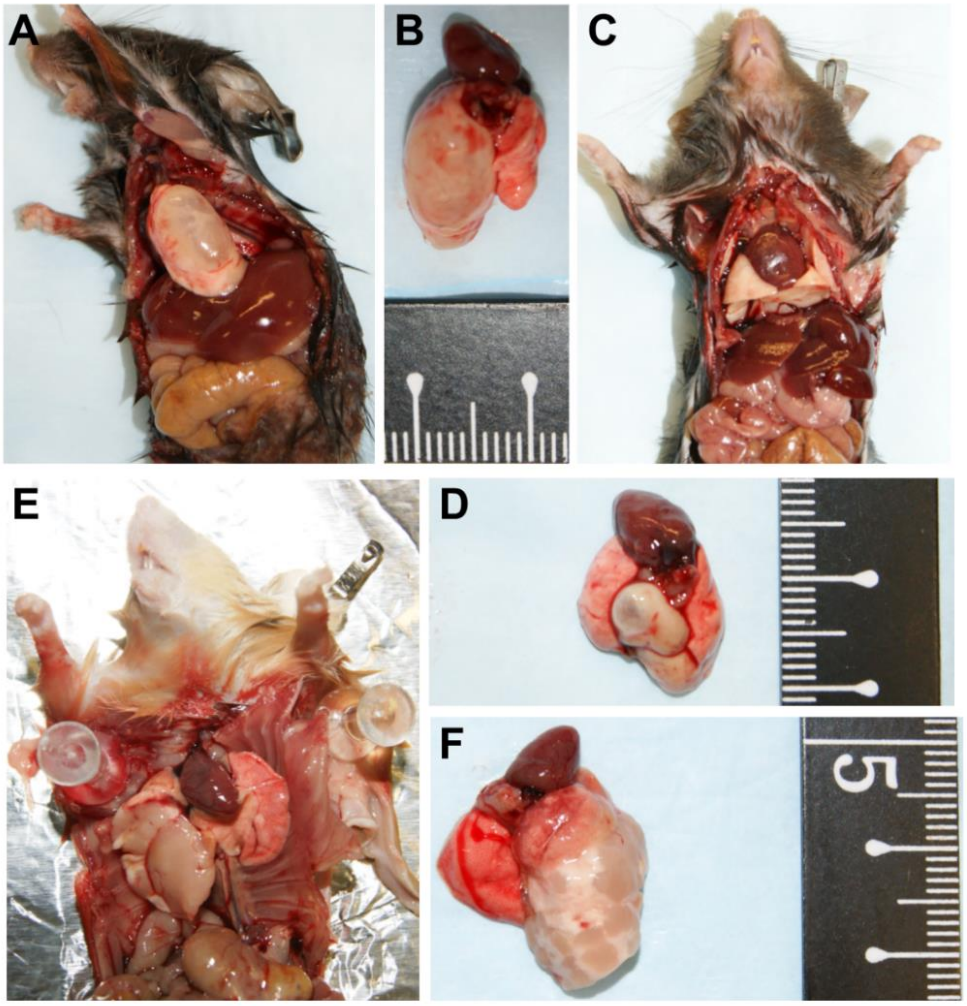

(A-B) K30$^{+/-}$C mouse, TP682, lungs *in situ*. **(B)** *Ex vivo*. (**C-D)** Additional K30$^{+/-}$C mice *in situ* and *ex vivo*. **(C)** TP752 *ex vivo*. **(D)**TP647 *in situ*. **(E)** One of two K30$^{-/-}$C to present with a pulmonary abnormality. TP634 *in situ*. **(F)** *Ex vivo*.

C7(A). Fluorescence-Activated Cell Sorting (FACS) of *Tip30*-wild-type pancreatic cancer cells

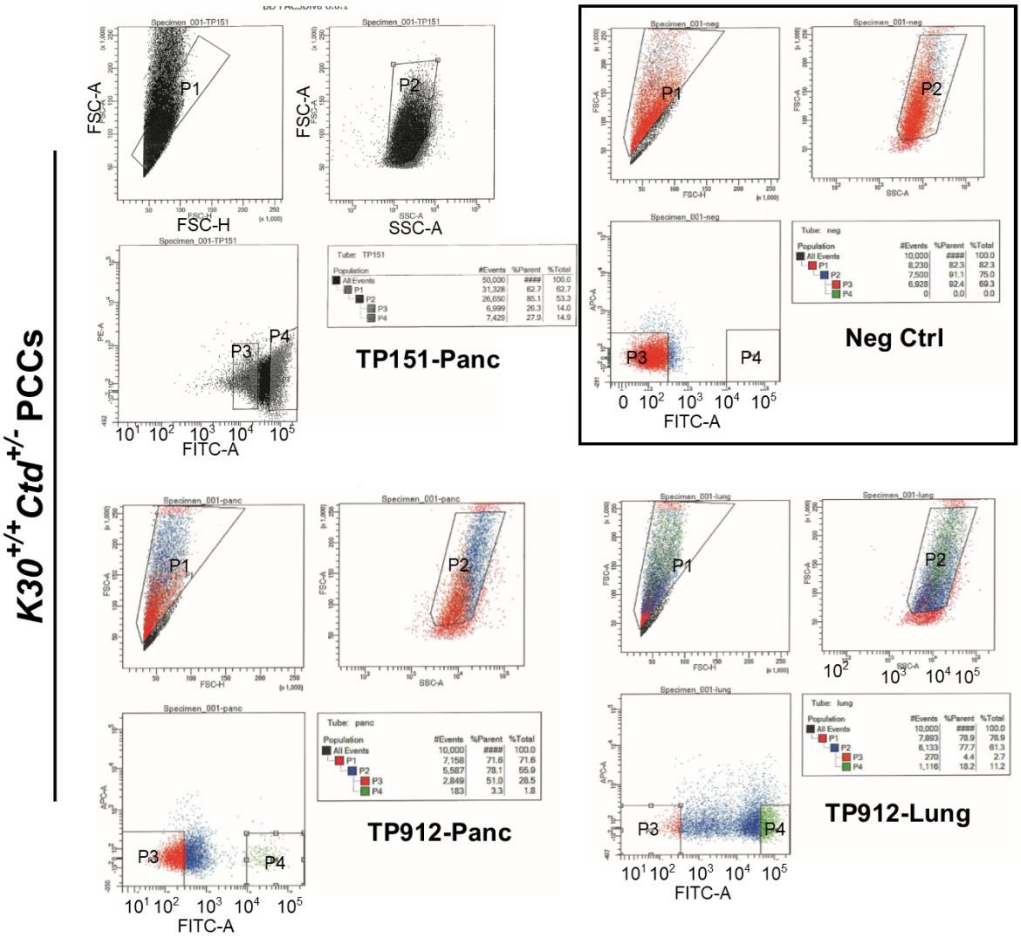

P4 is the population of cells that was collected to establish the GFP-positive pancreatic cancer cells (PCC) lines. P3 was considered to be a GFP-negative population. Gating was to the negative control (a non td+/- cell line).

C7(B). Fluorescence-Activated Cell Sorting (FACS) of *Tip30*-deficient pancreatic cancer cells (PCCs)

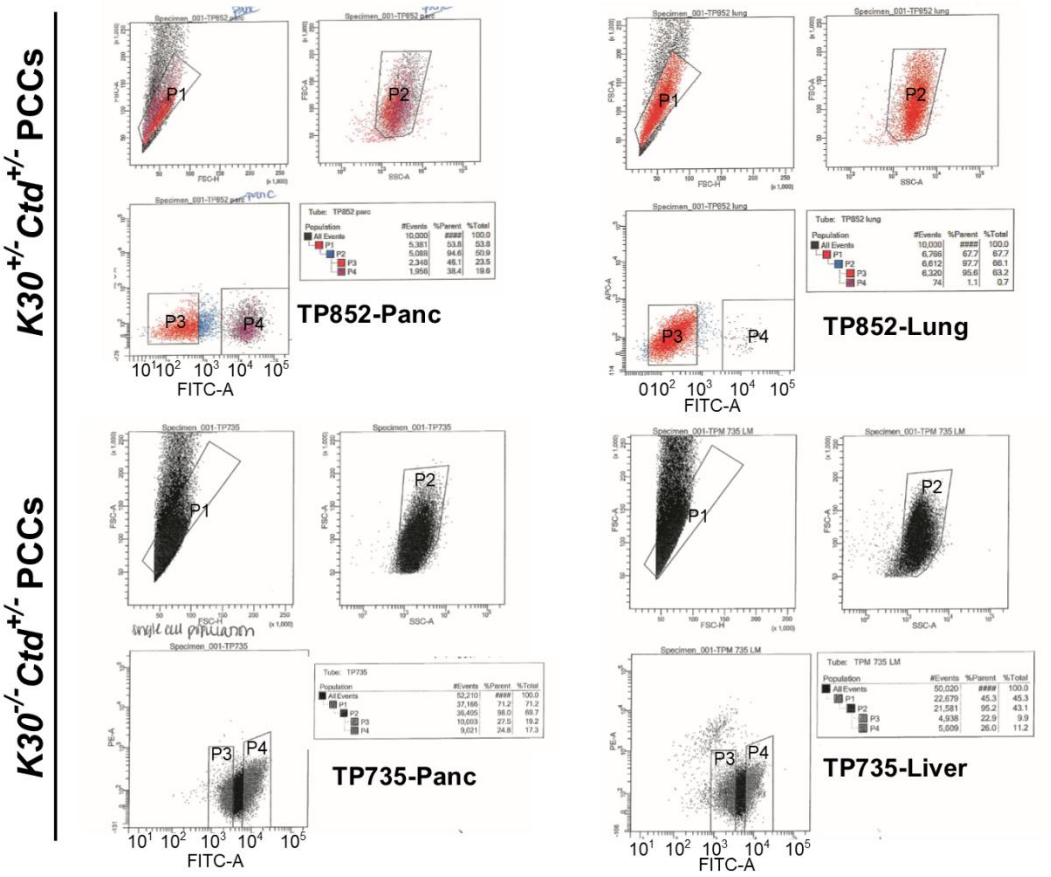

P4 is the population of cells that was collected to establish GFP-positive pancreatic cancer cells (PCC) lines. P3 is considered to be a GFP-negative population. Gating was to the negative control (a non td+/- cell line.

C8. Genomic DNA from K30$^{+/-}$C mouse pancreas and pulmonary lesion tissues is 1-*Lox*P-*Kras*^{G12D}-PCC positive

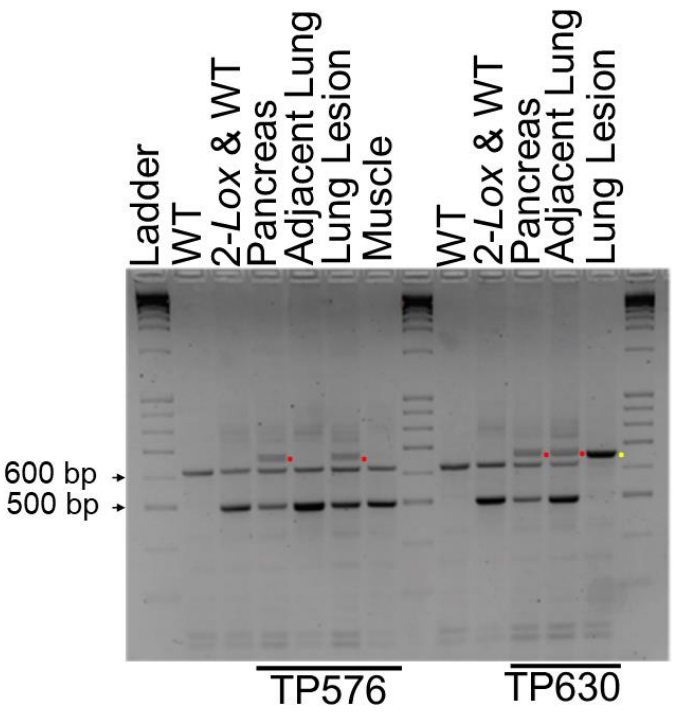

Recombined 1-*Lox-Kras*^{G12D} (red dot) is shown for both pancreas and lung lesion biopsies but not the adjacent normal lung tissue in five-week-old mouse ID TP576. Kras G12D Conditional PCR method (Jacks, 2017). PCR products were run with increased gel electrophoresis separation. DNA from the muscle tissue was negative for recombination. Mouse ID TP630 (3.5 months of age) has recombined 1-*Lox-Kras*^{G12D} (red dot) in the pancreas and evidence of DNA that tests positive for full recombination (yellow dot) in its pulmonary lesion. The adjacent normal lung tissue, although appeared normal by gross observation, was positive for both recombined (1-*LoxP-Kras*^{G12D}) and unrecombined (2-*LoxP-Kras*^{G12D}). This suggested that this tissue biopsy consisted of both 1-*LoxP-Kras*^{G12D} PCCs and lung cells. *Pdx1*-Cre results in stochastic expression of Cre in the pancreas epithelium, hence lack of full recombination for those tissues. First two columns under each mouse are controls, the first being a negative control for both the *LSL-Kras*^{G12D} transgene and the *Pdx1*-Cre transgene, DNA from pancreas tissue of mouse ID TP418 (WT); and the second a K30$^{+/+}$C control (however this sampling of pancreas tissue for this mouse (TP228) appears not to be positive for *LSL-Kras*^{G12D} recombination, although originally genotyped as a K30$^{+/+}$C mice at weaning) is positive for both the *LSL-Kras*^{G12D} and the *Pdx1*-Cre transgenes (2-*Lox*) as well as wild-type *Kras* (WT). Ladder, 10 kB.

C9. Micrometastatic seeding detected in two-month-old K30$^{+/-}$Ctd$^{+/-}$-TP852 pulmonary tissue

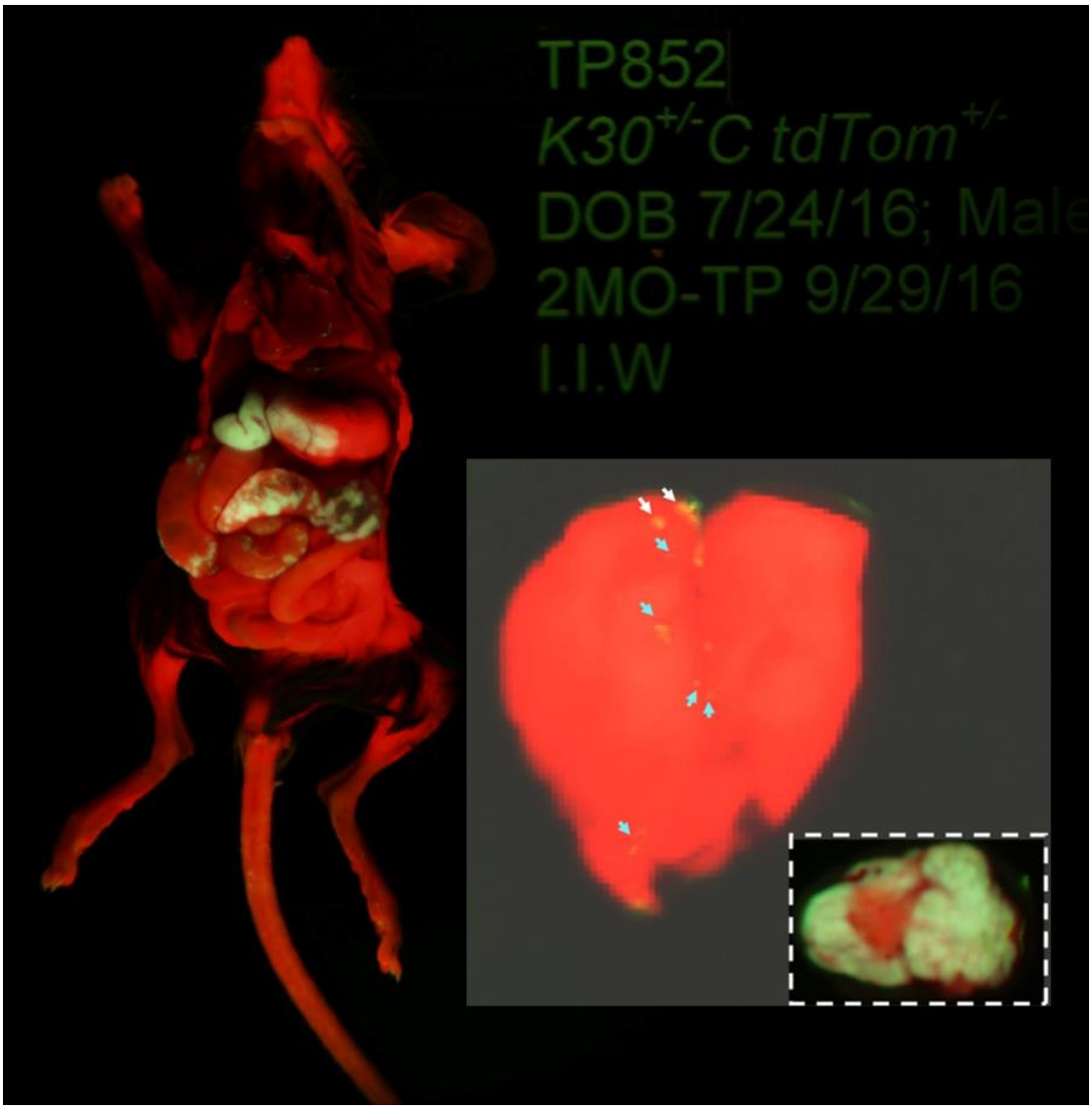

Frank pancreatic tumor was not grossly observed (inset, unaltered). Lung tissue was imaged using RFP and GFP filters and a fluorescent light box imaging resource. Lung image has been brightened and contrasted both by 70% to better allow for visualization of observed micrometastatic seeding at necropsy (white arrows). Upon brightening and contrasting the captured image one can also see additional sites of potential metastatic seeding (cyan arrows).

C10. Detectable GFP positivity in pancreas and small intestine of $K30^{+/+}C$ mice using RFP/GFP fluorescent light box imaging

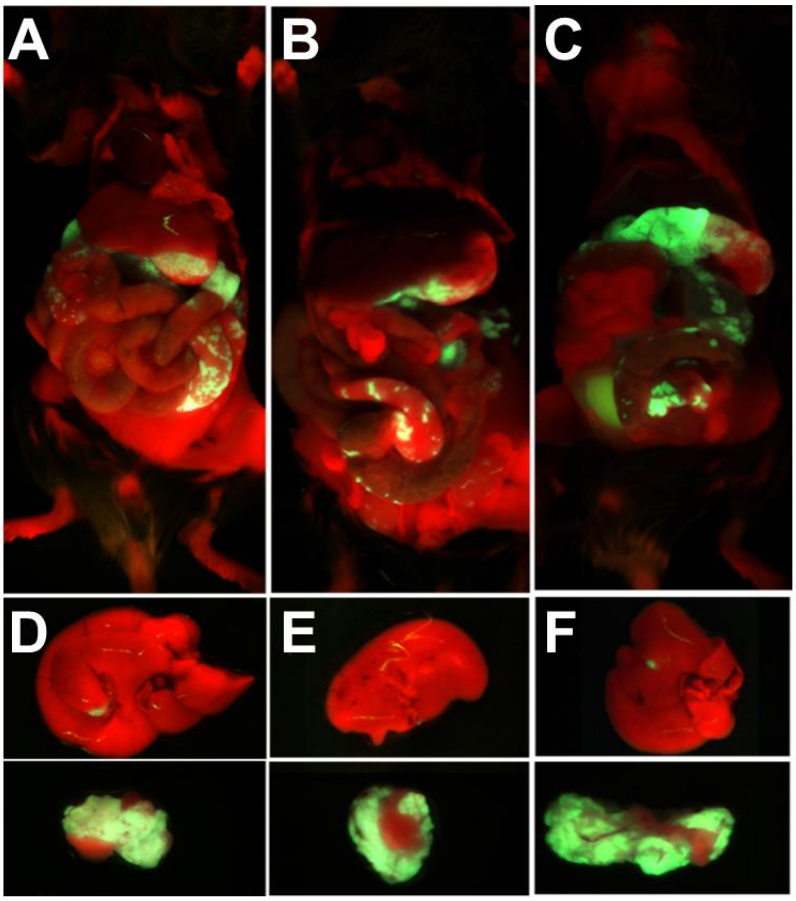

(A) TP834 (Generation 0, male, 2 months). **(B)** TP912 (Generation 3, male, 3 months). **(C)** TP957 (Generation 4, male, 3 months). **D-F** Liver (top row) and pancreas (bottom row) tissues from corresponding mice in A-C, TP834, TP912, and TP957, respectively. Generation reflections number of backcrosses to the C57BL/6 background.

C11. An 11-month old K30$^{-/-}$Ctd$^{+/-}$ mouse with GFP positive micrometastatic seeding in the intestines and liver

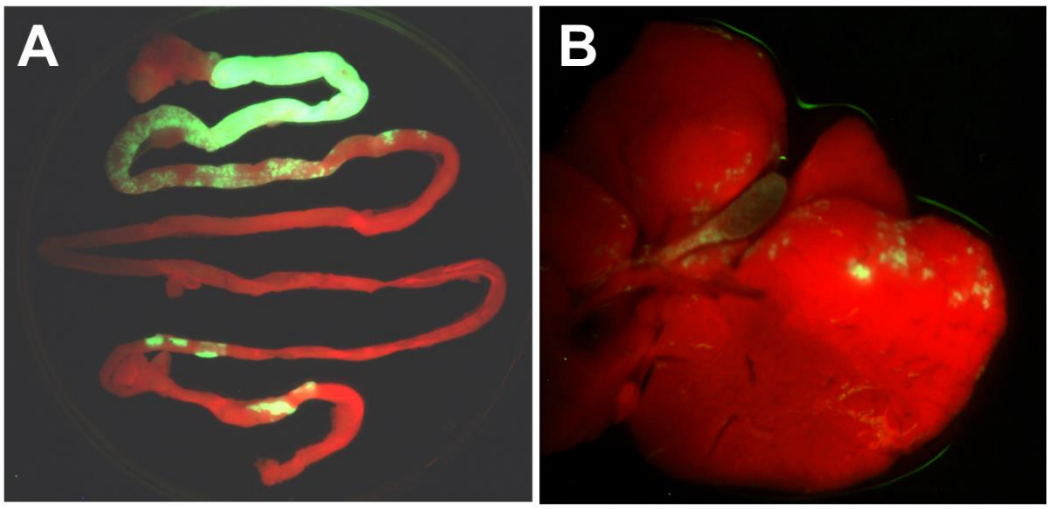

(A) *Pdx1-Cre* activity in the intestines. **(B)** Micrometastatic seeding in the liver. Mouse ID is TP746.

REFERENCES

Adamska, A., Domenichini, A., Falasca, M. (2017). Pancreatic ductal adenocarcinoma: current and evolving therapies. *Int J Mol Sci* 18(7), 1338.

Ahrendt, S. A., and Pitt, H. A. (2002). Surgical management of pancreatic cancer. *Oncology* (Williston Park) 16, 725-734; discussion 734, 736-728, 740, 743.

Aguirre, A.J., Bardeesy, N., Sinha, M., Lopez, L., Tuveson, D.A., Horner, J., Redston, M.S., Depinho, R.A. (2003). Activated Kras and *Ink4a/Arf* deficiency cooperate to produce metastatic pancreatic ductal adenocarcinoma. *Genes Dev* 17(24), 3112-3126.

Al-Hawary, M. M., Francis, I. R., Chari, S. T., Fishman, E. K., Hough, D. M., Lu, D. S., Macari, M., Megibow, A. J., Miller, F. H., Mortele, K. J., et al. (2014). Pancreatic ductal adenocarcinoma radiology reporting template: consensus statement of the Society of Abdominal Radiology and the American Pancreatic Association. *Gastroenterology* 146, 291-304.e291.

Almoguera, C., Shibata, D., Forrester, K., Martin, J., Arnheim, N., and Perucho, M. (1988). Most human carcinomas of the exocrine pancreas contain mutant c-K-ras genes. *Cell* 53, 549-554.

Alsamarrai, A., Das, S. L., Windsor, J. A., and Petrov, M. S. (2014). Factors that affect risk for pancreatic disease in the general population: A systematic review and meta-analysis of prospective cohort studies. *Clin Gastroenterol Hepatol* 12, 1635-1644.e1635; quiz e1103.

Alteri, R., Kalidas, M., and Yadao, L. (2017, December 18). Pancreatic Cancer Stages. Retrieved from https://www.cancer.org/cancer/pancreatic-cancer/detection-diagnosis-staging/staging.html on October 18, 2018.

Amaravadi, R. and Thompson, C. B. (2005). The survival kinases Akt and Pim as potential pharmacological targets. *J Clin Invest* 115(10), 2618-2624.

American Cancer Society. Cancer Facts & Figures 2017. Atlanta: American Cancer Society; 2017. Retrieved from https://www.cancer.org/content/dam/cancer-org/research/cancer-facts-and-statistics/annual-cancer-facts-and-figures/2017/cancer-facts-and-figures-2017.pdf on October 18, 2018.

American Cancer Society. Cancer Facts & Figures 2018. Atlanta: American Cancer Society; 2018. Retrieved from https://www.cancer.org/content/dam/cancer-org/research/cancer-facts-and-statistics/annual-cancer-facts-and-figures/2018/cancer-facts-and-figures-2018.pdf on October 18, 2018.

Andersen, D. K., Korc, M., Petersen, G. M., Eibl, G., Li, D., Rickels, M. R., Chari, S. T., and Abbruzzese, J. L. (2017). Diabetes, Pancreatogenic Diabetes, and Pancreatic Cancer. *Diabetes* 66, 1103-1110.

Ankeny, J. S., Court, C. M., Hou, S., Li, Q., Song, M., Wu, D., Chen, J. F., Lee, T., Lin, M., Sho, S., et al. (2016). Circulating tumour cells as a biomarker for diagnosis and staging in pancreatic cancer. *Br J Cancer* 114, 1367-1375.

Ardito, C.A., Gruner, B.M., Takeuchi, K.K., Lubeseder-Martellato, C. et al. (2013). EGF Receptor is required for KRAS-induced pancreatic tumorigenesis. *Cancer Cell* 22(3), 304-317.

Arnoult, D., Parone, P., Martinou, J. C., Antonsson, B., Estaquier, J., Ameisen, J. C. (2002). Mitochondrial release of apoptosis-inducing factor occurs downstream of cytochrome c release in response to several proapoptotic stimuli. *J Cell Biol* 159(6), 923-929.

Babu, D. A., Deering, T. G., and Mirmira, R. G. (2007). A feat of metabolic proportions: Pdx1 orchestrates islet development and function in the maintenance of glucose homeostasis. *Mol Genet Metab* 92(1-2), 43-55.

Bachem, M. G., Schünemann, M., Ramadani, M., Siech, M., Beger, H., Buck, A., Zhou, S., Schmid-Kotsas, A., and Adler, G. (2005). Pancreatic carcinoma cells induce fibrosis by stimulating proliferation and matrix synthesis of stellate cells. *Gastroenterology* 128, 907-921.

Baker, M. E. (1999). TIP30, a cofactor for HIV-1 Tat-activated transcription, is homologous to short-chain dehydrogenases/reductases. *Curr Biol* 9, R471.

Baker, M. E., Yan, L., and Pear, M. R. (2000). Three-dimensional model of human TIP30, a coactivator for HIV-1 Tat-activated transcription, and CC3, a protein associated with metastasis suppression. *Cell Mol Life Sci* 57, 851-858.

Bang, U. C., Benfield, T., Hyldstrup, L., Bendtsen, F., and Beck Jensen, J. E. (2014). Mortality, cancer, and comorbidities associated with chronic pancreatitis: A Danish nationwide matched-cohort study. *Gastroenterology* 146, 989-994.

Bao, L., Al-Assar, O., Drynan, L. F., Arends, M. J., Tyers, P., Barker, R. A., and Rabbitts, T. H. (2017). A non-cell autonomous mouse model of CNS haemangioblastoma mediated by mutant KRAS. *Scientific Reports* 7, 44899.

Bardeesy, N. and DePinho, R.A. (2002). Pancreatic cancer biology and genetics. *Nature Rev Cancer* 2, 897-909.

Bardeesy, N., Agugirre, A.J., Chu, G.C., Cheng, K., Lopez, L.V., Hezel, A.F., Feng, B., Brennan, C., Weissleder, R., Mahmood, U., Hanahan, D., Redston, M.S., Chin, L., DePinho, R.A. (2006a). Both $p16^{INK4a}$ and the p19Arf-p53 pathway constrain progression of pancreatic adenocarcinoma in the mouse. *Proc Natl Acad Sci U S A* 103(15), 5947-5952.

Bardeesy, N. Cheng, K., Berger, J.H., Chu, G.C., Pahler, J., Olson, P., Hezel, A.F., Horner, J., Lauwers, G.Y., Hanahan, D., and DePhino, R.A. (2006b). Smad4 is dispensable for normal pancreas development yet critical in progression and tumor biology of pancreas cancer. *Genes Dev* 20, 31130-3146.

Barton, C. M., Hall, P. A., Hughes, C. M., Gullick, W. J., Lemoine, N. R. (1991). Transforming growth factor alpha and epidermal growth factor in human pancreatic cancer. *J Pathol* 162(2), 111-116.

Begley, D. A., Krupke, D. M., Neuhauser, S. B., Richardson, J. E., Bult, C. J., Eppig, J. T., and Sundberg, J. P. (2012). The Mouse Tumor Biology Database (MTB): a central electronic resource for locating and integrating mouse tumor pathology data. *Vet Pathol* 49, 218-223. http://tumor.informatics.jax.org/mtbwi/tumorFrequencyGrid.do;jsessionid=EFDBF4B70D60BCAD87D981CAAE82E84E, accessed on May 31, 2018.

Begley, D. A., Krupke, D. M., Neuhauser, S. B., Richardson, J. E., Bult, C. J., Eppig, J. T., and Sundberg, J. P. (2012). The Mouse Tumor Biology Database (MTB): a central electronic resource for locating and integrating mouse tumor pathology data. *Vet Pathol* 49, 218-223. http://tumor.informatics.jax.org/mtbwi/live/www/html/Lymphoma.html, accessed on November 14, 2018.

Ben-David, U., Beroukhim, R., and Golub, T. R. (2018). Genomic evolution of cancer models: perils and opportunities. *Nature Rev Cancer* 19, 97-109.

Berghe, T.V., Hulpiau, P., Martens, L., Vandenbroucke, R.E., Wonterghem, E.V., Perry, S.W., Bruggeman, I., Divert, T., Choi, S.M., Vuylsteke, M., Shestopalov, V.I., Libert, C., Vandenabeele, P. (2015). Passenger mutations confound interpretation of all genetically modified congenic mice. *Immunity* 43, 200-209.

Berman, D.M., Karhadkar, S.S., Maitra, A., et al. (2003). Widespread requirement for hedgehog ligand stimulation in growth of digestive tract tumors. *Nature* 425, 846-851.

Beroukhim, R., Getz, G., Nghiemphu, L., Barretina, J., Hsueh, T., Linhart, D., Vivanco, I., Lee, J. C., Huang, J. H., Alexander, S., et al. (2007). Assessing the significance of chromosomal aberrations in cancer: methodology and application to glioma. *Proc Natl Acad Sci U S A* 104, 20007-20012.

Bloomston, M., Frankel, W. L., Petrocca, F., Volinia, S., Alder, H., Hagan, J. P., Liu, C. G., Bhatt, D., Taccioli, C., and Croce, C. M. (2007). MicroRNA expression patterns to differentiate pancreatic adenocarcinoma from normal pancreas and chronic pancreatitis. *JAMA* 297, 1901-1908.

Borowicz, S., Van Scoyk, M., Avasarala, S., et al. (2014). The soft agar colony formation assay. *J Vis Exp*. 92:e51998.

Brembeck, F. H., Schreiber, F. S., Deramaudt, T. B., Craig, L., Rhoades, B., Swain, G., Grippo, P., Stoffers, D. A., Silberg, D. G., Rustgi, A., K. (2003). The mutant K-ras oncogene causes pancreatic periductal lymphocytic infiltration and gastric mucous neck cell hyperplasia in transgenic mice. *Cancer Res 63(9), 2005-2009.*

Brennecke, J., Stark, A., Russell, R. B., and Cohen, S. M. (2005). Principles of microRNA-target recognition. *PLoS Biol* 3, e85.

Brosens, L. A., Hackeng, W. M., Offerhaus, G. J., Hruban, R. H., and Wood, L. D. (2015). Pancreatic adenocarcinoma pathology: changing "landscape". *J Gastrointest Oncol* 6, 358-374.

Bu, F., Liu, X., Li, J., Chen, S., Tong, X., Ma, C., Mao, H., Pan, F., Li, X., Chen, B., Xu, L., Li, E., Kou, G., Han, J., Guo, S., Zhao, J., and Guo, Y. (2015) TGF-β1 induces epigenetic silence of TIP30 to promote tumor metastasis in esophageal carcinoma. *Oncotarget* 6(4), 2120-2133.

Burnet, N. G., et al. (2004). Defining the tumour and target volumes for radiotherapy. *Cancer Imaging* 4(2), 153-161.

Burris, H.A. III, Moore, M.J., Andersen, J., et al. (1997). Improvements in survival and clinical benefit with gemcitabine as first-line therapy for patients with advanced pancreas cancer: a randomized trial. *J Clin Oncol* 15, 2403-2413.

Carrière, C., Seeley, E. S., Goetze, T., Longnecker, D. S., Korc, M. (2007). The Nestin progenitor lineage is the compartment of origin for pancreatic intraepithelial neoplasia. *Proc Natl Acad Sci U S A* 104, 4437-4442.

Carrière, C., Gore, A. J., Norris, A. M., Gunn, J. R., Young, A. L., Longnecker, D. S., Korc, M. (2011). *Gastroenterology* 141(3), 1091-1101.

Celus, W., Di Conza, G., Oliveira, A. I., Ehling, M., Costa, B. M., Wenes, M., and Mazzone, M. (2017). Loss of Caveolin-1 in Metastasis-Associated Macrophages Drives Lung Metastatic Growth through Increased Angiogenesis. *Cell Rep* 21, 2842-2854.

Cerami, E., Gao, J., Dogrusoz, U., Gross, B. E., Onur Sumer, S., Arman Aksoy, B., Jacobsen, A., Byrne, C. J., Heuer, M. L., Larrson, E., Antipin, Y., Reva, B., Goldberg, A. P., Sander, C., Schultz. (2012). The cBio cancer genomics portal: an open platform for exploring multidimensional cancer genomics data. *Cancer Discovery* 2(5), 401-404.

Ceranowicz, P., Cieszkowski, J., Warzecha, Z., Kuśnierz-Cabala, B., and Dembiński, A. (2015). The beginnings of pancreatology as a field of experimental and clinical medicine. *Biomed Res Int* 2015, 128095.

Chaffer, C. L., and Weinberg, R. A. (2011). A perspective on cancer cell metastasis. *Science* 331, 1559-1564.

Chai, G., Liu, N., Ma, J., Li, H., Oblinger, J. L., Prahalad, A. K., Gong, M., Long-Sheng, C., Wallace, M., Muir, D., Guhu, A., Phipps, R. J., Hock, J., and Yu, X. (2010). MicroRNA-10b regulates tumorigenesis in neurofibromatosis type 1. *Cancer Science* 101(9), 1997-2004.

Chambers, A. F., Groom, A. C., MacDonald, I. C. (2002). Dissemination and growth of cancer cells in metastatic sites. *Nat Rev Cancer* 2, 563-572.

Chen, F., Zhuang, X., Lin, L., Yu, P., Wang, Y., Shi, Y., Hu, G., and Sun, Y. (2015). New horizons in tumor microenvironment biology: challenges and opportunities. *BMC Med* 13, 45.

Chen, X., Cao, X., Dong, W., Luo, S., Suo, Z., and Jin, Y. (2010). Expression of TIP30 tumor suppressor gene is down-regulated in human colorectal carcinoma. *Dig Dis Sci* 55, 2219-2226.

Chen, Y., Gao, S. G., Chen, J. M., Wang, G. P., Wang, Z. F., Zhou, B., Jin, C. H., Yang, Y. T., and Feng, X. S. (2015). Serum CA242, CA199, CA125, CEA, and TSGF are Biomarkers for the Efficacy and Prognosis of Cryoablation in Pancreatic Cancer Patients. *Cell Biochem Biophys* 71, 1287-1291.

Chen, V. and Shtivelman, E. (2010). CC3/TIP30 regulates metabolic adaptation of tumor cells to glucose limitation. *Cell Cycle* 9(24), 4941-4953.

Chou, A., Waddell, N., Cowley, M. J., Gill, A. J., Chang, D. K., Patch, A.-M., Nones, K., Wu, J., Pinese, M., Johns, A. L., Miller, D. K., Kassahn, K. S., Nagrial, A. M., Wasan, H., Goldstein, D., Toon, C. W., Chin, V., Chantrill, L., Humphris, J., Mead, Scott Mead, R., Rooman, I., Samra, J. S., Pajic, M., Musgrove, E. A., Pearson, J. V., Morey, A. L., Grimmond, S. M., and Biankin, A. V. (2013). Clinical and molecular characterization of *HER2*amplified-pancreatic cancer. *Genome Medicine* 5(78), 1-11.

Chung, W. J., Daemen, A., Cheng, J. H., Long, J. E., Cooper, J. E., Wang, B. E., Tran, C., Singh, M., Gnad, F., Modrusan, Z., et al. (2017). Mutant genetically

engineered mouse models of human cancers are genomically heterogeneous. *Proc Natl Acad Sci U S A* 114, E10947-E10955.

Clark, C. E., Hingorani, S. R., Mick, R., Combs, C., Tuveson, D. A., Vonderheide, R. H. (2007). Dynamics of the immune reaction to pancreatic cancer from inception to invasion. *Cancer Res* 67(19), 9518-9527.

Collins, M. A., Bednar, F., Zhang, Y., Brisset, J. C., Galbán, S., Galbán, C. J., Rakshit, S., Flannagan, K. S., Adsay, N. V., and Pasca di Magliano, M. (2012). Oncogenic Kras is required for both the initiation and maintenance of pancreatic cancer in mice. *J Clin Invest* 122, 639-653.

Conroy, T., Desseigne, F., Ychou, M., Bouché, O., Guimbaud, R., Bécouarn, Y., Adenis, A., Raoul, J. L., Gourgou-Bourgade, S., de la Fouchardière, C., et al. (2011). FOLFIRINOX versus gemcitabine for metastatic pancreatic cancer. *N Engl J Med* 364, 1817-1825.

Costa-Silva, Aielo, N. M, Ocean, A. J., Singh, S., Zhang, H., Thakur, B. K., Becker, A., Hoshino, A., Mark, M.T., Molina, H., Xiang, J., Zhang, T., Theilen, T. M., García-Santos, G., Williams, C., Ararso, Y., Huang, Y., Rodrigues, G., Shen, T. L., Labori, K. J., Lothe, I. M., Kure, E. H., Hernandez, J., Doussot, A., Ebbesen, S. H., Grandgenette, P. M., Hollingsworth, M. A., Jain, M., Mallya, K., Batra, S. K., Jarnagin, W. R., Schwartz, R. E., Matei, I., Peinado, H., Stanger, B. Z., Bromberg, J., Lyden, D. C. (2015). Pancreatic cancer exosomes initiate pre-metastatic niche formation in the liver. *Nat Cell Biol* 17(6), 816-826.

Coté, G. A., Smith, J., Sherman, S., and Kelly, K. (2013). Technologies for imaging the normal and diseased pancreas. *Gastroenterology* 144, 1262-1271.e1261.

Court, C. M., Ankeny, J. S., Sho, S., Winograd, P., Hou, S., Song, M., Wainberg, Z. A., Girgis, M. D., Graeber, T. G., Agopian, V. G., et al. (2018). Circulating Tumor Cells Predict Occult Metastatic Disease and Prognosis in Pancreatic Cancer. *Ann Surg Oncol* 25(4), 1000-1008.

Couvelard, A., O'Toole, D., Leek, R., Turley, H., Sauvanet, A., Degott, C., Ruszniewski, P., Belghiti, J., Harris, A. L., Gatter, K., and Pezzella, F. (2005). Expression of hypoxia-inducible factors is correlated with the presence of a fibrotic focus and angiogenesis in pancreatic ductal adenocarcinomas. *Histopathology* 46, 668-676.

Craven, K. E., Gore, J., Wilson, J. L., and Korc, M. (2016). Angiogenic gene signature in human pancreatic cancer correlates with TGF-beta and inflammatory transcriptomes. *Oncotarget* 7, 323-341.

Crawford, H. C., Scoggins, C. R., Washington, M. K., Matrisian, L. M., Leach, S. D. (2002). Matrix metalloproteinase-7 is expressed by pancreatic cancer precursors and regulates acinar-to-ductal metaplasia in exocrine pancreas. *J Clin Invest* 109(11), 1437-1444.

Crawford, H. C., Pasca di Magliano, M., Banerjee, S. (2019). Signaling networks that control cellular plasticity in pancreatic tumorigenesis, progression, and metastasis. *Gastroenterology* 1-12.

Dagogo-Jack, I. and Shaw, A. T. (2018). Tumour heterogeneity and resitance to cancer therapies. *Nat Rev Clin Oncol* 15, 81-94.

De Wilde, R. F., Hurban, R. H., Maitra, A., and Offerhaus, G. J. A. (2012). Reporting precursors to invasive pancreatic cancer: pancreatic intraepithelial neoplasia, intraductal neoplasms and mucinous cystic neoplasm. *Diagnositic Histopathology* 18(1), 17-30.

diSibio, G. and French, S.W. (2008). Metastatic Patterns of Cancers. *Arch Pathol Lab Med* 132, 931-939.

Dong, W., Shen, R., and Cheng, S. (2014). Reduction of TIP30 in esophageal squamous cell carcinoma cells involves promoter methylation and microRNA-10b. *Biochem Biophys Res Commun* 453, 772-777.

Downward, J. (2003). Targeting RAS signalling pathways in cancer therapy. *Nat Rev Cancer* 3, 11-22.

Dragatsis, I. and Zeitlin, S. (2001). A method for the generation of conditional gene repair mutations in mice. *Nucleic Acids Res* 29(3), e10.

Dreyer, S. B., Jamieson, N. B., Upstill-Goddard, R., Bailey, P. J., McKay, C. J., Biankin, A. V., Chang, D. K., and Initiative, A. P. C. G. (2018). Defining the molecular pathology of pancreatic body and tail adenocarcinoma. *Br J Surg* 105, e183-e191.

Ducreux, M., Cuhna, A. S., Caramella, C., Hollebecque, A., Burtin, P., Goéré, D., Seufferlein, T., Haustermans, K., Van Laethem, J. L., Conroy, T., et al. (2015). Cancer of the pancreas: ESMO Clinical Practice Guidelines for diagnosis, treatment and follow-up. *Ann Oncol* 26 Suppl 5, v56-68.

Edmondson, R., Jenkins Broglie, J., Adcock, A. F., Yang, L. (2014). Three-dimensional cell culture systems and their applications in drug discovery and cell-based biosensors. Assay Drug Dev Technol 12(4), 207-218.

El Omari, K., Bird, L. E., Nichols, C. E., Ren, J., and Stammers, D. K. (2005). Crystal structure of CC3 (TIP30): implications for its role as a tumor suppressor. *J Biol Chem* 280, 18229-18236.

Embuscado, E. E., Laheru, D., Ricci, F., Yun, K. J., de Boom Witzel, S., Seigel, A., Flickinger, K., Hidalgo, M., Bova, G. S., and Iacobuzio-Donahue, C. A. (2005). Immortalizing the complexity of cancer metastasis: genetic features of lethal metastatic pancreatic cancer obtained from rapid autopsy. *Cancer Biol Ther* 4, 548-554.

Erkan, M., Reiser-Erkan, C., Michalski, C. W., Deucker, S., Sauliunaite, D., Streit, S., Esposito, I., Friess, H., and Kleeff, J. (2009). Cancer-stellate cell interactions perpetuate the hypoxia-fibrosis cycle in pancreatic ductal adenocarcinoma. *Neoplasia* 11, 497-508.

Erkan, M., Reiser-Erkan, C., Michalski, C. W., and Kleeff, J. (2010). Tumor microenvironment and progression of pancreatic cancer. *Exp Oncol* 32, 128-131.

Eser, S., Schnieke, A., Schneider, G., Saur, D. (2014). Oncogenic KRAS signaling in pancreatic cancer. *Br J Cancer* 111(5), 817-822.

Feig, C., Gopinathan, A., Neesse, A., Chan, D. S., Cook, N., and Tuveson, D. A. (2012). The pancreas cancer microenvironment. *Clin Cancer Res* 18, 4266-4276.

Feil, S., Valtcheva, N., and Feil, R. (2009). Inducible Cre Mice. *Methods Mol Biol* 530, 343-363.

Fejerman, L., John, E. M, Huntsman, S., Beckman, K., Choudhry, S., Perez-Stable, E., González Burchard, E., Ziv, E. (2008). Genetic ancestry and risk of breast cancer among US Latinas. *Cancer Res* 68(23), 9723-9728.

Fjällskog, M. L., Lejonklou, M. H., Oberg, K. E., Eriksson, B. K., Janson, E. T. (2003). Expression of molecular targets for tyrosine kinase receptor antagonists in malignant endocrine pancreatic tumors. *Clin Cancer Res* 9(4), 1469-1473.

Fountzilas, G., Bobos, M., Kalogera-Fountzila, A., Xiros, N., Murray, S., Linardou, H., Karayannopoulou, G., Koutras, A. K., Bafaloukos, D., Samantas, E., Christodoulou, C., Economopoulos, T., Kalogeras, K.T., Kosmidis, P. (2008). Gemcitabine combined with gefitinib in patients with inoperable or metastatic pancreatic cancer: a phase II Study of the Hellenic Cooperative Oncology Group with biomarker evaluation. Cancer Invest 26(8), 784-793.

Friedrich, G. and Soriano, P. (1991). Promoter traps in embryonic stem cells: a genetic screen to identify and mutate developmental genes in mice. *Genes Dev* 5, 1513-1523.

Friess, H., Yamanaka, Y., Büchler, M., Ebert, M., Beger, H. G., Gold, L. I., and Korc, M. (1993). Enhanced expression of transforming growth factor beta isoforms in pancreatic cancer correlates with decreased survival. *Gastroenterology* 105, 1846-1856.

Friess, H., Berberat, P., Schilling, M., Kunz, J., Korc, M., Büchler, M. W. (1996). Pancreatic cancer: the potential clinical relevance of alterations in growth factors and their receptors. *J Mol Med* (Berl) 74(1), 35-42.

Fritscher-Ravens, A., Brand, L., Knöfel, WT. et al. (2002). Comparison of endoscopic ultrasound-guided fine needle aspiration for focal pancreatic lesions in patients with normal parenchyma and chronic pancreatitis. *Am J Gastroenterol* 97(11), 2768-2775.

Fukushima, N., Sato, N., Ueki, T., Rosty, C., Walter, K.M., Wilentz, RE, Yeo, C.J., Hruban, R.H., Goggins, M. (2002). Aberrant methylation of preproenkephalin and p16 genes in pancreatic intraepithelial neoplasia and pancreatic ductal adenocarcinoma. *Am J Pathol* 160(5), 1573-1581.

Gades, N. M., Ohash, A., Mills, L. D., Rowley, M. A., Predmore, K. S., Marler, R. J., and Couch, F. J. (2008). Spontaneous vulvar papillomas in a colony of mice used for pancreatic cancer research. *Comp Med* 58, 271-275.

Gagner, M., and Palermo, M. (2009). Laparoscopic Whipple procedure: review of the literature. *J Hepatobiliary Pancreat Surg* 16, 726-730.

Gannon, M., Gamer, L. W., and Wright, C. V. (2001). Regulatory regions driving developmental and tissue-specific expression of the essential pancreatic gene pdx1. *Dev Biol* 238, 185-201.

Gao, S., Li, A., Liu, F., Chen, F., Williams, M., Zhang, C., Kelley, Z., Wu, C.-L., Luo, R., Xiao, H. (2013) NCOA5 Haplo-insufficiency results in glucose intolerance and subsequent hepatocellular carcinoma. *Cancer Cell* 24(6), 725-37.

Gao, J., Arman Aksoy, B., Dogrusoz, U., Dresdner, G., Gross, B., Sumer, S. O., Sun, Y., Jacobsen, A., Sinha, R., Larsson, E., Cerami, E, Sander, C.,

Schultz, N. (2013). Integrative analysis of complex cancer genomics and clinical profiles using the cBioPortal. *Science Signaling* 6(269), pl1.

Garzon, R., Marcucci, G., and Croce, C. M. (2010). Targeting microRNAs in cancer: rationale, strategies and challenges. *Nat Rev Drug Discov* 9, 775-789.

Gay, L. J. and Malanchi, I. (2017). The sleeping ugly: tumour microenvironment's act to make or break the spell of dormancy. *Biochim Biophys Acta Rev Cancer* 1868(1), 231-238.

Gerlai, R. (1996). Gene-targeting studies of mammalian behavior: is it the mutation or the background geneotype? *Trends Neurosci* 19(5), 177-181.

Giancotti, F. G. (2013). Mechanisms governing metastatic dormancy and reactivation. *Cell* 155(4): 750-764.

Goel, M. K., Khanna, P., and Kishore, J. (2010). Understanding survival analysis: Kaplan-Meier estimate. *Int J Ayurveda Res* 1(4), 274-278.

Goggins, M., Shekher, M., Turnacioglu, K., Yeo, C. J., Hruban, R. H., Kern, S. E. (1998). Genetic alterations of the transforming growth factor β receptor genes in pancreatic and biliary adenocarcinomas. *Cancer Res* 58(23), 5329-5332.

Golan, T., Sella, T., Margalit, O., Amit, U., Halpern, N., Aderka, D., Shacham-Shmueli, E., Urban, D., and Lawrence, Y. R. (2017). Short- and Long-Term Survival in Metastatic Pancreatic Adenocarcinoma, 1993-2013. *J Natl Compr Canc Netw* 15, 1022-1027.

Goldman, M., Craft, B., Hastie, M., Repečka, K., Kamath, A., McDade, F., Rogers, D., Brooks, A. N., Zhu, J., Haussler, D. (2019). The UCSC Xena platform for public and private cancer genomics data visualization and interpretation. bioRxiv 326470; doi https://doi.org/10.1101/326470.

Gore, J., Imasuen-Williams, Imade, Conteh, A.M., Craven, K.E., Cheng, M., Korc, M. (2016). Combined targeting of TGF-beta, EGFR and HER2 suppresses lymphangiogenesis and metastasis in a pancreatic cancer model. *Cancer Lett* 379(1), 143-153.

Grabocka, E. and Bar-Sagi, D. (2016). Mutant KRAS enhances tumor cell fitness by upregulating stress granules. *Cell* 167, 1803-1813.

Green, R. P., Cohn, S. M., Sacchettini, J. C., Jackson, K. E., and Gordon, J. I. (1992). The mouse intestinal fatty acid binding protein gene: nucleotide sequence, pattern of developmental and regional expression, and proposed structure of its protein product. *DNA Cell Biol* 11, 31-41.

Groot, V. P., Rezaee, N., Wu, W., Cameron, J. L., Fishman, E. K., Hruban, R. H., Weiss, M. J., Zheng, L., Wolfgang, C. L., and He, J. (2018). Patterns, Timing, and Predictors of Recurrence Following Pancreatectomy for Pancreatic Ductal Adenocarcinoma. *Ann Surg* 267, 936-945.

Grovel, J.-P., Chavrier, P., Zerial, M., Gruenberg, J. (1991). rab5 controls early endosome fusion in vitro. *Cell* 64 (5), 915-925.

Gu, G., Dubauskaite, J., and Melton, D. A. (2002). Direct evidence for the pancreatic lineage: NGN3+ cells are islet progenitors and are distinct from duct progenitors. *Development* 129, 2447-2457.

Gu, G., Brown, J. R., and Melton, D. A. (2003). Direct lineage tracing reveals the ontogeny of pancreatic cell fates during mouse embryogenesis. *Mech Dev* 120, 35-43.

Guerra, C., and Barbacid, M. (2013). Genetically engineered mouse models of pancreatic adenocarcinoma. *Mol Oncol* 7, 232-247.

Guerra, C., Mijimolle, N., Dhawahir, A., Dubus, P., Barradas, M., Serrano, M., Campuzano, V., and Barbacid, M. (2003). Tumor induction by an endogenous K-ras oncogene is highly dependent on cellular context. *Cancer Cell* 4, 111-120.

Guo, S., Jing, W., Hu, X., Zhou, X., Liu, L., Zhu, M., Yin, F., Chen, R., Zhao, J., and Guo, Y. (2014). Decreased TIP30 expression predicts poor prognosis in pancreatic cancer patients. *Int J Cancer* 134, 1369-1378.

Gupta, G. P., and Massagué, J. (2006). Cancer metastasis: building a framework. *Cell* 127, 679-695.

Guzman, C., Bagga, M, Kaur, A., Westermarck, J., Abankwa, D. (2014). ColonyArea: an ImageJ plugin to automatically quantify colony formation in clonogenic assays. *PLoS One* 9(3): e924444.doi:10.1371/journal.pone.0092444

Geer LY, Marchler-Bauer A, Geer RC, Han L, He J, He S, Liu C, Shi W, Bryant SH. "HTATIP2 HIV-1 Tat interactive protein 2 [*Homo sapiens* (human)]" The NCBI BioSystems database. *Nucleic Acids Res.* 2010 Jan; 38(Database issue):D492-6. *(Epub 2009 Oct 23)*

Haeno, H., Gonen, M., Davis, M. B., Herman, J. M., Iacobuzio-Donahue, C. A., and Michor, F. (2012). Computational modeling of pancreatic cancer reveals kinetics of metastasis suggesting optimum treatment strategies. *Cell* 148, 362-375.

Hanahan, D., and Weinberg, R. A. (2000). The hallmarks of cancer. *Cell* 100, 57-70.

Hanahan, D., and Weinberg, R. A. (2011). Hallmarks of cancer: The next generation. *Cell* 144, 646-674.

Harder, J., Ihorst, G., Heinemann, V., Hofheinz, R., Moehler, M., Buechler, P., Kloeppel, G., Röcken, C., Bitzer, M., Boeck, S., Endlicher, E., Reinacher-Schick A., Schmoor, C., Geissler, M. (2012). Multicentre phase II trial of trastuzumab and capecitabine in patients with HER2 overexpressing metastatic pancreatic cancer. *Br J Cancer* 106(6), 1033-1038.

Hartwig W, Schneider L, Diener MK, et al. (2009). Preoperative tissue diagnosis for tumours of the pancreas. *Br J Surg* 96:5–20.

Hassan, M. M., Bondy, M. L., Wolff, R. A., Abbruzzese, J. L., Vauthey, J. N., Pisters, P. W., Evans, D. B., Khan, R., Chou, T. H., Lenzi, R., et al. (2007). Risk factors for pancreatic cancer: case-control study. *Am J Gastroenterol* 102, 2696-2707.

Hatley, M. E., Patrick, D. M., Garcia, M. R., Richardson, J. A., Bassel-Duby, R., van Rooij, E., Olson, E. N. (2010). Modulation of K-Ras-dependent lung tumorigenesis by MicroRNA-21. *Cancer Cell* 18(3), 282-293.

Hermann, P. C., Huber, S. L., Herrler, T., Aicher, A., Ellwart, J. W., Guba, M., Bruns, C. J., and Heeschen, C. (2007). Distinct populations of cancer stem

cells determine tumor growth and metastatic activity in human pancreatic cancer. *Cell Stem Cell* 1, 313-323.

Heron, M., and Anderson, R. N. (2016). Changes in the Leading Cause of Death: Recent Patterns in Heart Disease and Cancer Mortality. NCHS Data Brief, 1-8.

Herreros-Villanueva, M., Hijona, E., Cosme, A., and Bujanda, L. (2012). Mouse models of pancreatic cancer. *World J Gastroenterol* 18, 1286-1294.

Hezel, A. F., Kimmelman, A. C., Stanger, B. Z., Bardeesy, N., and Depinho, R. A. (2006). Genetics and biology of pancreatic ductal adenocarcinoma. *Genes Dev 20*, 1218-1249.

Hidalgo, M. (2010). Pancreatic cancer. *N Engl J Med* 362, 1605-1617.

Hidalgo, M., Cascinu, S., Kleeff, J., Labianca, R., Löhr, J. M., Neoptolemos, J., Real, F. X., Van Laethem, J. L., and Heinemann, V. (2015). Addressing the challenges of pancreatic cancer: future directions for improving outcomes. *Pancreatology* 15, 8-18.

Hingorani, S. R., Petricoin, E. F., Maitra, A., Rajapakse, V., King, C., Jacobetz, M. A., Ross, S., Conrads, T. P., Veenstra, T. D., Hitt, B. A., et al. (2003). Preinvasive and invasive ductal pancreatic cancer and its early detection in the mouse. *Cancer Cell* 4, 437-450.

Hingorani, S. R., Wang, L., Multani, A. S., Combs, C., Deramaudt, T. B., Hruban, R. H., Rustgi, A. K., Chang, S., Tuveson, D. A. (2005). *Trp53*^{R172H} and *Kras*^{G12D} cooperate to promote chromosomal instability and widely metastatic pancreatic ductal adenocarcinoma in mice. *Cancer Cell* 7(5), 469-483.

Hingorani, S. R., Zheng, L., Bullock, A. J., Seery, T. E., Harris, W. P., Sigal, D. S., Braiteh, F., Ritch, P. S., Zalupski, M. M., Bahary, N., et al. (2018). HALO 202: Randomized Phase II Study of PEGPH20 Plus Nab-Paclitaxel/Gemcitabine Versus Nab-Paclitaxel/Gemcitabine in Patients With Untreated, Metastatic Pancreatic Ductal Adenocarcinoma. *J Clin Oncol* 36, 359-366.

Hoess, R.H. and Abremski, K. Interaction of the bacteriophage P1 recombinase Cre with the recombining site loxP. *Proc Natl Acad Sci U S A* 81(4), 1026-1029.

Hruban, R. H., Adsay, N. V., Albores-Saavedra, J., Anver, M. R., Biankin, A. V., Boivin, G. P., Furth, E. E., Furukawa, T., Klein, A., Klimstra, D. S., Kloppel, G., Lauwers, G. Y., Longnecker, D. S., Luttges, J., Maitra, A., Offerhaus, G. J., Pérez-Gallego, L., Redston, M., Tuveson, D. A. (2006). Pathology of genetically engineered mouse models of pancreatic exocrine cancer: consensus report and recommendations. *Cancer Res* 66, 95-106.

Hruban, R. H., Goggins, M., Parsons, J., and Kern, S. E. (2000). Progression model for pancreatic cancer. *Clin Cancer Res* 6, 2969-2972.

Hruban, R. H., Takaori, K., Klimstra, D. S., Adsay, N. V., Albores-Saavedra, J., Biankin, A. V., Biankin, S. A., Compton, C., Fukushima, N., Furukawa, T., et al. (2004). An illustrated consensus on the classification of pancreatic intraepithelial neoplasia and intraductal papillary mucinous neoplasms. Am *J Surg Pathol* 28, 977-987.

Hruban, R. H., Wilentz, R. E., and Kern, S. E. (2000). Genetic progression in the pancreatic ducts. *Am J Pathol* 156, 1821-1825.

Hu, Y., Chen, F., Liu, F., Liu, X., Huang, N., Cai, X., Sun, Y., Li, A., and Luo, R. (2016). Overexpression of TIP30 inhibits the growth and invasion of glioma cells. *Mol Med Rep* 13, 605-612.

Huang, W. Y., Hsu, S. D., Huang, H. Y., Sun, Y. M., Chou, C. H., Weng, S. L., and Huang, H. D. (2015). MethHC: a database of DNA methylation and gene expression in human cancer. *Nucleic Acids Res* 43, D856-861.

Huang, Z., and Liu, F. (2014). Diagnostic value of serum carbohydrate antigen 19-9 in pancreatic cancer: a meta-analysis. *Tumour Biol* 35, 7459-7465.

Ijichi, H., Chytil, A., Gorska, A. E., Aakre, M. E., Fujitani, Y., Fujitani, S., Wright, C. V. E., Moses, H. L. (2006). Aggressive pancreatic ductal adenocarcinoma in mice caused by pancreas-specific blockade of transforming growth factor-β signaling in cooperation with active Kras expression. *Genes Dev* 20, 3147-3160.

Iodice, S., Gandini, S., Maisonneuve, P., and Lowenfels, A. B. (2008). Tobacco and the risk of pancreatic cancer: a review and meta-analysis. *Langenbecks Arch Surg* 393, 535-545.

Ischenko, I., Petrenko, O., Hayman, M.J. (2014). Analysis of the tumor-initiating and metastatic capacity of PDX1-positive cells from the adult pancreas. *Proc Natl Acad Sci U S A* 111(9), 3466-3471.

Itakura, J., Ishiwata, T., Friess, H., Fujii, H., Matsumoto, Y., Büchler, M. W., Korc, M. (1997). Enhanced expression of vascular endothelial growth factor in human pancreatic cancer correlates with local disease progression. *Clin Cancer Res* 3, 1309-1316.

Ito, M., Jiang, C., Krumm, K., Zhang, X., Pecha, J., Zhao, J., Guo, Y., Roeder, R. G., and Xiao, H. (2003). TIP30 deficiency increases susceptibility to tumorigenesis. *Cancer Res* 63, 8763-8767.

Jacks, T. (2017). Kras G12D Conditional PCR. [Protocol, Dr. Tyler Jacks and The Jacks Lab, Koch Institute for Integrative Cancer Research at MIT]. Retrieved from https://jacks-lab.mit.edu/protocols/genotyping/kras_cond on June 8, 2016.

Jackson, E. L., Willis, N., Mercer, K., Bronson, R. T., Crowley, D., Montoya, R., Jacks, T., and Tuveson, D. A. (2001). Analysis of lung tumor initiation and progression using conditional expression of oncogenic K-ras. *Genes Dev* 15, 3243-3248.

Jacobetz, M. A., Chan, D. S., Neesse, A., Bapiro, T. E., Cook, N., Frese, K. K., Feig, C., Nakagawa, T., Caldwell, M. E., Zecchini, H. I., et al. (2013). Hyaluronan impairs vascular function and drug delivery in a mouse model of pancreatic cancer. *Gut* 62, 112-120.

Jaganathan, S., Yue, P., Turkson, J. (2010). Enhanced sensitivity of pancreatic cancer cells to concurrent inhibition of aberrant signal transducer and activator of transcription 3 and epidermal growth factor receptor or Src. *J Pharmacol Exp Ther* 333(2), 373-381.

Jain, R., Fischer, S., Serra, S. Chetty, R. (2010). The use of Cytokeratin 19 (CK19) immunohistochemistry in lesions of the pancreas, gastrointestinal tract, and liver. *Appl Immunohistochem Mol Morphol* 18(1), 9-15.

Jenkins, B. D., Martini, R. N., Hire, R., Brown, A., Bennett, B., Brown, I., Howerth, E. W., Egan, M., Hodgson, J., Yates, C., Kittles, R., Chitale, D., Ali, H., Nathanson, D., Nikolinakos, P., Newman, L., Monteil, M., Davis, M. B. (2019). Atypical chemokine receptor 1 (*DARC/ACKR1*) in breast tumors is associated with survival, circulating chemokines, tumor-infiltrating immune cells, and African ancestry. *Cancer Epidemiol Biomarkers Prev* 28(4), 690-700.

Jiang, C., Ito, M., Piening, V., Bruck, K., Roeder, R. G., and Xiao, H. (2004). TIP30 interacts with an estrogen receptor alpha-interacting coactivator CIA and regulates c-myc transcription. *J Biol Chem 279*, 27781-27789.

Johnson, L., Mercer, K., Greenbaum, D., Bronson, R. T., Crowley, D., Tuveson, D. A., and Jacks, T. (2001). Somatic activation of the K-ras oncogene causes early onset lung cancer in mice. *Nature* 410, 1111-1116.

Jones, K. A. and Peterlin, B. M. (1994). Control of RNA initiation and elongation at the HIV-1 promoter. *Annu Rev Biochem* 63, 717-743.

Jörnvall, H., Persson, B., Krook, M., Atrian, S., Gonzàlez-Duarte, R., Jeffery, J., and Ghosh, D. (1995). Short-chain dehydrogenases/reductases (SDR). *Biochemistry* 34, 6003-6013.

Kallberg, Y., Oppermann, U., Jörnvall, H., Persson, B. (2002). Short-chain dehydrogenases/reductases (SDRs). *Eur J Biochem* 269(18), 4409-17.

Kanda, M. Fujii, T., Nagai, S., Kodera, Y., Kanzaki, A., Sahin, T. T., Hayashi, M., Yamada, S., Sugimoto, H., Nomoto, S., Takeda, S., Morita, S., and Nakao, A. (2011). Pattern of lymph node metastasis spread in pancreatic cancer. *Pancreas* 40(6), 951-955.

Kanda, M., Matthaei, H., Wu, J., Hong, S. M., Yu, J., Borges, M., Hruban, R. H., Maitra, A., Kinzler, K., Vogelstein, B., and Goggins, M. (2012). Presence of somatic mutations in most early-stage pancreatic intraepithelial neoplasia. *Gastroenterology* 142, 730-733.e739.

Kang, Y. and Massagué, J. (2004). Epithelial-mesenchymal transitions: Twist in development and metastasis. *Cell* 118(3), 277-9.

Karbowski, M., Jeong, S.-Y., and Youle, R.J. (2004). Endophilin B1 is required for the maintenance of mitochondrial morphology. *JBC* 166(7), 1027-1039.

Kaur, S., Kumar, S., Momi, N., Sasson, A. R., Batra, S. K. (2013). Mucins in pancreatic cancer and its microenvironment. Nat Rev *Gastroenterol Hepatol* 10(10), 607-620.

Kawaguchi, Y., Cooper, B., Gannon, M., Ray, M., MacDonald, R. J., and Wright, C. V. (2002). The role of the transcriptional regulator Ptf1a in converting intestinal to pancreatic progenitors. *Nat Genet* 32, 128-134.

Kern, H. F. (1993). Fine Structure of the Human Exocrine Pancreas. In V. L. W. Go et al. (Eds.), *The Pancreas: Biology, Pathobiology, and Disease, Second Edition* (9-19). New York: Raven Press Ltd.

Kern, S. E. (2000). Molecular genetic alterations in ductal pancreatic adenocarcinoma. *Med Clin North Am* 84, 691-695, xi.

Kharroubi, A. T., and Darwish, H. M. (2015). Diabetes mellitus: The epidemic of the century. *World J Diabetes* 6, 850-867.

Khawja, S. N., Mohammed, S., Silberfein, E. J., Musher, B. L., Fisher, W. E., and Van Buren, G. (2015). Pancreatic cancer disparities in African Americans. *Pancreas* 44, 522-527.

King, F. W. and Shtivelman, E. (2004). Inhibition of nuclear import by the proapoptotic protein CC3. *Mol Cell Biol* 24, 7091-7101.

Kobayashi, A., Okuda, H., Xing, F., Pandey, P.R., Watabe, M., Hirota, S., Pai, S.K., Liu, W., Fukuda, K., Chambers, C., Wilber, A., Watabe, K. (2011). Bone morphogenetic protein 7 in dormancy and metastasis of prostate cancer stem-like cells in bone. *JEM* 208(13), 2641-2655.

Konstantinidis, I. T., Vinuela, E. F., Tang, L. H., Klimstra, D. S., D'Angelica, M. I., Dematteo, R. P., Kingham, T. P., Fong, Y., Jarnagin, W. R., and Allen, P. J. (2013). Incidentally discovered pancreatic intraepithelial neoplasia: what is its clinical significance? *Ann Surg Oncol* 20, 3643-3647.

Koong, A. C., Mehta, V. K., Le, Q. T., Fisher, G. A., Terris, D. J., Brown, J. M., Bastidas, A. J., and Vierra, M. (2000). Pancreatic tumors show high levels of hypoxia. *Int J Radiat Oncol Biol Phys* 48, 919-922.

Korc, M., Chandrasekar, B., Yamanaka, Y., Friess, H., Buchier, M., Beger, H.G. (1992). Overexpression of the epidermal growth factor receptor in human pancreatic cancer is associated with concomitant increases in the levels of epidermal growth factor and transforming growth factor alpha. *J Clin Invest* 90(4), 1352-60.

Kuzminov, A. (2011). Homologous recombination-experimental systems, analysis, and significance. *EcoSal Plus* 4(2): .doi:10.1128/ecosalplus.7.2.6.

Lakso, M., Sauer, B., Mosinger, Jr., B., Lee, E.J., Manning, R.W., Yu, S.-H., Mulder, K.L., Westphal, H. (1992). Targeted oncogene activation by site-specific recombination in transgenic mice. *Proc Natl Acad Sci U S A* 89, 6232-6236.

Lee, C. J., Li, C., and Simeone, D. M. (2008). Human pancreatic cancer stem cells: implications for how we treat pancreatic cancer. *Transl Oncol* 1, 14-18.

Li, A., Zhang, C., Gao, S., Chen, F., Yang, C., Luo, R., and Xiao, H. (2013). TIP30 loss enhances cytoplasmic and nuclear EGFR signaling and promotes lung adenocarcinogenesis in mice. *Oncogene* 32, 2273-2281, 2281e.2271-2212.

Li, C., Heidt, D.G., Dalerba, P., Burant, C.F., Zhang, L., Adsay, V., Wicha, M., Clarke, M.F., and Simeone, D.M. (2007). Identification of pancreatic cancer stem cells. *Cancer Res* 67(3), 1030-1037.

Li, D., Xie, K., Wolff, R., and Abbruzzese, J. L. (2004). Pancreatic cancer. *Lancet* 363, 1049-1057.

Lin, Y., Tamakoshi, A., Kawamura, T., Inaba, Y., Kikuchi, S., Motohashi, Y., Kurosawa, M., and Cohort, J. S. G. J. C. (2002). A prospective cohort study of cigarette smoking and pancreatic cancer in Japan. *Cancer Causes Control* 13, 249-254.

Lin, Y., Tamakoshi, A., Kawamura, T., Inaba, Y., Kikuchi, S., Motohashi, Y., Kurosawa, M., and Ohno, Y. (2002). Risk of pancreatic cancer in relation to

alcohol drinking, coffee consumption and medical history: findings from the Japan collaborative cohort study for evaluation of cancer risk. *Int J Cancer* 99, 742-746.

Livak, K. J. and Schmittgen, T. D. (2001). Analysis of relative gene expression data using real-time quantitative PCR and the 2(-Delta Delta C(T)) Method. *Methods 25*, 402-408.

Löhr, M., Trautmann, B., Göttler, M., Peters, S., Zauner, I., Maillet, B., and Klöppel, G. (1994). Human ductal adenocarcinomas of the pancreas express extracellular matrix proteins. *Br J Cancer* 69, 144-151.

Longo, V., Brunetti, O., Gnoni, A., Cascinu, S., Gasparini, G., Lorusso, V., Ribatti, D., and Silvestris, N. (2016). Angiogenesis in pancreatic ductal adenocarcinoma: A controversial issue. *Oncotarget* 7, 58649-58658.

Lu, D. S., Reber, H. A., Krasny, R. M., Kadell, B. M., and Sayre, J. (1997). Local staging of pancreatic cancer: criteria for unresectability of major vessels as revealed by pancreatic-phase, thin-section helical CT. *AJR Am J Roentgenol* 168, 1439-1443.

Lusis, A. J., Yu, J., and Wang, S. S. (2007). The problem of passenger genes in transgenic mice. *Arterioscler Thromb Vasc Biol* 27, 2100-2103.

Magnuson, M. A. and Osipovich, A. B. (2013). Pancreas-specific Cre driver lines and considerations for their prudent use. *Cell Metab* 18(1), 9-20.

Maisonneuve, P. and Lowenfels, A. B. (2015). Risk factors for pancreatic cancer: a summary review of meta-analytical studies. *Int J Epidemiol* 44, 186-198.

Mao, C., Domenico, D. R., Kim, K., Hanson, D. J., and Howard, J. M. (1995). Observations on the developmental patterns and the consequences of pancreatic exocrine adenocarcinoma. Findings of 154 autopsies. *Arch Surg* 130, 125-134.

Martinez-Ruiz, G., Maldonado, V., Ceballos-Cancino, G., Reyes Grajeda, J. P., Melendez-Zajgla, J. (2008). Role of Smac/DIABLO in cancer progression. *J Exp Clin Cancer Res* 27(1), 48.

Masiak-Segit, Wioletta & Rawicz-Pruszyński, Karol & Skórzewska, Magdalena & Polkowski, Wojciech. (2018). Surgical treatment of pancreatic cancer. *Polski Przeglad Chirurgiczny* 90(2), 45-53. 10.5604/01.3001.0011.7493.

Massagué, J. (1998). TGF-β Signal Transduction. *Annu Rev Biochem* 67, 753-791.

McCleary-Wheeler, A.L, Lomberk, G.A., Weiss, F.U., Schneider, G. Fabbri, M., Poshusta, T.L., Dusetti, N. J., Baumgart, S., Iovanna, J. L., Ellenrieder, V., Urrutia, R., Fernandez-Zapico, M. E. (2013). Insights into the epigenetic mechanisms controlling pancreatic carcinogenesis. *Cancer Lett* 328(2), 212-221.

McKinnon, C. M. and Docherty, K. (2001). Pancreatic duodenal homeobox-1, PDX-1, a major regulator of beta cell identity and function. *Diabetologia* 44(10), 1203-1214.

Mebratu, Y. and Tesfaigzi, Y. (2010). How ERK1/2 activation controls cell proliferation and cell death is subcellular localization the answer? *Cell Cycle* 8(8), 1168-1175.

Miller, D. M., Thomas, S. D., Islam, A., Muench, D., and Sedoris, K. (2012). c-Myc and cancer metabolism. *Clin Cancer Res* 18, 5546-5553.

Mollenhauer, J., Roether, I., and Kern, H. F. (1987). Distribution of extracellular matrix proteins in pancreatic ductal adenocarcinoma and its influence on tumor cell proliferation in vitro. *Pancreas* 2, 14-24.

Mori, S., Chang, J.T. Andrecheck, E.R., Matsumura, N., et al. (2010). An anchorage-independent cell growth signature identifies tumors with metastatic potential. *Oncogene* 28(31), 2796-2805.

Morton, J.P., Timpson, P., Karim, S.A., Ridgway, R.A., Athineos, D., Doyle, B., Jamieson, N.B., Oien, K.A., Lowy, A.M., Brunton, V.G., Frame, M.C., Jeffry Evans, T.R., Sansom, O.J. (2010). Mutant p53 drives metastasis and overcomes growth arrest/senescence in pancreatic cancer. *Proc Natl Acad Sci U S A* 107(1), 246-251.

Mullendore, M. E., Koorstra, J. B., Li, Y. M., Offerhaus, G. J., Fan, X., Henderson, C. M., Matsui, W., Eberhart, C. G., Maitra, A., and Feldmann, G. (2009). Ligand-dependent Notch signaling is involved in tumor initiation and tumor maintenance in pancreatic cancer. *Clin Cancer Res* 15, 2291-2301.

Muller, P.A. and Vousden, K.H. (2014). Mutant p53 in Cancer: New functions and therapeutic opportunities. *Cancer Cell* 25(3), 304-317.

Muzumdar, M. D., Tasic, B., Miyamichi, K., Li, L., and Luo, L. (2007). A global double-fluorescent Cre reporter mouse. *Genesis* 45, 593-605.

Muzumdar, M. D., Chen, P.-Y., Dorans, K. J., Chung, K. M., Bhutkar, A., Hong, E., Noll, E. M., Sprick, M. R., Trump, A., Jacks, T. (2017). Survival of pancreatic cancer cells lacking KRAS function. *Nat Commun* 8, 1090.

National Cancer Institute. Cancer Disparities. (2018, March 29). Retrieved from https://www.cancer.gov/about-cancer/understanding/disparities on October 18, 2018.

National Cancer Institute Surveillance, Epidemiology, and End Results Program. Number of Persons by Race and Hispanic Ethnicity for SEER Participants (2010 Census Data). Retrieved from https://seer.cancer.gov/registries/data.html#a1 on October 18, 2018.

Navas, C., Hernández-Porras, I., Schuhmacher, A. J., Sibilia, M., Guerra, C., and Barbacid, M. (2012). EGF receptor signaling is essential for k-ras oncogene-driven pancreatic ductal adenocarcinoma. *Cancer Cell* 22, 318-330.

Neesse, A., Algül, H., Tuveson D.A., Gress, T.M. (2015). Stromal biology and therapy in pancreatic cancer: a changing paradigm. *Gut* 64, 1476-1484.

Nguyen, D.X., Bos, P.D., Massagué, J. (2009). Metastasis: from dissemination to organ-specific colonization. *Nature Rev Cancer* 9, 274-284.

NicAmhlaoibh, R. and Shtivelman, E. (2001). Metastasis suppressor CC3 inhibits angiogenic properties of tumor cells in vitro. *Oncogene* 20, 270-275.

Noone AM, Howlader N, Krapcho M, Miller D, Brest A, Yu M, Ruhl J, Tatalovich Z, Mariotto A, Lewis DR, Chen HS, Feuer EJ, Cronin KA (eds). SEER Cancer Statistics Review, 1975-2015, National Cancer Institute. Bethesda, MD, https://seer.cancer.gov/csr/1975_2015/, based on November 2017 SEER data submission, posted to the SEER web site, April 2018.

Norris, A. M., Gore, A., Balboni, A., Young, A., Longnecker, D. S., Korc, M. (2013). AGR2 is a SMAD4-suppressible gene that modulates MUC1 levels and promotes the initiation and progression of pancreatic intraepithelial neoplasia. *Oncogene* 32(33), 3867-3876.

Obenauf, A.C. and Massagué, J. (2015). Surviving at a distance: Organ specific metastasis. *Trends Cancer* 1(1), 76-91.

Oettle, H., Neuhaus, P., Hochhaus, A., Hartmann, J. T., Gellert, K., Ridwelski, K., Niedergethmann, M., Zülke, C., Fahlke, J., Arning, M. B., et al. (2013). Adjuvant chemotherapy with gemcitabine and long-term outcomes among patients with resected pancreatic cancer: the CONKO-001 randomized trial. *JAMA* 310, 1473-1481.

Offield, M. F., Jetton, T. L., Labosky, P. A., Ray, M., Stein, R. W., Magnuson, M. A., Hogan, B. L., and Wright, C. V. (1996). PDX-1 is required for pancreatic outgrowth and differentiation of the rostral duodenum. *Development* 122, 983-995.

Öhlund, D., Handly-Santana, A., Biffi, G., Elyada, E., Almeida, A. S., Ponz-Sarvise, M., Corbo, V., Oni, T. E., Hearn, S. A., Lee, E. J., et al. (2017). Distinct populations of inflammatory fibroblasts and myofibroblasts in pancreatic cancer. *J Exp Med* 214, 579-596.

Olive, K. P., Jacobetz, M. A., Davidson, C. J., Gopinathan, A., McIntyre, D., Honess, D., Madhu, B., Goldgraben, M. A., Caldwell, M. E., Allard, D., et al. (2009). Inhibition of Hedgehog signaling enhances delivery of chemotherapy in a mouse model of pancreatic cancer. *Science* 324, 1457-1461.

Ouyang, H., Gore, J., Deitz, S., Korc, M. (2013). microRNA-10b enhances pancreatic cancer cell invasion by suppressing TIP30 expression and promoting EGF and TGF-β actions. *Oncogene* 33(38), 4664-74.

Özdemir, B. C., Pentcheva-Hoang, T., Carstens, J. L., Zheng, X., Wu, C. C., Simpson, T. R., Laklai, H., Sugimoto, H., Kahlert, C., Novitskiy, S. V., et al. (2014). Depletion of carcinoma-associated fibroblasts and fibrosis induces immunosuppression and accelerates pancreas cancer with reduced survival. *Cancer Cell* 25, 719-734.

Padua, D. and Massagué, J. (2009). Roles of TGFbeta in metastasis. *Cell Research* 19(1), 89-102.

Pandol, Stephen J. The Exocrine Pancreas, Morgan & Claypool Life Science Publishers, 2011. ProQuest Ebook Central, https://ebookcentral.proquest.com/lib/iupui-ebooks/detail.action?docID=881318.

Pandol, S., Edderkaoui, M., Gukovsky, I., Lugea, A., and Gukovskaya, A. (2009). Desmoplasia of pancreatic ductal adenocarcinoma. Clin Gastroenterol Hepatol 7(11 0), S44-S47.

Pannala, R., Leirness, J. B., Bamlet, W. R., Basu, A., Petersen, G. M., and Chari, S. T. (2008). Prevalence and clinical profile of pancreatic cancer-associated diabetes mellitus. *Gastroenterology* 134, 981-987.

Pantel, K., Brakenhoff, R.H., Brandt, B. (2008). Detection, clinical relevance and specific biological properties of disseminating tumour cells. *Nat Rev Cancer* 8, 329-340.

Pap, M. and Cooper, G. M. (1998). Role of glycogen synthase kinase-3 in the phosphatidylinositol 3-Kinase/Akt cell survival pathway. *J Biol Chem* 273,19929–19932.

Park, S. W., Zhen, G., Verhaeghe, C., Nakagami, Y., Nguyenvu, L.T., Barczak, A. J., Kileen, N., Erle, D. J. (2009). The protein disulfide isomerase AGR2 is essential for production of intestinal mucus. *Proc Natl Acad Sci U S A* 106(17), 6950-6955.

Pasca di Magliano, M. and Logsdon, C. D. Roles for KRAS in pancreatic tumor development and progression. (2013). *Gastroenterology* 144(6), 1220-1229.

Pastushenko, I., Brisebarre, A., Sifrim, A., Fioramonti, M., Revenco, T., Boumahdi, S., Van Keymeulen, A., Brown, D., Moers, V., Lemaire, S., De Clercq, S., Minguijón., E., Balsat, C., Sokolow, Y., Dubois, C., De Cock, F., Scozzaro, S., Sopena, F., Lanas, A., D'Haene, N., Salmon, I., Marine, J.-C., Voet, T., Sotiropoulou, P. A., and Blanpain, C. (2018). Identification of the tumour transition states occurring during EMT. *Nature* 556, 463-468.

Peixoto, R. D., Speers, C., McGahan, C. E., Renouf, D. J., Schaeffer, D., Kennecke, H. F. (2015). Prognostic factors and sites of metastasis in an unresectable locally advanced pancreatic cancer. *Cancer Med* 4(8), 1171-1177.

Percy, D.H. and Barthold, S.W. (2008). Pathology of Laboratory Rodents and Rabbits, Third Edition. Print ISBN:9780813821016 |Online ISBN:9780470344613 |DOI:10.1002/9780470344613 Accessed on December 6, 2008 using https://onlinelibrary.wiley.com/doi/book/10.1002/9780470344613

Pericleous, M., Rossi, R. E., Mandair, D., Whyand, T., and Caplin, M. E. (2014). Nutrition and pancreatic cancer. *Anticancer Res* 34, 9-21.

Pernick, N. L., Sarkar, F. H., Philip, P. A., Arlauskas, P., Shields, A. F., Vaitkevicius, V. K., Dugan, M. C., and Adsay, N. V. (2003). Clinicopathologic analysis of pancreatic adenocarcinoma in African Americans and Caucasians. *Pancreas* 26, 28-32.

Petersen, G. M. (2016). Familial pancreatic cancer. *Semin Oncol* 43, 548-553.

Philip, P. A., Goldman, B., Ramanathan, R. K., Lenz, H. –J., Lowy, A. M., Whitehead, R. P., Wakatsuki, T., Iqbal, S., Gaur, R., Benedetti, J. K., Blanke, C. D. (2014). Dual blockade of epidermal growth factor receptor and insulin-like growth factor receptor-1 signaling in metastatic pancreatic cancer: Phase Ib and randomized phase II trial of gemcitabine, erlotinib, and cixutumumab versus gemcitabine plus erlotinib (SWOG S0727). *Cancer* 2014, 120, 2980-2985.

Pomerantz, J. H. and Blau, H. M. (2013). Tumor suppressors: enhancers or suppressors of regeneration? *Development* 140, 2502-2512.

Preis, M., Gardner, T. B., Gordon, S. R., Pipas, J. M., Mackenzie, T. A., Klein, E. E., Longnecker, D. S., Gutmann, E. J., Sempere, L. F., and Korc, M. (2011).

MicroRNA-10b expression correlates with response to neoadjuvant therapy and survival in pancreatic ductal adenocarcinoma. *Clin Cancer Res* 17, 5812-5821.

Protti, M. P. and De Monte, L. (2013). Immune infiltrates as predictive markers of survival in pancreatic cancer patients. *Front Physiol* 4, 210.

Provenzano, P. P., Cuevas, C., Chang, A. E., Goel, V. K., Von Hoff, D. D., and Hingorani, S. R. (2012). Enzymatic targeting of the stroma ablates physical barriers to treatment of pancreatic ductal adenocarcinoma. *Cancer Cell* 21, 418-429.

Puck TT, Marcus PI, Cieciura SJ. Clonal growth of mammalian cells in vitro; growth characteristics of colonies from single HeLa cells with and without a feeder layer. *J Exp Med* 1956(103), 273–283.

Puigserver, P. and Spiegelman, B. M. (2003). Peroxisome proliferator-activated receptor-gamma coactivator 1 alpha (PGC-1 alpha): transcriptional coactivator and metabolic regulator. *Endocr Rev* 24, 78-90.

Qiu, W., Sahin, F., Iacobuzio-Donahue, C. A., Garcia-Carracedo, D., Wang, W. M., Kuo, C. Y., Chen, D., Arking, D. E., Lowy, A. M., Hruban, R. H., et al. (2011). Disruption of p16 and activation of Kras in pancreas increase ductal adenocarcinoma formation and metastasis in vivo. *Oncotarget 2*, 862-873.

Qu, X., Yu, J., Bhagat, G., Furuya, N., Hibshoosh, H., Troxel, A., Rosen, J., Eskelinen, E.-L., Mizushima, N., Ohsumi, Y., Cattoretti, G., and Levine, B. (2003). Promotion of tumorigenesis by heterozygous disruption of the beclin 1 autophagy gene. *J Clin Invest* 112(12), 1809-1820.

Rahib, L., Smith, B. D., Aizenberg, R., Rosenzweig, A. B., Fleshman, J. M., and Matrisian, L. M. (2014). Projecting cancer incidence and deaths to 2030: The unexpected burden of thyroid, liver, and pancreas cancers in the United States. *Cancer Res* 74, 2913-2921.

Rankin, E.B. and Giaccia, A.J. (2016). Hypoxic control of metastasis. *Science* 352(6282), 175-180.

Raphael, B. J., Aguirre, A. J., Hruban, R. H., C. G. A. R. N. E. a., and Network, C. G. A. R. (2017). Integrated Genomic Characterization of Pancreatic Ductal Adenocarcinoma. *Cancer Cell* 32, 185-203.e113.

Reichert, M., Bakir, B., Moreira, L., Pitarresi, J. R. Feldmann, K., Simon, L., Suzuki, K., Maddipati, R., Rhim, A. D., Schlitter, A. M., Kriegsmann, M., Weichert, W., Wirth, M., Schuck, K., Schneider, G., Saur, D., Reynolds, A. B., Klein-Szanto, A. J., Pehlivanoglu, B., Memis, B, Adsay, N. V., Rustgi, A. K. (2018). Regulation of Epithelial Plasticity Determines Metastatic Organotropism in Pancreatic Cancer. *Developmental Cell* 45, 696-711.

Rhim, A. D., Mirek, E. T., Aiello, N. M., Maitra, A., Bailey, J. M., McAllister, F., Reichert, M., Beatty, G. L., Rustgi, A. K., Vonderheide, R. H., Leach, S. D., Stanger, B. Z. (2012). EMT and dissemination precede pancreatic tumor formation. *Cell* 148, 349-361.

Rhim, A. D., Oberstein, P. E., Thomas, D. H., Mirek, E. T., Palermo, C. F., Sastra, S. A., Dekleva, E. N., Saunders, T., Becerra, C. P., Tattersall, I. W., Westphalen, C. B., Kitajewski, J., Fernandez-Barrena, M. G., Fernandez-Zapico, M. E., Iacobuzio-Donahue, C., Olive, K. P., Stanger, B. Z. (2014).

Stromal elements act to restrain, rather than support, pancreatic ductal adenocarcinoma. *Cancer Cell* 25, 735-747.

Rich, J. T., Neely, J. G., Paniello, R. C., Voelker, C. C. J., Nussenbaum, B., Wang, E. W. (2010). *Otolaryngol Head Neck Surg* 143(3), 331-336.

Roberts, N. J., Norris, A. L., Petersen, G. M., Bondy, M. L., Brand, R., Gallinger, S., Kurtz, R. C., Olson, S. H., Rustgi, A. K., Schwartz, A. G., et al. (2016). Whole Genome Sequencing Defines the Genetic Heterogeneity of Familial Pancreatic Cancer*. Cancer Discov* 6, 166-175.

Romagosa, C., Simonetti, S., López-Vicente, L., Mazo, A., Lleonart, M.E., Castellvi, J., and Ramon y Cajal, S. (2011). $p16^{Ink4a}$ overexpression in cancer: a tumor suppressor gene associated with senescence and high-grade tumors. *Oncogene* 30, 2087-2097.

Rozenblum, E., Schutte, M., Goggins, M., Hahn, S. A., Panzer, S., Zahurak, M., Goodman, S. N., Sohn, T. A., Hruban, R. H., Yeo, C. J., and Kern, S. E. (1997). Tumor-suppressive pathways in pancreatic carcinoma. *Cancer Res* 57, 1731-1734.

Rubins, J. B. (2003). Alveolar macrophages: wielding the double-edged sword of inflammation. *AJRCCM* 167(2), 103-104.

Ryan, J. F., Rosati, L. M., Groot, V. P., Le, D. T., Zheng, L., Laheru, D. A., Shin, E. J., Jackson, J., Moore, J., Narang, A. K., and Herman, J. M. (2018). Stereotactic body radiation therapy for palliative management of pancreatic adenocarcinoma in elderly and medically inoperable patients. *Oncotarget* 9, 16427-16436.

Sadowski, I., Ma, J., Triezenberg, S., and Ptashne, M. (1988). GAL4-VP16 is an unusually potent transcriptional activator. *Nature* 335, 563-564.

Sahin, I. H., Elias, H., Chou, J. F., Capanu, M., and O'Reilly, E. M. (2018). Pancreatic adenocarcinoma: insights into patterns of recurrence and disease behavior. *BMC Cancer* 18, 769.

Saka, B., Balci, S., Basturk, O., Bagci, P., Postlewait, L. M., Maithel, S., Knight, J., El-Rayes, B., Kooby, D., Sarmiento, J., et al. (2016). Pancreatic Ductal Adenocarcinoma is Spread to the Peripancreatic Soft Tissue in the Majority of Resected Cases, Rendering the AJCC T-Stage Protocol (7th Edition) Inapplicable and Insignificant: A Size-Based Staging System (pT1: ≤2, pT2: >2-≤4, pT3: >4 cm) is More Valid and Clinically Relevant. *Ann Surg Oncol* 23, 2010-2018.

Sauer, B. (1993). Manipulation of transgenes by site-specific recombination: use of Cre recombinase. *Methods Enzymol* 225, 890-900.

Sauer, B. and Henderson, N. (1988). Site-specific DNA recombination in mammalian cells by the Cre recombinase of bacteriophage P1. *Proc Natl Acad Sci U S A* 85, 5166-5170.

Sedoris, K. C., Thomas, S. D., Clarkson, C. R., Muench, D., Islam, A., Singh, R., and Miller, D. M. (2012). Genomic c-Myc quadruplex DNA selectively kills leukemia. *Mol Cancer Ther* 11, 66-76.

Seidler, B., Schmidt, A., Mayr, U., Nakhai, H., Schmid, R. M., Schneider, G., Saur, D. (2008). A Cre-loxP-based mouse model for conditional somatic gene

expression and knockdown in vivo by using avian retroviral vectors. *Proc Natl Acad Sci U S A* 105(29), 10137-10142.

Sempere, L. F., Gunn, J. R., and Korc, M. (2011). A novel 3-dimensional culture system uncovers growth stimulatory actions by TGFβ in pancreatic cancer cells. *Cancer Biol Ther* 12, 198-207.

Seo, Y., Baba, H., Fukuda, T., Takashima, M., Sugimachi, K. (2000). High expression of vascular endothelial growth factor is associated with liver metastasis and a poor prognosis for patients with ductal pancreatic adenocarcinoma. *Cancer* 88(10), 2239-2245.

Seyfried, T. N. and Huysentruyt, L. C. (2013). On the origin of cancer metastasis. *Crit Rev Oncog* 18, 43-73.

Shi, Y. and Massagué, J. (2003). Mechanisms of TGF-β signaling from cell membrane to the nucleus. *Cell* 113(6), 685-700.

Shi, M., Yan, S., G., Xie, S.T., and Wang, H.N. (2008). Tip30-induced apoptosis requires translocation of Bax and involves mitochondrial release of cytochrome c and Smac/DIABLO in hepatocellular carcinoma cells. *Biochim Biophys Acta* 1783, 263-274.

Shibue, T. and Weinberg, R.A. (2017). EMT, CSCs, and drug resistance: the mechanistic link and clinical implications. *Nature Reviews Clinical Oncology* 14(10), 611-629.

Shin, S-I., Freedman, V.H., Risser, R., and Pollack, R. (1975). Tumorigenicity of virus-transformed cells in nude mice is correlated specifically with anchorage independent growth in vitro. *Cell Biology* 72(11), 4435-4439.

Shtivelman, E. (1997). A link between metastasis and resistance to apoptosis of variant small cell lung carcinoma. *Oncogene* 14, 2167-2173.

Siegel, R., Ma, J., Zou, Z., and Jemal, A. (2014). Cancer statistics, 2014. *CA Cancer J Clin* 64, 9-29.

Siegel, R. L., Miller, K. D., and Jemal, A. (2018). Cancer statistics, 2018. *CA Cancer J Clin* 68, 7-30.

Simpson, E. M., Linder, C. C., Sargent, E. E., Davisson, M. T., Mobraaten, L. E., and Sharp, J. J. (1997). Genetic variation among 129 substrains and its importance for targeted mutagenesis in mice. *Nat Genet* 16, 19-27.

Slaughter, D. P., Southwick, H.W., Smejkal, W. (1953). Field cancerization in oral stratified squamous epithelium; clinical implications of multicentric origin. *Cancer* 6, 963-968.

Snider, P., Tang, S., Lin, G., Wang, J., Conway, S. J. (2010). Generation of *Smad7*^{Cre} recombinase mice: a useful tool for the study of epithelial-mesenchymal transformation within the embryonic heart. *Genesis* 47(7), 469-475.

Sohn, T.A., Yeo, C.J., Cameron, J. L., Koniaris, L., Kaushal, S., Abrams, R.A. Sauter, P. K., Coleman, J., Hruban, R. H., Lillemoe, K. D. (2000). Resected adenocarcinoma of the pancreas-616 patients: results, outcomes, and prognostic indicators. *J Gastrointest Surg* 4(6), 567-579.

Song, J., Xu, Y., Hu, X., Choi, B., and Tong, Q. (2010). Brain expression of Cre recombinase driven by pancreas-specific promoters. Genesis 48, 628-634.

Soriano, P. (1999) Generalized lacZ expression with the ROSA26 Cre reporter strain. *Nature Genetics* 21, 70-71.

Spiegelman, B. M., and Heinrich, R. (2004). Biological control through regulated transcriptional coactivators. *Cell* 119, 157-167.

Stacker, S.A., Achen, M.G., Jussila, L., Baldwin, M.E., and Alitalo, K. (2002). Lymphangiogenesis and cancer metastasis. *Nature Rev Can* 2, 573-583.

Stanger, B. Z. and Dor, Y. (2006). Dissecting the cellular origins of pancreatic cancer. *Cell Cycle* 5(1), 43-46.

Sternberg, N. and Hamilton, D. (1981). Bacteriophage P1 site-specific recombination: recombination between *lox*P sites. *J Mol Biol* 150, 467-486.

Szafranska, A. E., Davison, T. S., John, J., Cannon, T., Sipos, B., Maghnouj, A., Labourier, E., and Hahn, S. A. (2007). MicroRNA expression alterations are linked to tumorigenesis and non-neoplastic processes in pancreatic ductal adenocarcinoma. *Oncogene* 26, 4442-4452.

Szklarczyk, D., Fanceschini, A., Wyder, S., Forslund, K., Heller, D., Huerta-Cepas, J., Simonovic, M., Roth, A., Santos, A., Tsafou, K. P., Kuhn, M., Bork, P., Jensen, L. J., von Mering, C. (2015). STRING v10: protein-protein interaction networks, integrated of the tree of life. Nucleic Acids Res 43(Database issue): D447-D452.

Tao, Z., Deepak Muzumdar, M., Detappe, A., Huang, X., Xu, E. S., Yu, Y., Mouhieddine, T. H., Song, H., Jacks, T., and Ghoroghchian, P. P. (2018). Differences in nanoparticle uptake in transplanted and autochthonous models of pancreatic cancer. *Nano Lett* 18, 2195-2208.

Tehler, D., Høyland-Kroghsbo, N. M., and Lund, A. H. (2011). The miR-10 microRNA precursor family. *RNA Biol* 8, 728-734.

Tempero, M. A., Malafa, M. P., Al-Hawary, M., Asbun, H., Bain, A., Behrman, S. W., Benson, A. B., Binder, E., Cardin, D. B., Cha, C., Chiorean, E. G., Chung, V., Czito, B., Dillhoff, M., Dotan, E., Ferrone, C. R., Hardacre, J., Hawkins, W. G. (2017). Pancreatic Adenocarcinoma, Version 2.2017, NCCN Clinical Practice Guidelines in Oncology. *J Natl Compr Canc Netw* 15, 1028-1061.

Thayer, S.P., di Magliano, M. P., Heiser, P.W. (2003). Hedgehog is an early and late mediator of pancreatic cancer tumorigenesis. *Nature* 425,851-856.

Threadgill, D. W., Yee, D., Matin, A., Nadeau, J. H., and Magnuson, T. (1997). Genealogy of the 129 inbred strains: 129/SvJ is a contaminated inbred strain. *Mamm Genome* 8, 390-393.

Tian, Y., Luo, A., Cai, Y., Su, Q., Ding, F., Chen, H., Liu, Z. (2010). MicroRNA-10b promotes migration and invasion through KLF4 in human esophageal cancer cell lines. J Biol Chem 285(11), 7986-94.

Tobita, K., Kijima, H., Dowaki, S., Kashiwagi, H., Ohtani, Y., Yamazaki, H., Nakamura, M., Ueyama, Y., Tanaka, M., Inokuchi, S., Makuuchi, H. (2003). Epidermal growth factor receptor expression in human pancreatic cancer: significance for liver metastasis. *Int J Mol Med* 11(3), 305-309.

Tong, X., Li, K., Luo, Z., Lu, B., Liu, X., Wang, T., Pang, M., Liang, B., Tan, M., Wu, M., et al. (2009). Decreased TIP30 expression promotes tumor metastasis in lung cancer. *Am J Pathol* 174, 1931-1939.

Turajlic, S. and Swanton, C. (2016). Metastasis as an evolutionary process. *Science* 352(6282), 169-175.

Tuveson, D. A. and Neoptolemos, J. P. (2012). Understanding metastasis in pancreatic cancer: a call for new clinical approaches. *Cell* 148, 21-23.

Valle, S., Martin-Hijano, L., Alcalá, S., Alonso-Nocelo, M., Sainz, B. Jr. (2018). The ever-evolving concept of the cancer stem cell in pancreatic cancer. *Cancers (Basel)* 10(2), pii:E33.

Van Duyne, G. D. (2001). A structural view of cre-loxp site-specific recombination. *Annu Rev Biophys Biomol Struct* 30, 87-104. doi:10.1146/annurev.biophys.30.1.87. PMID 11340053

van Heek, N. T., Meeker, A. K., Kern, S. E., Yeo, C. J., Lillemoe, K. D., Cameron, J. L., Offerhaus, G. J., Hicks, J. L., Wilentz, R. E., Goggins, M. G., et al. (2002). Telomere shortening is nearly universal in pancreatic intraepithelial neoplasia. *Am J Pathol* 161, 1541-1547.

Varadhachary, G. R., Tamm, E. P., Abbruzzese, J. L., Xiong, H. Q., Crane, C. H., Wang, H., Lee, J. E., Pisters, P. W., Evans, D. B., and Wolff, R. A. (2006). Borderline resectable pancreatic cancer: definitions, management, and role of preoperative therapy. *Ann Surg Oncol* 13, 1035-1046.

Vinay, D. S., Ryan, E. P., Pawelec, G., Talib, W. H., Stagg, J., Elkord, E., Lichtor, T., Decker, W. K., Whelan, R. L., Kumara, H. M. C. S., et al. (2015). Immune evasion in cancer: Mechanistic basis and therapeutic strategies. *Semin Cancer Biol* 35 Suppl, S185-S198.

Wagner, M., Greten, F. R., Weber, C. K., Koschnick, S., Mattfeldt, T., Deppert, W., Kern, H., Adler, G., and Schmid, R. M. (2001). A murine tumor progression model for pancreatic cancer recapitulating the genetic alterations of the human disease. *Genes Dev* 15, 286-293.

Wagner, G. P., Kin, K., and Lynch, V. J. (2012). Measurement of mRNA abundance using RNA-seq data: RPKM measure is inconsistent among samples. *Theory Biosci* 131, 281-285.

Wang, M., Zhao, J., Zhang, L., Wei, F., Lian, Y., Wu, Y., Gong, Z., Zhang, S., Zhou, J., Cao, K., Li, X., Wiong, W., Li, G., Zeng, Z., and Guo, C. (2017). Role of tumor microenvironment in tumorigenesis. *J Cancer* 8(5), 761-773,

Ward, J.M. (2006). Lymphomas and leukemias in mice. *Exp Toxicol Pathol* 57(5-6), 377-81.

Warshaw, A. L., and Fernández-del Castillo, C. (1992). Pancreatic carcinoma. *N Engl J Med* 326, 455-465.

Wei, D., Wang, L., Yan, Y., Jia, Z., Gagea, M., Li, Z., Zuo, X., Kong, X., Huang, S., and Xie, K. (2016) KLF4 is essential for induction of cellular identity change and acinar-to-ductal reprogramming during early pancreatic carcinogenesis. Cancer Cell 29(3), 324-338.

Westphalen, C. B. and Olive, K. P. (2013). Genetically engineered mouse models of pancreatic cancer. *Cancer J* 18(6), 502-510.

Witkiewicz, A. K., McMillan, E. A., Balaji, U., Baek, G., Lin, W. C., Mansour, J., Mollaee, M., Wagner, K. U., Koduru, P., Yopp, A., et al. (2015). Whole-exome sequencing of pancreatic cancer defines genetic diversity and therapeutic targets. *Nat Commun* 6, 6744.

Whitman, S., Wang, X., Shalaby, R, Shtivelman, E. (200). Alternatively spliced products CC3 and TC3 have opposing effects on apoptosis. *Mol Cell Biol* 20(2), 583-93.

Wray, C. J., Castro-Echeverry, E., Silberfein, E. J., Ko, T. C., and Kao, L. S. (2012). A multi-institutional study of pancreatic cancer in Harris County, Texas: race predicts treatment and survival. *Ann Surg Oncol* 19, 2776-2781.

Wu C, Jin X, Tsueng G, Afrasiabi C, and Su AI (2016) BioGPS: building your own mash-up of gene annotations and expression profiles. *Nucl Acids Res* 44 (D1), D313-D316. (*Database Issue*)

Wu C, MacLeod I, Su AI (2013) BioGPS and MyGene.info: organizing online, gene-entric information. *Nucl Acids Res* 41(D1), D561-D565. (*Database Issue*)

Wu C, Orozco C, Boyer J, Leglise M, Goodale J, Batalov S, Hodge CL, Haase J, Janes J, Huss JW 3rd, Su AI (2009) BioGPS: an extensible and customizable portal for querying and organizing gene annotation resources. *Genome Biol* 10(11):R130.

Xiao, H., Palhan, V., Yang, Y., and Roeder, R. G. (2000). TIP30 has an intrinsic kinase activity required for up-regulation of a subset of apoptotic genes. *EMBO J* 19, 956-963.

Xiao, H., Tao, Y., Greenblatt, J., and Roeder, R. G. (1998). A cofactor, TIP30, specifically enhances HIV-1 Tatactivated transcription. *Proc Natl Acad Sci U S A* 95(5), 2146-2151.

Xie, G., Ji, A., Yuan, Q., Jin, Z., Yuan, Y., et al. (2014). Tumor-initiating capacity is independent of epithelial-mesenchymal transition status in breast cancer cell lines. *BJC* 110, 2514-2523.

Xu, T., Jin, Z., Yuan, Y., Zheng, H., Li, C., Hou, W., Guo, Q., and Hua, B. (2016). Tat-Interacting Protein 30 (TIP30) Expression Serves as a New Biomarker for Tumor Prognosis: A Systematic Review and Meta-Analysis. *PLoS One* 11, e0168408.

Xu, Z., Vonlaufen, A., Phillips, P. A., Fiala-Beer, E., Zhang, X., Yang, L., Biankin, A. V., Goldstein, D., Pirola, R. C., Wilson, J. S., and Apte, M. V. (2010). Role of pancreatic stellate cells in pancreatic cancer metastasis. *Am J Pathol* 177(5), 2585-2596.

Yachida, S., and Iacobuzio-Donahue, C. A. (2009). The pathology and genetics of metastatic pancreatic cancer. *Arch Pathol Lab Med* 133, 413-422.

Yachida, S., Jones, S., Bozic, I., Antal, T., Leary, R., Fu, B., Kamiyama, M., Hruban, R. H., Eshleman, J. R., Nowak, M. A., et al. (2010). Distant metastasis occurs late during the genetic evolution of pancreatic cancer. *Nature* 467, 1114-1117.

Yamamoto, S., Tomita, Y., Hoshida, Y. et al. (2004). Prognositc significance of activated Akt expression in pancreatic ductal adenocarcinoma. *Clin Canc Res* 10(8), 2846-2850.

Ying, H., Kimmelman, A. C., Lyssiotis, C. A., Hua, S., Chu, G. C., Fletcher-Sananikone, E., Locasale, J. W., Son, J., Zhang, H., Coloff, J. L., et al. (2012). Oncogenic Kras maintains pancreatic tumors through regulation of anabolic glucose metabolism. *Cell* 149, 656-670.

Yu, J. B., Gross, C. P., Wilson, L. D., and Smith, B. D. (2009). NCI SEER public-use data: applications and limitations in oncology research. *Oncology* (Williston Park) 23, 288-295.

Zhang, C., Mori, M., Gao, S., Li, A., Hoshino, I., Aupperlee, M.D., Haslam, S.Z., and Xiao, H. (2010). Tip30 Deletion in MMTV-Neu mice leads to enhanced EGFR signaling and development of estrogen receptor-positive and progesterone receptor-negative mammary tumors. *Cancer Res* 70(24), 10224-10233.

Zhang, C., Li, A., Zhang, X., Xiao, H. (2011). A novel TIP30 protein complex regulates EGF receptor signaling and endocytic degradation. *J Biol Chem* 286(11), 9373-81.

Zhang, D. H., Wong, L. L., Tai, L. K., Koay, E. S., and Hewitt, R. E. (2005). Overexpression of CC3/TIP30 is associated with HER-2/neu status in breast cancer. *J Cancer Res Clin Oncol* 131, 603-608.

Zhang, H., Zhang, Y., Duan, H. O., Kirley, S. D., Lin, S. X., McDougal, W. S., Xiao, H., and Wu, C. L. (2008). TIP30 is associated with progression and metastasis of prostate cancer. *Int J Cancer* 123, 810-816.

Zhang, Y. Yan, W., Mathew, E., Bednar, F., Wan, S., Collins, M. A., Evans, R. A., Weilling, T. H., Vonderheide, R. H., Pasca di Magliano, M. (2014). $CD4^+$ T lymphocyte ablation prevents pancreatic carcinogenesis in mice. *Cancer Immunol Res* 2(5), 423-435.

Zhang, Y., Velez-Delgado, A., Mathew, E., Li, D., Mendez, F.M., Flannagan, K., Rhim, A.D., Simeone, D.M., Beatty, G. L., Pasca di Magliano, M. (2017). Myeloid cells are required for PD-1/PD-L1 checkpoint activation and the establishment of an immunosuppressive environment in pancreatic cancer. *Gut* 66, 124-136.

Zhao, J., Ni, H., Ma, Y., Dong, L., Dai, J., Zhao, F., Yan, X., Lu, B., Xu, H., and Guo, Y. (2007). TIP30/CC3 expression in breast carcinoma: relation to metastasis, clinicopathologic parameters, and P53 expression. *Hum Pathol* 38, 293-298.

Zhao, J., Lu, B., Xu, H., Tong, X., Wu, G., Zhang, X., Liang, A., Cong, W., Dai, J., Wang, H., et al. (2008). Thirty-kilodalton Tat-interacting protein suppresses tumor metastasis by inhibition of osteopontin transcription in human hepatocellular carcinoma. *Hepatology* 48, 265-275.

Zheng, B., Sage, M., Sheppeard, E. A., Jurecic, V., and Bradley, A. (2000). Engineering mouse chromosomes with Cre-*loxP*: range, efficiency, and somatic applications. *Mol Cell Biol* 20(2), 648-655.

Zheng, X., Carstens, J. L., Kim, J., Scheible, M., Kaye, J., Sugimoto, H., Wu, C. C., LeBleu, V. S., and Kalluri, R. (2015). Epithelial-to-mesenchymal transition is dispensable for metastasis but induces chemoresistance in pancreatic cancer. *Nature* 527, 525-530.

Zhu, M., Yin, F., Fan, X., Jing, W., Chen, R., Liu, L., Zhang, L., Liu, Y., Liang, Y., Bu, F., et al. (2015). Decreased TIP30 promotes Snail-mediated epithelial-mesenchymal transition and tumor-initiating properties in hepatocellular carcinoma. *Oncogene* 34(11), 1420-1431.

Zhu, Y.-Y. and Yuan, Z. (2015). Pancreatic cancer stem cells. *Am J Cancer Res* 5(3), 894-906.
Zou, W. and Restifo, N. P. (2010). T_H17 cells in tumour immunity and immunotherapy. *Nat Rev Immunol* 10(4), 248-256.

CURRICULUM VITAE

IMADE E. IMASUEN WILLIAMS

EDUCATION

2013-2019	Indiana University (IU) Indianapolis, IN **Ph.D., Biochemistry and Molecular Biology**
2007-2012	Vanderbilt University Nashville, TN **B.A., Molecular and Cellular Biology, Russian Language**

TRAINING

2019	Indiana University School of Medicine Indianapolis, IN **Jumpstart to Teaching Series: Teaching and Learning in the Biomedical Sciences** *Planning and Structuring a Lesson; Strategies for Teaching in the Sciences; Measuring and Improving Teaching and Learning; Inclusive Teaching and Learning; Practical Teaching Session, 5/13/19-5/17/19*
2012-2013	Emory University Atlanta, GA **Post-Baccalaureate Research Education Program (PREP)**
2010	St. Petersburg State University Department of Political Science St. Petersburg, Russia **CIEE-Russian Language Program**

PROFESSIONAL ASSOCIATIONS

2018	Yale Ciencia Academy, ***Fellow*** *(Science career development and leadership program for Ph.D. students. 1 of 40 selected in US, 1 of 2 first IU School of Medicine Ph.D. students to be awarded.)*
2018	American Association for the Advancement of Science (AAAS), ***Member***
2018	Cancer Research Club, ***Organizer***

2017-2018	Project Grow: Pass the Torch for Women, ***Participant***
2018-2019	Dress for Success Indianapolis: Professional Women's Group, ***Member***
2016-2019	Southern Regional Education Board (SREB), ***Doctoral Scholar***
2010-Present	American Association for Cancer Research (AACR), ***Associate Member***

HONORS & AWARDS

2019	**William M. Plater Civic Medallion**, Community service commitment during graduate studies, IUPUI, Indianapolis, IN
2018	**Cancer Disparities Research Network Travel Award,** Travel Scholarship to attend 2018 AACR Annual Meeting, Chicago, IL
2017	**Reagent Validation Award,** Received funds for a cell line verification proposal as part of a NIH T32 supplement to support the "Reagent Validation as a Means for Enhanced Research Reproducibility" Course at IU School of Medicine, Indianapolis, IN
2017	**Lustgarten Foundation Travel Award,** Partial travel award to attend CSHL Workshop on Pancreatic Cancer, Cold Spring Harbor, NY
2017	**Cancer Disparities Research Network Travel Award,** Early Career Travel Award to attend National Cancer Institute's Center to Reduce Health Disparities (CRCHD) Career Development Workshop, Workshop on Grant Writing, Philidelphia, PA
2014	**IU Cancer Center Annual Research Day First Place Poster Presentation,** Translational/Clinical Research by Graduate/Medical Student. *PD-0332991 induces epithelial to mesenchymal transition in pancreatic cancer*, Imasuen, I.E., Gore, A.J., Korc, M.K., Indianapolis, IN
2014	**AACR Minority Scholar in Cancer Research**, Travel Award for AACR Special Conference on Pancreatic Cancer: Innovations in Research and Treatment. *PD-0332991*

induces epithelial to mesenchymal transition in pancreatic cancer, Imasuen, I.E., Gore, A.J., Korc, M.K. New Orleans, LA

2012 **Ninth Annual Tennessee Louis Stokes Alliance for Minority Participation (TLSAMP) Research Conference First Place Oral Presentation,** Life Sciences. *The effect of mutant KRAS on colorectal cancer cell-derived exosome composition,* Imasuen, I.E, Demory Beckler, M., Coffey, R.J., Murfreesboro, TN

2011 **Joseph S. Silber Student Research Fellowship**, *Dual-photon confocal microscopy analysis of EGFR targeted therapy mechanism of resistance in lung cancer.* Advisor: Dr. Patrick Ma, American Cancer Society, Cleveland Clinic, Cleveland, OH. *Declined in order to accept NHLB summer research award*

2009 **Sixth Annual TLSAMP Research Conference**, Tennessee State University, Nashville, TN, Poster presentation winner (1st place), *DMAPT enhances radiation induced cell killing in p53 null prostate cancer cells*, Imasuen, I., Watson, C.N., Smolen, N., Borgmann, A., Dhaemers, R., Chin-Sinex, H., Crooks, P., Sweeney, C., Mendonca, M.S. Nashville, TN

2007-2009 **Ingram Scholarship**, Full Tuition-4 years; transitioned year 3 to pursue research, Vanderbilt University, Nashville, TN (*Fosters service to community in conjunction with academic excellence. Selection criteria is based on previous community service involvement, leadership potential, and character.)*

PUBLICATIONS

Imasuen-Williams, I.E., Enane, F., Korc, M. Perturbations in tat-interacting protein 30 (TIP30) levels contribute to pancreatic aggressiveness. [abstract]. In: AACR 2018 Proceedings; April 14-18; Chicago, IL. Abstract nr 4079.

Mendonca, M.S., Turchan, W.T., Alpuche, M.e., Watson, C.N., Estabrook, N.C, Chin-Sinex, H., Shapiro, J.B., **Imasuen-Williams, I.E.,** Rangel, G., Gilley, D.P., Huda, N., Crooks, P.A., Shapiro, R.H. DMAPT inhibits NF-kB activity and increases sensitivity of prostate cancer cells to X-rays in vitro and in tumor xenografts *in vivo*. *Free Radic Biol Med.* (2017) Nov 112:318-326.

Gore, J., **Imasuen-Williams, I.E.,** Conteh, A.B, Craven, K.E., Cheng, M., Korc, M. Combined targeting of TGF-β, EGFR and HER2 suppresses

lymphangiogenesis and metastasis in a pancreatic cancer model. *Cancer Letters.* (2016) Jun 3; 379(1):143-153.

Imasuen, I.E., Gore, A.J., Korc, M. PD0332991 induces epithelial to mesenchymal transition in pancreatic cancer. [abstract]. In: Proceedings of the AACR Special Conference on Pancreatic Cancer: Innovations in Research and Treatment; May 18-21, 2014; New Orleans, LA. Philadelphia (PA): AACR; Cancer Res 2015;75(13 Suppl):Abstract nr 115.

Srivatsan S., Patel J.M., Bozeman E.N., **Imasuen, I.E.**, He, S., Daniels D., Selvaraj P. Allogeneic tumor cell vaccines: The promise and limitations in clinical trials. *Human Vaccines and Immunotherapeutics.* (2014) 10(1):52-63.

Imasuen, I. Bozeman, E., He, S., Patel, J., Selvaraj, P. Increased B7-1 (CD80) expression reduces overall tumorigenicity and metastatic potential of the murine pancreatic cancer cell model Pan02. [abstract]. In The Journal of Immunology, 2013, 190 (1 Suppl) 53.43: Abstract nr P2085.

Demory Beckler, M., Higginbotham, J.N., Franklin, J.L., Ham, A.J., Halvey, P.J., **Imasuen, I.E.**, Whitwell, C., Li, M., Liebler, D.C., Coffey, R.J. Proteomic analysis of exosomes from mutant KRAS colon cancer cells identifies intercellular transfer of mutant KRAS. *Molecular and Cellular Proteomics*. (2013) Feb; 12(2):343-55.

EXPERIENCE

Research Experience

2013-2019 **Graduate Research Assistant**
Department of Biochemistry and Molecular Biology
Department of Medicine: Division of Endocrinology
Indiana University (IU) School of Medicine, Indianapolis, IN

Research Advisors: Dr. Murray Korc; Dr. Thomas Hurley and Dr. Hari Nakshatri (June 2018 to July 2019)

Project: *Generation and Characterization of a Novel Genetically Engineered Mouse Model (GEMM) to Elucidate Tat-Interacting Protein 30 (TIP30) Loss in Pancreatic Cancer*

Description: Pancreatic ductal adenocarcinoma (PDAC) is an aggressive and metastatic disease characterized by a high frequency of driver mutations, including *KRAS* mutations (93%), increased expression of growth factor receptors and aberrant TGF-beta signaling, and chemoresitance. The survival rate for PDA is 8-9%. Tat-interacting protein 30 (TIP30) is a putative tumor and

metastasis suppressor and direct target of micro-RNA-10b (an upregulated micro-RNA in PDAC). My dissertation research focused on the role of *Tip30* copy number loss in a novel transgenic mouse model of murine PDAC (K30C). TIP30 is genetically altered in 49% of human PDAC, according to data obtained from TCGA. *TIP30* monoallelic loss results in slightly more than half of *TIP30* alterations in TCGA. *Tip30*-heterozygosity in the mice with germline $Kras^{G12D}$ directed to the pancreas epithelium resulted in pancreatic cancer cell metastatic lung seeding, accelerated pulmonary lesion presentation, and increased EGFR protein levels in PCCs derived from primary pancreatic tumors. *Tip30*-null K30C mice had increased metastatic seeding to the liver, with frank PDAC tumor formation and increased macrometastases at later timepoints. *Tip30* genetic dosage may contribute levels may contribute to metastatic organotropism in PDAC metastasis.

Techniques: Transgenic mouse modeling, ketamine injection, mouse husbandry, genotyping PCR, whole-body fluorescent light box imaging, tissue collection for formalin fixation, OCT, and liquid nitrogen, tissue sectioning, cell line derivation from tissues, DNA, RNA protein extraction from tissues and cell lines, cell culture, immunohistochemistry(IHC), IHC-immunofluorescence(IF), pancreas and lung histopathological analysis, PCR and gel electrophoresis, qRT-PCR for mRNA and microRNA, Western blotting and signaling analysis, immunoprecipitation, immunofluorescent confocal microscopy, whole exome sequencing, large database mining (cBioportal, Xenabrowser), CRISPR-Cas9 genome editing, FACS, flow cytometry, MTT assay, three-dimensional growth assay, clonogenic assay, Integrative Genomics Viewer (IGV), transfections, transductions, molecular cloning (by restrictive enzyme digestion and ligation), plasmid purification (miniprep and maxiprep), IncuCyte, BrdU assay, siRNA knockdown studies, inhibitor dose response, data quantitation and statistical analysis (ImageJ, Cell Profiler, GraphPad Prism, SigmaPlot)

2012-2013 **PREP Research Fellow**
Department of Pathology and Laboratory Medicine, Emory University, Atlanta, GA

Research Advisors: Dr. Periasamy Selvaraj, Dr. Erica Bozeman

Project: *The effect of GPI-anchored immunocostimulatory molecules on tumor development in a murine model of pancreatic cancer.*

2011-2012 **Undergraduate Research Assistant**
Departments of Medicine and Cell and Developmental Biology, Vanderbilt University Medical Center, Nashville, TN

Research Advisors: Dr. Robert J. Coffey, Dr. Michelle Demory Beckler

Projects: *1. The effect of mutant KRAS on colorectal cancer cell-derived exosome composition. 2. The role of amphiregulin-enriched exosomes in non-transformed rat intestinal epithelial (RIE-1) cell proliferation.*

Summer 2010 & Summer 2011 **National Heart, Lung, and Blood (NHLB) Institute Summer Research Fellow**
Case Western Reserve School of Medicine, Cleveland Clinic, Taussig Cancer Institute, Cleveland, OH

Research Advisor: Dr. Patrick Ma

Projects: *1. Confocal immunofluorescence studies on activated EGFR and STAT3 signaling in response to targeted EGFR inhibitors in lung cancer cells. 2. Phosphorylated EGFR up-regulation in H1975 non-small cell adenocarcinoma cells after HKI-272 irreversible inhibitor treatment.*

2008-2009 **Undergraduate Researcher**
Department of Biological Sciences, Vanderbilt University, Nashville, TN

Research Advisor: Dr. Julián Hillyer

Project: *Enzymatic activity in disease vector Anopheles gambiae and Aedes aegypti mosquitoes.*

Summer 2008 **Systems Biology and Bioengineering Undergraduate Research Experience (SyBBURE) Fellow**
Vanderbilt Institute for Integrative Biosystems Research and Education, Nashville, TN.

Research Advisor: Dr. Philip Samson

Project: Fabrication of the BAMBI multi-well microfluidic device for cell trapping, in a controlled perfused environment.

Summer 2006 & Summer 2007 — Indiana University Cancer Center Summer Research Program (IUCCSRP), Departments of Radiation Oncology and Medical and Molecular Genetics, Indiana University School of Medicine, Indianapolis, IN.

Research Advisor: Dr. Marc Mendonca

Projects: *1. The sensitivity of radioresistant tumorigenic hybrid cervical cancer cells after siRNA silencing of BCL-2. 2. Dimethylamino-parthenolide (DMAPT) enhances radiation-induced killing in p53 null prostate cancer cells.*

Summer 2005 — IUCCSRP, Division of Pulmonary and Critical Care Medicine, Indiana University School of Medicine, Indianapolis, IN.

Research Advisor: Dr. Homer L. Twigg

Project: The effect of Highly Active Antiretroviral Therapy (HAART) on cytokine and chemokine concentrations in bronchoalveolar lavage (BAL) and plasma of HIV infected patients.

Clinical Experience

2011 — VANDERBILT UNIVERSITY MEDICAL CENTER, Nashville, TN, Colon and Rectal Surgery, Observational Student to Dr. Paul E. Wise, 36 hours

Professional Experience

2011-2012 — VANDERBILT UNIVERSITY CENTER FOR HEALTH SERVICES, Vanderbilt University, Nashville, TN,
Community Outreach Worker, Pilot Project Developer
Achievements**:** Completed and evaluated nutrition/body image focus groups for hard of hearing/deaf community at Hearing Bridges and fifth to seventh grade female students at New Visions Academy.

2008-2010	VANDERBILT UNIVERSITY RESIDENT LIFE EDUCATION, Nashville, TN, ***Resident Advisor***
2008-2012	VANDERBILT UNIVERSITY DEPT OF TEACHING AND LEARNING, Nashville, TN, ***Office Assistant***
2009	VANDERBILT UNIVERSITY TUTORING SERVICES, Nashville, TN, ***Russian Language Tutor***

Leadership Experience

2018	IUPUI Underrepresented Professional and Graduate Student Organization, ***President***
2018	IU School of Medicine Cancer Research Club, ***Facilitator***
2009-2010	Vanderbilt University Prison Project, ***President***

GRANTS

2018-Present	Ruth L. Kirschstein National Research Service Award (NRSA) Individual Predoctoral Fellowship (Parent F31) NIH, National Cancer Institute (NCI), CA23633201, *Novel Molecular Mechanisms Dictating Pancreatic Cancer Metastasis in Tip30-Deficient Kras-Mutant Mice.* Awarded 9/19/2018.
2015-2018	Research Supplement (to Primary Investigator's RO1 Parent Grant) to Promote Diversity in Health-Related Research, NIH, National Cancer Institute (NCI), CA075059-19S1, *Novel Aspects of Epithelial-Mesenchymal Transition (EMT) in Pancreatic Cancer,* 6/1/2015-4/30/2018. Principle Investigator: Murray Korc
2016-2019	Southern Regional Education Board (SREB) Doctoral Scholar

INVITED PRESENTATIONS

2018	IU Simon Cancer Center Workshop on Fellowships and Funding Opportunities Available to Trainees, *A Successful F31 Application*, Imasuen-Williams, I., Indianapolis, IN
2018	Annual Biomedical Research Conference for Minority Students (ABRCMS), *Ph.D. Green-book: A Survival Guide*

for Navigating Graduate School, Hernández Borrero, L. J., Canela, V. H., Bloom, B., Imasuen-Williams, I., Miles, K., Santos Cancel, M., Indianapolis, IN

CONFERENCES & WORKSHOPS

2019 **American Association for Cancer Research (AACR) Annual Meeting**, Atlanta, GA

2019 **Amelia Project Annual Meeting for Breast Cancer Research**, Kokomo, IN

2018 **25th Institute on Teaching and Mentoring**, Compact for Faculty Diversity, Arlington, VA

2018 **American Association for Cancer Research (AACR) Annual Meeting**. Poster Presenter. *Perturbations in tat-interacting protein 30 (TIP30) levels contribute to pancreatic cancer aggressiveness*, Imasuen-Williams, I.E., Enane, F., Korc, M. Chicago, IL.

2018 **American Association for the Advancement of Science** (AAAS) Annual Meeting, Austin, TX

2017 **24th Institute on Teaching and Mentoring**, Compact for Faculty Diversity, Atlanta, GA

2017 **Continuing Umbrella of Research Excellence (CURE) Session Grant Writing Workshop**: "Strategies for CURE Funding Success for Students, Fellows, and New Investigators", Philadelphia, PA

2017 **Cold Spring Harbor Laboratory Workshop on Pancreatic Cancer**. Cold Spring Harbor Laboratory Banbury Campus, Lloyd Harbor, NY

2016 **Fourth International RB Meeting.** The James-Ohio State University, Comprehensive Cancer Center, University of Illinois at Chicago, Columbus, OH

2016 **23rd Institute on Teaching and Mentoring**, Compact for Faculty Diversity, Tampa, FL

2015 Annual Biomedical Research Conference for Minority Students (ABRCMS), Seattle, WA

2014 **IU School of Medicine Biochemistry Research Day** Poster Presenter. *PD-0332991 induces epithelial to mesenchymal transition in pancreatic cancer*, Imasuen, I.E., Gore, A.J., Korc, M. IU School of Medicine, Biochemistry and Molecular Biology Department, Indianapolis, IN

2014 **IU Simon Cancer Center Annual Cancer Research Day** Poster Presenter. *PD-0332991 induces epithelial to mesenchymal transition in pancreatic cancer*, Imasuen, I.E., Gore, A.J., Korc, M. Indianapolis, IN

2014 **AACR Special Conference on Pancreatic Cancer**, Innovations in Research and Treatment. Poster Presenter. *PD-0332991 induces epithelial to mesenchymal transition in pancreatic cancer*, Imasuen, I.E., Gore, A.J., Korc, M.K. Hyatt Regency New Orleans, New Orleans, LA.

2013 **American Association of Immunologists Annual Meeting** Poster Presenter. *Increased B7-1 (CD80) expression reduces overall tumorigenicity and metastatic potential of the murine pancreatic cancer cell model (Pan02)*, Imasuen, I.E., Bozeman, E.N., He, S., Patel, J., Selvaraj, P. Hawaii Convention Center, Honolulu, HI.

2013 **Emory University Stem Symposium.** Poster Presenter. *Increased B7-1 (CD80) expression reduces overall tumorigenicity and metastatic potential of the murine pancreatic cancer cell model (Pan02)*, Imasuen, I.E., Bozeman, E.N., He, S., Patel, J., Selvaraj, P. Emory University, Atlanta, GA.

2012 **Ninth Annual (TLSAMP) Undergraduate Research Conference**, Oral Presenter. Middle Tennessee State University, Murfreesboro, TN.

2009 **Sixth Annual (TLSAMP) Undergraduate Research Conference.** Poster Presenter. *DMAPT enhances radiation induced cell killing in p53 null prostate cancer cells*, Imasuen, I., Watson, C.N., Smolen, N., Borgmann, A., Dhaemers, R., Chin-Sinex, H., Crooks, P., Sweeney, C., Mendonca, M.S. Tennessee State University, Nashville, TN.

2008	**Fifth Annual TLSAMP Undergraduate Research Conference.** Poster Presenter**.** *DMAPT enhances radiation induced cell killing in p53 null prostate cancer cells*, Imasuen, I., Watson, C.N., Smolen, N., Borgmann, A., Dhaemers, R., Chin-Sinex, H., Crooks, P., Sweeney, C., Mendonca, M.S. LeMoyne-Owen College and University of Memphis, Memphis, TN.

SERVICE

2018	IU Simon Cancer Center Summer Research Program Science Outreach Workshop Facilitator, *Describe Your Research in Five Minutes or Less*; *How to Give a Stellar Research Presentation*, Imasuen-Williams, I. and Hugo Canela , V., IU School of Medicine, Indianapolis, IN
2017-2019	IBMG Ph.D. Program Mentor. IUSM, Indianapolis, IN. *Mentor to two first-year IBMG Ph.D. students.*
2016-2019	IBMG Ph.D. Program Recruitment. IUSM, Indianapolis, IN. *Assist IBMG staff with recruiting future scholars at scientific research conferences.*
2009-2010	DAVIDSON COUNTY JUVENILE COURT, Nashville, TN, Foster Care Review Board. *Board Member.*
2008-2010	DISMAS HOUSE, Nashville, TN. *Cook, Presenter, and Community Outreach Facilitator.*
2009	TENNESSEE PRISON FOR WOMEN, Nashville, TN, Better Decisions One on One Mentoring Program. *Mentor.*
2008-2009	CALDWELL ENHANCED OPTION ELEMENTARY SCHOOL, Nashville, TN, Monroe Harding Project Share. *Mentor.*
2007-2009	WOODBINE COMMUNITY CENTER, Nashville, TN, Manna Project International ESL. *ESL Instructor, Coordinator.*
2007-2008	SYLVAN PARK ELEMENTARY SCHOOL, Nashville, TN, PENCIL PROJECT FOUNDATION. *Reading Partner.*